NANOPARTICLE DELIVERY OF MOLECULAR AGENTS TO TACKLE HIV LATENCY

Abdalla Abbas Jafer Ali

MSc, B. Pharm

ORCID ID: 0000-0002-6946-4343

From Elgada, Sudan

Submitted in total fulfilment of the requirements of the degree of
Doctor of Philosophy (PhD)

Of

The Medical Faculty

The Rheinische Friedrich-Wilhelms-Universität Bonn

and

The Department of Microbiology and Immunology
Faculty of Medicine, Dentistry and Health Sciences
The University of Melbourne

Bonn/Melbourne, 2022

Performed and approved by The Medical Faculty of The Rheinische Friedrich-Wilhelms-Universität Bonn and The University of Melbourne

1. Supervisor: Prof. Dr. Martin Schlee

2. Supervisor: Prof. Dr. Sharon Lewin

Month and year of the original thesis submission: 12/2021

Month and year of the oral examination: 08/2022

Institute in Bonn:
Institute of Clinical chemistry
& Clinical Pharmacology

Director: Prof. Dr. med
Gunther Hartmann

Table of Contents

List of Abbreviations

AEs	Adverse effects
AIDS	Acquired Immunodeficiency Syndrome
ART	Antiretroviral therapy
ATI	Analytical Treatment Interruption
AxV	Annexin V
BACH2	BTB domain and CNC homolog 2
BAX	BCL-2-associated X protein
Bcl-2	B-cell lymphoma 2
BET	Bromodomains and extra-terminal
BG	bovine glycogen
BIR	Baculoviral IAP repeat
BiTEs	Bispecific T cell engagers
bNAbs	Broadly neutralising antibodies
bsAbs	Bispecific antibodies
CA	Capsid protein
CA	Cell associated
CA RNA	RNA Cell associated unspliced RNA
CAR	Chimeric antigen receptor
cDCs	Conventional dendritic cells
CDK	Cyclin-dependent kinase
cDNA	Complementary DNA
CF	Cell-free
CLL	Chronic lymphocytic leukaemia
CMV	Cytomegalovirus
CNS	Central Nervous System
CRISPR/CAS-9	CRISPR associated protein-9 nuclease system
CTLA4	Cytotoxic T-lymphocyte-associated antigen 4
CTLs	Cytotoxic T-lymphocyte
DCs	Dendritic cells

ddPCR	Digital droplet PCR
DDX 3	DEAD-box protein 3
DDX 5	DEAD-box protein 5c
DLS	Dynamic light scattering
DMEM	Dulbecco's modified eagle medium
DMSO	Dimethyl sulfoxide
DNTMs	DNA methyltransferase
ds	Double strand
EC	Elite controllers
EC	Endothelial cell
EDA	Ethylenediamine
EDTA	Ethylenediaminetetraacetic acid
EF1α	Elongation factor 1-α
HTLV-1	Human T cell leukemia virus type 1
EMT	Effector-to-memory transitioning T cells
Env	Envelope
FBS	Fetal Bovine serum
FDCs	Follicular dendritic cells
FLIPS	Full-Length Individual Proviral Sequencing
GALT	Gut Associated Lymphoid Tissue
GFP	Green Fluorescent Protein
GSH	Glutathione
HDAC	Histone deacetylase
HDACi	Histone Deacetylase Inhibitors
HEK	Human embryonic kidney
HIV	Human Immunodeficiency Virus
HMTases	Histone methyltransferases
HMTi	Histone methyltransferase inhibitors
HTLV-1	Human T cell leukemia virus type 1
IAP	Inhibitors of Apoptosis
IC	Immune checkpoint
IFI16	Interferon-gamma-inducible protein 16
IFN I	Type I interferon

IN	Integrase
Ing3A	Ingenol-3-angelate
IngB	Ingenol B
Iono	Ionomycin
IPDA	Intact proviral DNA assay
IRES	Internal Ribosome entry site
IRF 3	Interferon regulatory factor 3
IS	Internal standard
ISG	Interferon stimulating genes
JAK1	Janus kinase 1
LbL	Layer-by layer
LbL	Latency-reversal agents
LTR	Long-terminal repeat
MA	Matrix protein
MAbs	Monoclonal antibodies
MATR3	Matrix-associated RNA binding matrix 3
mDCs	Myeloid dendritic cells
MDDCs	Monocyte-derived dendritic cells
MHC	Major histocompatibility complex
MS	Mesoporous silica
MS	Multiply spliced mRNA
NC	Nucleocapsid Protein
NEFAT1	Nuclear Enriched Abundant Transcript 1
NFEAT	Nuclear factor of activated T cells
NF-κB	Nuclear Factor κ-light chain-enhancer
NSG	Next genome sequencing
NHP	Non-human primate
NTA	Nanoparticle tracking analysis
NP	Nanoparticle
Nuc-0	Nucleosome-0
Nuc-1	Nucleosome-1
OD	Optical density
PAMPs	Pathogen-associated molecular patterns

PBMC	Peripheral blood mononuclear cells
PCR	Polymerase chain reaction
PD-1	Programmed cell death protein-1
pDC	Plasmacytoid dendritic cells
PDI	polydispersity index
PEG	Polyethylene glycol
PHA	Phytohaemagglutinin
PI	Propidium iodide
PI3K	Phosphoinositide 3-kinase
PKC	Protein Kinase C
PLL	Poly L-lysine
PLWH	People living with HIV
PMA	Phorbol 12-myristate 13-acetate
PMA_{SH}	Thiolated Poly (methacrylic acid)
PPR	Pattern recognition receptor
PR	Viral protease
P-TEFb	Positive Transcription Elongation Factor b
qPCR	Quantitative PCR
RA	Retinoic acid
RCC	Renal cell carcinoma
rhIFN-α	Recombinant human interferon-alpha subtype
RIG-I	Retinoic acid-inducible gene *I*
RMD	Romidepsin
RMDLNP	Romidepsin loaded PMA_{SH} nanoparticle
RNAPII	RNA polymerase II
ROS	Reactive oxygen species
RRE	Rev responsive element
RT	Reverse Transcriptase
RT-qPCR	Reverse Transcription qPCR
SAMHD1	Sterile motif and histidine aspartic domain and HD domain-containing protein 1
SEC	Super elongation complex
SeV	Sendai virus

SHIV	Chimeric Simian Human Immunodeficiency Virus
SIV	Simian Immunodeficiency virus
SMAC	Second mitochondria-derived activator of caspases
Sp1	Specificity protein 1
SS	Singly spliced mRNA
STAT1	Signal transducer and activator of transcription 1
STAT2	Signal transducer and activator of transcription 2
SU	gp 120 external glycoprotein
TAR	Tat-responsive region
TCM	Central memory T cells
TCR	T cell receptor
TEM	Effector memory T cells
TFH	Follicular helper T cells
TIGIT	T cell immunoreceptor Immunoglobulin and ITM domain
TILDA	Tat/Rev Induced Limiting Dilution Assay
TLR	Toll-like receptor
TM	Transmembrane protein
TN	Naïve T cells
TNF	Tumour necrosis factor
TRM	Tissue-resident memory T cells
TRM	Tissue-resident memory T cells
TSCM	Stem cell memory T cells
TTE	Terminally differentiated T cells
TTM	Transitional memory T cells
Tyk2	Tyrosine kinase 2
US	Unspliced mRNA
VSV-G	Vesicular Stomatitis Virus Envelope Glycoprotein
XIAP	X-linked inhibitors of apoptosis

List of Tables

List of Figures

Chapter 1

Chapter 2

Chapter 3

Chapter 4

Chapter 5

Abstract

Antiretroviral therapy (ART) effectively suppresses HIV replication in people living with HIV (PLWH), but treatment is lifelong due to the persistence of long-lived, latently infected resting $CD4^+$ T cells. During the early course of infection, HIV integrates into the genome of $CD4^+$ T cells (provirus) and establishes a reservoir of latently infected cells. These latently infected cells contain a transcriptionally silent provirus that can evade ART, resist immune-mediated clearance and are a significant challenge in achieving a cure for HIV infection. One strategy toward eliminating HIV latency is the activation of HIV viral production by latency reversal agents (LRAs) to induce virus-mediated cytolysis or clearance through immune recognition in the presence of ART (often called "shock and kill"). A range of pharmacological and immunological interventions have been investigated to eliminate latency and purge the HIV latent reservoir, including epigenetic modifiers such as the histone deacetylase inhibitor romidepsin and compounds that work through the NF-κB pathway such as agonists of retinoic acid-inducible gene I (RIG-I). However, the shock and kill strategy has demonstrated limited efficacy both *in vitro* and in clinical trials based on lack of specificity, toxicity issues, inability to directly target the $CD4^+$ T cells and the failure to reduce reservoir size. One approach to overcome some of these limitations is using nano-engineered particle delivery systems to encapsulate and deliver LRAs to latently infected T cells, which possess several advantages over more traditional drug delivery methods and could potentially increase potency and reduce toxicity. We developed two different nanocarrier solutions to encapsulate two distinct LRAs; romidepsin (a small hydrophobic molecule) and 5'triphosphate double-stranded RNA (a nucleic acid RIG-I agonist).

In this thesis, first, we fabricated thiolated Poly (methacrylic acid) (PMA_{SH}) particles using the Layer-by-Layer (LbL) assembly technique with varying sizes, from 100 nm to 1 μm. In addition, we surface-functionalized the negatively charged PMA_{SH} particles to neutral (PMA_{SH}-PEG) and positive

surface charge (PMA_{SH}-PLL). Using these platforms, we investigated the influence of surface charge and size in particle association and internalization in T cells and within physiological mixtures of primary human blood immune cells (human whole blood and PBMC) using flow cytometry and confocal microscopy. We demonstrated that negatively charged PMA_{SH} particles are more readily associated with T cells than neutral PMA_{SH}-PEG and positively charged PMA_{SH}-PLL. Furthermore, smaller negatively charged particles (400 nm) were preferentially internalized in T cells compared to larger particles. In contrast, we found that PMA_{SH}-PEG and PMA_{SH}-PLL 400 nm particles were highly associated with T cells in human PBMC mix culture. Interestingly, in human whole blood, 400 nm particles were taken up by monocytes and DCs irrespective of their surface charge.

We then utilized the PMA_{SH} particle drug delivery system to encapsulate romidepsin (RMDLNPs) and investigated their potency to reactive HIV latency and cytotoxic effects compared to romidepsin free drug formulation in cell line models of HIV latency. We successfully delivered RMDLNPs to a latently infected T cell line and demonstrated enhanced potency to reverse HIV latency with reduced toxicity.

Finally, we optimized a delivery carrier platform for a RIG-I agonist using ethylenediamine modified bovine glycogen (BG_{EDA}) nanoparticles. This RNA/glycogen complex was able to induce type I interferon (IFN-I) in primary $CD4^+$ T cells and reversed HIV latency in a cell line model of HIV latency.

In summary, these data illustrate the potential use of nano-engineered particles in HIV shock and kill strategies and demonstrate the capacity of nanoparticle drug delivery systems to enhance the future of HIV cure.

Declaration

I declare that this thesis:

I. Comprises of my original work towards the Doctor of Philosophy except where indicated in the Preface

II. Due acknowledgment has been made in the text to all other material used.

III. This thesis is less than 100,000 words in length, exclusive of tables, figures, references and the appendices

Preface

This PhD thesis contains the research undertaken at the Lewin Laboratory, the Peter Doherty Institute for Infection and Immunity, the Department of Microbiology and Immunology, and the Nanostructured Interfaces and Material Science Group (Caruso Nanoengineering Group), Department of Chemical Engineering-The University of Melbourne, Australia. This work was carried under the supervision of Prof. Sharon Lewin with co-supervision of Prof. Damian Purcell and Dr Jori Symons. Components of this PhD thesis contain contributions from collaborators, and their contributions are mentioned below.

Dr Yi Ju synthesised the mesoporous silica (MS) particles (Figure 2.1) used to fabricate PMA_{SH} nanoparticles in Chapters 3 and Chapter 4. Dr Rene Lafleur contributed directly to the generation of the data for chapter 2, Figures 2.3, 2.4 and 2.5 and chapter 4, Figure 4.3. Dr Christina Cortez also contributed to generating the data for chapter 3, Figure 3.7 and 3.9. Jared Stern provided J-Lat 10.6 cells for the *in vitro* model of HIV latency. Additionally, Marvin Holz provided us with the Sendai virus, THP-1 cells and HEK blue cells. Paula Cevaal assisted with synthesis of bovine glycogen nanoparticles and helped generate the data for Figures 5.1 and 5.2.

Acknowledgements

Firstly, I want to take this opportunity to thank and acknowledge the people that significantly contributed and who made this work possible. Foremost, I want to thank Allah for giving me strength and peace through all the difficulties. I have experienced your guidance day by day, and I will keep trusting you for my future.

I would like to thank my supervisors, Prof. Sharon Lewin, Prof. Damian Purcell, Prof. Martin Schlee and Dr Jori Symons. Sharon, I am deeply indebted to you for taking me on as your student and for the supervision and guidance you have provided over the last few years. Thank you for the opportunity to work in such a great laboratory/group and for the knowledge and for skills I have gained during my time in the lab. Indeed, I will carry these fruitful experiences through my career. Your excellent mentorship and advice on becoming a better scientist have played a pivotal role in my growth as a scientist, sharpened my thinking, and brought my work to a higher level. One example amongst many is giving me the confidence to respond to criticisms and questions towards my research.

I would also like to thank Damian for his support as a supervisor and also beyond the science when I first arrived in Australia; your genuine nature has helped me persevere. Your meticulous scrutiny, informed advice, and scientific approach has helped me to expand my approaches to address my research questions. Martin is the brilliant mind behind the RIG-I agonist delivery to T cells hypothesis. You have always been there when I needed extra advice on research questions. Jori, where and how to start? I owe you a deep sense of gratitude for believing in me. I still remember our first meeting, and I appreciated your honesty while working together and doing good science. Your guidance in formulating the research questions and providing support enabled me to complete my work. Without your help, advice, expertise and encouragement, this research would not have

happened. Beyond the lab, I appreciated our relationship and the deep conversations; it opened my mind and influenced my thinking. Your support during the challenging times I have encountered during my PhD was beyond my expectations, and it was one of the few reasons that I kept going. Thank you for being a consistent source of advice and support in the lab and beyond in other areas of life. I will forever be appreciative of your kindness, empathy, and support. It would also be remiss not to mention and sincerely thank Dr Christina Cortez-Jugo. Thank you for co-supervising, introducing me to the “nano-world”, intellectual guidance and patience. This thesis would also not have been possible without your assistance.

Dr Michael Roch, the process of writing a thesis is long and arduous, especially in these challenging times we are going through, and it is undoubtedly not done single-handedly. Your guidance, insight, feedback, and advice were essential throughout the thesis writing process (just like a fish, keep swimming). It is a credit to you, Michael, that I have become more confident in my scientific writing. You are such a great mentor, and I am very blessed to have worked with you.

I would also like to express my gratitude to my thesis advisory committee, Prof. Bill Health, Prof. Paul Gory and Dr. Francesca Cavalieri. Collectively, I would like to thank them for challenging my knowledge and guiding experiments, especially in the first year of my PhD and as my thesis developed. Your valuable inputs into my thesis have helped me keep in perspective where my research fits into the bigger picture. Additionally, your constructive criticisms have helped me strengthen my thesis.

I would like to acknowledge all the Lewin, Purcell and Caruso lab members who have helped in this enormous process. It was a privilege to work with each one of you. In addition, I am greatly appreciative of the reservoir group members (The Lewin lab), who have contributed to my research and the insight provided from great discussion with our brilliant PhD students, postdocs, and research assistants. I also owe gratitude to our lab manager Ajantha Rhodes for being such a supportive colleague on the professional

and personal level during my time at the Lewin lab. My special thanks also to our research assistant Carolin Trumps for training me on PC2, PC3 and several assays required for my thesis and always being willing to go for a coffee break or have a walk around the campus. Rachel Pascoe and Danielle Fong, thank you for being my PC3 buddies during the week and weekends. I would also like to thank our research managers Dr Jasminka Sterjovski and Dr Catherine Kennedy. Jasminka, you have been supportive and understanding when I first moved to the Lewin lab and helped me settle. Catherine, thank you for assisting me towards the end with helping me to plan my thesis writing and proof-reading some of the thesis.

Many thanks to the past members of the Lewin lab, especially to Prof. Paul Cameron for his insightful suggestions; A/Prof Thomas Rasmussen for helping with statistics; Dr Jenny Anderson for her helpful advice on imaging, confocal microscopy assays and technical input in HIV latency reversal experiments; and lastly, Dr Zuwena Richardson for her help during my stressful thesis writing and going for a walk around Princess Park.

I would like to extend my deepest gratitude to the Nano-team. Paula Cevaal and Haoming Lu, you are a fantastic team, and I always enjoyed our brainstorming ideas on how to bring the nanoparticles to the world. Paula, what a colleague and friend you are! Thank you for always being so supportive and considerate. You are always happy to help and give brilliant ideas to my thesis.

Also many thanks to the Joint PhD program, Bonn and Melbourne Research and Graduate School. Prof. Sammy Bedoui (programme director-University of Melbourne), Prof. Christian Kurts (programme director-University of Bonn), Dr Marie Greyer (programme coordinator -University of Melbourne), and Lucie Delforge (programme coordinator-University of Bonn), thank you for being very supportive during the programme and always listening to our concerns. Additionally, I am grateful for such a fantastic opportunity to grow and transform myself into a scientist.

My little family in Australia, Yousif, Amaya, Omar, and Oz, thank you for always being there for me and bringing joy to my life during my PhD. Yousif, thank you for being a wonderful human, giving me a shelter for few months when I first arrived in Australia and always offering financial support when funds are tight. Amaya, thank you for being a true amiga and a good listener, cooking meals while I was writing this thesis, going for walks, and just inviting me to almost every social event you attend. Omar and Oz, it was always joyful whenever I met you. Your support was tremendous.

Finally, to my family back home. My mother Nawal, sisters Suzi and Roja, your prayers for me was what sustained me so far. I appreciate your understanding when I have been away from you during the past few years and have not supported you during difficult times. Nawal, your words of wisdom always kept me strong. Suzi, thank you for the sacrifices you made; your endless support and unconditional love made it possible to pursue my dream. Every time I was ready to quit, you did not let me, and I am forever grateful. Roja, your smart and wise thinking and encouragement provided me with much energy throughout this journey. My father Abbas and brother Khalid, I wish you were here to see this. You have been such an inspiration, and I would not be the person I am today without you.

Chapter 1: Introduction and Literature review

1.1 INTRODUCTION

"Progress in scientific research rarely follows a straight path. Generally, it entails many unexpected meanderings, with a mix of good and bad ideas, good and bad luck. The discovery of the human immunodeficiency virus as the cause of AIDS did not avoid this pattern". Robert C. Gallo (1).

1.2 THE GLOBAL HIV PANDEMIC

The human immunodeficiency virus (HIV) continues to be the cause of a devastating global health crisis, causing significant morbidity and mortality following the recognition of acquired immunodeficiency syndrome (AIDS) (2). Since the start of the epidemic in 1981, worldwide, an estimated 78.7 million have contracted HIV infection, and approximately 38 million people have died of HIV-related illnesses, with a majority of them concentrated in Eastern and Southern Africa (3). According to the UNIAIDS Global report, in 2020 there were 1.5 [1.1-2.1] million new infections globally compared to 2.1 [1.8-24] million in 2015, and 0.68 [0.48-1.0] million HIV-related deaths compared to 1.1 [0.94-1.3] million in 2015 (4). This is mainly attributed to the advent of ART, an essential player in preventing HIV transmission and progression of HIV to AIDS. As of 2020, 73 % [56 %-88 %] of people living with HIV (PLWH) globally were accessing life-saving antiretroviral therapy (ART) compared to 50 % in 2015 (4). Despite ART substantially reducing HIV-related morbidity and mortality, ART is not curative, and treatment is lifelong. In addition, access to ART can be difficult, particularly in high burden regions and is a great financial burden with an estimated cost to treat all PLWH with ART to reach 30 billion US dollars by 2030 (5). Therefore, there is great interest in developing a strategy to cure HIV infection so PLWH can cease ART.

1.3 HIV: STRUCTURE AND REPLICATION CYCLE

1.3.1 Structure

The core of the HIV virion consists of two identical single-stranded positive sense ribonucleic acid molecules (ssRNA), and an enzyme called reverse transcriptase (RT) that converts viral RNA to Deoxyribonucleic DNA (6) (Figure 1.1). The HIV particle has a 120 nm diameter and is surrounded by a lipid bilayer (7, 8). The viral particle membrane contains non-covalently bound trimers of the viral glycoprotein gp 120 and the transmembrane spanning gp 41 glycoprotein (9). The virus membrane and the matrix protein enclose the capsid composed of polymers of the core antigen (p24). The viral capsid is composed of two copies of the HIV RNA, nucleoprotein and reverse transcriptase enzymes such as integrase (IN), reverse transcriptase (RT) and protease (PR), which are required for reverse transcription (10).

The 9.8 kb genome of HIV contains nine open reading frames (ORFs) that produce 15 proteins classified into structural and regulatory proteins expressed during the HIV life cycle (11). In the direction 5′ to 3′ (Figure 1.2), the gag gene $Pr55^{gag}$ encodes the proteins of the outer core membrane matrix protein (MA) p17, which is implicated in the nuclear import of the HIV pre-integration complex (12, 13); capsid protein (CA) p24, nucleocapsid protein (NC) p7 and p6 gag protein which participate in late steps of the HIV replication cycle, specifically virion budding (14). The pol gene encodes a variety of viral enzymes including, protease (PR), reverse transcriptase (RT), RNAse H and Integrase (IN) (15). The envelope glycoprotein (Env) encodes two envelope glycoproteins located on the outer surface (SU) membrane, gp 120 and the transmembrane (TM) protein, gp 41, collectively enable viral fusion into the host cell (16).

HIV encodes two regulatory proteins; the transactivation protein Tat, and RNA splicing regulator Rev, which is essential for HIV gene expression and nuclear export. In addition HIV encodes four accessory genes, viral protein R (Vpr), negative factor (Nef), viral protein U (Vpu) and viral infectivity factor (Vif), which are involved in pathogenicity and promoting the ideal environment for viral replication (17–19). Flanking the genome at the 5' and 3' ends are the long terminal repeats (LTRs) which are a consequence of reverse transcription and are identical sequence of HIV DNA (11). In an

integrated provirus, they are products formed through reverse transcription and are located on each side of the HIV genome (20). The LTR region is further divided into three distinct regions, the U3, R and U5 segments, where HIV transcription initiates from the promotor region in the R section of the 5'LTR and terminates at the polyadenylation (PolyA) signal in the R region of the 3'LTR (21, 22).

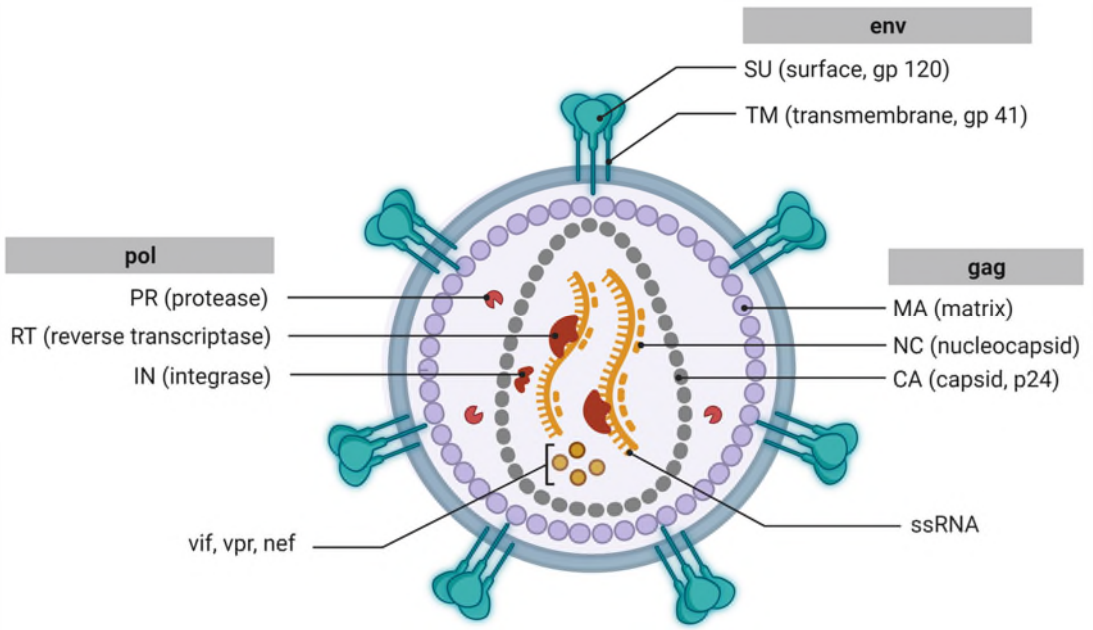

Figure 1.1 HIV virion.

HIV is an envelope virus of approximately 120 nm in diameter. The plasma membrane is surrounded by envelope protein, consisting of an outer glycoprotein (gp) 120 and a transmembrane domain gp 41. HIV contains a core protected by a lipid bilayer shield (matrix, MA) and a capsid protein, and includes several host proteins, the positive-sense ssRNA genome and various proteins such as Vif, Vpr, Nef and enzymes such as protease, integrase, and reverse transcriptase (11).

Created with biorender.com

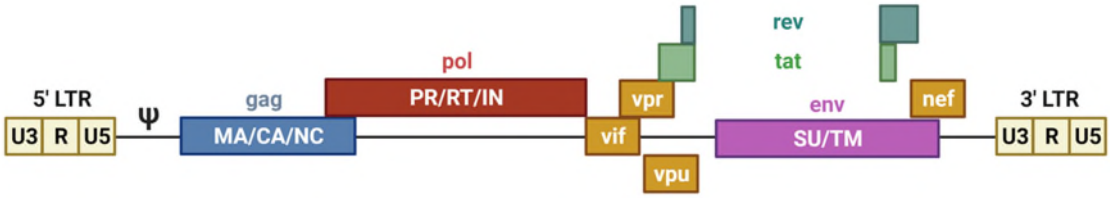

Figure 1.2 HIV genomic structure

The HIV genome structure varies in size between 119-207 bp (23). The HIV genome contains 15 open reading ORFs that can produce proteins translated from spliced mRNA and unspliced mRNA to liberate the protein into their functional units. Created with biorender.com

1.3.2 Replication cycle

HIV predominantly targets $CD4^+$ T cells but can infect other cell types that express CD4, including monocytes, macrophages and dendritic cells (DCs) (24). The first step of the HIV life cycle begins upon adhesion of the virus to the host cell, which is mediated by the binding of the viral gp 120 envelope protein to the host cell receptor CD4 (25, 26). This induces a conformational change in gp 120, enabling the co-receptor binding domain to bind to the cellular chemokine C-C motif receptors 5 (CCR5) or C-X-C motif receptor type 4 (CXCR4), and subsequently, gp 41 leads to fusion of the viral membrane with the cellular membrane and the viral core is deposited in the cytoplasm (27) (Figure 1.3). Once in the cytoplasm, the core houses and the single-stranded viral RNA genome are reverse transcribed by the viral protein reverse transcriptase to form double-strand (ds) DNA (28). The conversion to dsDNA leads to the pre-integration complex (PIC) assembly, which then moves from the cytoplasm to the nucleus (29, 30). The PIC is imported into the host cell nucleus, where the viral DNA (provirus) is integrated into the host genome by the action of the viral Integrase protein (31). The irreversible integration of HIV DNA into a host cell chromosome is facilitated with a strong preference for sites in introns of transcriptionally active genes (32–34).

The HIV DNA genome is flanked at both ends by the LTR sequences. The 5'LTR region contains many protein binding sites such as negative regulatory elements, modulating HIV transcription by utilising it as landing pads to host transcription factors. The HIV LTR contains two direct nuclear factor-kB ($NF\text{-}_kB$), the nuclear factor of activated T cells (NFAT) and three repeats of specificity protein 1 (SP-1) and TATA box, which are required to trigger transcription (35). Tat recruits viral and cellular transcriptional factors on the LTR to upregulate the transcription of the HIV genome. Following

integration, transcription can be actively silenced (in a resting $CD4^+$ T cell) or proceeds efficiently (in an activated $CD4^+$ T cell) (36, 37). Once the viral transcription is efficiently initiated, this results in messenger RNA synthesis (mRNA) (38).

There are two NF-$_k$B and three SP1 binding sites positioned in the enhancer region and the core promoter region of the LTR, respectively (36). Availability of transcriptional factors (TFs) to bind to these sites is critical for efficient transcriptional initiation from the viral promoter (37, 39). In the absence of the viral regulatory protein Tat, transcriptional elongation is inefficient (40). However, interactions between TFs at the HIV LTR produce a low level of transcription events, which can proceed to completion and produce full-length transcripts from the HIV genome (41, 42). The HIV regulatory protein Tat, encoded by the *tat* gene, is essential for virion production in natural HIV infection and influences the balance between productive and latent infection after HIV DNA integrates into the host cell chromosome. The regulatory Rev protein encoded by the *rev* gene exports unspliced or singly-spliced viral mRNAs from the nucleus into the cytoplasm before it undergoes complete splicing (43). As the levels of complete viral transcripts start to increase, Tat and Rev levels gradually accumulate, creating a powerful positive feedback loop with Tat that facilitates efficient transcriptional elongation at the LTR, in the process positively regulating it is own production (44). In the early transcription phase, the 9.8 kb HIV transcript is spliced, resulting in a 1.8 kb fragment class of unspliced (US) or single spliced (SS) mRNA and transported back to the cytoplasm, where structural proteins of new virions are synthesised (45, 46). Herein, only part of HIV transcripts is completely processed as Rev facilitates the export of intron-containing mRNA out of the nucleus by associating with the Rev Responsive Element (RRE) (47). Moreover, the coordinated actions of the two regulatory proteins, Tat and Rev, are essential for successfully expressing the structural and envelope proteins required to assemble viral particles (48, 49).

The formation of new viral particles is a stepwise process: These mRNAs lead to the translation of viral Gag, Gag-Pol polyprotein (US RNA), Env (SS RNA) structural polyproteins and multiple spliced RNA encoding additional

regulatory proteins forming the virus capsid (45, 50, 51). This immature particle migrates towards the plasma membrane with two copies of full-length ssRNA and buds of the cell generating new immature virions. The large precursor molecules (Gag-Polyprotein) are then cleaved by the HIV protease, resulting in new infectious viral particles, which bud through the host cell membrane (52, 53).

1.4 ANTIRETROVIRAL THERAPY (ART)

HIV replication can be effectively inhibited with ART and has decreased overall mortality among PLWH (54). ART treats HIV and consists of at least two or three antiviral agents that target viral enzymes or proteins required for HIV replication (55). Multiple antiretrovirals are now available, targeting different steps in the virus life cycle (56) (Figure 1.3). Currently, there are several classes of antiretroviral drugs classified based on their molecular targets including, nucleoside reverse transcriptase inhibitors (NRTIs), non-nucleoside reverse transcriptase inhibitors (NNRTIs), co-receptor antagonists, fusion inhibitors, integrase inhibitors and protease inhibitors (Figure 1.3). Recent new antiretrovirals progressing through clinical development include long-acting injectables and broadly neutralising antibodies (57, 58).

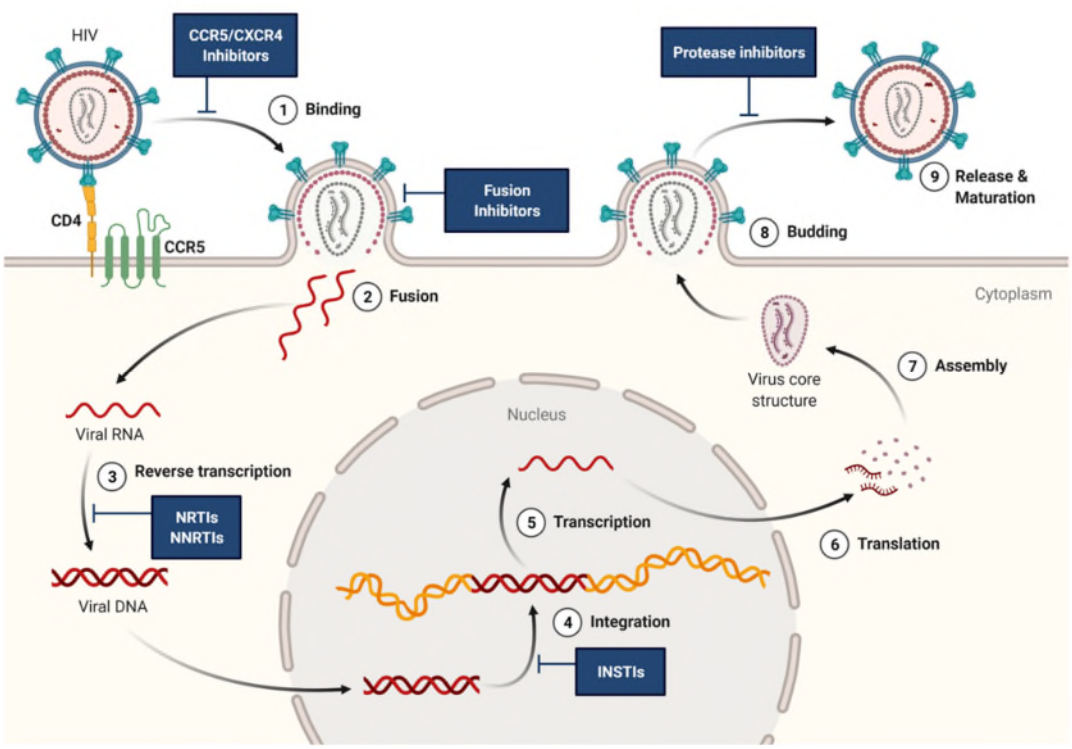

Figure 1.3 HIV replication cycle and site of action of antiretroviral therapy

The life cycle of HIV infection mainly consists of nine stages: (1) binding, (2) fusion, (3) reverse transcription, (4) integration, (5) transcription, (6) translation, (7) assembly, (8) budding and (9) release and maturation of virion. The virus glycoprotein envelope gp 160 binds to the cellular receptor CD4 and evokes a conformational change, exposing a co-receptor binding domain of gp 120. This is followed by binding to either CCR5 or CXCR4, inducing another conformational change enabling the viral and cellular membranes fusion. HIV deposits its core in the cytoplasm where there is uncoating, and then the RNA is reverse transcribed to DNA to form the pre-integration complex (59). The PIC translocates to the nucleus and with the help of viral integrase. Following HIV integration into the host genome, HIV utilises the cellular machinery to initiate transcription, and viral RNAs are exported to the cytoplasm and translated into protein. Finally, maturation occurs, allowing the viral RNA and proteins to assemble at the surface and bud off the cell membrane forming a new virion (60). Antiretroviral therapy targets multiple steps of the HIV life cycle, including attachment, fusion, reverse transcriptase, integration, maturation, and formation of complete infectious virions. Created with biorender.com

1.5 HIV PERSISTENCE IN PLWH ON ART

Following ART initiation, rapid decay in plasma viral load is usually observed (61, 62). These phases of viral RNA decay are classified into three phases (Figure 1.4). The first decay phase is rapid and lasts between 1-2 days, and is related to the death of productively infected activated $CD4^+$ T cells with a short life span (63, 64). The second decay phase shows another infected cell population that are resistant to viral cytopathic effect, such as macrophages with a life span of 1-4 weeks (65). The third phase corresponds to a constant phase caused by the stable pool of latently infected cells with a lifespan of approximately 39 weeks. During this phase, occasional viremic episodes, known as viral blips, are observed in PLWH on ART (66). Although prolonged ART treatment, residual low-level viremia ranging from 1 to 5 copies/ml with an overall median viral load of 3.1 copies/ml can be detected in >80% of participants using ultrasensitive RT-PCR assays (67). However, as soon as ART is stopped, the virus rapidly rebounds within 2-3 weeks (68–70). This is because HIV can persist in PLWH on ART in multiple forms.

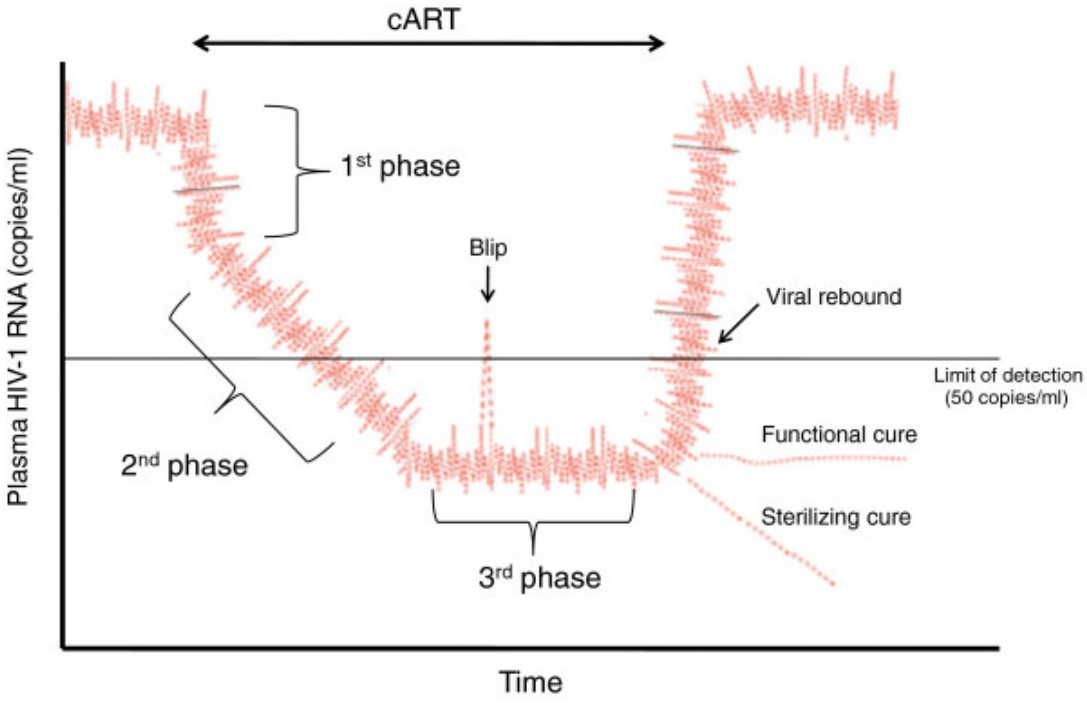

Figure 1.4 Dynamics of HIV RNA in the context of ART and treatment interruption in PLWH.

In PLWH on ART, there are three phases of viremia decay. The first rapid phase is the death of productively infected CD4+ T cells that die quickly after infection, and the second phase is the decay of cells that are more resistant to viral cytopathic effects, such as macrophages. The third phase refers to the stable pool of latently infected cells, which viremia reaches a level below the limit of detection and are estimated to have a half-life of 3.7 years. In the context of treatment interruption, the rapid viral rebound is observed and can reseed plasma viremia within 2-3 weeks. Although, several PLWH have shown transiently elevated HIV RNA levels which are known as blips.
(Figure taken from (71)).

1.6 HIV LATENCY

Latently infected cells are defined as cells harbouring an intact HIV proviral genome that is transcriptionally silent. HIV can establish a state of latent infection in PLWH on suppressive ART, which is unaffected by therapy nor immune system (viral cytopathic effect and CTL recognition) and characterised by the detection of integrated HIV DNA but minimal or no cell-associated HIV RNA, proteins or free virions (72–77). This pool of latently infected cells or viral reservoirs is sufficient to refuel viral replication if ART fails or is interrupted (78). Latently infected cells are located in peripheral blood and distinct tissue compartments (79–83). However, peripheral blood is thought to harbour a smaller share of HIV reservoir than tissues (84). HIV DNA can be found in all $CD4^+$ T cells populations (79), but the differentiated memory populations, including central memory (T_{CM}), transitional memory (T_{TM}), and effector memory (T_{EM}), are considered to support HIV infection and harbour more viral DNA (79, 85, 86). The latent reservoir is established very soon following initial infection (87). Early initiation of ART seems not to prevent the formation of HIV reservoirs but can reduce the frequency of infected cells (88–90). The vast majority of integrated HIV DNA within the $CD4^+$ T cell reservoir is defective, whereby the provirus contains large internal deletions of genes or lethal mutations (91–93). It is estimated that at least 90 % of proviruses are defective (94). Thus traditional quantitive PCR (qPCR) based measures of the reservoir, which estimate the reservoir

to be 100-10,000 copies/million $CD4^+$ T cells, likely present a significant overestimation of the replication-competent reservoir (95).

Furthermore, not all proviruses are inducible, whereby stimulus can be applied to the latently infected cell leading to virus production (96, 97). Indeed some proviruses require multiple rounds of maximal T cell stimulation *in vitro* to produce HIV RNA and protein (97). Thus, the true size of the inducible replication-competent reservoir (where viral rebound emerges from in the absence of ART) is more likely 1-10 per million CD4+ T cells in the blood (69, 98). This estimation may be higher in tissue (97). Therefore, it is these cells that represent the primary barrier to curing HIV.

1.7 PATHWAYS TO THE ESTABLISHMENT OF HIV LATENCY

Despite being the primary HIV reservoir in PLWH on ART, resting $CD4^+$ T cells that have not received activating stimuli and have not entered cell cycle G (1b) are poorly permissive to HIV infection *in vitro* (99). In addition, CCR5 is highly expressed on activated $CD4^+$ T cells but poorly expressed on resting cells, hindering the first step of viral infection of these cells.

It has been demonstrated in several studies that *in vitro* infection of resting $CD4^+$ T cells are achievable with the use of chemokines (99–101), and it was also determined that direct infection of resting cells *in vivo* is efficient (102–104), which might be explained by the chemokines microenvironment within lymphoid tissues. It is currently hypothesised that there are two ways wherein HIV can establish latency: post-activation and pre-activation latency (Figure 1.5). Infection of an activated $CD4^+$ T cell at the time of transition to a resting state in the absence of cell death induced by viral replication and infection of an activated $CD4^+$ T cell and reversion to quiescence state may offer a narrow window of opportunity that permits HIV silencing and persistence of the infected cell (Post-activation latency) (Figure 1.5) (74, 76, 105, 106). The role of cytokines in promoting post-activation latency, such as transforming growth factor-beta (TGF-β), interleukin 8 (IL-8) and interleukin (IL-10), has been demonstrated in *in vitro* experiments. Additionally, immune checkpoint molecules such as PD-1 diminish T cell activation, subsequently favour HIV latency (107, 108). Alternatively, direct infection of a resting $CD4^+$ T cell results in integration of

the genome but does not lead to productive infection (pre-activation HIV latency) (109, 110). *In vitro,* direct infection of resting $CD4^+$ T cells appears to be inefficient due to the presence of multiple blocks to the viral life cycle and a consequence of inefficient reverse transcription and integration (109, 111, 112). Inhibition of viral replication may occur through several pathways, including; (a) mutation in the HIV genome (113, 114), (b) transcriptional interference (115–117), (c) remodelling of chromatin structure (118, 119), (d) epigenetic silencing, (e) presence of negative transcriptional factors TFs (120, 121), (f) absence of positive transcriptional factors (122) and (g) issues with RNA processing and transport (123, 124). Altogether, these mechanisms may occur individually or in multiple combinations to suppress HIV transcription. However, multiple lines of evidence demonstrated that pre-treating resting $CD4^+$ T cells with soluble factors such as chemokine C-C motif ligand 19 (CCL19) or chemokine C-C motif ligand 20 (CCL20) enhance direct latent infection (Figure 5) (125, 126). CCL19 and CCL20 are believed to increase the susceptibility of resting $CD4^+$ T cells to latent infection by modifying the actin cytoskeleton, thus increasing nuclear entry and integration of the viral DNA (125). Similarly, interleukin 7 (IL-7), and interleukin 15 (IL-15) are cytokines also involved in T cell development and homeostasis, inactivating the restriction factor SAMHD1, thus increasing the susceptibility of resting $CD4^+$ T cells to HIV infection (127, 128). In addition, cell-cell contact of resting $CD4^+$ T cells and antigen-presenting cell (APCs) such as dendritic cells (DCs), mDCs and $CD14^+$ monocytes favour latency establishment (129, 130), suggesting that cell-cell interaction alter the transcription network of $CD4^+$ T cells to establish a pro-latency environment in a cell-specific manner (131).

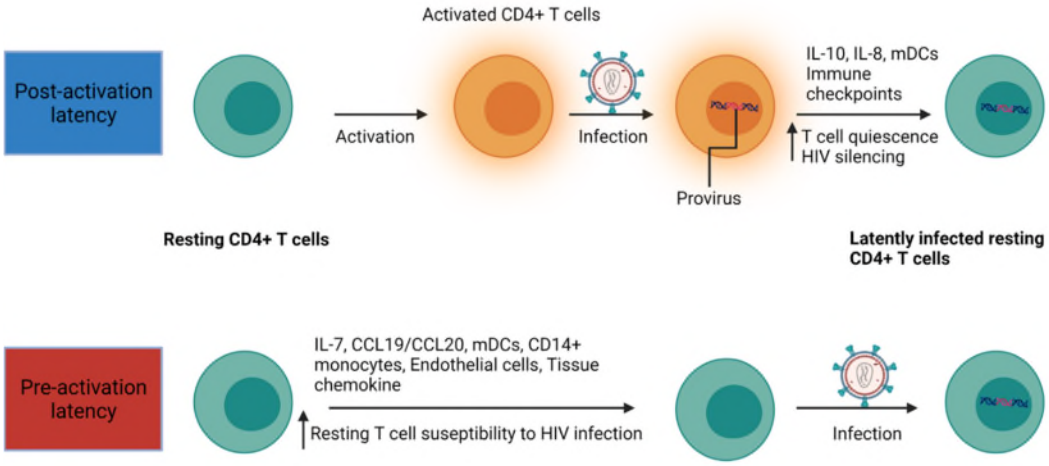

Figure 1.5 Formation of HIV latency in CD4⁺ T cells

The establishment of HIV latency mainly occurs in two major forms. Post activation latency refers to a phenomenon by which HIV infects activated CD4⁺ T cells that can revert to the quiescent state harbouring HIV provirus that is unable to produce viral proteins (latently infected CD4⁺ T cell). Alternatively, in the absence of T cell activation, resting CD4⁺ T cells may be directly infected with HIV in the presence of chemokine, dendritic cells, and monocytes. Infected resting CD4⁺ T cells harbour viral DNA but fail to express viral proteins termed pre-activation latency. (Figure adapted from (132)). Created with Biorender.com

1.8 MAINTENANCE OF HIV LATENCY IN RESTING CD4⁺ T CELLS

Once the virus is integrated into resting CD4⁺ T cells, multiple factors and different mechanisms effectively contribute to the maintenance of HIV latency, which involves a diverse range of cellular processes. (Figure 1.6). First, the site of integration is likely important because it can affect the transcriptional state of a latently infected cell. Provirus integration in latently infected cells usually favours actively transcribed regions of the host DNA (133, 134). Transcription of the HIV genome can be disrupted by the transcriptional activity of the surrounding cellular genes, a phenomenon that may promote the formation of latency and is known as transcriptional interference (135). Transcriptional interference involves promoter occlusion, where the provirus integrates downstream of the host gene in the same transcriptional orientation (116, 136). This effect may result in the displacement of constitutively expressed transcriptional factors such as Sp-

1 that bind to the HIV LTR and are essential for viral gene expression (116). In addition, another mechanism of transcriptional interference is referred to as convergent transcription. It occurs when the provirus integrates into the opposite orientation relative to the host gene causing the collision of RNA Polymerase II (RNAPII) from the host and viral promoters, leading to the early arrest of transcription (137). Additionally, convergent transcription may also occur when both strands of viral DNA are elongated and ultimately lead to the silencing of viral transcription or translation through RNA interference (138, 139).

The 5′LTR of HIV contains multiple binding sites for cellular transcription factors, including NF-κB, nuclear factor of activated T cells (NFAT), Sp1, and AP1. These key cellular factors can either promote or repress transcription of the provirus. Additionally, in resting cells, NF-κB and NFAT are sequestered in the cytoplasm (and cannot promote HIV transcription in the nucleus) but undergo nuclear translocation following appropriate cellular activation. Both NFAT and NF-κB can bind to κB sites in the HIV LTR (140, 141). Therefore, the absence of these factors leads to minimal HIV gene expression.

Another critical factor in the regulation of latency is the control of transcriptional elongation by the HIV Transactivator Tat and positive transcription elongation Factor b (P-TEFb) Tat- P-TEFb complex. The HIV Transactivator Tat protein is produced early in the HIV replication cycle and plays a significant role in the elongation phase of transcription (142). During the earlier initiation phase, RNA Polymerase II and host transcriptional factors, including NF-κB and P-TEFb), are recruited to the HIV LTR promoter region to initiate transcription, the complex pauses early after initiation and Tat is crucial to the continuation of transcriptional elongation (143–145). The absence of Tat would naturally limit the efficiency of expression of the stalled RNA polymerase II at the viral promoter, as this would severely incapacitate the recruitment of P-TEFb to the HIV LTR (146, 147). P-TEFb is an essential co-factor for transcription in the cell, and its subunits Cyclin T1 and CDK9 are stringently modulated. In resting cells, the active form of P-TEFb is present at a minimum: Cyclin T1 protein levels are low in resting $CD4^+$ T cells due to microRNAs (miRNA)-mediated

translational repression of Cyclin T1 mRNA (148, 149). While phosphorylation of Thr-186 in the T-loop of CDK9 is required for its activity and is inhibited in resting cells (150, 151). Both where shown experimentally in an in vitro based system (152). Although not confirmed in resting $CD4^+$ T cells derived from PLWH on ART, there are generally low levels of 7SK RNA and HEXIM1 in latently infected cell models (152–154), hence the previous suggestion that sequestration of P-TEFb in an inactive complex with HEXIM1 (inhibitor of CDK9 kinase activity) and 7SK snRNA (forming the 7SK snRNP complex) as a contributor to the regulation of latency may not be relevant (155).

MicroRNAs (miRNAs) have also been implicated in promoting HIV latency (156). Several binding sites for cellular miRNA have been elucidated on the 3' region of HIV RNA (157). Finally, in latently infected cells, there is nuclear retention of transcripts and transport that may impose or restrict HIV gene expression in latently infected cells (123).

Collectively, a better understanding of these factors and other mechanisms that support the initiation and regulation of HIV transcription and target them therapeutically is needed.

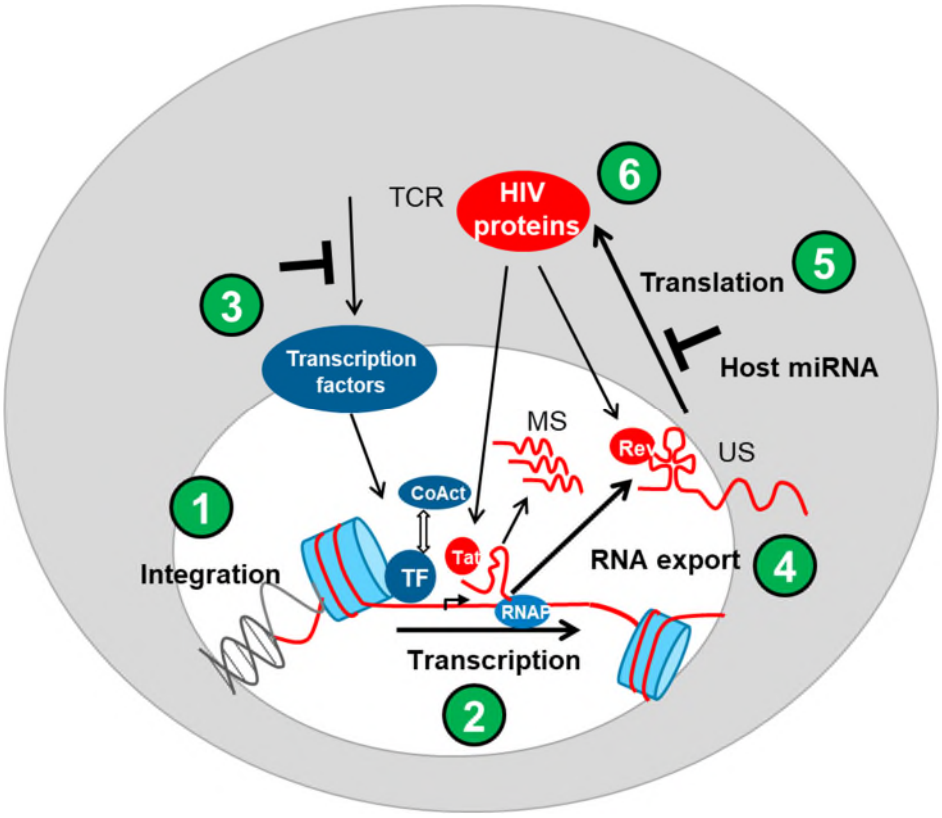

Figure 1.6 Mechanisms that maintain HIV latency in resting CD4⁺ T cells

Multiple blocks exist in CD4⁺ T cells that lead to the maintenance of HIV latency. These blocks include 1. Site of integration 2. epigenetic silencing of transcription 3. Lack of cellular transcription factors.

4. Incomplete elongation of the viral transcript. 5. Nuclear retention of the transcript. 6. MicroRNAs. TCR, T cell receptor.

(Figure taken from (158)).

1.9 CELLULAR HIV RESERVOIR FOR HIV PERSISTENCE

HIV preferentially targets CD4⁺ T cells but potentially can infect other cell types that express CD4, such as macrophages, monocytes and DCs (159–161). Among CD4⁺ T cells, a wide range of subsets contribute differently to the immune response (161). These cells are characterised by their effector functions, anatomical locations and longevity, which may present them as an ideal host for HIV persistence (162, 163) (Figure 1.7). Cells of the myeloid lineage are also known to be infected by HIV, and together with lymphoid cells, have the capacity to migrate throughout the body, facilitating

the widespread of the virus to various anatomical compartments, either harbouring latent or productive HIV (164).

1.9.1 T cell reservoir

HIV was initially shown to persist in a latent form in a subset of memory T cells including, including central memory (T_{CM}), effector memory (T_{EM}), transitional memory (T_{TM}), terminally differentiated (T_{TD}) and naïve (T_N) $CD4^+$ T cells (86, 165, 166). Subsequent papers showed persistence in T cell subsets, including T_{CM} and T_{TM} cells (79, 167).Another subset of cells in the memory lineage is the immature human stem cell-like memory T cells (T_{SCM}), which have also been shown to support replication-competent virus in PLWH on ART (85) (Figure 1.7). Furthermore, T_{SCM} cells are long-lived and capable of spreading the provirus to other types of memory T cells and with the potential of self-renewal and differentiation upon stimulation (85). Recently, other $CD4^+$ T cells subsets including, T_H1, T_H17 and T_H22 subsets of T helper cells and a significant class of the peripheral gamma delta t cells known as $V\gamma9V\delta2^+$ T cells, have been shown to harbour HIV latent infection in PLWH on ART (168, 169). Moreover, resting regulatory $CD4^+$ T cells (Tregs) identified as ($HLA\text{-}DR^-CD69^-CD25^{hi}FoxP3^+CD4^+$ T cells) was also found to contribute to the proviral reservoir (170).

On the other hand, tissue-resident memory $CD4^+$ T cells (T_{RM}) are enormously distributed around the body and may exhibit potential tissue-specific reservoirs of latent HIV infection (84, 171–173). However, this potential reservoir remains poorly studied as the majority of sampling for latently infected cells has been done in the circulating lymphocyte compartments (174, 175). Given that the diversity of cell types and anatomic compartments harbouring HIV provirus, it is unlikely a single intervention or modalities will be sufficient to eradicate or reduce the HIV from the body in all possible reservoir compartments.

1.10 T CELL PROLIFERATION AND IT IS ROLE IN MAINTAINING THE HIV RESERVOIR

In addition to long-lived infected cells, HIV can also persist through cellular proliferation, although the driver for proliferation remains unclear (176, 177).

Evidence of the proliferation of infected $CD4^+$ T cells came from studies that analysed HIV integration sites within a given subject (178). These studies showed that a large pool of infected $CD4^+$ T cells has identical integration sites (178–181). T_{CM} and T_{TM} are considered a key HIV reservoir in PLWH on ART and are thought to be primarily maintained through antigen driven expansion and homeostatic proliferation respectively as evidenced by identical sequences and integration sites of the virus in multiple cells (85, 182). The T_{EM} subset has also been demonstrated to contain clonally expanded HIV provirus (183, 184). Whether the site of integration is an essential driver of proliferation and cell survival, or proliferation is due to the low-level antigen-driven proliferation or cytokine-mediated homeostatic proliferation remains unclear.

1.11 MONOCYTES, MACROPHAGES, AND DENDRITIC CELLS COMPARTMENTS (NON- T CELL RESERVOIR)

Although memory $CD4^+$ T cells are a long-term cellular reservoir for HIV, they are not the only cells that may contain latent proviruses. Macrophages, dendritic cells (DCs), and tissue macrophages, such as microglial cells, are part of the viral reservoir (84, 173, 185). Cells of the myeloid lineage, including monocytes, macrophages, and, DCs are susceptible to HIV infection, but the virion production frequency in these cells is far lower than in activated T cells (161, 186). Monocytes and macrophages that reside in the gastrointestinal tract, brain and lungs have been shown to contain HIV DNA in PLWH on ART, but it is still unclear whether these cells harbour the replication-competent virus and represent a stable-long term latent reservoir (187–193). Macrophages play an essential role in the innate immune system, engulfing infected or dead cells through the phagocytosis mechanism (194). It is not certain whether the HIV detected in these samples in macrophages is due to receptor-mediated infection, phagocytic mediated infection or residual DNA from engulfed infected T cells (186). Follicular dendritic cells (FDCs) are not permissive for HIV infection (195). However, it has been proposed that FDCs can retain HIV in immune complexes by expressing virions on their surface in the presence of ART. These virions potentially may remain infectious for several months (196–

198), while peripheral blood DCs seems to be less likely to harbour any form of HIV (199, 200).

1.12 ANATOMICAL TISSUE SITES OF THE HIV RESERVOIR

Latently infected cells are found in peripheral blood as well as distinct tissue compartments (81). However, the majority of studies of the HIV reservoir under suppressive ART have been in peripheral blood $CD4^+$ T cells. The blood harbours only 2 % of total lymphocytes, as most T cells reside in lymphoid tissue (201, 202). Several studies in human and non-human primates (NHP) have extensively highlighted the importance of lymphoid tissue as a potential sanctuary reservoir for HIV persistence, suggesting a consequence of the limited access of ART, cytotoxic $CD8^+$ T cells or cellular proliferation (84, 203–206). In addition, $CD4^+$ T cells subsets in lymph nodes (LNs) differ phenotypically and functionally compared to blood. In particular, follicular helper T cells (T_{FH}) are enriched in LNs and harbour replication-competent provirus despite the presence of ART, suggesting that lymphoid tissue play a crucial role in HIV persistence (198, 207, 208).

The gut-associated lymphoid tissues (GALT) is known as the largest immune organ in the body and is considered to also serve as the primary source of residual viremia in PLWH on ART, given its high concentration of HIV target cells and its role as a site of initial HIV exposure and early infection (209–212). Given this early establishment of infection, the wide distribution of GALT and its essential role in immune function, substantial evidence has suggested this compartment poses important sites of virus persistence on ART (83, 212–214). GALT is the largest component of the lymphoid system (85 % of lymphoid tissue) and is made up of four compartments: the tonsils; Peyer's patches (PPs), located in the small intestine; lymphoid follicles (lymphoid aggregates) in the stomach and small intestine and lymphoid cell in the lamina propria (LP), located beneath the intestinal epithelium (215).

Several clinical observations have shown ongoing detection of HIV RNA and DNA from the rectum of PLWH on ART (83, 216, 217). Evidence of HIV persistence on ART and adaptation in different tissues was demonstrated in an early study, where gut biopsies of PLWH on ART revealed

compartmentalisation of viral diversity in the gut (212, 218). Additionally, another study estimated that the gut harbours 1.2 x 10^9 infected $CD4^+$ T cells (213). These studies may reflect HIV adaptation within various tissues, suggesting that the GALT is an essential source of persistent viral infection (188, 212, 219, 220). However, these reservoirs have been challenging to study, and the full extent of these putative ongoing foci of HIV replication is poorly understood. In addition, HIV DNA has also been detected in PLWH on ART in non-lymphoid tissue, including skin, bone marrow, liver, thymus, genital tract, liver and the central nervous system (CNS) (217, 221, 222). Thus, HIV persists in different cell types within distinct anatomical compartments, and these studies highlight the importance of targeting sites other than peripheral blood in cure strategies.

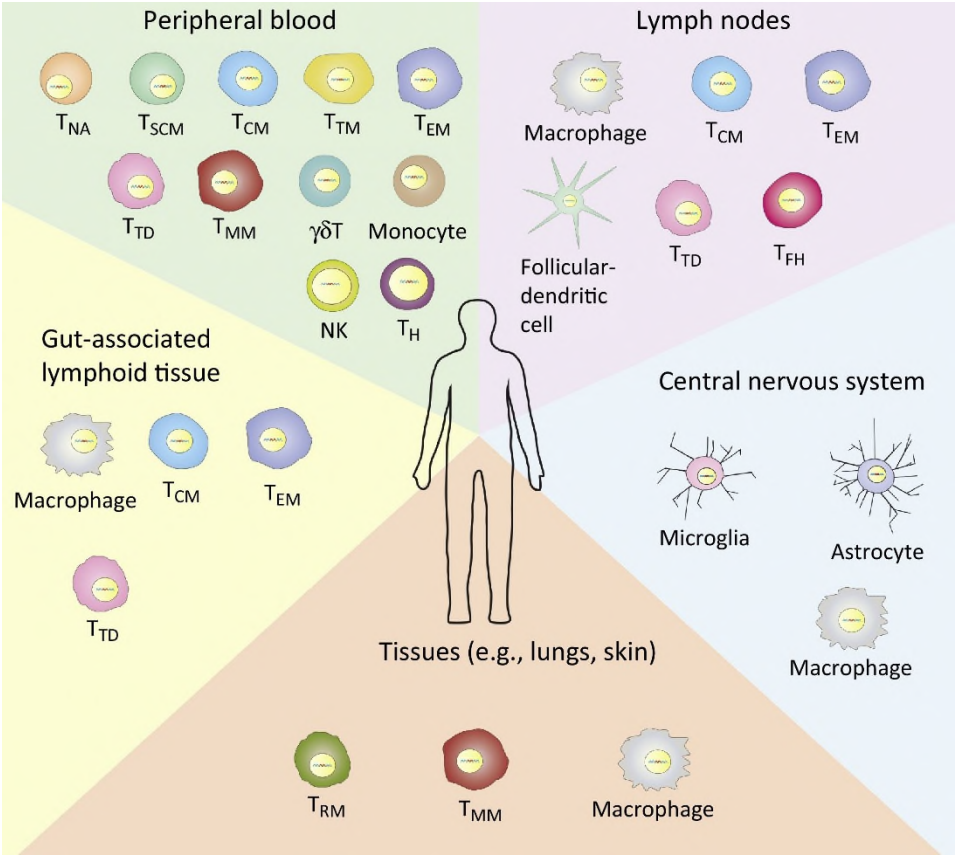

Figure 1.7 Potential cellular and tissue sites for HIV persistence

In addition to cellular compartments that exhibit HIV latent reservoirs such as $CD4^+$ memory T cells subsets, macrophages, the lymphoid tissue, gut-associated lymphoid tissue, and the central nervous system (CNS) are also potential anatomical reservoirs that may represent a source of residual

viremia in PLWH on suppressive ART. Tissue sites, lymphoid nodes and CNS represent significant sanctuary sites for ART to penetrate, which results in the persistence of HIV during ART therapy. T_{NA}= Naïve T cells, T_{SCM}= Stem memory T cells, T_{CM}= Central memory T cells, T_{TM}=Transitional memory T cells, T_{EM}= Effector memory T cells, T_{TD}= Terminally differentiated T cells, T_{MM}= Migratory memory T cells, γδT= Gamma Delta T cells, T_H= Helper T cells, T_{FH}= T follicular helper cells.
(Figure taken from (223)).

1.13 MODELS OF LATENT INFECTION

In PLWH on long term ART, the frequencies of latently infected $CD4^+$ T cells are low (1 in 10^6) and compromise an exceedingly infrequent proportion of total $CD4^+$ T cells (224). In addition, this minor population of latently infected cells do not have distinct phenotypic markers that can distinguish them from uninfected cells. Interestingly, the majority of latently infected cells contain a provirus that is defective (97, 225). Only a median of ~1 in 10^6 $CD4^+$ T cells harbours an intact HIV provirus that can be activated following a single round of maximal in vitro stimulation (74). This low frequency of infected cells poses a substantial challenge to studying HIV latency in samples from PLWH. While ex vivo samples are invaluable for investigating HIV latency and examining drug compounds that could be used to purge latently infected cells in PLWH, multiple *in vitro* models have been successfully established to investigate the molecular mechanisms that contribute to the establishment and maintenance of HIV latency (226). These models can facilitate the screening for different pharmacological and immunological interventions aimed at depleting latently infected cells (227–230). While T cell line models of latency have been useful in studying HIV latency and screening compounds that reactivate the latent provirus, they do not entirely replicate HIV infection *in vivo* (231). Immortalised T cell line models are limited by their clonal and cycling nature, which means that the viral integration site is similar in all cells (179). In such a setting, many groups have designed primary cellular models that recapitulate the generation of latently infected cells *in vivo* to study latency and evaluate anti-latency compounds *in vitro*.

1.13.1 Primary cell models of HIV latency

While no one model perfectly replicates latently infected cells, each model system attempts to mirror the *in vivo* conditions to create a cell system that will permit the latently infected cells to be manipulated in culture (76, 101, 145, 232–236). These models systems offer several advantages over *ex vivo* samples regarding their availability, ease of access, frequent infection, known proviral sequence, and integration site. A variety of primary T cell models of HIV latency are currently established using freshly isolated $CD4^+$ T cells from healthy donors infected with HIV or HIV derived vectors followed by the transition of infected cells to a resting state to establish HIV latency in memory $CD4^+$ cells (232). This modelling of latent infection contains one or more aspects of latency. The model developed by Sahu et al. and colleagues models post-activation latency (234). This model involved $CD4^+$ T cell infection after activation through T cell receptor (TCR) and co-culture with brain-tumour feeder cell line H80, allowing the transition back to the resting state. The major problem is that most $CD4^+$ T cells die soon after activation if not continuously cultured in the presence of specific cytokines (such as IL-2, IL-7) or anti-apoptotic proteins (such as Bcl-2) (237, 238). However, IL-2 and IL-7 have been implicated in the reactivation of latent HIV (237, 238). Alessandra Marini et al developed a model that relies on latently infected primary CD4+ T cells activated in response to stimulation with Monocyte-derived dendritic cells (MDDC) (239). Interestingly addition of low doses of IL-7 did not induce cell activation and proliferation or viral reactivation. Another model uses activated $CD4^+$ T cells transduced with a lentiviral vector expressing the Bcl-2 gene enabling cells to increase their survival and allowing time for more cells to transition to a memory state with integrated HIV (236, 240). The expression level of Bcl-2 in these cells is similar to that in freshly isolated $CD4^+$ T cells, and thus cells can continuously be cultured for several weeks without exogenous cytokines (236).

Another HIV latency model created by the Lewin laboratory involves direct infection of resting $CD4^+$ T cells treated with chemokines such as CCL19 (101). Pre-treatment of non-permissive resting $CD4^+$ T cells before infection increases the efficiency of HIV infection in resting $CD4^+$ T cells leading to

more latently infected cells. In addition, the Lewin laboratory has also shown that culturing resting $CD4^+$ T cells in the presence of $CD14^+$ monocytes or myeloid dendritic cells (mDCs) exhibited a substantial increase in the frequency of HIV-DNA and enhanced the latent infection in nonproliferating memory $CD4^+$ T cell (129).

1.13.2 T cell lines models of HIV latency

In vitro immortalised T cell lines have been extensively relied on to investigate the mechanism of HIV latency establishment and the screening of repurposed drugs in reactivation of HIV transcription (241–243). The main advantage of these systems is that they are easy to maintain for a long time with higher transfection efficiency than primary T cell model systems (244). On the other hand, immortalised T cell lines consciously proliferate, making them fundamentally different from quiescent resting $CD4^+$ T cells in the G0 state (245). There are several cell line models harbouring stably integrated latent full-length or HIV LTR with reporter gene including ACH2 (246), U1 (247), J89EGFP cells (248) and various J-Lat clones (249). These latently infected cell lines differ in (i) the parental cell line (ACH2: A3.01 subclone of CEM T cells; U1: U937 pro-monocytic cells; J89EGFP and J-Lats: Jurkat T cells), (ii) the site of viral integration and (iii) the replication capacity of the provirus (ACH2 and U1 harbour replication-competent virus mutated in Tat and TAR respectively (113, 114), while J89EGFP contains wild type replication-competent virus and J-Lat cells harbour replication-defective virus). This thesis will focus exclusively on the J-Lat T cell line model of latency.

The J-Lat T cell line series is one of the most heavily used transformed cell line models in HIV research. The J-Lat T cell line is a latently infected Jurkat T cell containing integrated HIV DNA that is transcriptionally silent (a small amount of HIV RNA can be measured but little to no viral protein) but can be activated upon treatment with various stimuli (249). HIV reactivation can be quantified through the detection of a reporter fluorescent protein using flow cytometry. Several clones on J-Lat-T cell lines mostly contain the full-length provirus (e.g., J-Lat 10.6 cells), with a frameshift in env and GFP in place of the Nef coding sequence that expresses GFP upon activation. The

second form of the J-Lat cells line contains a single integrated copy of the HIV LTR (LTR-Tat-IRES-GFP) driving the expression of the viral Tat- and green fluorescent protein (GFP) genes. Translation of GFP is provided by an internal ribosomal entry site (IRES) leading to LTR-Tat-IRES-GFP (249). Following reactivation of the J-Lat A2 clone, only part of the HIV (Tat) activates the HIV LTR promoter and subsequently drives GFP expression. Although all J Lat clones are derived from Jurkat cells, these cell lines may have different sensitivity to different activating stimuli and latency-reversing agents (115, 232). Suggesting that a better understanding of the accumulation of latently infected cells with different integration sites of the HIV provirus is warranted (179).

1.14 MEASURING HIV PERSISTENCE ON ART

A cure for HIV infection remains elusive due to the persistence of intact replication-competent HIV provirus in PLWH on ART. The intact replication-competent provirus is identified based on whether the integrated provirus can produce infectious particles following reactivation (97). However, there are significant challenges in measuring the HIV reservoir because of heterogeneity in the provirus sequence composition in latently infected cells *in vivo*, with most proviral sequences being replication-defective (250). The frequency of latently infected cells carrying replication-competent provirus in PLWH on ART was estimated to be 1 in 10^6 resting $CD4^+$ T cells in peripheral blood (73, 251). However, the total number of these cells could be much higher (95, 97). In addition, quantifying precisely the frequency of latently infected cells has been challenging due to the lack of a specific biomarker and the ability to discriminate between intact and defective viruses (158). Investigators debate the best way to measure HIV persistence on ART as different assays have been used to quantify the frequency of intact, replication-competent provirus or the number of latently infected cells containing an intact provirus sequence (96, 158, 173, 252).

PCR based assays, including quantitive real-time PCR (q-RT-PCR) or digital droplet PCR (ddPCR), are designed to quantify viral RNA and DNA from $CD4^+$ T cells. The DNA qPCR assays were characterised to quantify integrated HIV DNA, and a number of these assays can quantify

unintegrated HIV DNA (proviral 2-LTR circle DNA) (253–258). A worthy note here; these assays directly measure provirus but do not provide information about their inducibility (259). These assays approach depends on targeting conserved regions of HIV genes, *gag*, the LTR, or *pol* (257). PCR-based assays have also been used to measure the HIV proviral DNA in $CD4^+$ T cells from the gut-associated lymphoid tissue (GALT), where HIV replication persists in PLWH on ART (95, 212, 213, 260). However, it is often challenging to perform comparative analysis on DNA measurements across different assays (assay design and performance), individual (proviral genetic information heterogeneity) and different extraction efficiencies on tissue samples (261).

1.14.1 Direct measurement of the HIV genome

Digital droplet PCR assays of HIV DNA has also been established, and overall, they are relative to qPCR with greater precision due to the limited dilution format of the assay and tolerance for primer or probe mismatch (262–264). Additionally, as mentioned above, most of these DNA PCR assays are designed to detect a conserved region inside the HIV provirus region; they also detect unintegrated 2-LTR circle DNA, though this unintegrated form is less frequent and their stability in PLWH on suppressive ART is not apparent (95, 251, 265). Based on this notion, assays for integrated HIV DNA have been developed that target the Alu short interspersed element (a common repeat element disperse through the human genome) within the host genome to guarantee the exclusion of unintegrated HIV DNA (266, 267). This assay includes one primer that targets the Alu element and a second primer that targets the HIV gag, followed by a second-round nested PCR for the HIV LTR resulting in the detection of integrated HIV DNA (256, 267). A major caveat with all DNA PCR-based assays (qPCR and ddPCR) is overestimating total or integrated HIV DNA due to their failure to distinguish between defective, intact or replication-competent viral sequences (95, 97). To some extent, to overcome such limitations, several groups have developed near full-length HIV genome sequencing assays and provided critical insights into the HIV reservoir (94, 97, 225, 268). In addition, sequencing and mapping of HIV

integration sites have also provided information about the importance of clonal expansion in HIV reservoir dynamic maintenance to develop new cure strategies for HIV infection (180, 181, 269–271).

1.14.2 Measurement of the basal or inducible reservoir expression

An alternative approach that measures the basal or inducible HIV reservoir expression has been proposed to estimate the size of the reservoir. This culture method involves using highly sensitive PCR methods that are now employed to quantify the level of HIV RNA from cells (Cell-associated RNA, CA) or cell supernatant (Cell-free RNA, CF) (272). These PCR assays measure the inducible transcription status of the latent reservoir following activation in CA or CF from resting or total $CD4^+$ T cells samples of virally suppressed PLWH on ART, indicating the frequency of infected cells capable of producing viral RNA (273–277). However, while the quantification of transcriptional competency may reflect the capacity to generate viral RNA, it does not assess the ability of a provirus to produce viral particles. In addition, quantification of CA-RNA can also overestimate the HIV latent reservoir as it detects defective HIV genome that can be partially or entirely transcribed (277, 278).

1.14.3 Measurement of intact provirus

Most DNA-PCR assays use primers and probes designed to bind to a highly conserved proviral region that is defective or mutated in regions external of the assay amplicon, resulting in failing to exclude many defective proviruses (95, 225). Recently, Bruner et al. developed a high-throughput DNA assay, the intact proviral DNA (IPDA), that can distinguish intact and defective proviruses (279). This innovative approach is based on ddPCR multiplex technology, which enables estimates of intact proviral DNA by using primers that bind to regions of the virus that commonly contain hypermutation or large deletions. Using this novel detection method, it was found that approximately 10 % of all proviruses were intact(279). In the following study by Gaebler et al., the percentage of proviruses called intact by the IPDA probes that were truly intact by near-full-length sequencing varied from 9.1 % to 96 % (280). In addition, recently, Peluso et al. used combined IPDA and bioinformatics analysis to estimate the rate of change of intact and

defective proviruses from PLWH on ART (281). This study demonstrated that intact and defective proviruses have different decay rates, with intact viruses decaying more rapidly than defective proviruses and showing a faster decline in PLWH with higher $CD4^+$ T cell nadirs (281).

Recently, a limited dilution single-cell RNA-PCR assay has been developed to provide insights into the frequency of HIV ca-RNA expressing cells (275). In the tat/rev induced limiting dilution assay (TILDA) assay, $CD4^+$ T cells from PLWH are stimulated with PMA/Ionomycin, and the levels of tat/rev multiply spliced RNA are measured using RT-qPCR. An important advantage of TILDA is that it does not require virus amplification, and only a small quantity of samples is needed for the measurement. In addition, the TILDA assay reduces reservoir frequency overestimation by assaying multiply spliced HIV RNA because multiply spliced HIV RNA is less likely to arise from non-intact proviruses (275, 282, 283). The quantitative viral outgrowth assay (QVOA) was the first to characterise the frequency of latently infected cells. QVOA identifies the frequency of resting $CD4^+$ T cells from PLWH on ART that harbour replication-competent proviral sequences using a single round of T cell activation. (73, 74, 91, 173). Isolated resting $CD4^+$ T cells are plated in serial dilution format before being stimulated with the mitogen phytohemagglutinin (PHA) or with anti-CD3 plus anti-CD28 antibodies in the presence of irradiated allogeneic peripheral blood mononuclear cells (PBMC). Following T cell activation, the viruses released from these cells are expanded in $CD4^+$ lymphoblasts from HIV-negative donors and detected after 2–3 weeks by an ELISA assay for HIV p24 antigen in the supernatant (173, 284). This assay quantifies individual latently infected cells that release a replication-competent virus, and the frequency of latently infected cells are expressed in terms of infectious units per million (IUPM) resting $CD4^+$ T cells. However, The QVOA assay usually detects released virus particles capable of robust replication following a single round of T cell activation; therefore, it only provides an estimate of viral quantity following strong T cell activation. Furthermore, a number of studies have demonstrated that the second round of mitogen stimulation of wells negative for viral outgrowth resulted in the activation of some intact

but previously non-induced proviruses, increasing the number of proviruses detected using QVOA (97, 250).

1.15 WHY DO WE NEED A CURE FOR HIV INFECTION?

Latently infected $CD4^+$ T cells are the foremost hurdle to eliminating HIV infection in PLWH on ART (79). Despite the great success of ART in reducing mortality and morbidity, treatment is not curative and thus lifelong (158, 285). Furthermore, limited accessibility to ART remains a burden, particularly in low-income countries that carry a disproportionate burden of HIV infection. For those who have access to the treatment, stigma, associated health risks such as kidney, cardiovascular and bone diseases, and an inordinate economic burden for individuals and health care systems exist (286). Therefore, there is an urgent need to develop a cure that aims to eliminate or reduce the latent reservoir that could lead to the cure or lifelong remission of HIV infection.

1.16 HIV CURE STRATEGIES

HIV cure traditionally is defined as the complete elimination of HIV from the body. However, it is now excepted that there may be two different outcomes of cure strategies including; I) sterilising cure, where there is complete eradication of infected cells, and II) functional cure (also called HIV remission), where HIV persists at a low level off ART but causes no adverse events and cannot be transmitted. Strategies can be divided into those that target the virus directly and those that target the immune system. Accumulation of knowledge over the last two decades of the molecular and cellular factors influencing this silent form of HIV infection has facilitated a range of potential approaches to cure HIV.

1.16.1 Gene therapy

Numerous potential strategies have been implemented to cure HIV infection. Gene therapy approaches have been pursued to mediate the knockdown of the co-receptor CCR5 or directly target the HIV genome. Zinc finger nucleases (ZFNs) has been investigated *in vitro* for HIV inactivation(287, 288). In a clinical trial (NCT00842634), a single dose of

ZFN CCR5-modified autologous $CD4^+$ T cells was administrated to PLWH on ART. The approach was well-tolerated and long-term persistence of the modified cells after engraftment was observed, thus preserving a pool of cells refractory to HIV infection (289). In addition, clustered regularly interspaced short palindromic repeats paired with CRISPR associated protein-9 nuclease system (CRISPR/CAS-9) has been investigated to generate a knock-out of CCR5 or a CCR5Δ32 mutation in host cells, to induce resistance to infection with CCR5-tropic HIV. However, the achieved percentage of CCR5 disruption was insufficient to induce HIV remission (290). However, each of these curative strategies appeared to have limitations and challenges, such as the optimal route of delivery and concern of emergence of CXCR4-utilising viruses (291–293).

1.16.2 Deep silencing latency (Block and Lock)

One functional cure strategy of HIV infection is a permeant silencing of HIV gene expression, also known as 'Block and Lock'. Unlike the shock and kill approach, this strategy focuses on rendering permanent silencing of the integrated provirus in the infected cell. The HIV Tat inhibitor Didehydro-cortistatin A (dCA) was found to bind Tat and effectively disrupted the Tat/TAR axis, resulting in restriction of HIV transcription and replication (294). dcA effectively suppresses HIV transcription *in vitro* by blocking the TAR binding domain of Tat (295, 296). Studies with *ex vivo* $CD4^+$ T cells from PLWH on ART with dcA have shown restriction of viral reactivation and delayed viral rebound following ART cessation in animal models (297). Alternatively, targeting host factors has also been proposed to reinforce deep latency. Targeting of DEAD-box protein 3 and 5 (DDX3/5) splicing factors, up frameshift (UPF) proteins, involved in HIV post-transcriptional processing, including inhibitors of mTOR, cardiotonic steroids, and Serine and arginine-rich (SR) proteins, have been shown to inhibit HIV latency reversal and lead to a block in translation (298–303).

1.16.3 Therapeutic HIV vaccines

Therapeutic HIV vaccines are mainly designed to induce HIV-specific immune responses that can control the virus in the absence of ART (304).

Ideally, a robust vaccine would enhance long-term immunity and control residual viremia (< 20 copies/ML) when treatment is interrupted (305). Nevertheless, the exceptional ability of HIV to escape the immune system based on the genetically diverse envelope and variable protein products have made it challenging to achieve an efficient therapeutic vaccine. Several methods have been applied in the therapeutic vaccine, including mRNA, nanoparticles, native-like envelope trimers, viral vectors, among other vaccine strategies, to achieve a durable, efficient immune response against HIV (306). These strategies have shown promise in animal models and limited progress in human phase I and II clinical studies (307–311). Given that these strategies were not the focus of this thesis, we will not cover them in detail. A pharmacological and immunological compound used to reactivate HIV latency was the main focus of this thesis.

1.16.4 Activation of HIV latency

Alternatively, a widely addressed approach to achieve HIV remission is the so-called "shock and kill" (Figure 1.8). This approach seeks to reverse HIV latent infection through various pharmacological agents (latency-reversing agents). Induction of HIV transcription and translation will ultimately lead to the production of infectious viruses - the ’shock‘. This is followed by recognition and clearance of the shocked cell by a rejuvenated immune response or death of the infected cell through HIV cytopathic effects – the ‘kill’ (272, 312).

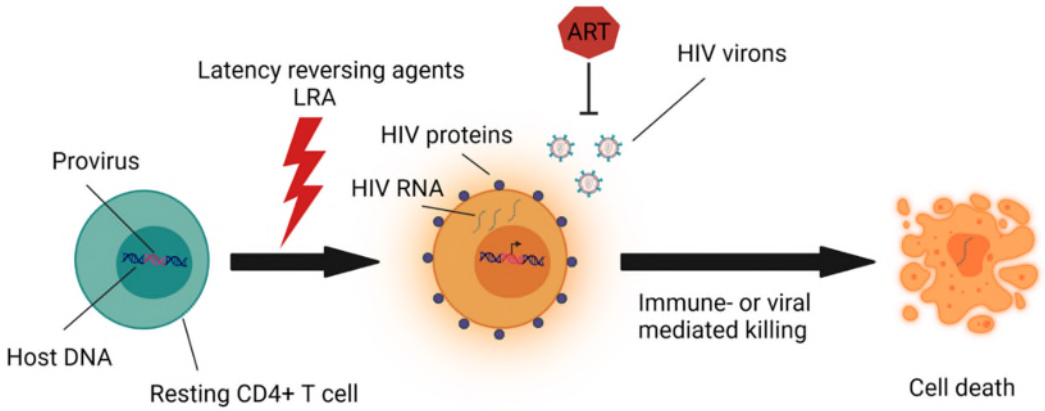

Figure 1.8 Shock and Kill.

This paradigm proposes to combine a latency-reversing agent to reactivate HIV transcription or virion production (312) with immune effectors such as $CD8^+$ cytotoxic T lymphocytes or NK cells, to induce cytolysis and eliminate HIV infected cells. Importantly, this is done under the protection of ART to prevent *de novo* infection.

1.17 LATENCY-REVERSAL AGENTS (LRAS)

Latency reversal agents (LRAs) are molecules that can reverse HIV latency by activating virus transcription and production so that the infected cell will be susceptible to immune-mediated killing or virus-induced apoptosis (312). This is done in the presence of suppressive ART so that newly produced virions cannot infect uninfected cells. Many compounds with a range of different mechanisms of action have been investigated *in vitro* to reverse latency (313). Early attempts at reversing HIV latency that reached clinical trials used global T cell activators; IL-2 and IL-7 with or without IFN-γ were administrated while participants maintained on ART to prevent *de novo* infection from occurring in bystander T cells (314–318). Additionally, two subsequent trials assessed the response to anti-CD3 mAb, muromonab-CD3 (OKT3), followed by IL-2 (319, 320). Both studies outcomes showed a lack of efficacy, and severe adverse effects were reported in the OKT3 trials. Several classes of latency-reversing agents have been investigated *in vitro,* and some have been tested in clinical trials. These include histone deacetylase inhibitors (HDACi) (321, 322), bromodomain and extra terminal domain inhibitors (BETi), protein kinase C (PKC) agonists, toll-like receptor-7 agonists (323), mitogen-activated protein kinase (MAPK) agonists and

unclassified compounds such as the anti-alcoholism drug disulfiram (324–326). These LRAs can reactivate HIV in latent cell line models and $CD4^+$ T cells isolated from PLHW on ART (327). Various interventions have appeared promising and reached human clinical trials, but the results have thus far shown an inability of the candidate therapeutically to reduce the frequency of infected cells (106, 320, 326).

1.17.1 LRAs for HIV cure

HIV propagation in latently infected cells depends on many host transcriptional factors , including NF-κB, NFAT and the cyclin T1 component of P-TEFb (328). A promising lead in this line is the PKC (329) activator bryostatin, which is a macro-cyclic lactone (330, 331). It has been shown that bryostatin promotes activation of the canonical NF-κB signalling pathway via translocation of the two functional units P50 and P65 to the nucleus at the NF-κB in the HIV LTR, which is optimal for mRNA viral transcription from the HIV LTR, subsequently reactivating the HIV provirus (331–333). However, two studies have reported bryostatin association with adverse effects, including severe myalgia and nausea in patients with advanced renal cell carcinoma (RCC) (334, 335). In addition, dose limitation is considered a major concern to reduce the toxicity caused by a systematic release of cytokines (336, 337). An *in vitro* study investigated the impact of LRAs on HIV antigen expression. The study elaborates the effect of two classes of LRA, the histone deacetylase inhibitors, romidepsin and PKC activator, bryostatin on MHC-1 expression; romidepsin transiently reduced MHC-1 expression and relatively bryostatin increases T cell activation and T cell proliferation (338). Importantly, these effects were only observed promptly. In addition, combination treatment with romidepsin and bryostatin was shown to affect primary HIV-specific $CD8^+$ T cells, which failed to eliminate autologous resting $CD4^+$ T cells that had been reactivated with these agents (332).

Prostratin is another anti-HIV latency candidate that has been described to reactivate HIV transcription via PKC signalling (339). Prostratin has been shown to strongly stimulate HIV LTR transcription in *in vitro* models of HIV

latency (339, 340) and resting $CD4^+$ T cells and activating the transcription factor NF-κB (341).

Ingenol is another promising candidate that showed potential reactivation activity of HIV gene expression at the viral mRNA level through the activation of the canonical NF-κB pathway (342). The combination of this agent with the bromodomain and extra-terminal inhibitor (BETi), JQ1, showed synergetic reactivation, releasing infectious viruses to levels similar to the positive control (227). Ingenols also showed clinical safety and tolerability (328, 343), whereas it has been demonstrated that bryostatin and prostratin significantly decrease PBMC and $CD8^+$ T cells survival upon administration in a dose-dependent manner 10 nM and 300 nM, respectively (337, 338). Nevertheless, the author suggested it is difficult to determine *in vitro* doses that reflect clinically relevant effects for these compounds. An Ingenol derivative (Ingenol-3-hexanoate, Ingenol B) induced HIV gene expression *in vitro* and *ex vivo* in $CD4^+$ T cells from PLWH on ART (328). Similarly, another Ingenol derivative, ingenol-3-angelate (PEP005), has been shown to effectively enhance HIV gene transcription *in vitro* and *ex vivo* (344). Interestingly, both compounds (Ingenol B and PEP005) have shown additive synergism effect with JQ1 in boosting HIV transcription.

An alternative to PKC activators is represented by tetraethyl thiuram disulphide disulfiram (disulfiram), a drug approved for the treatment of alcoholism (345). In the first clinical trial of disulfiram in PLWH on ART, disulfiram was administered for 14 days. The drug was well tolerated but did not change the levels of plasma HIV RNA or affect HIV DNA levels (346). A dose-escalation study (500 mg, 1000 mg, and 2000 mg) of short-term administration of disulfiram on PLWH on ART disulfiram showed that administration of all doses increases cell-associated unspliced HIV RNA during and after treatment. Disulfiram treatment of all doses was well tolerated among participants (326). However, in both studies, no change in the size of the reservoir was observed.

Recently, a new class of latency-reversing agent have gained much attention due to their multifactorial effects on the HIV reservoir. SMAC mimetics (SMs) are characterised by acting through the non-canonical NF-$_k$B pathway activation and induction of apoptosis. SMs target several cellular

inhibitors of apoptosis factors including, baculoviral IAP repeat (BIR) 2 (BIRC2, also known as a cellular inhibitor of apoptosis; cIAP1/ BIRC2) and X-linked inhibitor of apoptosis protein (XIAP), (also known as a cellular inhibitor of apoptosis protein 3 (cIAP3) and baculoviral IAP repeat-containing protein 4 (BIRC4) (347, 348). Thus, aside from their capacity to reverse latency, SMs also act as pro-apoptotic compounds, a class of drugs that has become the focus of intense study for their ability to kill latently infected cells (313). Additionally, SMs compounds alone or combined with other LRAs have shown promising results in reversing latency and induced apoptosis selectively in HIV-infected (but not uninfected) central memory $CD4^+$ T cells isolated from PLWH on ART (349–352).

1.17.2 Epigenetic modulation agents

1. Histone Deacetylase inhibitors (HDACis) (Vorinostat, Panobinostat and Romidepsin)

HDACis increase histone acetylation, which leads to a change in chromatin structure, allowing for increased access of transcription factors to their target DNA sequences (353). HDAC are classified based on their structure homology (354) (355). Class I HDACs (HDAC1,2,3 and 8), class II HDACs (HDAC4,5,6,7,9 and10) and the class IV HDAC (HDAC11) are all zinc-dependent, whereas class III deacetylases (SIRT1-7) are nicotinamide adenine dinucleotide (NAD+ dependent) (356). Among these groups, only class I HDACs (HDAC 1, HDAC 2, HDAC 3) are localised at the integrated HIV LTR, as demonstrated by chromatin immunoprecipitation (ChIP) assays (357).

Pharmacologically, HDAC inhibitors can be classified as members of five classes of compounds: (I) hydroxamic acids (hydroxamates); (II) short-chain fatty (aliphatic) acids; (III) benzamides; (IV) cyclic tetrapeptides; and (V) sirtuin inhibitors including the pan-inhibitor nicotinamide and the specific SIRT1 and SIRT2 inhibitors sirtinol and cambinol, respectively (358).

Vorinostat (359) (Zolinza, Merck) is a potent pan-HDAC inhibitor and is approved for the treatment of relapsed or refractory cutaneous T cell

lymphoma (360). In humans, vorinostat acts on class I, II and IV HDACs, increasing histone acetylation and, therefore, upregulating the cellular transcription of HIV in $CD4^+$ T cells (272, 361, 362).

In an early study, a single dose of vorinostat administrated to PLWH on ART resulted in a nearly five-fold increase in HIV transcription measured by cell-associated unspliced (CA-US) HIV RNA (272). A single-arm, proof of concept study of 20 PLWH study participants on ART received 400mg of vorinostat that led to a significant increase in HIV transcription as measured by (CA-US) HIV RNA in $CD4^+$ cells after 8 hours of drug exposure (361). Interestingly, in another study of vorinostat, when administrated on multiple doses three days a week for eight weeks, there was only a minimal increase in HIV gene expression (363). Furthermore, a recent study of 2 years extended follow up of 20 PLWH demonstrated no long-term adverse effects, that US-RNA returned to baseline levels, and there were no significant changes in the number of T cell subsets ($CD4^+$ and $CD8^+$) although the ratio of $CD4^+$ to $CD8^+$T cells were significantly higher at 24 months. In addition, total HIV DNA, plasma HIV RNA and CA-US HIV RNA remain unchanged over time (362). This study may highlight that administration of vorinostat may require more frequent doses for a more extended period (362).

Panobinostat (364) is a potent non-selective HDAC. In a phase I/II clinical trial (NCT01680094), PLWH study participants on ART received oral panobinostat 20 mg three times per week every other week for 8 weeks. The study demonstrated a significant increase in plasma viremia levels and cell-associated unspliced HIV RNA in total $CD4^+$ cells. Side effects were well-tolerated, but no cohort-wide reduction in the total or integrated HIV DNA levels was observed. Furthermore, viral rebound occurred (median time 17 days) in all participants undergoing an analytical treatment interruption (365).

Romidepsin (RMD, FK228) is a bicyclic depsipeptide antibiotic HDACi with antineoplastic activity known for its high toxicity profile (366, 367). RMD is a small prodrug molecule (MW = 540.7) and is activated inside the cell by glutathione (GSH) (368). RMD has been shown to reactivate HIV expression in latently infected cells *in vitro* and *ex vivo* $CD4^+$ T cells from PLWH on ART (369).

In PLWH on ART, romidepsin was administrated at 5mg/m^2 IV over 14 days, confirming the drug's bioactivity *in vivo,* which safely increased HIV transcription measured by cell-associated HIV RNA without blunting T cell-mediated immune responses. However, no significant reservoir depletion was observed (370). In contrast, in a randomised controlled placebo trial, 43 PLWH on ART-treated with RMD showed that RMD infusions were safe but did not increase plasma viremia or unspliced CA-RNA despite the increased histone acetylation (371). In a recent trial, RMD administration to PLWH on ART effectively activated HIV transcription from peripheral $CD4^+$ T cells (372). Interestingly, the viremia induced by RMD contained few defective mutations and low genetic diversity (373). Importantly, this study highlighted the consideration for the complex and variable composition of the different viral reservoirs in cure strategies and the role of cellular proliferation and cellular clonal expansion in enhancing HIV persistence.

2. Histone Deacetylase Inhibitors Adverse effects AEs

To date, all HDACi are non-specific drugs for HIV infection and have off-target effects and generate adverse reactions, inhibiting their pharmacologic potency (374, 375). Toxicity and tolerability are essential considerations in LRAs screening and moving towards the clinical setting. Although agents administrated at clinically accepted doses may still influence T cell viability that could compromise HIV specific T cell function to eliminate reactivated HIV infected cells.

HDACi can have a range of non-specific off-target effects, in addition to the induction of transcription of the latent HIV genome. In one study, three HDACis had a negative impact on the effector and functions of CTL due to T cell exhaustion (376). In a recent *ex vivo* study, Reardon et al. showed that vorinostat upregulated gene expression in resting $CD4^+$ T cells in a dose-dependent manner and demonstrated that increased VOR dose appeared to downregulate T cell function (377).

In addition, combination treatment with HDACi romidepsin and PKC agonist bryostatin was shown to affect primary HIV specific $CD8^+$ T cells, which

failed to eliminate autologous HIV-infected resting $CD4^+$ T cells that had been reactivated with these agents (374).

The effects of such LRAs on the viral reservoir size are likely to be influenced by host immune responses in addition to the impact of these drugs on innate and adaptive immune systems (378). In addition to adverse effects on immune function, HDAC inhibition can also modulate the transcriptional activity of all cells, including innate and adaptive immune cells. For instance, it has been reported that HDACis showed a high level of toxicity to activated T cells and $CD8^+$ T cells clones. In contrast, these effects were limited in resting $CD4^+$ T cells (376).

In a recent study, analysis of results in which 15 individuals received 12 dosages of panobinostat identified a significant impact on both T cell activation status and regulatory T cell suppressive marker expression also showed decreased level of monocytic responsive to inflammatory stimuli (338). Altogether, these results suggest that it might be challenging to eliminate HDACi toxicity in an ordinary drug formulation. Immunomodulatory LRA

1.17.3 Cytokines and cytosolic pattern recognition receptor (PPR) agonist

Interleukin-7 (IL-7) plays an essential role in the early development and maintenance of human T cell function through it is γ-chain cytokine receptor family (IL-2, IL-4, IL-7, IL-9, IL-15, IL-21) (379). Several studies have focused on the ability of IL-7 to induce viral outgrowth in resting $CD4^+$ T cells. These studies showed conflicting results in activation of HIV latency or promoting HIV persistence during ART (323, 380–383).

Earlier work done by Jones et al. has provided a proof-of-concept that the IL-15 super agonist (ALT-803 and IL-15SA) can reverse HIV latency and sensitised previously reactivated cells for HIV-specific $CD8^+$ T cell recognition in $CD4^+$ T cells from PLWH on ART (384). In another study, autologous CTL clones were used as bio detectors for $CD4^+$ T cells from PLWH on ART undergone latency reversal with ALT-803 and IL-15SA (385). Although a reduction in total HIV DNA was observed, no reduction in the inducible intact reservoir was measured by QVOA (385).

PPR agonist

Toll-like receptor (TLR) agonists are microbial-sensing proteins of the PRRs, which are involved in the non-specific recognition of pathogen-associated molecular patterns (PAMPs) by innate immune system cells, including $CD4^+$ T cells macrophages DCs, neutrophils, NK cells, and fibroblasts (386–388). Once PAMPs bind to the corresponding TLR, the signalling pathways downstream from these TLRs recruit specific intracellular adaptor proteins such as TIR-domain-containing adaptor protein inducing beta interferon, IFN-β (TRIF) or myeloid differentiation primary response protein 88 (myD88). This will lead to initiate signalling pathways culminating in activation of NF-κB, MAP kinases, and IRFs that control the transcription of genes encoding type I interferon (IFN I), chemokines and other inflammatory cytokines to create an anti-viral state (389, 390). Multiple TLR agonists are being investigated as LRAs to reactivate HIV transcription, including TLR2, TLR3, TLR7 and TLR9.

A recent *in vitro* study investigated the latency reversal activity of several TLR agonist panels in a latently infected human microglia cell line (hμglia) using a single-round HIV. Challenging these cells with a panel of TLRs agonists (TLR1,2,3,4,5 and 6 agonists) demonstrated the capability of TLR3 to reactivate HIV latency, while other TLRs (1,2,4,5 and 6) showed weaker reactivation in the hμglia /HIV cell line. Interestingly, apart from the level of TLRs potency among this panel, TLR3 agonist-induced latency reversal by activation of the interferon regulatory factor 3 (IRF3) transcriptional factor cascade while other TLRs target NF-κB induction pathway. However, results showed a distinct activation profile of TLR agonists in latently infected monocyte cell lines (391). TLRs are present and serve significant roles in subsets of $CD4^+$ T cells, constituting a significant part of the HIV reservoir. An *ex vivo* study demonstrated TLR1-2 agonist ability to reactivate HIV latency through the cooperation of NF-$_k$B, NFAT and AP-1 signalling pathways (392).

The TLR7 agonists are among the well-studied TLRs ligands that induce HIV RNA and active HIV-specific cytotoxic $CD8^+$ T cells in PBMC isolated from PLWH on ART (393). Studies of TLR7 agonists (GS-986 and GS-9620) have shown *in vivo* viral reactivation and reduction of viral reservoir size

both in blood and tissue in simian immunodeficiency virus (SIV) infected rhesus macaque (RM) on ART (323). However, the subsequent studies failed to produce similar results showing viral reactivation in SIV-infected or simian-human immunodeficiency virus (SHIV) RM nor PLWH (394–398). The TLR7 agonist GS-9620 (Vesatolimod) was recently investigated in a phase 1b, randomized, double-blind, placebo-controlled study; only isolated and modest induction of HIV RNA was observed (399).

The TLR9 agonist, MGN1703 which stimulates IFN I from pDCs, was also advanced to clinical trials. In a preclinical evaluation study of TLR9 agonist MGN1703, peripheral blood mononuclear cells were isolated from aviremic PLWH on ART and treated with MGN1703 resulting in enhanced levels of HIV transcription and induction of the potent antiviral activity of NK cells mediated suppression of HIV infection (400).

A recent phase I clinical trial (TEACH, NCT02443935) involved 15 PLWH on ART. This trial provided a unique opportunity to investigate whether the antiviral immune response can be induced and/or viral transcription reactivated following administration of single drug molecule TLR9 agonist (MGN1703) for four weeks (401). This study showed TLR9 agonists might exhibit dual characteristics by activating HIV transcription and enhancing cytotoxic NK cell activation and specific- HIV $CD8^+$ T cells.

Retinoic acid-inducible gene I RIG-I agonist

RIG-I is a cytosolic pattern recognition receptor of the cytoplasmatic DEAD-box dsRNA helicase family (RIG-I like receptors, RLRs) that detects non-self RNA as a pathogen-associated molecular pattern (402). It has been shown to activate IFN I and NF-$_k$B signalling pathways following RIG-I activation. There is an increased interest in harnessing the potential of RIG-I activation to purge the latent reservoir. However, whether RIG-I agonist treatment can disrupt HIV latency and induce preferential apoptosis of latently infected cells *in vitro* and *ex vivo* has been controversial. Li et al. showed that pharmacological stimulation of the RIG-I pathway using acitretin (RIG-I agonist, FDA approved for the management of psoriasis) in the latently infected TZM-bl cell line or primary $CD4^+$ T cells from PLWH on ART, induced RIG-I expression and increased HIV transcription, but also

RIG-I signalling selectively induced IFN-mediated apoptosis of HIV-positive cells (133). In contrast, Garcia-Vidal et al. and Palermo et al. found that acitretin mediated stimulation of RIG-I expression but failed to induce potent HIV reactivation and lacked selective cell death of HIV- positive cells in the latently infected J-Lat T cell line or primary $CD4^+$ T cells from PLWH on ART (403, 404). The discrepancies between acitretin efficacy and outcome obtained from those two studies may be attributed to differences in a cell culture setting and virus strains used. Recently Indra Sarabia et al, showed that RIG-I agonist (dsRNA) reactivated latent HIV through the mitochondrial antiviral signalling (MAVS) protein (405). The study stressed the central role of MAVS in mediating signalling from RIG-I and reversing HIV latency.

1.18 COMBINATION LRA APPROACHES

Considering the vast array of known factors or blocks that maintain HIV latency, a combination approach of LRA classes that synergistically target different latency pathways may be required for efficient activation of HIV gene expression in infected resting $CD4^+$ T cells and also limit LRA toxicity by using smaller doses of each agent (406).

For example, Laird *et al.* compared two LRAs combinations (bryostatin-1 + romidepsin and bryostatin + JQ1 inhibitor) (338). These results showed a significant synergetic effect in reactivating HIV latency following combination LRAs treatment in the same system without the release of proinflammatory cytokines by resting $CD4^+$ T cells. However, the synergetic effect of LRA may impair primary HIV-specific $CD8^+$ T cells and cause immune suppression.

Interestingly, an innate immune agonist (cGAS-STING agonist) combined with the HDACi resminostat amplified viral reactivation and induced specific death of HIV-infected cells in the J-Lat T cell line and ACH2 cells (404). However, this magnitude of reactivation and immune response against latently infected cells was not observed *ex vivo*. Importantly, these studies highlighted the therapeutic potential in synergising innate immune agonists with other LRA classes (e.g. HDACi) or immunotherapeutic modalities such as PD-1 immune checkpoint blockade (ICB) reinvigorating T cell effector function and cytotoxic activity (407, 408).

Collectively, these observations suggested that LRAs may exhibit several effects on innate and adaptive immune responses. In addition, not all LRAs within the same pharmacological class have the same detrimental effects directly on infected cells, such as affecting antigen processing or presentation or on HIV-specific $CD8^+$ T cells. Moreover, in the shock and kill strategy, early studies highlighted the need to reactivate all cells harbouring HIV integrated DNA without triggering a systematic inflammatory response (314, 318). We aim to investigate possible approaches to overcome these unwanted effects, including reducing or eliminating hazardous systematic effects using a nanoparticle drug delivery platform.

1.19 NANOMEDICINE MEDIATED DRUG DELIVERY

Nanomedicine has raised tremendous attention in biomedical research towards therapeutic development based on smart delivery nanoparticles (409–411). The current development of nano-therapeutics focuses on designing and engineering nano- carrier systems for drug and vaccine delivery (412–415). However, recently it has become clear that engineered nanoparticle systems often lack in-depth characterisation towards their interaction with immune cells (416).

In recent years nanotechnology-based drug delivery systems have received tremendous interest and showed remarkable ability to overcome an anatomical and physiological barrier in animal models and deliver the therapeutic agents at the site of systemic diseases such as blood cancer and HIV (417–420). Particle-based delivery has several potential advantages compared to free drug formulations, owing to its power to load and protect various payloads, sustained kinetic release, improved drug pharmacokinetics and biodistribution. In addition, the ability to navigate to a specific organ or cell increase nanomedicines efficiency and reduce off-target related toxicity effects (410, 411, 417, 421). A significant advance in nanocarrier drug delivery using a nanoscale particle system is their ability to encapsulate efficiently different types of therapeutic payloads. A second significant advance has been made by understanding mechanisms that govern cellular binding, internalisation and trafficking of particles at the plasma membrane (422–424).

1.19.1 T cell-targeting nanoparticles drug delivery systems

Nanoscale drug delivery vehicles are available in various forms and materials, e.g., nanoparticles, nanoshells, liposomes, carbon nanotubes and dendrimers (Figure 1.9). A major common advantage of these systems is the flexibility in tuning their physicochemical properties such as size, shape, rigidity, surface chemistry, stability and structure, which are key factors that impact cellular uptake, biodistribution patterns, and clearance (425).

Cellular uptake of nanoparticles is different from that of free drug formulations. Therefore, nanocarriers are designed to overcome barriers in endocytosis. Nanoparticulate systems with encapsulated drugs can be internalized either by non-specific endocytosis or receptor-mediated endocytosis (426). Nanotechnology can also facilitate receptor-mediated endocytosis through particle surface modification with a specific ligand that can allow enhanced binding to target cells that overexpress its receptor (285, 414, 427–429).

T cells are one of the adaptive immune system arms that respond to T cell receptor (TCR) recognition of their specific antigen presented by APC on MHC-II (CD4) or MHC-I (CD8) (430). T cells are susceptible to many diseases, including blood cancers (e.g., acute lymphoblastic leukemia and T cell Lymphoma) and viral infections (e.g. HIV and HTLV-1), making them attractive targets for therapeutics and prevention approaches (312, 431–433). Consequently, this has led to the development of T cell-based immunotherapy to tackle diseases or boost T cell responses to diseased or infected cells (408).

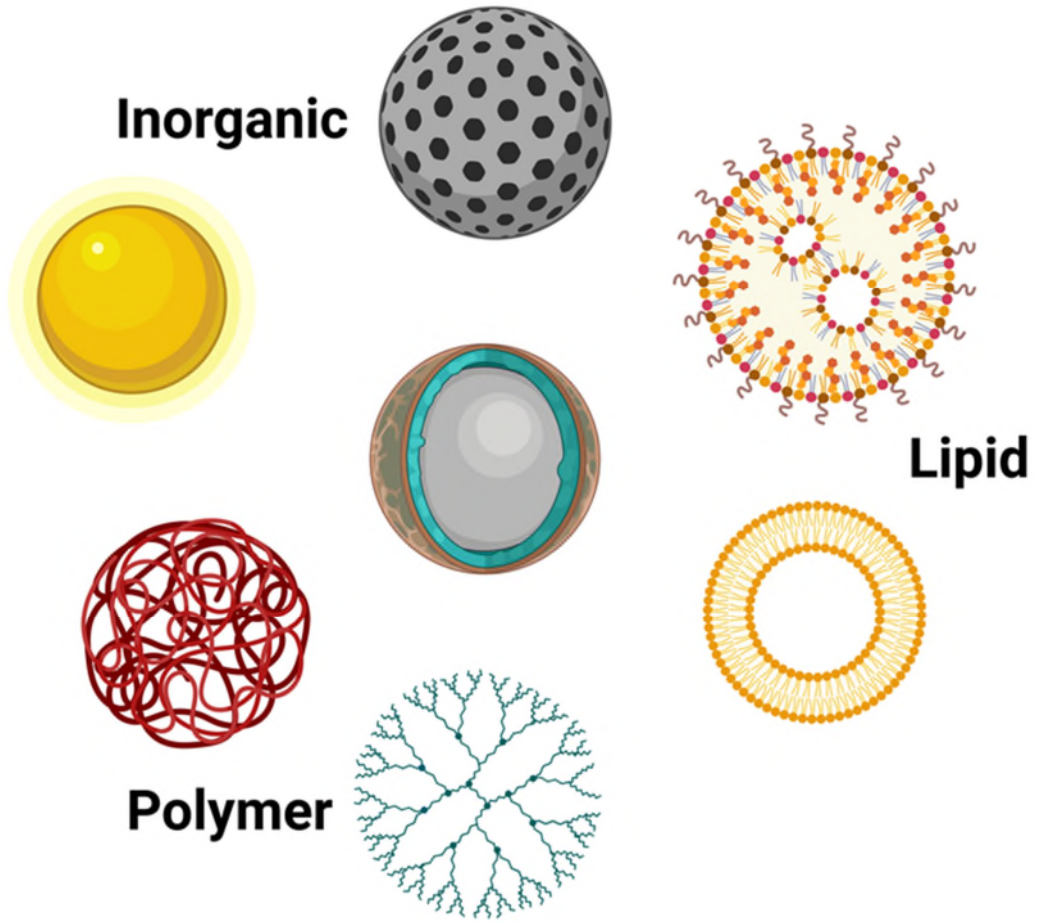

Figure 1.9 Potential nanoparticle drug delivery platforms.

Nanoparticles can be broadly subdivided into three main classes: lipid-based, polymer-based, and inorganic nanoparticles. Lipid-based nanoparticles include liposomes (aqueous core) or micelles (hydrophobic core). Polymer-based nanoparticles include cationic polymer-based particles or micelles, or capsules made from hydrophobic polymer (red) combined with an amphiphilic coating (blue). Inorganic nanoparticles include gold and iron oxide spheres. The diversity of nanoparticle types available is far beyond the basic categories depicted here. Nanoparticles share common features such as drug loading capacity, specificity multifunctionality, biocompatibility and improved drug stability.

1.19.2 Nanostructured drug delivery system for improving latency reversal

In the context of HIV infection, the efficacy of LRAs is impaired by the systematic toxicity induced by the cytotoxic effect of these compounds (Table 1.1) (375, 434). Nanoengineered particles-based delivery of LRAs to T cells may circumvent these unwanted effects. However, safe delivery of particles remains a major technological challenge, primarily due to the non-phagocytic nature of $CD4^+$ T cells. Therefore, the first step to overcome cellular barriers and improve LRA delivery of nanoengineered particles is to study their interaction with the cell membrane. The negatively charged plasma membrane surrounding a living cell forms a boundary between the cytosolic and external microenvironment and provides structural support to the cell (423, 435). In particular, non-phagocytic T cells strictly control charged molecule intake from the extracellular environment (423). However, particle adsorption onto the membrane and subsequent internalization depends on particle size and surface charge (436, 437). Small soluble molecules with a molecular weight below 1 KDa (e.g. medical drugs) pass quickly through passive diffusion, whereas polar molecules require energy-dependent or membrane modelling (438). Micropinocytosis is an intracellular uptake mechanism of particles > 200 nm that relies on membrane ruffling and results from actin polymerisation (439, 440). These rearrangements are induced by growth factors and mitogens such as phorbol esters (441). Another uptake mechanism that has played an essential role in receptor-mediated endocytosis is clathrin-dependent endocytosis, where larger molecules (< 200 nm) use this pathway for cellular uptake (442, 443). Several studies have shown that clathrin-mediated uptake of nanoparticles < 90 nm in diameter is possible (364, 416, 442, 444). The surface charge of particles is another critical parameter that influences particle uptake and may have a dominant effect over particle size (445, 446). In general, particles carrying positive charge (cationic) often have a higher association rate than negatively charged and neutral particles of similar dimension with the negatively charged cell membrane (anionic) through electrostatic interaction of an electrical potential gradient (53, 445, 447–449). However, particles may acquire different identities when

interacting with biological fluids such as blood and cell culture media. In biological fluids, the surface charge may change drastically by the adsorption of biomolecules, including proteins biological molecules, to form a protein corona (449–453). This new biological identity of nanoparticles can significantly alter the behaviour and fate of their interaction with cells. Therefore, studying the fundamental influence of nanoparticle physiochemical properties (size and surface charge) in interaction with T cells in physiologically relevant of *in vitro* and *ex vivo* experimental models is critical for developing efficient delivery of LRA loaded nanoparticles.

1.19.3 Potential drug delivery system as carrier for LRAs

The most well-investigated particle systems are Poly (lactic-co-glycolic acid) (PLGA) and lipid-based and have attracted considerable attention due to their biocompatibility, delivery of multiple drugs and sustained cargo release (454–456). In reactivation, the latent HIV proviral PLGA nanoparticles loaded with an HIV protease inhibitor (nelfinavir) were targeted to $CD4^+$ T cells in PBMCs culture. This nanoformulation reversed latency and inhibited *de novo* infection (455). A similar effect was observed when PLGA-PEG particles were used to target delivery of SAHA and nelfinavir to latently infected $CD4^+$ T cells. In a proof-of-concept study for nanoparticle encapsulation of LRAs, lipid nanoparticles incorporating the PKC agonist bryostatin, HDACi sodium butyrate and supplemented nelfinavir were delivered into a range of latently infected cell lines and primary cells (455). The authors showed significant binding/uptake of the nanoparticle in various cell lines, including macrophage (positive control), Hela and CEM (as these cell lines have endocytosis characters), and the nanoparticles also reversed latency in J-Lat cells and resting $CD4^+$ T cells. However, this prototype nanoparticle system lacked specificity to target resting $CD4^+$ T cells. In another study, Jones RB *et al.* showed targeted drug delivery lipid nanoparticles linked to antigen recognition which would localize payload release to the site of antigen expression in $CD8^+$ T cells (457).

In a recent study, Cao et al. synthesized hybrid lipid-coated PLGA nanocarriers loaded with diverse LRAs. These lipid-coated nanocarriers could selectively activate $CD4^+$ T cells *in vitro* and in non-human primate

PBMCs as well as targeted murine lymph nodes with substantially reduced toxicity (458).

Nanoparticle delivery of shock/ pro-apoptotic compounds or kill agents would require developing a biodegradable, efficient, highly specific, stable, and multifunctional particle system that can maximally activate HIV gene expression in latent reservoirs with minimal off-target effects and lead to clearance of infected cells.

Table 1.1 Summary of nanoparticle delivery platforms used to improve the delivery of molecules and macromolecules to tackle HIV infection

Nanostructure class	Nanoparticle (NP)	Application	Reference
Polymer-based	Poloxamer-based NP	Delivery of ART to T cells	(459, 460)
Copolymer-based	PLGA/Pluronic NP	Delivery of ART	(461)
Polymer-based	PLGA	Delivery of LRA to T cells	(462)
Copolymer based	PLGA/PEG NP	Co-delivery of ART and LRAs to T cells	(463)
Lipid-based	Lipid NP	Targeted Co-delivery of ART and LRA to lymph nodes	(464)
Lipid-based	Lipid NP	Targeted delivery of LRA to lymph nodes	(458)
Lipid-based	Lipid NP	Delivery of LRA to T cells	(457)
Hybrid lipid and polymer-based	Lipid-coated PLGA NP	Co-delivery of LRAs to T cells	(465)
Inorganic-based	Gold	Delivery of CRISPR-Cas9 components to T cells	(466)

Nanostructure class	Nanoparticle (NP)	Application	Reference
Inorganic-based	Metallic NP (Iron oxide)	Targeted delivery of nanoART and LRA formulations to the brain	(467)

1.20 POLYMERIC NANOCARRIERS

Polymeric nanostructured materials have played an important role in different biomedical applications, such as therapeutic drug delivery, diagnostic, and imaging applications (468, 469). Non-biodegradable polymeric nanoparticles, such as, polyacrylamide (PAM), polymethylmethacrylate (PMMA) and polystyrene (PS), have been used for drug delivery systems; however, significant toxicity and detrimental health consequences from non-biodegradable polymers have been observed (470). Therefore, biodegradable polymers (able to integrate with biological systems without eliciting an immune response) have attracted considerable interest over recent years due to their properties and biocompatibility for *in vivo* diagnosis and treatment of diseases (471). The unique features of smart polymeric-based nanostructured systems such as stability, tunable size, porosity, shape and surface charge, their mechanical strength and non-immunogenic properties enable them to meet the needs of different targeted biomedical applications (469, 470, 472–474). Different type of natural and synthetic polymer nanoparticles play a vital role in a targeted drug delivery system (475–477). Ideally nanoparticles prepared from natural or synthetic polymeric materials are inexpensive, have easy accessibility, bio-decomposition properties, and are easily modified. Reactive groups present on polymers such as amines, thiols and carboxylic groups, can be linked to fluorophore tags, drugs, or other synthetic materials endowing advantageous properties of different polymers (478–480). There are various types of polymers and are classified based on their origin or structural backbone (481). Based on origin, polymers are classified into either natural or synthetic polymers.

1.20.1 Natural and synthetic polymers nanoparticles

There are numerous types of natural polymers nanoparticles, and they are classified mainly into polysaccharide (polymeric carbohydrates) and protein-based polymers (469, 482, 483). On the other hand, synthetic polymer-based nanoparticles are classified into biodegradable such as phosphorous based, polyester and polyamides and non-biodegradable such as cellulose derivatives and acrylic based polymers (484). Herein we will focus on acrylic and polysaccharide-based nanoparticles.

1.20.2 Layer-by layer poly(methacrylic acid) engineered nanoparticle delivery system

Several nanoparticles drug delivery systems have been utilised to improve the delivery of ART and LRAs (Table 2.1). However, the most promising system to fulfil the above-mentioned needs is the layer-by-layer (L-bL) technique, which is applied to generate nanocapsules or core-shell particles by layered polymers on a silica template (485, 486). The LbL technique allows for better tailor-made nanoparticle generation due to its flexibility in size, composition, drug loading, surface charge and surface functionality (487, 488). In particular, layering poly(methacrylic acid) containing activated thiol moieties (PMA_{SH}) generates biologically interesting nanoparticles as these are stable under physiological conditions but degradable in the intracellular reductive endosomal environment (487, 489, 490). PMA_{SH} nanoparticles are fabricated from a mesoporous silica core that can be loaded with a drug and subsequently layered with alternatively negatively charged PMA_{SH} and positively charged poly(vinylpyrrolidone) (PVPON) at pH 4. At this pH, the two polyelectrolytes form stable multilayers that can be crosslinked through disulphide bonds, after which the PVPON is washed off at physiological pH to create negatively charged PMA_{SH} nanoparticles (491).

Recent applications of PMA_{SH} nanoparticles for drug delivery systems have included controlled drug delivery of stimuli-responsive carriers in the field of nanomedicine (491). The versatility of the PMA_{SH} nanoparticle system is compatible for encapsulation of different cargo types, including water-soluble and insoluble drugs, which have all successfully been adsorbed into

the mesoporous silica core, resulting in delivery into the same intracellular compartment (487, 492). An important advantage of the PMA_{SH} nanoparticles is the capacity to encapsulate a larger drug load due to large mesopores of 15 to 30 nm, resulting in efficient loading capacity for hydrophobic and hydrophilic drugs (492). In addition, the size of PMA_{SH} particles can be controlled in contrast to other particle systems by varying the size of the template (493, 494). The mesoporous silica core can be generated at different sizes by varying solvent, synthesis temperature, and silica source, resulting in cores ranging from ~100 nm up to 2 µm (495). Multifunctional properties of PMA_{SH} nanoparticles could play an essential role in targeted delivery and combinational therapy. It has been demonstrated that sub 500 nm-sized huA33 mAb-coated nanoparticles can bind with specificity to the A33 antigen that presents on almost all colorectal cancer cells (496). Nevertheless, toxicological considerations, chemical stability, specificity and a convenient biodistribution are still areas for improvement.

1.20.3 Bovine Glycogen nanoparticles (BG-NP)

In general, glycogen NP can be synthesised from different biological sources such as bovine liver (BG), rabbit liver (RG) and oysters (OG) (482, 497). Soft bovine glycogen nanoparticles (BG-NP) are a promising delivery system that efficiently encapsulates nucleic acid (418, 498). The advantages of soft glycogen NP over other synthetic and natural polymers (Table 1.1) are their tunable size, degradability, and lack of toxicity at high concentrations (418). The hyperbranched BG- NPs are a favourable non-viral gene delivery system because they have endo-lysosomotropic properties allowing for cytosolic localisation and endosomal escape. Second, they can deliver multiple copies of nucleic acid encoding genes and finally, they have reduced cytotoxicity (418, 499, 500). BG-NP surface charge can be easily modified to incorporate different therapeutic and targeting molecules. For intracellular delivery of nucleic acids, the otherwise neutrally charged BG-NP are modified with ethylenediamine (EDA) to generate a positive surface-charge (BG_{EDA}-NP) (418). BG_{EDA} engineered NP have previously been used to deliver small nucleic acids (such as

siRNA) *in vivo*, which make them a better candidate to deliver nucleic acid-based therapeutic into T cells due to (i) their smaller size and (ii) endoplasmic delivery of payload which are critical factors for efficient translation of RNA based therapies to T cells (418, 501).

1.21 HYPOTHESIS

We hypothesise that the delivery of nanoparticles loaded with latency-reversing agents (LRAs) will lead to efficient uptake in $CD4^+$ T cells and reverse HIV latency with enhanced potency and reduced toxicity. To investigate this hypothesis, we will utilize PMA_{SH} particles loaded with the hydrophobic LRA romidepsin and glycogen particles encapsulating an RNA RIG-I agonist ligand. PMA_{SH} particles were chosen because they can encapsulate hydrophobic drugs efficiently and have tunable physiochemical characteristics that allow for varying pore size and volume, surface area, and surface modification. Glycogen particles were chosen for their ability to complex with RNA and a range of other properties, including biocompatibility, stability during circulation against serum proteins, adequate cellular uptake, and early endosomal escape. All of which are crucial elements for the efficient delivery of RNA molecules into T cells. We addressed the hypothesis through the following aims.

1.22 AIMS

1. To identify an optimal nanoparticle (NP) that can encapsulate a hydrophobic drug and that can be taken up by $CD4^+$ T cells
2. To deliver NPs loaded with latency-reversing agents (LRAs) to HIV-infected $CD4^+$ T cells to enhance both potency and specificity

To optimize nanoparticle delivery of a nucleic acid-based RIG-I agonist to HIV-infected $CD4^+$ T cells and determine the effects of RIG-I signalling on HIV latency.

This page has been left intentionally blank

2 Materials and Methods

Section one, “Material”, compiles tables listing all materials including reagents, buffers, labware, equipment and software’s used to acquire, analyse, and present the data. Section two, “Methods”, describes procedures and protocols.

2.1 SECTION ONE- MATERIAL

This section compiles tables listing all materials, including reagents, buffers, labware, types of equipment and software’s used to acquire, analyse, and present the data.

Table 2.1 Chemicals, buffers, cell culture media, reagents, and pharmaceutical compounds

Name	Manufacture	Cat no
MS 1 µM particles	Sigma-Aldrich (St. Louis, Missouri)	89904
Poly (methacrylic acid)	Polysciences (Warrington, Pennsylvania)	00578-50
Pyridine dithioethylamine	Shanghai Speed Chemicals (Shanghai, China)	FB52790
Dithiothreitol (DTT)	Sigma Aldrich (St. Louis, Missouri)	3483-12-3
MOPS buffer	Chem Supply[1]	Chem Supply
DMTMM	Chem Supply	Chem Supply
Sodium acetate NaOAc buffer	Chem Supply	Chem Supply

Name	Manufacture	Cat no
Chloramine T CaT	Sigma Aldrich (St. Louis, Missouri)	402869
Poly(N-vinylpyrrolidone) PVPON	Sigma Aldrich (St. Louis, Missouri)	PVP40
2-(N morpholino) ethanesulfonic acid) MES	Chem Supply	Chem Supply
Milli-Q water	Millipore Corporation (Burlington, Massachusetts)	Millipore Milli-Q plus 185 purification system
Tetraethyl orthosilicate (TEOS)	Sigma-Aldrich (St. Louis, Missouri)	131903
Poly (acrylic acid)	Sigma-Aldrich (St. Louis, Missouri)	9003-01-4
Cetyltrimethylammonium bromide (CTAB)	Sigma-Aldrich (St. Louis, Missouri)	57-09-0
Cetyltrimethylammonium tosylate (CTAT)	Sigma-Aldrich (St. Louis, Missouri)	138-32-9
Ammonium hydroxide	Sigma-Aldrich (St. Louis, Missouri)	221228
(3-aminopropyl) triethoxysilane (APTES, 99%)	Sigma-Aldrich (St. Louis, Missouri)	440-140
Ethanol (EtOH)	Sigma-Aldrich (St. Louis, Missouri)	Chem supply
Triethanolamine	Sigma-Aldrich (St. Louis, Missouri)	90279
5,5′-dithiobis-2-nitrobenzoic	Sigma-Aldrich (St. Louis, Missouri)	D218200
mPEG5K-b-PLKC50	Alamanda polymers (Huntsville, Alabama)	599393

Name	Manufacture	Cat no
PLKC50/250	Alamanda polymers (Huntsville, Alabama)	26124-78-7
Romidepsin (FK228, Depsipeptide)	Jomar life research (Victoria, Australia)	S3020
dimethyl sulfoxide (DMSO)	Sigma Aldrich (St. Louis, Missouri)	D2650
phorbol ester phorbol myristate acetate, PMA	Sigma-Aldrich (St. Louis, Missouri)	P1585-1MG
Ionomycin	Sigma-Aldrich (St. Louis, Missouri)	I3909-1ML
Phytohaemagglutinin, PHA	Sigma-Aldrich (St. Louis, Missouri)	R30852701
Human IFN alpha 2a Recombinant Protein	Life Technologies (Victoria, Australia)	111011
Boc-D-glutamic acid 1-benzyl ester	Sigma-Aldrich (St. Louis, Missouri)	34404-30-3
Potassium phosphate monobasic	Sigma- Aldrich (St. Louis, Missouri)	7778-77-0
Hydrochloric acid	Thermo Fisher (Victoria, Australia)	7647
Methanol	Chem-supply	Chem-supply
RPMI 1640	Life Technologies (Victoria, Australia)	21870092
Gibco Dulbecco's Modified Eagle Medium (*DMEM*)	Life Technologies (Carlsband, CA)	11960069
Penicillin	Life Technologies (Carlsbad, CA)	10378016
Streptomycin	Life Technologies (Carlsbad, CA	10378016

Name	Manufacture	Cat no
L-glutamine	Life Technologies (Carlsband, CA)	10378016
Blasticidin	InvivoGen (San Diego, CA)	ant-bl-05
Zeocin	InvivoGen (San Diego, California)	ant-zn-05
Fetal bovine serum (FBS)	Interpath (Victoria, Australia)	AUFBS/PG
Ficoll-Paque Plus	GE Healthcare Pharmacia (Champaign, Illinois)	17-1440-02
Pancoll human density	PanBiotech (Kaohsiung, Taiwan)	P04-60500
BD 10x Pharm Lyse buffer	BD Biosciences (San Jose, CA)	(BD 555899)
Stabilizing Fixative	BD Biosciences (San Jose, CA)	338036
10% Tris-borate-EDTA (TBE)	Life Technologies (Carlsband, CA)	EC6365BOX
Phosphate buffer saline PBS	Gibco (Victoria, Australia)	10010023
Dulbecco's Phosphate buffer saline D-PBS	Gibco (Victoria, Australia)	141190144
DNA loading buffer	Thermo Fisher (Victoria, Australia)	10816015
3p dsRNA (RIG-I agonist)	Martin Schlee lab (Bonn, Germany)	Martin Schlee lab
dsRNA (control ligand)	Martin Schlee lab (Bonn, Germany)	Martin Schlee lab
Lipofectamine 2000 Transfection Reagent	Life Technologies (Carlsband, CA)	11668019

Name	Manufacture	Cat no
Sendai virus	Charles River (Victoria, Australia)	PI-1, SV

(1) Chem supply indicate where reagents were supplied by the Department of Chemical Engineering at the University Of Melbourne

Table 2.2 Laboratory plasticware

Name	Manufacture
Chamber furnace	Jetlow (Victoria, Australia)
Micro cuvette	ZEN0040, Malvern Instruments (Malvern, UK)
Capillary cell	DTS1070, Malvern Instruments (Malvern, UK)
Vacuette blood collection tubes (Heparin K2 EDTA)	Greiner Bio-One (Kremsmunster, Austria)
Falcon 50ml Conical Polypropylene Tube	In Vitro Technologies (Victoria, Australia)
Falcon 15 ml Conical Polypropylene Centrifuge Tube	In Vitro Technologies (Victoria, Australia)
96well Tissue Culture plate, round bottom	Interpath (Victoria, Australia)
µ-Slide 8 Well ibiTreat	DKSH Australia pty (Victoria, Australia)
CryoGen tubes 2 mL	Bio sigma (Cona, Italy)
Formvar carbon-coated grid EMSFCF400-NI-UC	ProSciTech (QLD, Australia

Table 2.3 Equipment and software

Platform	Manufacture	Facility
Apogee A50-Microflow cytometer	Apogee Flow Systems (Northwood, UK)	Materials Characterisation and Fabrication Platform
Zetasizer (Nano-ZS)	Malvern Analytical (Malvern, UK)	Materials Characterisation and Fabrication Platform
Nano Sight NS400	Malvern Analytical (Malvern, UK)	Materials Characterisation and Fabrication Platform
LSR Fortessa II flow cytometry	BD Biosciences (San Jose, CA)	Doherty Institute Flow Facility
Confocal microscopy Nikon A1R	Nikon, (Victoria, Australia)	Materials Characterisation and Fabrication Platform
Transmission electronic microscopy TEM	FEI Tecnai TF20 (Hillsboro, Oregon)	Materials Characterisation and Fabrication Platform
High-performance chromatography (HPLC)	Shimadzu Prominence (Victoria, Australia)	Bio21 Molecular Science and Biotechnology institute
Microplate luminometer reader	FLUOstar Omega, BMG LABTECH	Lewin group laboratory[2]
Electrophoresis system	Bio-rad (Hercules, California)	Lewin group laboratory
Automated cell isolation-autoMACS	Miltenyi Biotec (Galdbach)	Lewin group laboratory
Image J	National Institute of Health (Bethesda, Maryland)	Open-source software
FCS express	De Novo software (Los Angeles, CA)	Lewin group laboratory[2] licence
FlowJo	v10 (Ashland, Oregon)	Lewin group laboratory[2] licence
GraphPad prism	GraphPad (San Diego, CA)	Lewin group laboratory[2] licence

Platform	Manufacture	Facility
Origin Viewer	Origin Lab (Northampton, Massachusetts)	Open-source software

(1) Equipment or software's licence provided by Lewin group laboratory

Table 2.4 Cell lines

Cell type	Manufacture	Catalogue number
THP-1 dual reporter cell	InvivoGen (Hennigsdorf)	thpd-nfis
HEK-Blue IFN-α/β	InvivoGen (Hennigsdorf,)	Hkb-ifnab
Jurkat cell line	NIH AIDS Reference Reagent Program (Bethesda, Maryland)	ARP-177
J-Lat A2	NIH AIDS Reference Reagent Program (Bethesda, Maryland	ARP-9854
J-Lat 10.6	NIH AIDS Reference Reagent Program (Bethesda, Maryland)	ARP-9849
TZM-bl	NIH AIDS Reference Reagent Program (Bethesda, Maryland)	ARP-8129

Table 2.5 Primary antibodies and stains

Antibody/Reagent	Manufacture	Cat no
Anti-human CD69 G46-6. BUV395	BD Biosciences (San Jose, CA)	564364
Anti-human CD25 MA-25. PE-CY7	BD Biosciences (San Jose, CA)	341009
Anti-human HLA-DR L243. FITC	Pharmingen (Lahore, Pakistan)	S101618
Anti-human HLA-DR L243. PB	BD Biosciences (San Jose, CA)	307633
Anti-human CD4 RPA-T4. FITC	BD Biosciences (San Jose, CA)	555346

Antibody/Reagent	Manufacture	Cat no
Anti-human CD3 HIT3A. PE	BD Biosciences (San Jose, CA)	555340
Anti-human CD3 UCHT1. Brilliant Violet-510	BD Biosciences (San Jose, CA)	563109
Anti-human CD56 B159. AF488	BD Biosciences (San Jose, CA)	557699
Anti-human CD19 HIB19. PE	BD Biosciences (San Jose, CA)	561741
Anti-human CD66B G10FS. PE/Dazzle-594	BioLegand (San Diego, CA)	305122
Anti-human CD14 M5E2. Brilliant Violet-785	BioLegand (San Diego, A)	301840
Anti-human CD8 OKT-8	ATCC (Manassas, Virginia)	CRL-8014
Anti-human CD11b OKM-1	ATCC (Manassas, Virginia)	CRL-8026
Anti-human CD14 FMC-17	Flinders Medical Centre, Adelaide, AUS	-
Anti-human CD16 3G8	Steinman Lab and Assoc. Prof. Anthony Jaworowski	-
Anti-human CD19 FMC63	Heidi Zola, Flinders Medical Centre (Adelaide, Australia)	-
glycophorin-A 107MN	ATCC (Manassas, Virginia)	HB-8162
Mouse IgG Isotype control MOPC-21. PE	BD Biosciences (San Jose, CA)	555749
Goat anti-mouse IgG microbeads	Miltenyi Biotech (Galdbach, Germany)	130-048-401
Alexa Flour 488 C_5 Maleimide	Thermofisher Scientific (Victoria, Australia)	A10254
Alexa Flour 647 C_2 Maleimide	Thermofisher Scientific (Victoria, Australia)	A20347

Antibody/Reagent	Manufacture	Cat no
Hoechst 33342 solution	Thermo Fisher Scientific (Victoria, Australia)	62249
1,1'-Dioctadecyl-3,3,3',3'-Tetramethylindocarbocyanine Perchlorate (DiI) stain	Thermo Fisher Scientific (Victoria, Australia)	D3911
Propidium iodide-cell viability	Invitrogen (Waltham, Massachusetts)	37670
Annexin V. Pacific blue	BioLegand (San Diego, CA)	640918
Annexin V buffer	Invitrogen (Waltham, Massachusetts)	V13246
CellTitre-Glo viability assay kit	Promega (Victoria, Australia)	G7570
SYBR Gold	Thermo Fisher Scientific (Victoria, Australia)	S11494
QUANTI-Luc	Jomar Life Research (Victoria, Australia)	rep-qlc2
QUANTI-Blue	Jomar Life Research (Victoria, Australia)	rep-qbs

2.2 SECTION TWO-METHODS

This section compiles all protocols and procedures performed at the Lewin and Caruso laboratories.

2.2.1 Synthesis and preparation of mesoporous silica (MS) particles

This procedure was performed at the Department of Chemical Engineering, Caruso Nanoengineering Group.

Three sizes of primary MS particles were used; 100 nm, 400 nm, and 800 nm in diameter were synthesised in-house (502). Polyelectrolyte-surfactant complexes were used as a template to synthesise the MS particles of 400 nm and 800 nm (503, 504). Cetyltrimethylammonium bromide (CTAB) (1.1 g) (Table 2.1) was dissolved in 50 mL Milli-Q water with continuous stirring. Poly (acrylic acid) (PAA, MW ~ 250 kDa, 35 weight % (wt %) solution in water) (Table 2.1) was added to CTAB solution under a vigorous stirring

condition at room temperature for 20 minutes to obtain a clear solution. A 3.5 mL of ammonium hydroxide solution (25 %) (Table 2.1) was added to the above mixture with vigorous stirring for 20 minutes, yielding a milky suspension. Subsequently, a 4.46 mL solution of tetraethyl orthosilicate (TEOS) (Table 2.1) was added to the above solution, followed by continuous stirring for 15 minutes. Then, the mixture was placed into a Teflon-sealed autoclave at 100 ◦C for 48 hours. The mesopores silica particles were washed twice with Milli-Q water and ethanol, then dried at 80 °C. Finally, to purify the formed MS, particles were placed in a chamber furnace (Table 2.2) and calcinated at 550°C in the air at 823 K for 30 hours.

100 nm MS particles were fabricated in accordance with a previously published method (505). 960 mg of cetyltrimethylammonium tosylate (CTAT) (Table 1), and 174 mg triethanolamine (Table 2.1) were suspended in 50 mL milli-Q water at 80 °C. Then, 7.8 mL of TEOS (Table 2.1) solution was added, and the mixture was stirred under vigorous conditions at 80 °C. After 2 hours, the mixture was transferred to a Teflon-sealed autoclave at 80 ◦C. After 48 hours, the resulting MS particles were twice with milli-Q water and ethanol, dried at 80 °C, and calcined at 550 °C in the air for 6 to remove any organic materials.

Finally, the primary MS particles of 1 µm in diameter were purchased from Sigma Aldrich (Table 2.1). On the basis of synthesised MS particles, transmission electron microscopy (TEM) was used to characterise the size and surface morphology of particles. TEM evaluation of the prepared MS supraparticles revealed the spherical morphology of the particles with a corresponding diameter of each particle of 100 nm, 400 nm, 800 nm and 1µm (Figure 2.1)

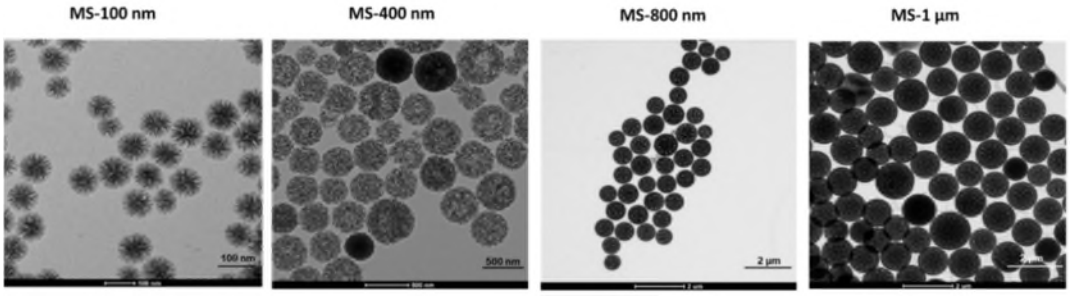

Figure 2.1 Characterisation of size and surface morphology of different mesoporous silica (MS) particles.

TEM images were performed to visualise the primary 100 nm, 400 nm, 800 nm, and 1 µm MS particles to confirm particles size and spherical shape.

2.2.2 Thiolated Poly (methacrylic acid) (PMAPDA) synthesis and reagent preparation

Poly (methacrylic acid) (PMA) (Table 2.1) was synthesised from PMA solution and cystamine dihydrochloride via carbodiimide coupling as described previously (487). $PMASH_{PDA}$ was synthesised by introducing the thiol (PDA) functionality. The functionalisation with cystamine dihydrochloride was performed in PBS. Dithiothreitol (DTT), 4-(4,6-dimethoxy-1,3,5-triazin-2-yl)-4 methylmorpholinium chloride (DMTMM) (20 gL^{-1}) (Table 2.1) was added to PMA solution and stirred for 15 minutes at room temperature. PDA (20 gL-1) was added to the above mixture and incubated overnight under moderate stirring conditions to obtain $PMASH_{PDA}$. The resulting polymer was purified by dialysis against Milli-Q water for 3 days with at least 6 times water exchange. Finally, the product was recovered via freeze-drying. The thiol content in the resulting polymer was characterised using 5,5′-dithiobis-2-nitrobenzoic acid (Table 2.1) via carbodiimide coupling, which corresponded to 12.9 mol % thiol groups modification.

^1H NMR: δ_H (400 MHz; D_2O): PMA_{PDA}: 0.5–1.25 (CH_3), 1.25–2.2 (CH_2 backbone), 2.65–3 (S–CH_2), 3.2–3.5 (NH–CH_2), 7.0–7.3, 7.5–7.9, 8.25–8.4 (C*H* pyridine).

A stock solution of poly(N-vinylpyrrolidone) (PVPON) (Table 2.1.1) (50 mg mL-1) was prepared in 10 mM sodium acetate buffer NaOAc (pH 4) (Table 2.1). For sequential disposition, PMA_{PDA} was synthesised by amide bond formation between the carboxyl groups of thiolated poly (methacrylic acid) (PMA) (Table 2.1) and the amine groups of pyridine dithioethylamine (PDA) (Table 2.1). Activation of thiol groups to generate PMA_{SH} was achieved by dissolving PMA_{PDA} in 100 mg/mL into 0.5M solution of 1,4-Dithiothreitol (DTT) (Table 2.1) at pH 8, followed by thermo mixing for 15 mins at 37°C,

800rpm. A 1:25 dilution of the 100 mg/mL PMA_{SH} into 50mM sodium acetate buffer NaOAc (Table 2.1) at pH 4 was performed to generate the final solution for layering.

2.2.3 Layer by layer assembly of PMA_{SH} nanoengineered particles

PMA_{SH} nanoengineered particles were synthesised using Layer-by-Layer assembly of a biopolymer via hydrogen-bonding multilayer particles assembly (489). This method is based on the alternate deposition of polymers containing a hydrogen bond acceptor and a hydrogen-bond donor. Herein, we synthesised various particles sizes ranging from 100 nm to 1 µm and with different surface charges, including negative (PMA_{SH}), neutral (PEGylated, PMA_{SH}-PEG) and positive (Poly-L-lysine, PMA_{SH} -PLL).

The layering procedure of MS cores included four subsequent layers of PMA_{SH} (donor, MW 15 kDa) and PVPON (Acceptor, MW 55 kDa) polymers (Table 2.1). After resuspension in 50µl of NaOAc pH 4, 50µl of 4mg/mL PVPON (Table 1) was added and incubated for 10 minutes at room temperature (RT), then washed three times in NaOAc to remove excess polyelectrolyte. The cores were then resuspended in 50µl NaOAc and incubated with 50µl 4mg/mL PMA_{SH} (Table 2.1). This process was repeated until eight bilayers were formed, ending with a final layer of PMA_{SH}. Finally, particles were washed three times with NaOAc and discarded the supernatant before cross-linking PMA_{SH} layers. To ensure an equal spread of the polymers across the cores, samples were vortexed immediately before and after the addition of 50 µl PVPON or PMA_{SH}.

2.2.4 Cross-linking procedure for PMA_{SH} particles

Following the final washing steps to stabilise the PMASH particles of PMASH particles, 500 µl (2.7 mM) of chloramine T (CaT) solution (Table 2.1) was added and vortexed for 1 minute to induce cross-linking of thiol groups (487). The layered particles (core shells) were then slowly brought up to physiological pH by washing twice in 2-(N-morpholino) ethane sulfonic acid buffer (MES) (Table 2.1), pH 6, and three times in phosphate buffer saline (PBS) (Table 2.1) pH 7.4 (Table 2.1) to expel the PVPON from the

shell. The particles were stored in 200 µL of PBS before surface functionalisation.

2.2.5 Surface modification

One-step surface modification between the PMA_{SH} particles surface and the modifier was used to tailor the particles surface chemistry. We used chemical conjugation treatment of Methoxy-poly (ethylene glycol)-block-poly (L-lysine hydrochloride) (mPEG5K-b-PLKC50, MW = 1000 Da and 8200 Da) (Table 2.1) for a neutral charge (PMA_{SH}-PEG) and Poly-L-lysine hydrochloride PLKC50/250 (MW = 41000 Da) (Table 2.1) for a positive charge (PMA_{SH}-PLL). Synthetic mPEG5K-b-PLKC50 or PLKC50/250 were prepared in a 10 mg/mL concentration in milli-Q water. 200 µL of mPEG5K-b-PLKC50 or PLKC50/250 solutions were added to PMA_{SH} particles (5 mg) to form an electrostatic interaction with the PMA_{SH} particles negative charged shell. Samples were incubated at room temperature (22 °C) under mild stirring conditions for 1 hour, followed by washing three times in PBS. Finally, particles were resuspended in 100 µL PBS before fluorophore labelling of particles.

2.2.6 PMA_{SH} particles labelling

To fluorescently label the particles for visualisation, we used Alexa Flour 488 C_5 Maleimide (AF488) and Alexa Flour 647 C_2 Maleimide (AF647) (Table 2.5). 5 µL (1 mg mL^{-1}) of AF488 or AF647 were added to 5 mg of particles suspension in PBS. Samples were first incubated at room temperature under mild stirring conditions, followed by incubation at 4°C. After 24 hours, the excess dye was removed by washing three times with PBS and particles were stored in PBS at 4°C until used.

2.2.7 Characterisation of PMA_{SH}, PMA_{SH}-PEG and PMA_{SH}-PLL nanoengineered particles

PMA_{SH} particles size may be adjusted depending on the size of the silica core. To determine the size and particles intensity, dynamic light scattering (DLS) (Table 2.3) (particles size > 100 nm) and nanoparticles tracking analysis (NTA) (Table 2.3) (particles ≤ 100 nm) were used. The particles

morphology of MS-100 nm, MS-400 nm, MS-800 nm and MS-1 µm were further characterised using transmission electron microscopy (TEM) (Table 2.3) using the previously described method (502). The TEM samples were prepared by placing 2 µL of diluted (1:1000 in Milli-Q) 100 nm, 400 nm, 800 nm and 1 µm MS particles on Formvr carbon-coated grids (Table 2.2). The TEM images were acquired immediately using an FEI Tecnai TF20 instrument at an operation voltage of 120 kV under liquid nitrogen cooling. Characterization of each layer was not performed, only the final product was characterized.

2.2.8 Dynamic light scattering (DLS), zeta potential and polydispersity index (PDI) measurements

The particles hydrodynamic diameter, zeta potential, and PDI were measured using a Zetasizer (Nano-ZS) Nano-ZS instrument (Table 2.3). For size distribution and PDI measurements, 1 mL of diluted particle (i.e., PMA_{SH}, PMA_{SH} -PEG and PMA_{SH} -PLL) solution (1:1000 dilution in Milli-Q water) (Table 1) was analysed in a micro cuvette (Table 2.2). We used Zetasizer (Nano-ZS) Nano-ZS instrument (Table 2.2). The measurements were performed using a standard operating procedure with automatic attenuation and measurement position.

The microelectrophoresis technique measured particle zeta potential before and after polymer layering to confirm particle surface charge. To measure particles zeta potential, 1 mL of particle dispersion (1:1000 dilution in Milli-Q water) was introduced into a folded capillary cell (Table 2.2), and measurements were performed similarly.

2.2.9 Nanoparticles tracking analysis (NTA) measurement

The hydrodynamic diameter of 100 nm nanoparticles was analysed via the nanoparticle tracking analysis (NTA) technique; 1 mL of diluted nanoparticle solution (1:2000) in Milli-Q water was analysed using Malvern Nano Sight NS400 instrument (Table 2.3) fitted with a 405 nm laser (65 mW output).

2.2.10 Particles counting

Particle counting for 400 nm, 800 nm and 1 µm of PMASH, PMA_{SH}-PEG and PMA_{SH}-PLL particles was performed using an Apogee A50-Microflow cytometer (Table 2.3). Particle counting for PMA_{SH}-100 nm, PMA_{SH}-PEG-100 nm and PMA_{SH}-PLL- 100 nm nanoparticles could not be accurately performed by flow cytometry due to their small size. Instead, the concentration of these particles was determined via nanoparticle tracking analysis performed on a Malvern Nano Sight NS400 instrument (Table 2.3) fitted with a 405 nm laser (65 mW output).

2.2.11 Pharmaceutical compounds and formulations

The following pharmaceuticals were dissolved in dimethyl sulfoxide (DMSO) (Table 2.1.1) to make stock concentrations stored at -80˚C: 10mM romidepsin (RMD; FK228) (Table 2.1) and 1mM PMA (Table 2.1). The following compounds were reconstituted in DMSO and stored at -20˚C: 1mg/ml phytohaemagglutinin (PHA) (Table 2.1) and 1mM Ionomycin (IONO) (Table 2.1). Interleukin-2 (IL-2) was constituted in PBS and stored at -20 ˚C.

2.2.12 Cell culture and latently infected cell lines

The human monocyte cell line THP-1 dual reporter (506, 507), human T lymphocyte cell line Jurkat (508), J-Lat A2 clone (249, 509) and J-Lat 10.6 clone (249) (Table 2.4) were cultured in RPMI 1640 based cell culture media plus 10% heat-inactivated fetal bovine serum (FBS) (Table 2.1), supplemented with 100 U/ml penicillin, 100 µg/ml streptomycin and 2 mM L-glutamine (Table 2.1) (RF10). TZM-bl reporter cell line (510) and HEK-Blue IFN-α/β reporter cell line (511) (Table 2.4) were cultured in Dulbecco's modified eagle medium (DMEM10) (Table 2.1) supplemented with glucose (4.5 g/L) 10 % FBS, 100 U/ml penicillin, 100 µg/ml streptomycin and 2 mM L-glutamine (Table 2.1). In addition, HEK-Blue IFN-α/β reporter cells were supplemented with antibiotic resistance 30 µg/mL and 100 µg/mL of blasticidin and zeocin, respectively (Table 2.1). All cells were maintained in a humidified 37˚C and 5 % CO_2 humidified atmosphere.

2.2.13 Ethics statement

The Human Research Ethics and Integrity committee from the University of Melbourne (Ethics ID:1443071) approved the use of blood samples packs from healthy volunteers. Adult donors blood was obtained from the Red Cross Blood Transfusion Service, and all provided written informed consent for the use of their blood products for the research purpose.

2.2.14 Study participant-Healthy human donor blood collection

After obtaining informed consent per the Department of Chemical Engineering, Blood was collected from healthy donors, The University of Melbourne Human ethics approval 1750753.2. Blood was collected in Vacuette blood collection tubes containing NH Sodium Heparin K2 EDTA as an anti-coagulant (Table 2.2). Tubes were inverted 5 times to mix with anti-coagulant. Total blood count was performed, and blood was examined within 1 hour of collection.

2.2.15 Isolation of peripheral blood mononuclear cells (PBMC) from whole blood

The peripheral blood mononuclear cells (PBMCs) were isolated from whole blood from healthy donors as previously described (101) using Ficoll-Paque (Table 2.1) density separation. Whole blood was diluted in an equal volume of PBS and layered over Ficoll-Paque. The samples then underwent density gradient centrifugation at 800xg for 20 minutes at room temperature. The PBMC layer was collected, resuspended in cold PBS, and then subjected to centrifugation at 500xg for 10 minutes at 4˚C. The pellet was resuspended in cold PBS and pelleted at 300xg, and the above step repeated at 200xg. Finally, the pelleted cells were resuspended in 10 % fetal calf serum RPMI 1640 media (Table 2.1) and spun down at 500xg for 2 minutes. Isolated PBMC were counted per donor, recorded, used immediately or stored in liquid nitrogen until used.

2.2.16 Isolation of total $CD4^+$ T cells from PBMC

PBMCs were isolated from healthy volunteers buffy obtained from the Australian Red Cross Blood Bank as previously early described. Total $CD4^+$

T cells were isolated using negative bead depletion as previously published (101), isolated PBMC were added to a total depletion cocktail compromised for human cell surface markers using a monoclonal antibody cocktail targeting as follow; anti αCD8 (OKT-8 hybridoma); αCD11b (OKM-1 hybridoma); αCD14 (FMC-17 hybridoma); αCD16 (3G8 hybridoma); glycophorin-A (Gly A) (107MN hybridoma,); CD19 (FMC-63 hybridoma,) (Table 2.5). Goat anti-mouse IgG microbeads (Table 2.5) were added, and an autoMACS (Table 2.3) was then used for magnetic bead depletion. T cell purity was assessed using CD4-FITC (Table 2.5) and CD3-PE (Table 5) staining, followed by analysis on the Fortessa II (Table 2.3). Purity percentage was analysed using FlowJo software (Table 2.3) and ranged between 96-98 %. Isolated cells were used immediately or frozen in freezing media (90 % FBS + 10 % DMSO) and stored in liquid nitrogen until further used.

2.2.17 *In vitro* PMA_{SH} particle association studies

Total $CD4^+$ T cells were thawed in a 42 C° in a water bath, 1 mL warm (37 °C) heat-inactivated FBS (Table 2.1) was added dropwise manner to thawed cells and transferred into a 15 mL falcon tube (Table 2.2). Cryovials were washed with 1ml of warm RF10, added dropwise to the 15 mL Falcon tube, and further toped to 13 mL with RF10 media. The tube was inverted carefully 8 times, and cells were spun down for 7 minutes at 400xg at room temperature. The supernatant was discarded, and the pellet was resuspended in 13 mL of warm (37 °C) PD and washed again. The pellet was resuspended in a warm (37 °C) RF10 medium, and the number of cells in each donor (15 mL tube) was counted using a haemocytometer. For particle association study, cells were seeded at a concentration of $8.5x10^6$ cells/mL in RF10 + 3U/ML IL-2. The next day, Jurkat cell line and primary $CD4^+$ T cells were harvested and reseeded in a 96-well U bottom plate (Table 2.2) at a density of 0.2 X 10^6 cells per 100 µL in RF10. The positive control cell line, TZM-bl, were seeded at the same concentration in a 96-well flat plate (Table 2.2) in DMEM10 (Table 2.1). Cells were treated with AF488 (Table 2.5) fluorescent labelled 400 nm, 800 nm or 1 µm of PMA_{SH}, PMA_{SH}-PEG and PMA_{SH}-PLL particles, at a ratio of 200:1- particles: cells

for 24 hours at 37°C, CO_2 humidified atmosphere. Subsequently, cells were washed three times with PBS buffer to remove free particles from the medium. Particles-cells was association analysed after gating on single cells and analysing AF488 signals by flow cytometry (Table 2.3). Data were analysed using FlowJo V10.4 and GraphPad prism 8 (Table 2.3).

2.2.18 *In vitro* confocal laser scanning microscopy image analysis (CLSM) quantification

To obtain quantitive data on particles association (binding and internalisation) in T cells, we employed a confocal laser scanning microscopy image analysis (CLSM)-based approach coupled with ImageJ® software (Table 3.2) to distinguish between bound and internalised particles. TZM-bl cell line, Jurkat cell line and primary $CD4^+$ T cells were treated as previously described. Cells were washed three times with PBS buffer to remove free particles from the medium, then stained with 1,1'-Dioctadecyl-3,3,3',3'-Tetramethylindocarbocyanine Perchlorate (DiI) stain (1:1000 dilution) (membrane) and Hoechst 33342 (1:100 dilution) (nucleus) (Table 5.2) to localise associated particles. Cells were fixed with 1 % paraformaldehyde for 15 mins and rinsed twice in PBS before transferring 100 µL in duplicate 8 wells microscopic chamber (Table 2.2). Cells were imaged by Nikon A1R confocal microscopy using 20× and 63× oil immersion objectives (Table 2.3). To scan conditions and acquire images for quantitive analysis, we divided each well into four quadrants to quantify all possible ROI events. Quantification of positive cells for surface-bound particles or/and internalised particles was carried out through blind-randomised ROI scanning of each condition (Figure 2.2 A). Field view images of scanned ROI were taken, and particles localisation within the cells were analysed as shown in the representative slice (Figure 2.2 B). Particle–cell interactions (binding and internalisation) were quantitated using ImageJ software (512) (Table 2.3) by stepping through z-stacks and counting the percentage of cells containing AF488-labelled particles at the surface or inside the cell. The quantification strategy we employed in this study based on (i) the presence of one particle or aggregates within the cell, was counted as an internalisation positive cell , (ii) a cell with one particle internalised and

another adhered to the membrane would also count as an internalised positive cell . In contrast, a cell with only particles adhered to the surface will count as a binding positive cell (>1500 cells per condition). (Figure 2.2 C).

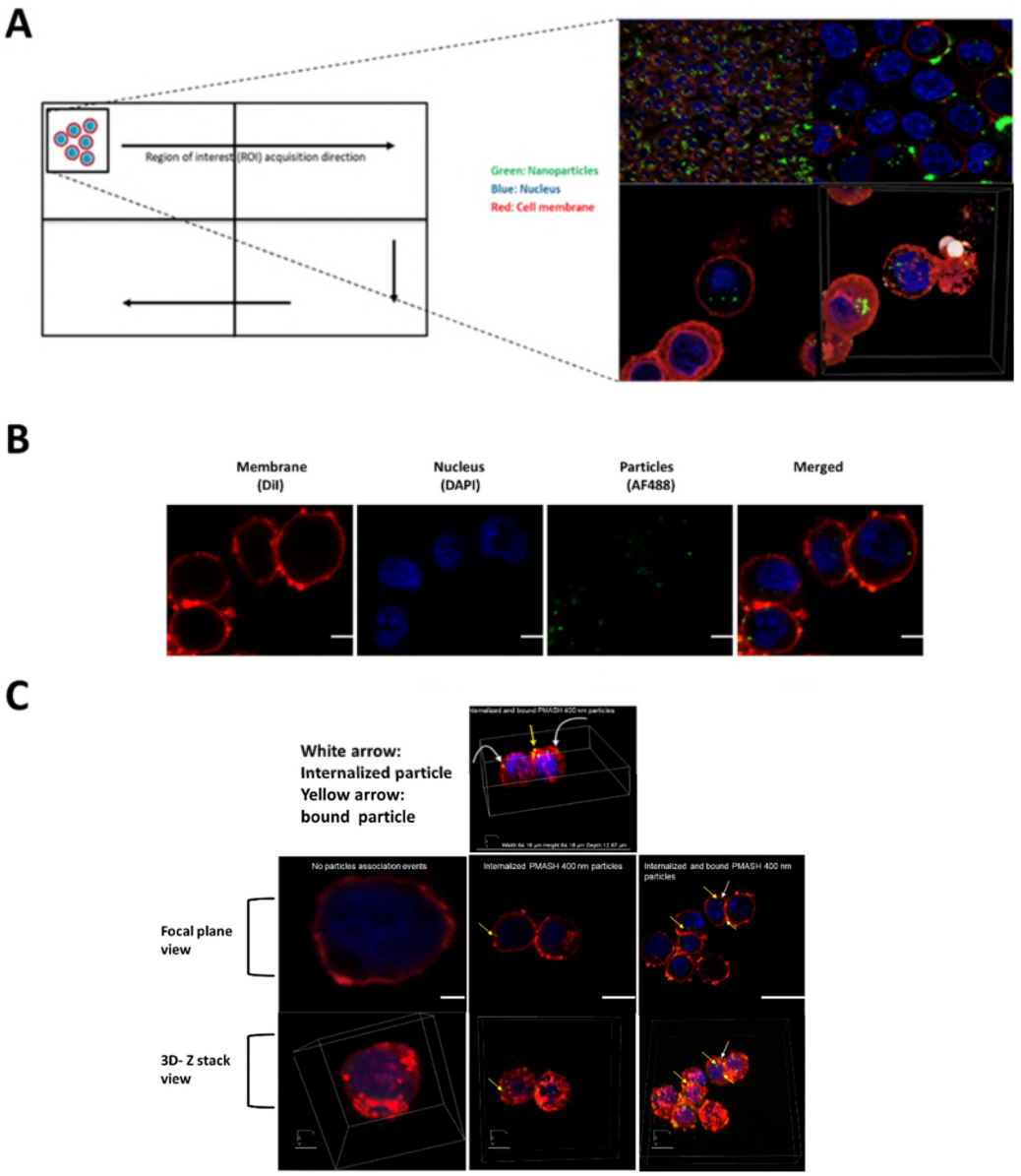

Figure 2.2 Quantification and localisation of associated particles with T cells

A) Cells were plated on confocal chambers, and while acquisition, we divided each well into four quadrants to further collect images of the region of interest (ROI) and capture 3D-Z stack images to localised associated particles. B) Representative confocal images showing staining for the membrane (DiI, red), nucleus (DAPI, blue) and PMA_{SH} 400 nm particles (AF 488, green). C) representative images displaying a field of view and Z stack to localise bound and internalised particles into primary $CD4^+$ T cells. Scale bar: A. 4 µm. B, 10 µm.

2.2.19 Particles association with human whole blood and PBMC

We investigated 400 nm negatively charged PMA_{SH}, neutral PMA_{SH}-PEG and positive PMA_{SH}-PLL particles interaction with cells using fresh human whole blood and PBMC as previously described (513). Whole blood from healthy volunteers (obtained with informed consent) was collected into tubes containing NH Sodium Heparin K2 EDTA as an anti-coagulant. 200 µL of fresh blood per well were seeded into a 96-well U bottom plate (Table 2.2), and 10 X 10^6 fluorescent labelled AF647 particles were added to the blood and incubated at 37 ◦C, 5% CO_2 humidified atmosphere for 1 hour. PBMC were isolated as described above and treated similarly.

Following incubation, particles interaction with cells was terminated by placing the samples on ice. Samples were diluted into H_2O BD 10 X Pharm lysate buffer (Table 2.1) was added to samples to lysate red blood cells, vortexed for 5 seconds, incubated on ice for 15 min, and washed twice with PBS. Whole blood and PBMC were phenotyped with a panel of anti-human antibodies fluorophores for 1 hour on ice to identify different cell subsets. Cells were surface stained for CD3 BV 510, CD14 BV785, CD56 AF488, Human leukocyte antigen - DR isotype (HLA-DR) Pacific Blue, CD19 PE and CD66b PE/Dazzle 594 (Table 2.5). Samples were washed three times with FACS Wash Buffer (1x PBS containing 1% bovine serum albumin (Table 2.1), resuspended in 200 µL stabilising fixative buffer (Table 2.1) and analysed by flow cytometry (Fortessa II, Table 1.3). Gated populations of single cells were analysed for association with particles using FCS Express version 9 (Table 2.3), and percentage cells associated with particles (% Association) summarised using GraphPad Prism 8 (Table 2.3).

2.2.20 Viability assay (propidium Iodide)

Jurkat and primary $CD4^+$ T cells (0.2 X 10^6 in 0.2 mL) were seeded in 96 wells U bottom plate, and then all cells were treated with different sizes and surface charge NPs (400 nm, 800 nm and 1µm, PMA_{SH}, PMA_{SH}-PEG and PMA_{SH}-PLL) particles in a ratio of 200: 1 NPs: cell and incubated at 37° C and 5% CO_2 humidified environment for 24 hours. Cells were washed three times with PD to remove free particles, followed by PI staining (0.25 µg/ml) (Table 2.5) and analysed immediately using LSR Fortessa II. Viable cells (PI^-) and dead cells (PI^+) populations were analysed using FCS Express version 9.

2.2.21 Cellular activation

To examine whether PMA_{SH} particles 400 and 100 nm induce T cell activation in $CD4^+$ T cells at different time points: 12 h, 24 hours and 48 hours. T cells activation was assessed by quantifying the expression of activation antigens (activation markers); CD25, CD69 and HLA-DR using flow cytometry analysis.

A day before the experiment, $CD4^+$ T cells were thawed as previously described. $CD4^+$ T cells were platted at 3 X 10^5 per well in a 96-well U bottom plate. Cells were stimulated with PHA/IL-2 (Table 2.1) or exposed to PMA_{SH} 100 nm and 400 nm particles for 12 hours, 24 hours, 48 hours and 72 hours and incubated in a 37 °C incubator with 5% CO_2 humidified atmosphere. Cells were harvested by centrifugation at 400xg for 5 minutes and washed twice with cold PD at study termination. Cellular stained for activation markers following the manufacturer's suggested protocol, with minor changes in the concentration (optimal antibodies concentration were standardised). Cells were surface stained for CD69 G46-6 (Table 2.1.5), CD25 M-A25 (Table 2.5) and HLA-DR L243 (Table 2.5) and incubated on ice. After 30 minutes of incubation, cells were washed twice with cold PD before being stained with live/dead cell viability stain PI for 10 minutes on ice. After washing off the unbound antibodies, the expression level of activation markers was assessed immediately using LSR Fortessa II and data were processed using FCS Express 9.

2.2.22 Encapsulation of romidepsin (RMD) into mesoporous silica (MS) template

The hydrophobic romidepsin (FK228, Depsipeptide, RMD) (Table 2.1) was loaded in the 100 nm and 400 nm MS particles using the previously reported method (492). Approximately 6 mg of MS particles were dispersed in 0.5 mL of DMSO solution containing 0.5 mg ml^{-1} of RMD, and the mixture was shaken at room temperature (22 ◦C) for 6 hours. After centrifugation of particles at 3500xg for 3.5 min and 3000xg for 2 min for 100 nm and 400 nm particles, respectively, and removing the supernatant, the RMD loaded MS particles were dried in a vacuum desiccator to remove the DMSO. The RMD loaded MS particles were then processed to RMD loaded PMA_{SH} NPs (RMDLNP) fabrication following the above-described method in sections 2.2.3 and 2.2.4.

The encapsulation efficiency (EE %) and drug loading percentage (DL%) of NPs were calculated by Equations (1) and (2)

(1) $$Encapsulation\ efficiency\ \%\ (EE\%) = \frac{M0-Mn}{M0} X\ 100$$

Where M0 is the total amount of RMD (mg) added to the particles and Mn is the amount of free RMD found in the supernatant

(2) $$\text{Drug loading (DL \%)} = \frac{\text{amount of drug found in MS particles (mg)}}{\text{amount of particles added (mg)}}\ X\ 100$$

Measuring of the remining drug in solution post nanoparticle incubation is a good surrogates for drug encapsulation. However, does not account for the fraction of RMD stuck on the outside of the MS core particles.

2.2.23 Drug release study

The release kinetics of RMD loaded into PMA_{SH} particles depressed 400 nm RMDLNP in 100 µL pH 7.3 PBS were monitored in the presence or absence of physiological concentration of 5 mM glutathione (GSH) at 37 ◦C, 5% CO_2 humidified atmosphere. 90 µL of each sample was collected at 0 min, 30 min, and each hour up to eight hours, and daily up to six days to determine the cumulative-released dose by high-performance chromatography (HPLC) (Table 2.3, detailed in “Instrumentation section”).

2.2.24 Determination of drug loading and release kinetic of romidepsin 400 nm PMA_{SH} loaded particles (RMDLNP) using HPLC

Instrumentation

HPLC was performed using a Shimadzu Prominence LC system equipped with a SIL20A-HT autosampler, CTO-20A column oven and SPD-M20A photodiode array detector. The chromatography was performed using an ACE Excel 5 SuperC18 analytical column (150 x 4.6 mm). Data was collected using LabSolutions software version 5.97 SP1 from Shimadzu. For all chromatographic experiments, the mobile phase consisted of acetonitrile – potassium phosphate buffer (Table 2.1) (0.03 M, pH 3) in a 27:73 volumetric ratio, consistent with a chromatographic assay that was previously developed for romidepsin (514). The mobile phase was used at a flow rate of 1.0 mL/min, and the experiments were performed at room temperature.

Calibration curve

To determine the concentration of RMD in the supernatant following drug loading or when released from particles, a calibration curve was prepared by a similar method as reported previously (515). Boc-D-glutamic acid 1-benzyl ester (Table 2.1) was used as the internal standard (IS) and dissolved at a concentration of 100 µg/mL. The stock solution was prepared by first dissolving the IS in pure methanol, then adding MilliQ-water to reduce the methanol (Table 2.1) content to 2% by volume. This stock solution was stored at room temperature because precipitates were observed after thawing a frozen stock solution. RMD was dissolved at 10 mM in dimethyl sulfoxide (Table 2.1). Solutions containing 50 µg/mL I.S., but different concentrations of romidepsin: 0.5, 5, 50, 100, 250, 400 and 500 µg/mL, were prepared by serial dilution. These samples were run in triplicate with HPLC in isocratic mode, using a run time of 120 minutes. A concentration of 50 ng/mL RMD was observed to be the limit of detection. RMD and the IS had retention times of around 45 and 75 minutes, respectively. Chromatograms were plotted in Origin software (version 2019b), using the absorption at a wavelength of 215 nm as a function of

time. The area under the curve (AUC) of both the romidepsin and IS peaks was determined using the 'Peak Analyzer' user interface in Origin's 'Analysis' menu. The interactive modes of this user interface were used to select the relevant peaks manually. The ratio's $AUC_{RMD}/AUC_{I.S.}$ were calculated for all measurements. The average ratio's (with standard deviation) were plotted as a function of the known concentration of romidepsin in the samples. Using the 'Linear Fit' in the 'Analysis' menu of Origin, Linear regression of the data points gave a good (R^2 = 0.99) linear fit through the seven data points (see Figure 2.3), with equation y = 0.06895x – 0.01007.

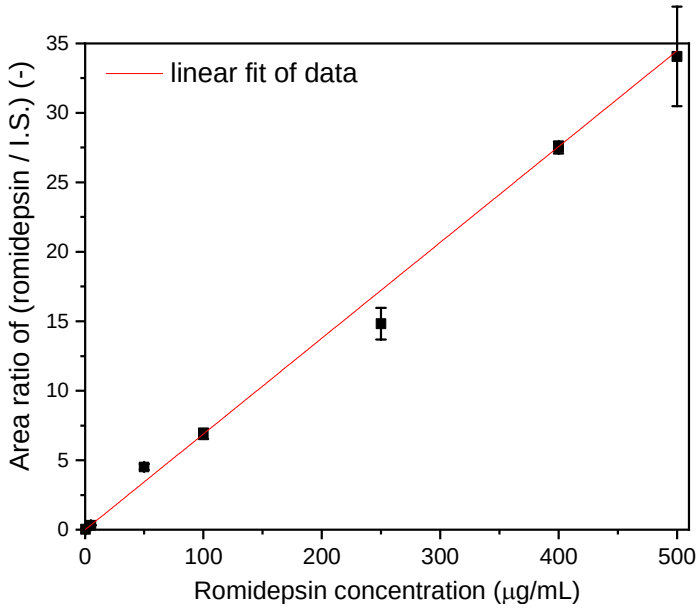

Figure 2.3 Calibration curve obtained from HPLC-runs with the romidepsin (RMD) / IS (Internal standard).

Peak area ratio as a function of the concentration of romidepsin in the samples (IS was constant at 50 µg/mL). Error bars represent the standard deviations from three separate measurements**.**

3. Determination of the romidepsin concentration in supernatant samples

The calibration curve (see above) was used to determine the unknown concentration of romidepsin in supernatant samples following the drug loading of nanoparticles. The supernatant samples were taken at time

points of 6 hours and 24 hours after loading nanoparticles with sizes of 100 nm and 400 nm with RMD. Since the drug loading was performed in DMSO, the samples were diluted four times or six times with MilliQ-water and spiked with 50 µg/mL IS prior to the HPLC runs. After the HPLC runs, the absorbance at 215 nm was plotted as a function of time (see Figure 2.4 for representative example), and the areas of the RMD and IS peaks were determined using Origin software as described above. The areas of the romidepsin peaks were multiplied with the dilution factor (4 or 6) to compensate for the dilution as mentioned earlier step. Subsequently, the area ratios of $AUC_{RMD}/AUC_{I.S.}$ were calculated and used (as 'y') to solve the equation y = 0.06895x – 0.01007 for x, thereby resulting in the concentration of the romidepsin (in µg/mL) that was present in the supernatant samples. Two of these samples were run in triplicate to determine the typical standard deviation of these measurements, which was ~ 2 µg/mL.

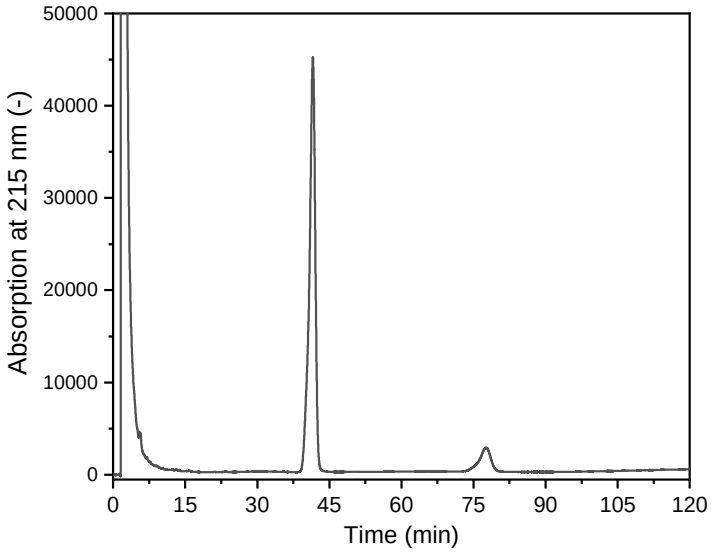

Figure 2.4 Chromatogram of a supernatant sample that was obtained six hours after loading nanoparticles of 100 nm in size.

Before the HPLC run, the sample was diluted fourfold and spiked with IS at 50 µg/mL. The peaks correspond to dimethyl sulfoxide (~ 5 min.), romidepsin (~ 40 min.), and IS (~ 75 min).

4. The release kinetics of romidepsin from 400 nm PMA_{SH} loaded particles RMDLNP

The calibration curve (Figure 2.3) was used to determine the unknown concentration of RMD while being released from nanoparticles. The drug release was studied in PBS for nanoparticles in the presence and absence of 5 mM glutathione, and samples were taken at multiple time points. Before the HPLC runs, the samples were diluted two times with MilliQ-water and spiked with 50 µg/mL IS. Whereas for previous runs (Figure 2.3), injection volumes of 20 µL were used, larger injection volumes were used in this series because of the anticipated lower concentrations of romidepsin in the samples, up to a maximum of 100 µL. After the HPLC runs, the absorbance at 215 nm was plotted as a function of time. For the four samples in which romidepsin was observed (see Figure 2.5 as an example), the areas of the romidepsin and IS peaks were determined using Origin software as described previously. The areas of the romidepsin peaks were multiplied by two to account for the dilution step. Subsequently, the area ratios of $AUC_{RMD}/AUC_{I.S.}$ were calculated and used (as 'y') to solve the equation y = 0.06895x – 0.01007 for x, thereby resulting in the concentration of romidepsin (in µg/mL) that is present in the samples obtained during the drug release experiment.

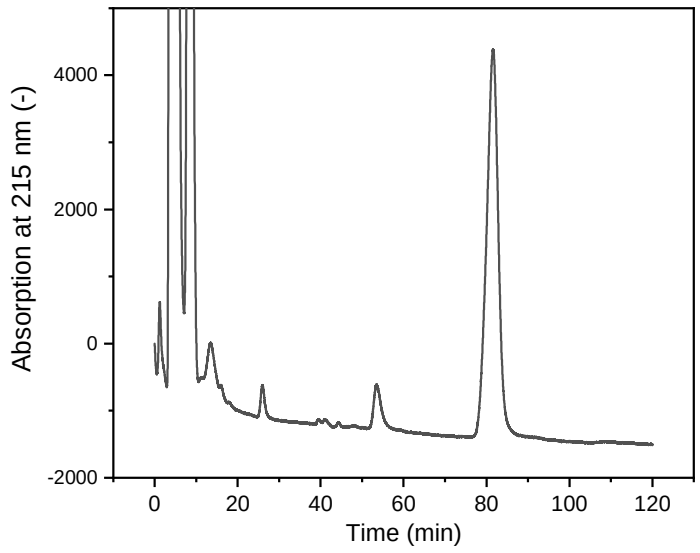

Figure 2.5 Chromatogram of a sample that was obtained four days after starting the romidepsin release experiment.

Before the HPLC run, the sample was diluted twice and spiked with IS at 50 µg/mL. The peaks correspond to glutathione (~ 5 min.), romidepsin (~ 50 min), and IS (~ 80 min).

2.2.25 2.2.25 Efficacy and cytotoxicity of RMD loaded particles in J-Lat cells A2 cells

Efficacy of formulations was measured simultaneously with the cytotoxicity study using propidium iodide (PI) cell viability assay and percentage of GFP cells measured by flow cytometry to indicate formulations reactivation potency.

J-Lat Tat-IRES-GFP (Table 2.4) were seeded at a concentration of 0.2×10^6 per well in a 96-well U bottom culture plate. Cells were maintained in RF10 cell culture media as described earlier and incubated at 37°C and 5% CO_2 humidified atmosphere. Cells were treated with free drug RMD or RMDLNP-formulations at different concentrations for continuous incubation of 48 hours and 72 hours or 4 hours pulse-wash treatment, followed by 48-and 72 hours continuous incubation. At the specified time, cells were washed three times with PBS to wash off free RMD or remove unbound RMDLNPs. Cells were incubated with viability PI cell stain for 15 minutes at room temperature. Cells were taken to flow cytometry analysis immediately. Flow cytometry analysis was performed on a BD Fortessa II, and data were analysed using FlowJo V10.2 and FCS express.

2.2.26 Efficacy of RMD loaded particles in J-Lat 10.6 cells

J-Lat 10.6 containing full-length HIV provirus (Table 2.4) were seeded at a concentration of 0.2×10^6 per well in a 96-well U bottom culture plate. Cells were maintained in RF10 cell culture media as described earlier and incubated at 37°C and 5% CO_2 humidified atmosphere. Cells were treated with free drug RMD or RMDLNP-formulations at different concentrations for continuous incubation of 48 hours, 72 hours and 96 hours or 4 hours pulse-wash treatment, followed by 48 hours, 72 hours and 96 h continuous incubation. At the specified time points, cells were washed three times with PBS to wash off free RMD or remove unbound RMDLNPs, and a 50 µL aliquot was taken for CellTitre-Glo luciferase (Table 2.5) cytotoxicity assay.

For reactivation assay, cells were fixed with 1% paraformaldehyde for 15 mins and rinsed twice in PBS before resuspending in 100 µL FACS WASH (PD + 1% FBS), transferred into FCAS tube and stored at 4 ◦C and protected from light until analysed on LSR Fortessa II (Table 2.3). Data were analysed using FCS Express 9 (Table 2.3).

2.2.27 Cytotoxicity assay

Cytotoxicity of free drug RMD and RMD loaded particles were tested using CellTitre-Glo cytotoxicity assay. The collected 50 ul of J-Lat 10.6 lysate containing approximately 50,000 cells were incubated with CellTitre-Glo luminescent cytotoxicity assay reaction buffer following the manufacturer's protocol (Table 2.5). After 10 minutes of incubation at room temperature, cells viability was immediately analysed. The colourimetric results were quantified using a microplate luminometer reader (Table 2.3) with an optimised gain setting for each condition.

2.2.28 Glycogen oxidation

100 mg of glycogen (corresponding to 0.6 mmol of glucose monomers) from bovine liver (Table 2.1) was dissolved into 5mL of 0.6 M acetic buffer (Table 2.1) (pH 5.5) with stirring in the dark. For 15 % glycogen modification, 20 mg of sodium periodate $NaIO_4$ (Table 2.1) was added to the above solution and incubated in the dark at 4◦C for 2 hours under continuous stirring conditions. To obtain 15 % modification, the added amount of $NaIO_4$ added was calculated using the following formula,

$$m_{NaIO_4} = n_{NaIO_4} \cdot M_{NaIO_4}$$

Where:

$$n_{NaIO_4} = \frac{modification\,\% \cdot n_{glucose\ monomers}}{100}$$

M = molar mass

m = mass of substance (in grams)

n = number of moles of substance

2.2.29 Reductive amination

27.8 mg of ethylenediamine (EDA) (Table 2.1), followed by 27.8 mg of sodium cyanoborohydride $NaBH_3CN$ (Table 2.1), was dissolved in the above solution. The pH was adjusted to 5.5, and then the solution was incubated overnight under continuous stirring conditions. The amount of ethylenediamine EDA and sodium cyanoborohydride $NaBH_3CN$ added to the oxidated glycogen was calculated using the following equations,

Weight of EDA = $n_{NaBH_3CN} = 10 \cdot n_{NaIO_4}$)

Weight of $NaBH_3CN$ = ($n_{EDA} = 5 \cdot n_{NaIO_4}$)

Where

M = molar mass

m = mass of substance (in grams)

n = number of moles of substance

2.2.30 Purification

The final 15 % EDA modified glycogen product was purified by dialysis (tube size14 kDa MWCO) against Milli-Q water for 3 days (6 times water change) and then freeze-dried.

2.2.31 Yield

80 % degree of substitution of modified glycogen (BG-$_{EDA}$) was determined by Nuclear Magnetic Resonance **(**NMR): 1H NMR (400 MHz, D2O, 78 C) d (ppm): 5.316 (s, 0.8H, H1-4), 5.11 (s, 0.05H, H1-4'), 4.99 (s, 0.1H, H1-6'), 4.91 (s, 0.04H. H1-6), 4.16e3.44 (m, 11H, H2, H3, H4', H5), 3.38 (t, J ¼ 8 Hz, 0.1H, H4), 3.26e2.41 (m, 1.65H, HA, HB).

2.2.32 Fabrication of glycogen-ethylenediamine (BG-$_{EDA}$) nanoparticles (NPs)

Glycogen (100 mg, corresponding to 0.6 mmol of glucose monomers) from bovine liver (bovine glycogen BG) was dissolved in 5mL of 0.6M acetic buffer (pH 5.5) (Table 2.1) with stirring to ensure proper dissolving (vortex and sonicate if necessary). Sodium periodate (26 mg, 0.12 mmol) (Table 2.1) was added and reacted in the dark. After two h, 36 mg of ethylenediamine (Table 2.1) (EDA; 0.6 mmol) was added, followed by ten

eq. of sodium cyanoborohydride to 76 mg of sodium periodate (1.2 mmol) (Table 2.1), and the mixture was stirred overnight. The product was purified by dialysis (tube size 10 kDa) against Milli-Q water for three days (6 times changed) and freeze-dried.

2.2.33 Synthesis of 5'triphosphate double-strand RNA

The 3p dsRNA, RIG-I agonist (RIG-I A) [sequence: Sense Oligo (5′-TTGTAATACGACTCACTATAGGGACGCTGACCCAGAAGATCTACTAG AAATAGTAGATCTTCTGGGTCAGCGTCCC3′) and dsRNA, Control ligand (Ctr ligand) antisense oligo (5′GGGACGCTGACCCAGAAGATCTACTATTTCTAGTAGATCTTCTGGG TCAGCGTCCCTATAGTGAGTCGTATTACAA-3′) (516) (Table 2.1) was generously synthesised and provided by the laboratory of prof. Martin Schlee at the Universitätsklinikum Bonn, Germany (516).

2.2.34 Complexation of BG-$_{EDA}$-3p dsRNA complexes for *in vitro* investigation

The modified bovine glycogen NPs, BG-$_{EDA}$ was synthesised as described above. The synthesised was diluted into Dulbecco's phosphate buffer saline (D-PBS) (ph. 7.2, 30 mM) (Table 2.1) to a final concentration of 10 mg mL^{-1}. This stock was further diluted to 0.5 mg mL^{-1} in PBS and rapidly mixed with either 3p dsRNA (RIG- A) or dsRNA (Ctr ligand) at different weight (w/w) ratios BG-$_{EDA}$: 3p/dsRNA between 1:1 6: 1, incubated at room temperature for 15 min. The formed complexes were further diluted into RF10 media and used immediately.

2.2.35 BG-$_{EDA}$ -3p/dsRNA complexes characterisation

BG-$_{EDA}$-3p/dsRNA constructs were mixed with OH-RNA as detailed above. The construct was monitored using 10 % tris-borate-EDTA (TBE) polyacrylamide gel electrophoresis (Table 2.1). Samples were prepared as follows: 500 ng/µL was mixed with BG-$_{EDA}$ at weight ratios (w/w 5: 1 and 6: 1). The prepared samples were allowed to equilibrate for 15 min at room temperature, and 2 µl of nucleic acid loading buffer (Table 2.1) was added to each sample. Then, 10 µl of each sample was loaded onto the gel and

ran in protein gel electrophoresis chamber for 30 min at 90 V. dsRNA retardation was evaluated by staining the gel with SYBR Gold reagent (Table 2.5) for 25 min and imaged using a digital ChemiDoc XRS þ Imaging System (Table 3).

2.2.36 THP-1-Dual NF-κB and type I IFN reporter cell line assay

THP-1-Dual cells stably express A nuclear factor κB (NF-κB)–inducible secreted alkaline phosphatase (SEAP) gene and an IFN regulatory factor (IRF) inducible Lucia luciferase reporters (517), (Table 2.4). Cells were seeded at 2 X 10^5 cells per well in a 96-well U bottom plate. Cells were then incubated with 500 ng/mL BG_{EDA}-RIG-I A, BG_{EDA}-Ctr ligand, BG_{EDA} only, RIG-I A, Ctr ligand, or transfected with lipofectamine 2000 (Table 2.1) as a positive control. The supernatant was collected after 24 hours and 48 hours to measure SEAP (NF-κB activity) and luciferase (IRF activity). QUANTI-Luc (Table 2.5) was used to detect the level of luciferase by adding to culture supernatant and reading immediately with a microplate luminometer reader at a 0.1-s reading time. QUANTI-Blue (Table 2.5) was used to detect the level of secreted embryonic alkaline phosphatase (SEAP) by adding to culture supernatant and incubating for 1-3 hours and reading with a microplate luminometer reader at 619 nm.

2.2.37 Stimulation and quantification of type IFN in human PBMC and primary $CD4^+$ T cells using HEK-Blue-α/β reporter assay

Thawed primary $CD4^+$ T cells were seeded at 3 X 10^5 cells per well in a 96-well U bottom plate. Cells were activated for 2 days, then human PBMC and primary $CD4^+$ T cells were challenged with BG_{EDA}-RIG-I A, BG_{EDA}-Ctr ligand or transfected with Sendai virus (Table 2.1) as the positive control for 1 and 3 days. The day after, HEK-Blue-α/β (518) (Table 2.4) were plated at 5 X 10^4 cells per well in a 96-well flat-bottom plate (Table 2.2). The following day, supernatant from stimulated and SeV infected cells (or control cells) was added, and a standard curve was generated in parallel by serial dilutions of Human IFN-α2a recombinant protein (Table 2.1) added in complete DMEM10 media. Post 16-20 h of incubation, 50 µL of HEK-Blue IFN-α/β supernatants was added to 150 µL of Quanti-blue substrates (Table

2.5) and incubated at 37°C, CO_2 humidified environment for 15-30 min. Absorbance was measured at 619 nm using a microplate luminometer reader. The standard curves were used to provide semiquantitative analyses of the IFN concentrations produced by the stimulated cells.

2.2.38 Quantification of apoptosis by flow cytometry assay

In order to study cell death in primary $CD4^+$ T cells, annexin V (AxV, Table 2.5) and propidium iodide (PI, Table 2.5) double staining have been used in flowcytometric analyses. AxV signal (AxV^+/PI^-) provides a sensitive method for detecting early apoptosis, while PI signal (AxV^-/PI^+) corresponds to late apoptosis or necrotic, apoptotic cells. Cells were harvested, washed twice with AxV buffer (Table 2.1). cells were stained with AxV (1:100 dilution) and PI (1:2000 dilution) and incubated on ice for 10 minutes with protection from light. Cell death kinetics was measured immediately using an LSR Fortessa II. The proportion of AxV^-/PI^- AxV^+/P^-, AxV^-/PI^+ or AxV^+/PI^+ cell population were analysed using FCS Express 9.

2.2.39 Statistical analysis

All statistical analyses were performed using GraphPad Prism software version 9, in which two-tailed, unpaired T test was used to compare experiments. The small sample size precluded the use of non-parametric tests. Therefore, parametric unpaired T tests were used. A P-value below 0.05 was considered significant, were used throughout.

3 The role of size and surface charge in cellular uptake of nanoparticles by CD4+ T cells for the elimination of HIV latency

3.1 INTRODUCTION

One promising nanoengineered particle system is the thiolated poly (methacrylic acid) mesoporous core-shell particle system, generated using the layer-by-layer (LbL) assembly technique (487). Synthesis of colloidal nanostructured materials using the LbL technique to fabricate shell materials involves the layered deposition of interacting polymers poly (methacrylic acid) (PMA) and polyvinylpyrrolidone (PVPON) on silica core template, representing a stable and highly versatile approach to formulate particles (487). PMA can be modified with thiol groups (PMA_{SH}) to allow cross-linking by disulphide linkages between PMA_{SH} layers (487, 492).

The physicochemical properties of PMA_{SH} particles, including size and surface charge, are essential parameters that can influence their internalisation into mammalian cells and improve delivery efficacy (446). Additionally, these properties can significantly modulate the fate of nanoparticles *in vivo* as they face multiple potential sites of clearance by immune cells (513, 519–521). There have been limited *in vitro* and *ex vivo* studies on the uptake of PMA_{SH} particles in T cells (513). To assess PMA_{SH} particle biodistribution in T cells, precise quantification of how particles and target cells interact is pivotal. However, there is currently no appropriate assay to quantify these interactions, including accurate measurement of cellular uptake of nanoparticle systems. The analytical techniques employed to measure nanoparticle association with cells are quite diverse and broad (522–524). This includes imaging flow cytometry (525, 526), laser

scanning microscopy (526), inductively-coupled mass spectrometry (ICP-MS) (527), mass cytometry(528), and flow cytometry (453, 529, 530).

Based on these observations, we hypothesised that the size and surface charge of PMA_{SH} particles would influence association with T cells. To test this hypothesis, we fabricated PMA_{SH} particles using the LbL technique with varying sizes, from 100 nm to 1 µm. In addition, particles were surface modified to neutral or positive charge using poly (ethylene glycol) (PEG) and poly-L-lysine (PLL), respectively. The interactions of particles with T cells were examined and quantified using confocal laser microscopy combined with image analysis software ImageJ (512). Additionally, to compare the effect of charge, we studied different particles (400 nm of PMA_{SH}, PMA_{SH}-PEG and PMA_{SH}-PLL) and their distribution *ex vivo* and assessed their association pattern with immune cells in human peripheral blood mononuclear (PBMC) and whole blood.

3.2 RESULTS

3.2.1 Synthesis and characterisation of different sizes and charges of a PMA_{SH} engineered particle delivery system

We synthesised varying sizes (100 nm, 400 nm, 800 nm and 1 µm) of PMA_{SH} particles via the deposition of thiolated PMA_{SH} and PVPON onto mesoporous silica (MS) particles to form PMA-based core-shell particles. The interaction between thiolated PMA_{SH} and PVPON promoted hydrogen bonding. Controlled oxidation of thiol groups (pH 4.0) allowed for bridging disulphide linkages in the PMA_{SH}. Altering the solution pH to 7.0 induced the release of PVPON, resulting in negatively charged PMA_{SH} particles that were held together via biodegradable disulphide bridges. Degradation of PMA_{SH} particles was facilitated in the presence of a physiological concentration of thiol group oxidation agents (Glutathione, GSH) through cleavage of the disulphide bonds (490) (Figure 3.1).

To systematically modulate the surface charge of PMA_{SH} particles to neutral, we electrostatically incorporated onto the negatively charged PMA_{SH} shell methoxy-poly (ethylene glycol)-block-poly-L-lysine hydrochloride (mPEG5K-b-PLKC50) that contained a poly-L-lysine

hydrochloride section and non-reactive poly (ethylene glycol) (PEG) section (PMA_{SH}-PEG). Separately, PMA_{SH} particles were coated by the positively charged synthetic poly amino acid poly-L-lysine hydrochloride (PLKC50/250) to form positive surface charged particles (PMA_{SH}-PLL) (Figure 3.1). The successful PEGylation and PLL coating of PMA_{SH} particles were confirmed using dynamic light scattering (DLS) analysis and zeta potential measurements. The physicochemical properties were determined as the size by intensity and Z average of the engineered particles by DLS. The polydispersity index (PDI) and the resulting Zeta potential measurement of the particles are shown in Table 3.1. DLS measurement of the synthesised PMA_{SH} particles (~ 431 nm) and functionalised PMA_{SH}-PEG (~ 436 nm) and PMA_{SH}-PLL (~ 441 nm) particles were almost all monodispersed with a single size distribution as shown in Figure 3.2 C. These results confirm that we had produced a single sized homogeneous nanoparticle. The surface charge of PMA_{SH}-PEG and PMA_{SH}-PLL particles was assessed and showed a neutral and positive zeta potential, respectively (Figure 3.2). These data indicate that both particles were successfully coated with PEG and PLL.

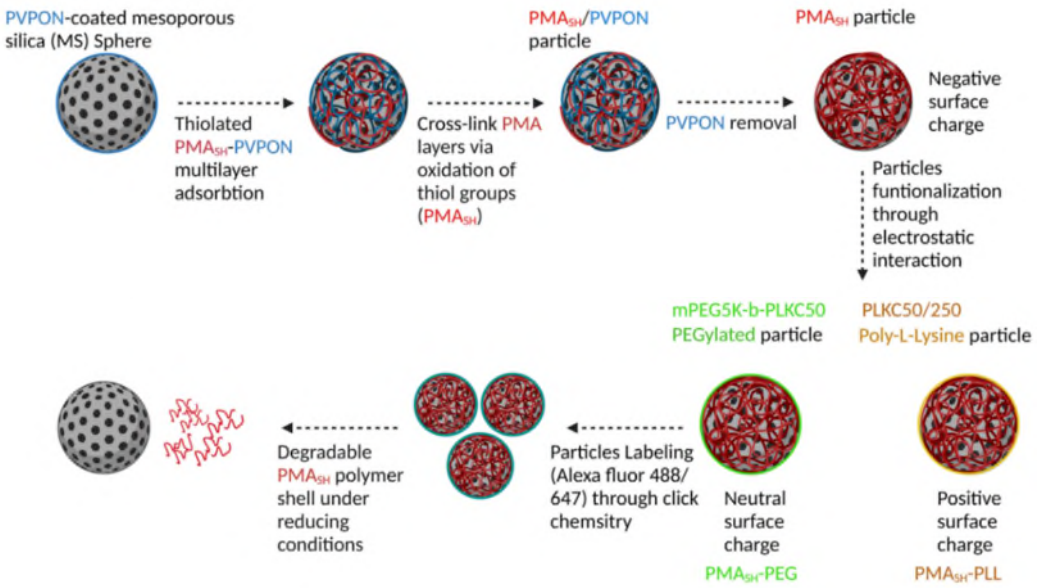

Figure 3.1 Schematic illustration of layer-by-layer (LbL) synthesis and surface modification of PMA_{SH} particles

PMA_{SH} nanoparticles were synthesised by the layering of interacting polymers PMA_{SH} and PVPON over mesoporous silica. The PMA_{SH} layers

were crossed-linked at pH 4.0 via disulphide bonds between thiol groups present on the PMA_{SH} molecules. Finally, PVPON layers were removed to form the final product of PMA_{SH} particles. Deposition of the copolymers mPEGG5-PLKC5 block and PLKC50/250 polymers onto the particle surface to induce neutral and positive charge, respectively. Fluorescent labelling of nanoparticles was performed by binding the dye to amine groups on the surface of particles.

Table 3.1 Physiochemical characterisation of multilayered PMA_{SH}, PMA_{SH}-PEG and PMA_{SH}-PLL particles measured by DLS and zeta potential.

Particles were measured in Milli-Q water for size and Z potential measurement. There was a slight increase in size measurements of PMA_{SH}-PEG and PMA_{SH}-PLL compared to PMA_{SH} particles. ND not determined. Data represent ± standard deviation (SD) from two independently formulated batches and three independent measurements.

Particle	Surface modified	Coating material (polymer outer layer)	Size (d.nm)	Polydispersity Index[a]	Zeta potential (mV)[b]
PMA_{SH} 100 nm	No	PMA_{SH}	119	ND	-37
PMA_{SH} 400 nm	No	PMA_{SH}	428	0.08 ± 0.01	-38
PMA_{SH} 800 nm	No	PMA_{SH}	814	0.2 ± 0.7	-38
PMA_{SH} 1 µm	No	PMA_{SH}	1026	0.3 ± 0.04	-40
PMA_{SH}-PEG 100 nm	Yes	mPEG5K-b-PLKC50	122	ND	+6
PMA_{SH}-PEG 400 nm	Yes	mPEG5K-b-PLKC50	429	0.4 ± 0.2	+4
PMA_{SH}-PEG 800 nm	Yes	mPEG5K-b-PLKC50	822	0.2 ± 0.1	+7
PMA_{SH}-PEG 1 µm	Yes	mPEG5K-b-PLKC50	1038	0.4 ± 0.05	+10
PMA_{SH}-PLL 100 nm	Yes	PLKC50/250)	121	ND	+29
PMA_{SH}-PLL 400 nm	Yes	PLKC50/250	434	0.3 ± 0.7	+26
PMA_{SH}-PLL 800 nm	Yes	PLKC50/250	826	0.6 ± 0.3	+23
PMA_{SH}-PLL 1 µm	Yes	PLKC50/250	1049	0.5 ± 0.01	+27

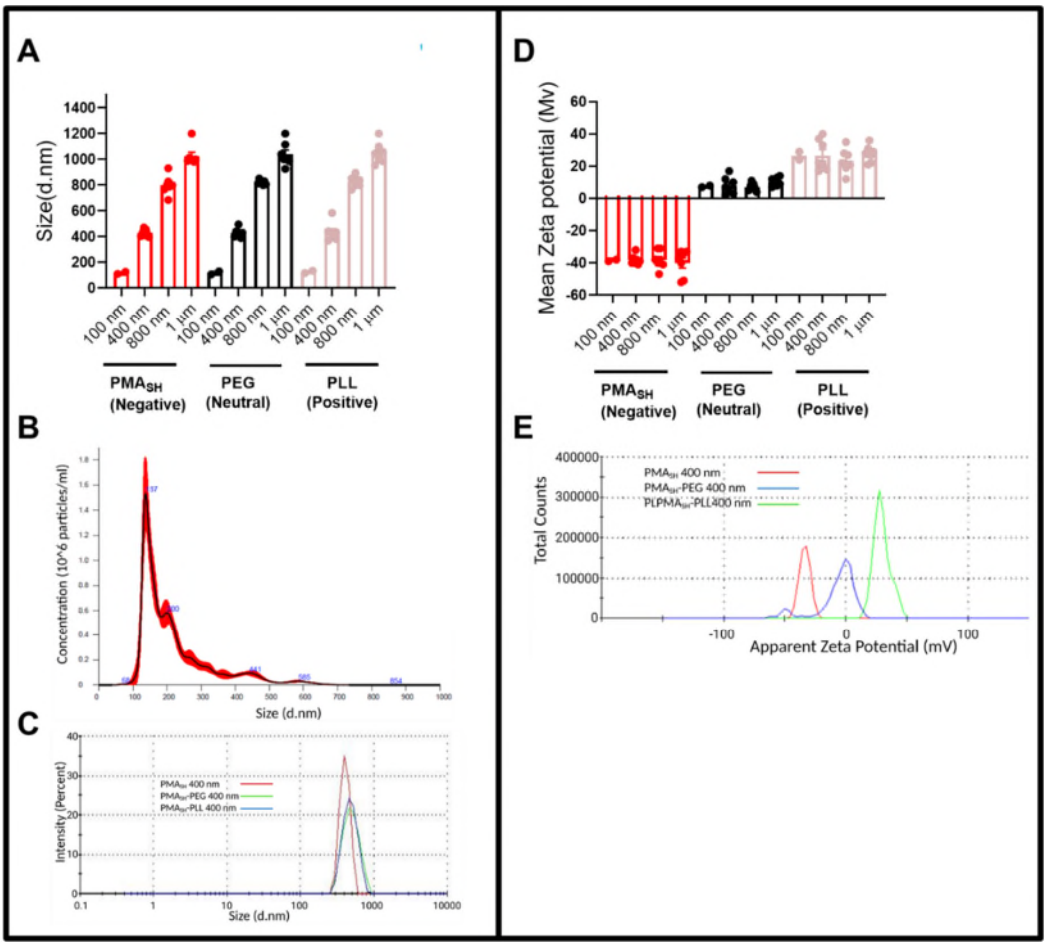

Figure 3.2 Characterisation of PMA$_{SH}$, PMA$_{SH}$-PEG and PMA$_{SH}$-PLL particles.

A) Size distribution of PMA$_{SH}$, PMA$_{SH}$-PEG and PMA$_{SH}$-PLL particles were measured by dynamic light scatter (DLS). B) Representative graph of the average size distribution and concentration of monodispersed PMA$_{SH}$ 100 nm particles measured by nanoparticle tracking analysis (particles ≤ 100 nm) capturing three videos of 60 seconds per measurement with a camera focus of -15 to +15 and camera lever 11. The red curve represents the standard deviation obtained from multiple measurements. The blue numbers indicate the mean of nanoparticles size in the sample. C) Representative graphic of size measurement of PMA$_{SH}$ [red, 431 nm], PMA$_{SH}$-PEG [green, 436 nm] and PMA$_{SH}$-PLL [blue, 441 nm] as measured by DLS. D) Zeta potential of the dispersed particles surface charge using micro electrophoresis. E) Representative graph of the Zeta potentials for PMA$_{SH}$ [Red, -36 mV], PMA$_{SH}$-PEG [Blue,+4 mV] and PMA$_{SH}$-PLL [Green,

+32 mV] measured by micro electrophoresis. Error bars indicate ± standard error of the mean from seven independently formulated batches [except 100 nm, two independent batches] and three independent measurements. (SEM; N = 2 and 7).

3.2.2 Size and surface charge properties of untargeted PMA_{SH} particles influence interaction with T cells

We next focused on the effect of size and surface charge on association with T cells. Fluorescent labelled (Alexa Fluor 488; AF488) particles of 400 nm, 800 nm and 1 μm in diameter carrying three distinctly different surface charges (negative, PMA_{SH}; neutral, PMA_{SH}-PEG; and positive, PMA_{SH}-PLL) were incubated at a 200:1 ratio of particles to cells with the TZM-bl cell line, Jurkat T cell line and primary $CD4^+$ T cells for 24 hours (Figure 3.3 A). The TZM-bl is a HeLa cell line with strong endocytic properties and was used as a positive control. We incubated particles with cells for 24 hours to minimize the effects of cellular proliferation. Additionally, we wanted to eliminate the possibility of particles recycling after binding or internalisation as the turnover time of most mammalian cells is greater than 24 hours (531). Evidence of particle-cell association was quantified using flow cytometry (the term particles association referred to particles that are bound to the cell membrane and internalized particles). The gating strategy was applied to discriminate cells, single cells and cells that are positive for particles (AF 488) (Figure 3.3 B).

Irrespective of the size and surface charge, all particles are associated highly with the TZM-bl cell line [mean = upper range 88.4 % and lower range 58%] (Figure 3.4 A). In addition, we observed a reduction in association of 800 nm PMA_{SH}-PLL [mean = 39%] (Figure 3.4 A), which we theorised might be due to particle aggregation. We observed a higher association of particles with the TZM-bl cell line, which may be explained by their endocytic properties and the fact that they are adherent, allowing for enhanced uptake as particles tend to settle on the cell surface due to gravity.

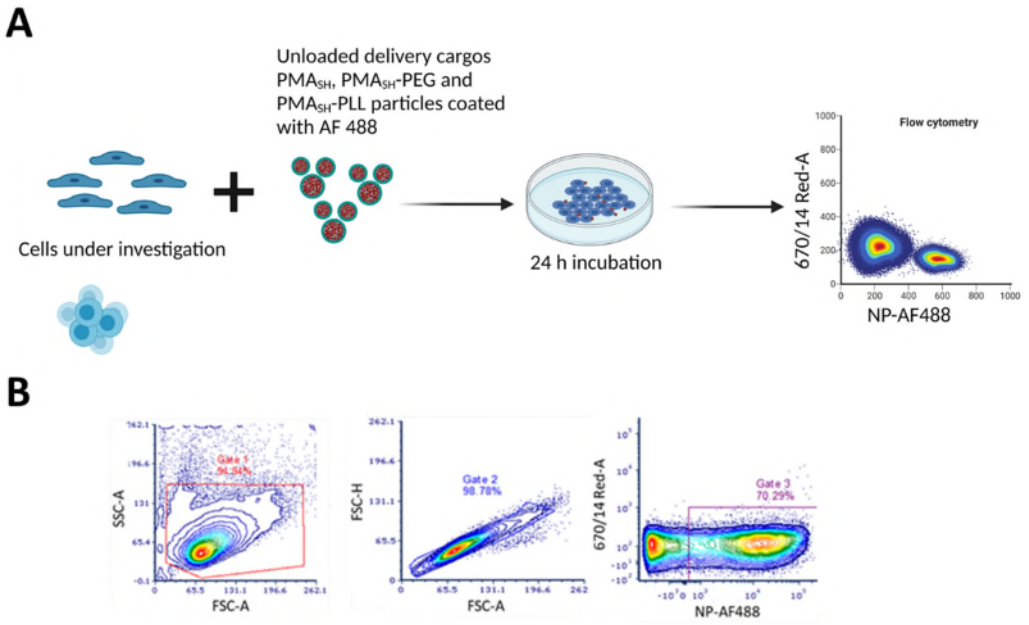

Figure 3.3 Effect of size and surface charge on particle association with cells.

(A) Schematic illustration showing the cell line of interest (TZM-bl cell line, Jurkat cell line or primary CD4$^+$ T cells) co-incubated with AF488-labelled 400 nm, 800 nm or 1 µm, PMA$_{SH}$, PMA$_{SH}$-PEG or PMA$_{SH}$-PLL particles (NP-AF488). Cells were exposed to particles in a ratio of 200:1 particle: cell for 24 hours at 37˚C before particles association to cells were examined by flow cytometry. (B) representative flow cytometry plots showing gating strategy for identifying single cells associated with AF488 labelled particles.

In contrast, in both T cell models, i.e., Jurkat cells and primary CD4$^+$ T cells, we observed different patterns of association. In the Jurkat T cell line, irrespective of size, negatively charged PMA$_{SH}$ particles were highly associated with cells compared to their counterparts of PMA$_{SH}$-PEG and PMA$_{SH}$-PLL (Figure 3.4 B). Irrespective of surface charge, we observed that 400 nm particles showed a similar or higher association with Jurkat cells compared to larger particles of 800 nm and 1 µm particles (Figure 3.4 B). We also observed that the smaller 400 nm PMA$_{SH}$ particles were highly bound to cells (mean = 94.4 %) compared to other particle sizes of PMA$_{SH}$, PMA$_{SH}$-PEG and PMA$_{SH}$-PLL (Figure 3.4 B). Interestingly, we observed substantially increased association of 400 nm negatively charged PMA$_{SH}$ particles (mean = 94.4 %) compared to 400 nm neutral PMA$_{SH}$-PEG [mean

= 66.2 % , p = 0.0501, unpaired t test] or 400 nm positive PMA_{SH}-PLL [mean = 62.1 %, p = 0.081, unpaired t test] (Figure 3.4 B).

In primary $CD4^+$ T cells, we observed a similar trend of association. Negatively charged PMA_{SH} particles were highly associated with cells compared to PMA_{SH}-PEG and PMA_{SH}-PLL (Figure 3.4 C). Overall, in $CD4^+$ T cells, size also mattered. The smaller size 400 nm PMA_{SH} particles had the strongest association to cells (mean = 72.1 %) than PMA_{SH}-PEG [mean = 35.7 %, p = 0.0247, unpaired t test] and PMA_{SH}-PLL [mean = 31%, p 0.0358, unpaired t test] (Figure 3.4 C).

In summary, size and surface charge mattered for the PMA_{SH} nanoparticle drug delivery system to associate with T cells. In both T cell models, the negatively charged PMA_{SH} particles 400 nm showed greater association than neutral and positively charged particles of the same size.

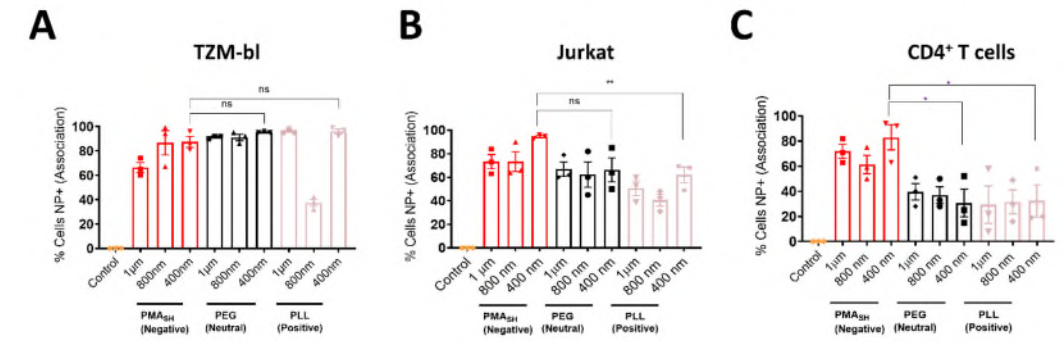

Figure 3.4 Quantification of association between different PMA_{SH} particles and TZM-bl, Jurkat cell lines and primary $CD4^+$ T cells.

Three different sized particles, 400 nm, 800 nm and 1 µm and three different charges negative PMA_{SH} [red], neutral PMA_{SH}-PEG [black] and positive PMA_{SH}-PLL [pink] were assessed using flow cytometry as described in Figure 3. The percentage of nanoparticles associated with a cell is shown for A) TZMbl cells, B) Jurkat cells, and C) primary $CD4^+$ T cells. All data are shown as the mean ± standard error of the mean of three independent experiments (SEM; N = 3). All P values were determined using a two-tailed, unpaired T test: *P<0.05 **P<0.01, and ns=not significant. Only comparison with PMA_{SH} 400 nm particles is shown.

3.2.3 Quantification of untargeted PMA_{SH}, PMA_{SH}-PEG and PMA_{SH}-PLL particles with T cells using Confocal Laser Scanning Microscopy image analysis (CLSM)

Disulphide-stabilised PMA_{SH} particles rely on intracellular reductive enzymes to oxidise the disulphide bonds on the particle shell and deliver loaded cargo into targeted cells (489, 490). Non-phagocytic T cells strictly control the entry of molecules (e.g. proteins and nanoparticles) from the extracellular environment (423). One mechanism that plays an essential role in receptor-mediated endocytosis is clathrin-dependent endocytosis. Smaller molecules (up to 300 nm) use this pathway for cellular uptake (532). In addition, particle size and the surface charge may also influence the uptake into T cells. We previously showed that 400 nm negatively charged PMA_{SH} particles exhibited a higher association with T-cells compared to other sizes or neutral and positively charged particles (Figure 3.5 A-C).

To confirm these findings, we next employed a confocal laser scanning microscopy image analysis (CLSM)-based approach coupled with ImageJ® software to distinguish between bound and internalised particles associated with T cells. In addition, multiple Z stacks images were taken to examine the presence of associated particles on the cell surface or within cells

We first quantified particle internalisation in an adherent cell line with endocytic properties (TZM-bl cell line) and T cells (Jurkat cell line and primary $CD4^+$ T cells). In the TZM-bl cell line, the confocal microscopy image data indicated that a mean value of 90% of cells were associated with particles irrespective of size and surface charge (Figure 3.5 A). The smaller sized particles (i.e., 400 nm PMA_{SH}, PMA_{SH}-PEG and PMA_{SH}-PLL) showed a slight decrease in internalisation events [mean = 73 %, 70 % and 65 %, respectively] compared to the larger particles (i.e., internalisation of PMA_{SH}, PMA_{SH}-PEG and PMA_{SH}-PLL for 800 nm with a mean value of 81 %, 79 % and 72 %; and for 1 μm were 79 %, 77 % and 85 %, respectively (Figure 3.5 A). These observations reflect that the endocytic properties of the TZM-bl cell line. Additionally, the endosomal recycling pathway is likely dependent on particle size, where smaller particle sizes may recycle back to the host membrane. This phenomenon may likely contribute to the

underestimation of internalized smaller particles compared to larger particles (533).

In contrast, assessment of particle association with the non-phagocytic Jurkat T cell line revealed that irrespective of size, PMA_{SH} particles were more highly associated with Jurkat cells compared to PMA_{SH}-PEG and PMA_{SH}-PLL particles (Figure 3.5 B). Further to this, the 400 nm PMA_{SH} particles showed the greatest internalization with a mean value of 24 % compared to negligible internalisation of 800 nm and 1 µm PMA_{SH} particles [p = 0.0126 and 0.0129 respectively, unpaired t test] (Figure 3.5 B). Interestingly, 400nm PMA_{SH} particles exhibit higher internalisation percentage with a mean value of 24 % compared to 400nm PMA_{SH}-PEG (mean = 4 %) [p = 0.0438, unpaired t test] and 400 nm PMA_{SH}-PLL (mean = 4 %) [p = 0.0465, unpaired t test] (Figure 3.5 B).

A similar trend of particle association was observed in non-phagocytic isolated $CD4^+$ T cells. All sizes of PMA_{SH} particles are highly bound to $CD4^+$ T cells compared to their counterparts of PMA_{SH}-PEG and PMA_{SH}-PLL (Figure 3.5 C). In addition, a mean value of 12.3 % of 400 nm PMA_{SH} particles internalized in $CD4^+$ T cells, while 800 nm and 1 µm of PMA_{SH}-PEG and PMA_{SH}-PLL never entered cells (Figure 3.5 C). remarkably, we observed reasonable efficient internalization of 400 nm PMA_{SH} particles (mean= 12.3 %) into $CD4^+$ T cells compared to 400 nm particles of PMA_{SH}-PEG and PMA_{SH}-PLL (3 % and 2 % respectively) [p = 0.0239 and 0.0191 respectively, unpaired t test] (Figure 3.5 C).

Finally, we identified aggregation of PMA_{SH}-PLL and, to a lesser degree, PMA_{SH}-PEG particles, compared to PMA_{SH}, which showed negligible aggregation (Figure 3.5 D). Aggregation may abrogate the internalization of particles into cells, or decrease association, as we observed earlier in the association study (Figure 3.4 B-C). Aggregation of these particles may only occur under the specific experimental setting we used (i.e., cell culture serum and/or incubation time), given the previously calculated dispersion data (Table 3.1) showing well-dispersed particles in MilliQ-water.

Taken together, quantification of particle association (percentage of cells have one or more membrane bound particles and/or internalized particle) with Jurkat and primary CD4+ T cells by flow cytometry and confocal

microscopy suggested that smaller, negatively charged particles were internalised more efficiently than particles of neutral (PMA_{SH}-PEG) or positive (PMA_{SH}-PLL) charge (Table 3.2).

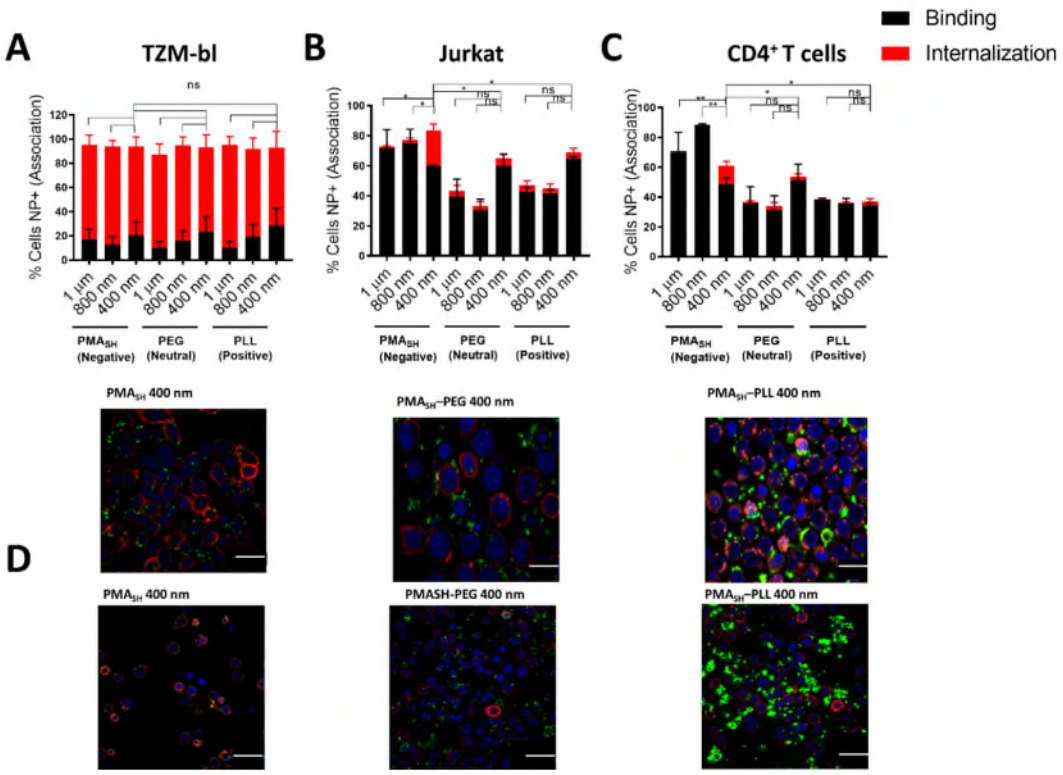

Figure 3.5 Negatively charged 400 nm PMA_{SH} particles are internalised into T cells.

A) Percentage of associated particles with the TZM-bl cell line, B) Jurkat cell line, and C) primary CD4+ T cells. Columns represent the percentage of cells with surface-bound particles (black) and those with internalised particles (red) as calculated by confocal microscopy with representative images. D) Representative confocal images of primary CD4+ T cells treated with particles showing minimal aggregation of PMA_{SH} 400 nm particles (left) compared to PMA_{SH}-PEG particles (middle) and PMA_{SH}-PLL (right). All data are shown as the mean ± standard error of the mean (SEM; N = 3). All P values were determined using a two-tailed, unpaired T test: *P<0.05, **P<0.001. NS = not significant. (1500 cells counted per condition). Representative confocal microscopy images of corresponding cells (Bottom) showing cell membrane (red), nucleus (blue) and associated particles (green). Scale bar: 10 µm.

3.2.4 Evaluation of particle association with isolated peripheral blood mononuclear cells.

We next aimed to understand particle uptake, association and biodistribution of untargeted PMA_{SH} particles in complex and diverse cell population subsets. Examining the association of nanoparticles drug delivery systems in such multi-cell systems is required for the systematic administration of nanomedicine.

First, we collected peripheral blood samples from 5 healthy donors, and peripheral blood mononuclear cells (PBMC) were isolated from heparinised blood using Ficoll-paque density gradients (Materials and Methods) (Figure 3.6 A). To identify different immune cell subsets in PBMC samples, cells were immunolabeled with fluorescently-conjugated antibodies against CD3, CD14, HLA-DR, CD56 and CD19 and samples were analysed on the same day using flow cytometry. To determine the biodistribution of particles among cell subsets, T cells were identified as $CD3^{+}CD14^{-}$, monocytes $CD3^{-}CD14^{+}$, and $CD3^{-}CD14^{-}$ cells were further gated for natural killer cells (NK) $CD56^{+}CD19^{-}$, B cells $CD56^{-}CD19^{+}$ and finally dendritic cells (DC) $HLA\text{-}DR^{+}CD56^{-}$ (Figure 3.6 B). Immune profiling analysis data revealed the frequency of cell population to be approximately (mean) 65 % T cells, 12 % monocytes, 7 % NK cells, 3 % B cells and 3 % DC (Figure 3.6 C) (Table 3.3).

With negatively charged PMA_{SH} particles, association with phagocytic monocytes was high (mean = 97 %) (Figure 3.7 A). In contrast and as expected, association with T cells and DC (mean of 50 %) and with NK cells and B cells was lower at 36 % and 64 %, respectively (Figure 3.7 A). PMA_{SH}-PEG and PMA_{SH}-PLL particles were preferentially associated with T cells and monocytes (mean = 84 % and 80 % and 8 5% and 78 % respectively) compared with DC, NK cells and B cells (Figure 3.7 B-C). Notably, PMA_{SH}-PEG particles were significantly more associated with T cells compared to NK cells and B cells [p = 0.0021 and 0.0335 respectively, unpaired t-test] (Figure 3.7 B), while PMA_{SH}-PLL particles were even more specific in their preference for T cells compared to DC, NK cells and B cells [p = 0.01, 0.0001, and 0.0001 respectively, unpaired t test] (Figure 3.7 C).

In these experimental settings, we concluded that in non-phagocytic cell populations, both neutral charged PMA_{SH}-PEG and positively charged

PMA_{SH}-PLL associate more efficiently with T cells compared to negatively charged PMA_{SH} particles (Table 3.3). In addition, the phagocytic properties of antigen-presenting cells (APC) such as monocytes likely leads to significant association due to uptake and may play a role in the clearance of particles.

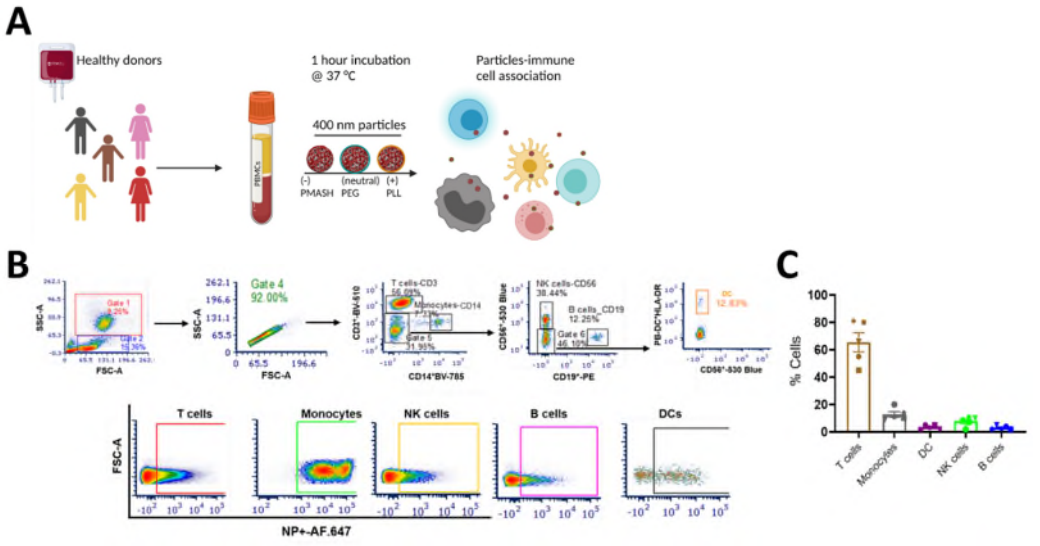

Figure 3.6 Biodistribution of PMA_{SH} 400 nm particles in human PBMC

A) blood was collected from healthy donors, and human PBMC were isolated by Ficoll density gradient centrifugation. PBMCs were exposed to particles for 1 hour at 37 ◦C. To characterise immune cell subsets, PBMC were immunolabeled with antibodies specific for CD3, CD14 (Monocytes), HLA-DR (DC), CD56 (NK), CD19 (B cells). B) Representative gating strategy for $CD3^{+}CD14^{-}$ T cells, $CD3^{-}CD14^{+}$ monocytes, HLA-DR^{+} $CD56^{-}$ dendritic cells (DC), $CD56^{+}CD19^{-}$ Natural killer cells (NK) and $CD56^{-}CD19^{+}$ B cells. C) The percentage of cell subsets in PBMC from 5 healthy donors. All values represent the mean ± standard error of the mean (SEM =2).

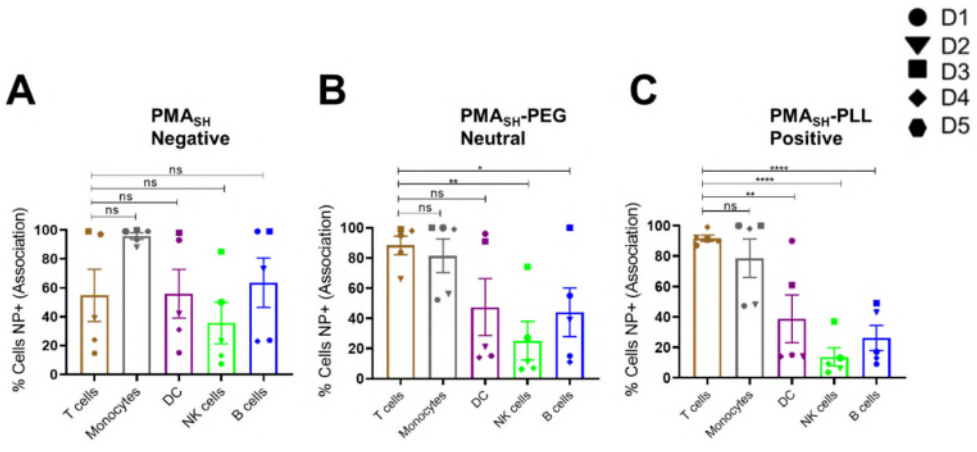

Figure 3.7 PMA$_{SH}$ particles are preferentially associated with antigen-presenting cells in human PBMC.

Particles were co-incubated with human PBMC for 1 hour at 37 ◦C at a concentration of 10 x 10^7 particles. The percentage of AF647 positive cells were determined for different cell subset and shown with A) PMA$_{SH}$. B) PMA$_{SH}$-PEG. C) PMA$_{SH}$-PLL particles. All data are shown as the mean ± standard error of the mean (SEM; N = 5). All P values were determined using two-tailed T test: *P<0.05, **P<0.01 and ****P<0.0001. NS = not significant.

3.2.5 Evaluation of particle association with cells in whole human blood.

One of the most significant challenges of nanomedicine in the clinical setting is achieving targeted drug delivery to a specific organ or tissue. Human whole blood contains a plethora of cell types, including white blood cells (WBCs), such as neutrophils, B cells, monocytes, T cells, DCs and NK cells, that potentially endocytose or phagocytose targeted particles. Additionally, human blood compromises the complexity of different plasma proteins (445, 534). Therefore, we next assessed the association of particles in the presence of blood components and the particle association rate with human blood.

Briefly, whole blood samples were collected in a heparin-anticoagulant tube from 5 healthy donors. Fresh 200 µl of whole blood was incubated with 400 nm PMA$_{SH}$, PMA$_{SH}$-PEG and PMA$_{SH}$-PLL with particles for 1 hour at 37 ◦C and particle association with cells was analysed using flow cytometry

(Figure 3.8 A). To identify different cell subsets, cells were harvested and immunolabelled against six separate immune cells populations; neutrophil, T cells, monocytes, natural killer (NK), B cells and dendritic cells (DC), as shown in the representative gating strategy we applied (Figure 3.8 B). Immune profiling analysis revealed the frequency of cell populations; a mean value of 17 % of whole blood were granulocytes, with 97% of this population neutrophils (Figure 3.8 C). Furthermore, the percentage of lymphocytes and monocytes cell populations were [mean = 62 %] T cells, [mean = 9 %] monocytes, [mean = 5 %] NK cells, [mean = 9 %] B cells and [mean = 8 %] DC (Figure 3.8 C) (Table 3.4).

3.2.6 The surface charge of particles does not influence particles association in human whole blood

To assess whether we can observe a similar association pattern with the immune cells we observed in PBMC, we examined the association pattern of 400 nm PMA_{SH}, PMA_{SH}-PEG and PMA_{SH}-PLL particles in human whole blood. Association data analysis showed that human blood phagocytic cell subsets, neutrophils, monocytes and Dcs were highly associated with all particle types, i.e., PMA_{SH}, PMA_{SH}-PEG and PMA_{SH}-PLL (Figure 3.9 A-C) (Table 3.4). Monocytes had the strongest association with particles compared to DCs and neutrophil cells, suggesting that surface charge may not influence particles clearance by phagocytic cells. Furthermore, we observed that T cells and NK cells had a negligible association with all particle types. We also found that all particles had a similar level of association with T cells. PMA_{SH} particles highly associated with monocytes and B cells [p = 0.0005 and 0.0167 respectively, unpaired t test] compared to T cells (Figure 3.9 A-C), while PMA_{SH}-PEG and PMA_{SH}-PLL particles displayed greater association with neutrophils, monocytes, DC, and B cells compared to T cells [p = 0.0050, 0.0001, 0.0313 and 0.0311 respectively, unpaired t-test] and [p = 0.0057, 0.0001, 0.0236 and 0.0087 respectively, unpaired t test] (Figure 3.9 B-C). Overall, these findings indicate that association is primarily driven by the phagocytic uptake of particles, irrespective of particles surface charge.

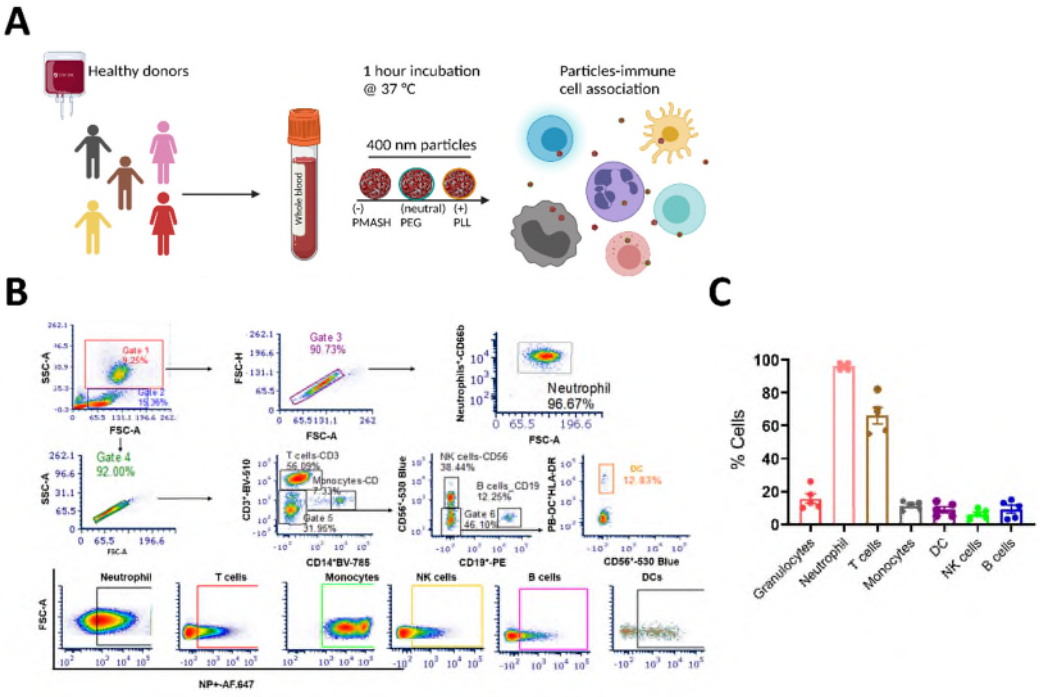

Figure 3.8 Biodistribution of PMA$_{SH}$, PMA$_{SH}$-PEG and PMA$_{SH}$-PLL 400 nm particles in whole human blood.

A) Blood was collected from 5 healthy donors and exposed to particles for 1 hour at 37 °C. To characterise different immune cell subsets, mixed human blood cell populations were immunolabelled with fluorescent-coupled antibodies specific for CD66b, CD3, CD 14 (Monocytes), HLA-DR (DC), CD56 (NK), CD19 (B cells). B) the representative gating strategy was applied as follow; CDD66^{+}, CD3^{+}CD14^{-} T cells, CD3^{-}CD14^{+} monocytes, HLA-DR^{+} dendritic cells (DC), CD56^{+}CD19^{-} Natural killer cells (NK) and CD56^{-}CD19^{+} B cells. C) Cell subsets distribution of human whole from 5 healthy donors. All values represent the mean ± standard error of the mean (SEM)

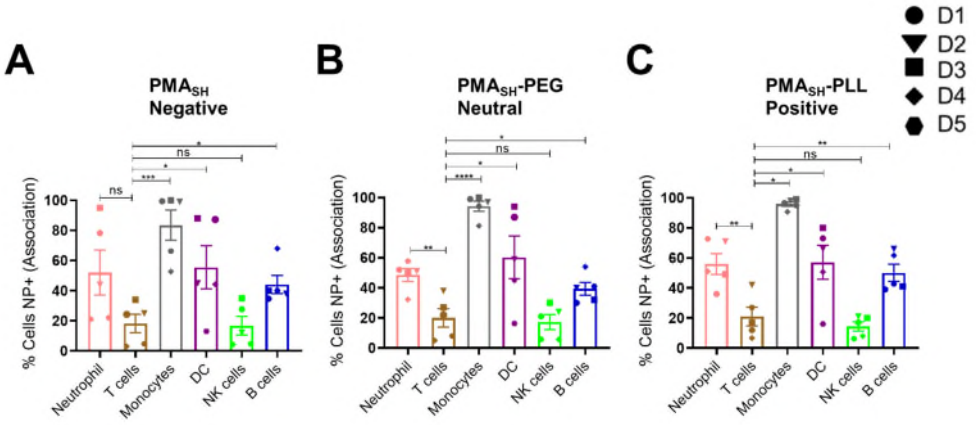

Figure 3.9 400 nm PMA_{SH}, PMA_{SH}-PEG and PMA_{SH}-PLL particles are taken up by phagocytic blood cells.

Fresh heparin-anticoagulated whole blood was treated with AF647 labelled negative PMA_{SH}, neutral PMA_{SH}-PEG and positive PMA_{SH}-PLL for 1 hour at 37 ◦C. Association with primary immune cells was analysed by flow cytometry and represented as a percentage of cells positive for AF647 within ease. The percentage of AF647 positive cells were determined for different cell subsets and shown with A) PMA_{SH}, B) PMA_{SH}-PEG. C) PMA_{SH}-PLL particles. All data are shown as the mean ± standard error of the mean (SEM; N = 5). All P values were determined using two-tailed T test: *P<0.05, **P<0.001, ***P<0.0005 and ****P<0.0001. NS = not significant.

3.2.7 3.2.7 Analysis of toxicity effects of PMA_{SH}, PMA_{SH}-PEG, and PMA_{SH}-PLL particles on T cells

Engineered nanoparticles represent a toxicological challenge; the interaction of particles with the cell membrane may disrupt the integrity and functionality of cellular membranes in a size and surface charge-dependent manner (535, 536). In order to understand whether 400 nm or 800 nm PMA_{SH}, PMA_{SH}-PEG, and PMA_{SH}-PLL particles are toxic to cells, we used a flow cytometer-based cell death assay. In this assay, we determined apoptosis (Annexin V staining) versus necrosis (PI). Representative plots of the gating strategy for analysis of cell viability are shown in Figure 3.10 A. Toxicity data analysis in Figure 3.10 B-C demonstrated that 400 nm and 800 nm particles independent of surface charge had no appreciable toxic effect

to Jurkat cells, while all particles induced negligible toxic effect to primary $CD4^+$ cells compared to mock-treated cells.

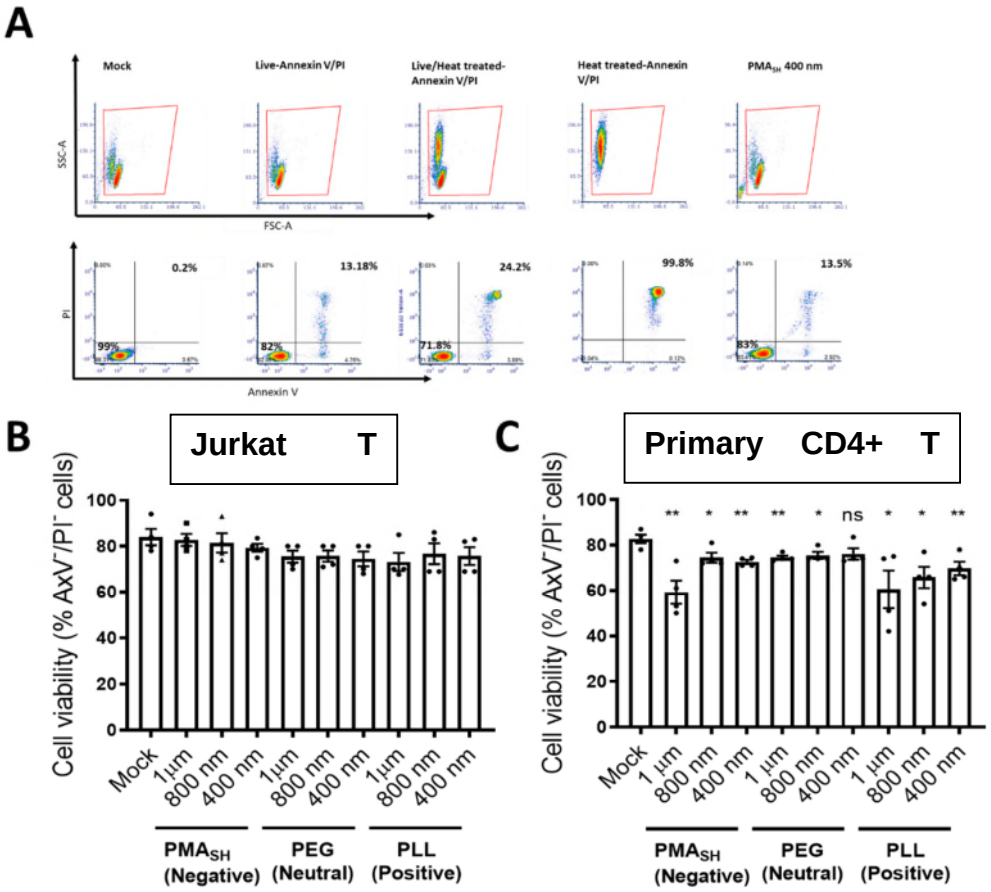

Figure 3.10 Percentage cell viability measured by PI and Annexin V assay relative to mock-treated cells.

A) representative gating strategy was used to discriminate $Annexin^+$ V (AxV)/ PI^+ cells. Analysis was performed on the cells shown in the scatter histograms comparing forward scatter vs side scatter (FSC-A/SSC-A) and PI vs Annexin V of cells alone (mock), untreated cells (live-Annexin V/PI), live and dead cells, dead cells and cells exposed to particles. B) Jurkat cells and C) primary CD4+ T cells. Cells were treated with PMA_{SH}, PMA_{SH}-PEG and PMA_{SH}-PLL in a 200:1 particle: cell ratio for 24 hours at 37 °C. All data are shown as the mean ± standard error of the mean (SEM; N = 4). All P values were determined using a two-tailed T test: *P<0.05 and **P<0.001. Only statistically significant comparisons are shown.

3.2.8 3.2.8 PMASH particles induced transient CD69 and CD25 activation in CD4+ T cells

Using flow cytometry and confocal microscopy analysis, we demonstrated that smaller negatively charged particles are highly associated with T cells. Therefore, we choose 400 nm PMA_{SH} as the optimal particle to further investigate. It is a worthy note that in the association studies, the fluorescent signal from 100 nm particles was undetectable under the settings and concentration we used. However, because of the attractive size of the 100 nm PMA_{SH} particles and their potential to internalize into T cells efficiently, we decided to examine their effect on cellular activation markers (416). Next, we tested the effect of 100 nm and 400 nm PMA_{SH} particles on T cell activation in primary $CD4^+$ T cells using flow cytometry. We included the 100 nm particles.

To measure the effect of particles and the kinetics of T cell activation, we analysed the surface expression level of different surrogate cell membrane markers of $CD4^+$ T cell, i.e., CD69, CD25 and HLA-DR, over time. CD69 (Cluster of Differentiation 69) is a classical early activation marker and is a vital regulator of the immune response through it is role in cytotoxic functions as well as T cell migration and retention (537, 538). Interleukin-*2* receptor α (CD25) is a component of the IL-2 receptor and is upregulated during T cell activation and promotes T cell proliferation and the development of regulatory T cells (Treg) (539, 540). Human leukocyte antigen-antigen D (HLA-DR) is a T cell late activation marker and plays a central role in the immune response to foreign antigens (541, 542).

$CD4^+$ T cells were exposed to PMA_{SH} 100 nm and 400 nm particles over time-course (i.e., 12, 24, 48 and 72 hours). Cells were harvested periodically for flow cytometry analysis. We analysed the expression of activation markers and the frequencies of $CD69^+$, $CD25^+$ and $HLA\text{-}DR^+$ cells as shown in representative Figure 3.11 A. The percentage of T cells positive for activation markers were compared to those induced by the "positive control" phytohemagglutinin (PHA), or untreated cells is reported. In general, particles induced a transient expression of CD69 and CD25 on $CD4^+$ T cells (Figure 3.11 B-C).

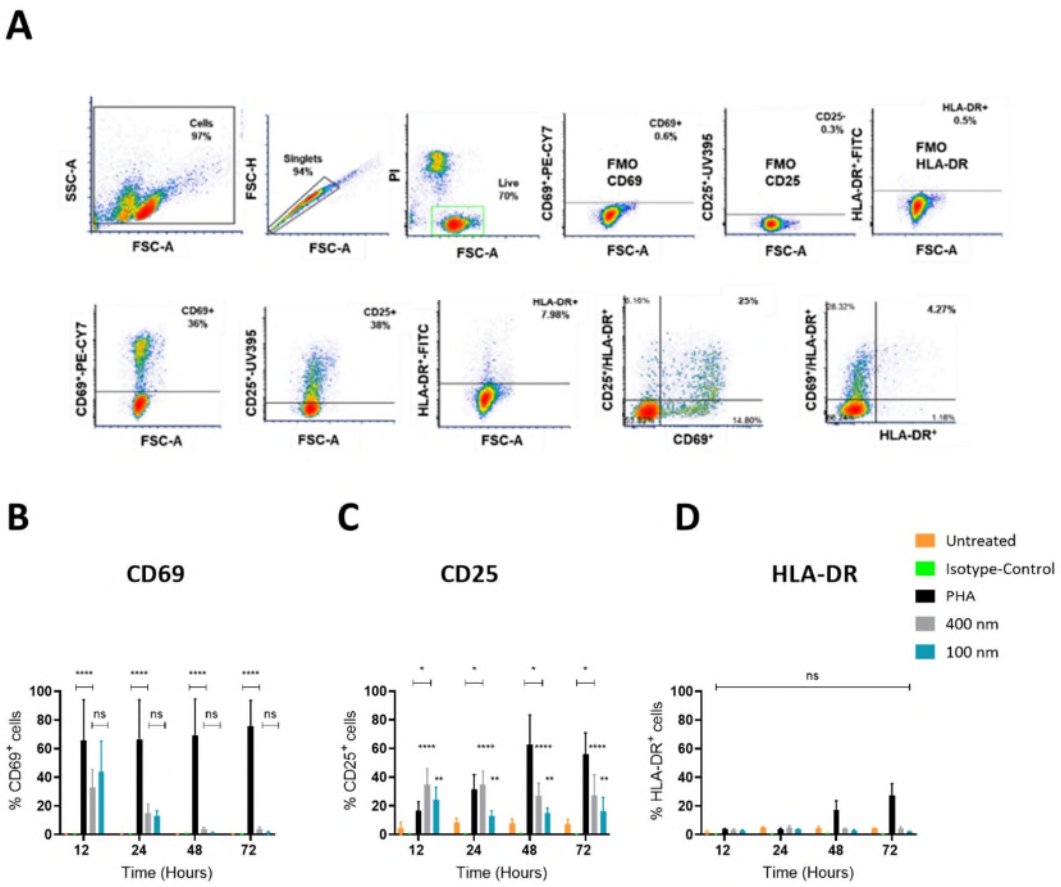

Figure 3.11 Expression of cell surface activation markers within CD4+ T cells following incubation with nanoparticles.

A) gating strategy for flow cytometric analysis of *in vitro* stimulation of $CD4^+$ T cells. The percentage expression of B) CD69, C) CD25, and D) HLA-DR following different stimuli over time is shown. All data are shown as the mean ± standard error of the mean (SEM; N = 3). All P values were determined using a two-tailed T test: *P<0.05 and ****P<0.0001. PHA =20 ng mL^{-1}.

Following incubation with both sized particles, we observed sustained expression of $CD25^+$ cells and transient expression of CD69 over time (Figure 3.11 C). In addition, cells exposed to particles showed no change in HLA-DR expression at 48 and 72 hours. In conclusion, at earlier time points (12 hours and 24 hours), cells treated with particles expressed the highest level of CD96 and CD25 compared to later time points (48 hours and 72 hours). We saw no difference between 100 and 400 nm.

Table 3.2 Interaction of nanoparticles with Jurkat cell line and primary CD4+ T cells

NP type	Association[a]		Binding[b]		Internalization[c]	
	Jurkat cell line	CD4+ T cells	Jurkat cell line	CD4+ T cells	Jurkat cell line	CD4+ T cells
PMA_{SH} 400 nm	94 %	83 %	60 %	48 %	23 %	17 %
PMA_{SH} 800 nm	73 %	61 %	72 %	88 %	1 %	Not detected
PMA_{SH} 1 µm	73 %	72 %	72 %	71 %	1 %	Not detected
PMA_{SH}-PEG 400 nm	66 %	30 %	59 %	52 %	5 %	3 %
PMA_{SH}-PEG 800 nm	62 %	37 %	30 %	32 %	3 %	3 %
PMA_{SH}-PEG 1 µm	67 %	39 %	39 %	37 %	4 %	1 %
PMA_{SH}-PLL 400 nm	62 %	32 %	64 %	35 %	3 %	3 %
PMA_{SH}-PLL 800 nm	40 %	31 %	41 %	36 %	3 %	2 %
PMA_{SH}-PLL 1 µm	50 %	29 %	42 %	37 %	4 %	1 %

(a)Association percentage refers to cells that have one or more particles absorb to extracellular membrane or subsequent internalization into cell. (b) binding percentage refers to cells that have one or more particles absorb to extracellular membrane. (c) Internalization refers to percentage of cells that have one or more particles internalized (crossed the extracellular membrane).

Table 3.3 Biodistribution of PMA_{SH} 400 nm particles in human PBMC

NP type	Association of cell Subset with NPs				
	T cells	Monocytes	DC	Nk cells	B cells
PMA_{SH} 400 nm	55 %	96 %	56 %	36 %	64 %
PMA_{SH}-PEG 400 nm	89 %	81 %	48 %	25 %	44 %
PMA_{SH}-PLL 400 nm	92 %	79 %	39 %	14 %	27 %

Association percentage refers to cells that have one or more particles absorb to extracellular membrane or subsequent internalization into cell.

Table 3.4 Biodistribution of PMASH 400 nm particles in human whole blood

NP type	Association of cell Subset with NPs					
	Neutrophils	T cells	Monocytes	DC	Nk cells	B cells
PMA_{SH} 400 nm	52 %	18 %	84 %	56 %	17 %	44 %
PMA_{SH}-PEG 400 nm	49 %	20 %	95 %	61 %	18 %	40 %
PMA_{SH}-PLL 400 nm	65 %	21 %	96 %	58 %	15 %	50 %

Association percentage refers to cells that have one or more particles absorb to extracellular membrane or subsequent internalization into cell.

3.2.9 Discussion

Although our knowledge regarding the influence of physicochemical properties of nanoengineered particles in association with cells has significantly advanced in the past decade (536, 543, 544), at present, there is a lack of data on the impact of physicochemical properties on functionalized polymer-based nanoparticles coming into contact with T cells. Cellular uptake, cell viability and cytotoxicity, and phenotypic and activation marker expression are unknown (416, 545, 546). Moreover, nanoparticles are exogenous synthetic structures that indeed may have immunomodulatory effects and subsequently face clearance upon interaction with immune cells (i.e. APC) (544), therefore studying particle-T cell interaction in *in vitro* monoculture settings may not represent the environment clinically (547–549).

We showed that negatively charged PMA_{SH} is highly associated with T cells compared to neutral PMA_{SH}-PEG and PMA_{SH}-PLL. In particular, we found that PMA_{SH} particles parameters such as size and charge are the main features affecting intracellular uptake. Smaller (i.e., 400 nm) and negatively charged (i.e., PMA_{SH}) particles were preferentially internalised in T cells compared to larger (i.e., 800 nm and 1 µm) and neutral and positive charged (i.e., PMA_{SH}-PEG and PMA_{SH}-PLL) nanoparticles (Figure 3.5 A-C). These

results suggest that the size and surface charge of PMA_{SH} particles plays an important role in interaction with T cells.

One possible explanation for these findings is the possibility that protein corona, the collection of biological proteins that collect on the surface of the PMA_{SH} particle shell, increases particle-cell binding, and consequently, the smaller size accelerates internalisation. This phenomenon has been shown in many studies. For example, specific proteins in the biomolecular corona were previously identified as crucial factors for nanoparticle association with cells (531). In contrast, the presence of PEG and PLL groups on PMA_{SH}-PEG and PMA_{SH}-PLL are known to drastically reduce the adsorption of protein corona on the particle surface (470, 550, 551). An additional explanation is that surface charge alters the T cell membrane. Specifically, the T cell surface marker $CD4^+$ contains a thiol group (-SH) (552, 553) that may form a covalent attachment with reactive disulphides present on the PMA_{SH} shell, facilitating particle adsorption into the membrane mimicking HIV entry into $CD4^+$ T cells (554). While the presence of PEG and PLL layers (PMA_{SH}-PEG and PMA_{SH}-PLL) on the top of the PMA_{SH} layer are likely to inhibit the interaction of thiol groups that present of the PMA_{SH} with the host membrane. Alternatively, several studies have shown that reactive disulphides can react with the transferrin receptor (TfRC, CD71) and will covalently bind to the thiol group present on the receptor leading to transport across the cellular membrane (555–557). Of note, to further support this hypothesis, TfRC usually cycles between the plasma membrane and the endosomal compartment and is upregulated following T cell activation (558–560). This observation supports our findings on T cell activation, where we observed a transient upregulation of CD69 and CD25 in $CD4^+$ T cells following exposure to negatively charged PMA_{SH} 400 nm (Figure 3.11 B-C). One possible way to test this hypothesis is by blocking the TfRC receptor (anti-TfRC antibody or TfRC knock out CD4+ T cells) before exposing cells to PMA_{SH} particles. Furthermore, PMA_{SH}-PEG and PMA_{SH}-PLL appeared to aggregate under the specific experimental setting we used (i.e., cell culture serum and/or incubation time) (Figure 3.5 D). Aggregation usually refers to the irreversible adherence of particles, leading to large and irregular particle clusters (561). When introduced to a complex biological media containing

proteins, electrolytes and lipids, particles are subjected to a range of forces, which determine their biological behaviour and colloidal stability in such an environment. Therefore, investigating the factors that influence particles colloidal stability when exposed to biological media is warranted to develop effective and safe nanomedicine. Future work is needed to delineate which endocytosis pathway PMA_{SH} 400 nm particles use to internalize. It would be interesting to investigate whether the cell can internalise PMA_{SH} particles using different endocytic pathways, given that the physiochemical parameters (size and surface charge) may direct particles internalisation to a subset of these pathways.

Next, we screened 400 nm PMA_{SH}, PMA_{SH}-PEG and PMA_{SH}-PLL particles and assessed their interaction with immune cells in human PBMC and whole blood. In human PBMC, we found 400 nm particles highly associated with monocytes and DCs (Figure 3.7 A-C). Particles association result was expected and agreed with previous reports (449, 562, 563) as these cells have a classical phagocytotic function and are triggered once they encounter foreign bodies. Interestingly, we found that PMA_{SH}-PEG and PMA_{SH}-PLL 400 nm particles were also highly associated with T cells (Figure 3.7 B-C). This finding was different from our flow cytometry and confocal microscopy association data and could be due to the difference in how particles behave in isolated $CD4^+$ T cells compared to a homogeneous mix of immune cell subsets in PBMC.

In contrast, in human whole blood, all particles, regardless of surface charge, are associated preferentially with neutrophils, monocytes and DCs (Figure 3.9 A-C). We also found that all particles had approximately 20% association with T cells in human whole blood, regardless of the charge. These findings support the potential use of all particles (i.e., 400 nm PMA_{SH}, PMA_{SH}-PEG and PMA_{SH}-PLL) *in vivo* to target T cells. A notable observation of our PBMC association with particles experiment was the large variability across various human donors, reflecting the diversity of the human population. In examining the association of particles with human whole blood and PBMC, at least two of five donors displayed exceptionally high association of their T cells, DCs and B cells with PMA_{SH}, PMA_{SH}-PEG, PMA_{SH}-PLL particles.

In contrast, the remaining displayed a lesser amount of association (Figure 3.7 A-C). In human whole blood, we observed a similar effect of particles association with neutrophils, monocytes, and DC cells population with PMA_{SH}, DC association with PMA_{SH}-PEG and PMA_{SH}-PLL particles (Figure 3.9 A-C). These observations highlight the need for studies in biologically relevant conditions when evaluating bio-nano interactions.

PEGylation of nanoparticles involves adding a protective coating of polyethylene glycol (PEG). PEGylated nanoparticles become hydrophilic and attain near-zero zeta potential, thus inhibiting the attachment of opsonins; as a result, nanoparticle PEGylation can increase particles in the circulation, avoiding immune recognition subsequent clearance by APC cells (449, 564–566). The PEGylation technique has been widely used in different nanoparticle drug delivery systems and is often called “stealth” because it can escape immune system surveillance (325, 567, 568). In our experiments, neutrally charged PMA_{SH}-PEG did not recapitulate the protective effect of PEGylation when examined with either human PBMC or whole blood (Figure 3.7 B and Figure 3.9 B). Several explanations are to be considered here. First, the size of the coated PMA_{SH} particle can influence particles clearance by immune cells (opsonisation) (436, 453, 534, 547, 569, 570). Recently, Yi Ju *et al*. showed that the association of the particle with monocytes and B cells in PBMC culture was more prominent with the decreased particle size (453). Second, the length and concentration of coated PEG is also crucial factor in achieving stealth properties (563, 571, 572). PEGylating brush regimes are mostly preferred to improve the stealth properties and pharmacokinetics of nanoparticles because, in this regime, the interaction of the particles with neighbouring molecules is less, and particles diffuse faster through tissue than other used regimes (553, 573, 574). Veronese *et al.* and others highlighted that PEG configuration and sufficient coating on the nanoparticle surface is crucial to prevent immune recognition (436, 575, 576). In addition to different regimes, Suk *et al.* and others summarised the effect of PEG content, mainly the molecular weight (MW), nanoparticles core properties and grafting density are the main parameters affecting PEG configuration on the surface of the nanoparticle in order to evade immune detection (553, 566, 575, 577, 578). These

observations reflect that the stealthiness introduced into PMA_{SH} particles must be proportionately designed and sufficiently cover the surface of PMA_{SH} particles to provide complete protection against opsonization and subsequent uptake by phagocytic immune cells.

It is important to note that PEG is an exogenous material that can induce an anti-PEG immune response against nano-materials and lead to particle clearance by antibody-mediated opsonization (416, 579). Although PEGylated drugs and nanomedicines have been approved for safe use in humans by the USA Food and Drug Administration (FDA), the administration of PEGylated particles or drugs may lead to the induction of anti-PEG antibodies (anti-PEG immunoglobulin M (IgM)) and lead to immune recognition and clearance of the particle (576, 580, 581). Due to this phenomenon, we think PMA_{SH}-PEG may have triggered an immunogenic response that led to their rapid clearance by phagocytic cells in human whole blood and PBMC. This hypothesis can be further tested by depleting the anti-PEG function in whole blood by depleting the immunoglobin fraction (582).

We also examined whether the physicochemical properties of nanoparticles can induce a specific biological response in T cells. Specifically, nanoparticles could induce cytotoxicity, apoptosis, or activation through the change in expression of surface receptors. Several studies have confirmed that nanoparticles can trigger toxicity by injuring the plasma membrane (583–585). To this end, understanding the modest toxicity we observed in $CD4^+$ T cells caused by particles (in particular PMA_{SH} and PMA_{SH}-PLL) could be related to the higher association of PMA_{SH} particles and higher aggregation of positively charged particles with PMA_{SH}-PLL. The results also suggest no clear, direct correlation between particle size and surface charge and induced cytotoxicity. In contrast, we did not observe a significant drop in viability in Jurkat cells treated with particles, and this may be primarily because Jurkat cells are immortalized cell lines and inherently more resistant to apoptosis.

We investigated the impact of prototype PMA_{SH} 100 nm and 400 nm particles exposure on activating $CD4^+$ T cell surface markers (CD69, CD25 and HLA-DR). Particle exposure to primary $CD4^+$ T cells at a ratio of 200:1

particles: cells for 24 hours induced transiently increased expression of CD69 and sustained upregulation of CD25. Our data suggest that the effect is due to the direct interaction between particles and cells. In support of this hypothesis, we observed an increase in expression of activation markers at the earlier time points (12 hours and 24 hours) compared to later time points (Figure 3.11 B-C). It would be interesting to study a similar response in human PBMC and assess whether APCs affect the expression of these markers.

The ability to engineer nanoparticles with tunable physicochemical properties is increasingly important. Here we demonstrate that the size and charge of PMA_{SH} particles (i.e., PMA_{SH}, PMA_{SH}-PEG and PMA_{SH}-PLL) can influence their association with primary $CD4^+$ T cells. The smaller 400 nm PMA_{SH} particles were efficiently taken up by primary $CD4^+$ T cells. In contrast, 400 nm PMA_{SH}-PEG and PMA_{SH}-PLL demonstrated increased association with T cells in human PBMC. Notably, the effect of physicochemical properties was not distinct when we evaluated $CD4^+$ T cells in human whole blood. Therefore, the influence of size and surface charge on particle internalization warrants further quantification. Studies should be performed in both human PBMC and whole blood as these particles may display different characteristics in relation to cellular uptake in the presence of protein corona. In subsequent chapters in this thesis, we expanded these findings and explored the role of 400 nm PMA_{SH} particles to effectively deliver small pharmacological molecules (LRAs) to $CD4^+$ T cells. In addition, the relative distribution of immunocyte subsets obtained from the respective immune profiling analysis found in PBMC and whole blood (figure 3.6 C and 3.8 C, respectively) vary considerably from donor to donor. Therefore, further studies are warranted since understanding the source of intra-donor variability may unlock clinically relevant principles of how immune cells response to particles varies from donor to donor in *ex vivo* models or *in vivo* of humanized animal models.

3.2.10 Conclusion

In summary, we fabricated, functionalised, and characterised nanoengineered PMA_{SH} particles of different sizes and charges using the

Layer-by-Layer assembly technique. Particles were grouped by (a) size (i.e., 100 nm, 400 nm, 800 nm and 1 µm) and (b) surface charge (i.e., negative PMA_{SH}, neutral PMA_{SH}-PEG and positive PMA_{SH}-PLL). To investigate the influence of particle size and surface charge on the association of particles with T cells, we developed a confocal microscopy-based quantification method to determine the level of particle uptake in the Jurkat T cell line and primary $CD4^+$ T cells. Next, we characterised their interaction with T cell line, primary $CD4^+$ cells, human PBMC and human whole blood. Further, we studied the biological response of particles with a T cell line and primary $CD4^+$ T cells. We found that smaller and negatively charged PMA_{SH} particles efficiently internalized in Jurkat cells and primary $CD4^+$ T cells. In primary $CD4^+$ T cells, particles had only a limited biological effect on toxicity and some modest short-lived T cell activation. We aim to encapsulate the hydrophobic drug romidepsin into these particles to target latently infected $CD4^+$ T cells selectively.

4 Delivery of romidepsin loaded particles to latently infected T cell line models

4.1 INTRODUCTION

Antiretroviral therapy (ART) effectively suppresses HIV replication in people living with HIV (PLWH), but treatment is lifelong. The persistence of long-lived, latently infected resting $CD4^+$ T cells is a significant challenge in achieving a cure for HIV infection (74, 79, 80, 586). During the early course of infection, HIV integrates into the genome of $CD4^+$ T cells (provirus) and establishes a reservoir of latently infected cells (74, 145, 233). These latently infected cells contain a transcriptionally silent provirus that can evade ART and resist immune-mediated clearance. One strategy toward eliminating HIV latency is the activation of HIV viral production by latency reversal agents (LRAs) to induce virus-mediated cytolysis or clearance through immune recognition in the presence of ART (often called "shock and kill") (272, 312). However, the shock and kill strategy has had limited progress in clinical trials, given the off-target effects of most LRAs and the failure to reduce reservoir size (61, 375, 587). Several hypotheses have been suggested to contribute significantly to these limitations. Many LRAs can have toxic effects (e.g., romidepsin) as they are not specific to HIV. Additionally, current LRAs are probably may not be sufficiently potent to induce cell death (312, 313, 588, 589). Other evidence suggests that latently infected cells may be primed to survive through the expression of pro-survival proteins such as B-Cell Lymphoma-2 (Bcl-2) (590, 591).

While the frequencies of latently infected cells are low *in vivo*, multiple *in vitro* models have been successfully established to investigate the molecular mechanisms that contribute to the establishment and maintenance of HIV latency. These models can facilitate the screening for different pharmacological and immunological interventions aimed at

depleting latently infected cells (227–230). *In vitro* cell line models of HIV latency, including the J-Lat T cell line, are latently infected Jurkat T cell containing integrated HIV DNA but is transcriptionally silent (provirus) and could be transcriptionally activated upon treatment with a various stimulus (249). HIV transcription can be quantified through the detection of GFP using flow cytometry.

Several pharmacological and immunological interventions have been investigated to eliminate latency and purge the HIV latent reservoir (61, 313, 589, 592). The HDACi romidepsin (RMD) is well characterised and approved for the management of cutaneous T cell lymphoma (593, 594). RMD is a prodrug; its activity occurs only after internalisation into a host cell (595). However, *in vitro* and *in vivo* studies have demonstrated that RMD is not specific for HIV, has off-target effects, and lacks sufficient potency to eliminate latently infected $CD4^+$ T cells from PLWH on ART (118, 357, 369, 370). We hypothesised that we could overcome these limitations by using a nano-engineered particle delivery system loaded with RMD to increase potency and reduce toxicity to latently infected T cells. This approach possesses several advantages over more traditional drug delivery methods (410, 565, 596). Specifically, nano-engineered particles can protect the encapsulated drug from degradation, increase drug solubility and bioavailability, and have sustained slow release kinetics (416, 597–599). However, a growing body of studies have reported on the use of nano-engineered carriers for HDACi inhibitors, and most of those studies originate from the field of oncology (458, 463, 599–601). Primarily, there are two strategies for targeting delivery, passive targeting, and active targeting.

Furthermore, various approaches have been proposed on controlled drug release at the targeted site. In one study, Denis et al. developed a pH-responsive vorinostat-polymer conjugate nanoparticle, thus achieving enhanced intratumor accumulation and drug controlled release (601). In another study, Kuai et al. reported a self-assembly peptide- panobinostat loaded nanoparticles that were able to activate HIV latency *in vitro* moderately (37). However, none of these studies has investigated the potential to deliver the HDACi RMD in the nano-engineered drug delivery formulation to T cells. Therefore, here we utilised RMD loaded nanoparticles

(RMDLNPs) and evaluated the PMA_{SH} particle drug delivery system. We hypothesised that RMDLNPs would have greater potency to reactive HIV latency and reduced cytotoxic effects in various models of HIV latency. We used the PMA_{SH} delivery system given our earlier work showing increased uptake of these specific particles by resting $CD4^+$ T cells (chapter 3).

4.2 RESULTS

4.2.1 Development and characterisation of 100 nm and 400 PMA_{SH} particles loaded with the HDAC inhibitor romidepsin (RMDLNP)

First, we assessed the hydrophobic LRA RMD loading capacity into PMA_{SH} particle prototypes that we have evaluated previously (i.e., 100 nm and 400 nm negatively charged PMA_{SH} particles). It is important to note that we could not quantify the association of 100 nm nanoparticles with resting T cells due to a higher detection limit related to particle size. In general, most flow cytometers have a detection limit of particles in a size range between 200 nm and 500 nm (602–604). Thus, based on our quantitive data (chapter 3) and previously published reports (416, 441, 598, 605, 606), we found that smaller particles (in our study, i.e. 400 nm) compared to larger particles (in our study, i.e. 800 nm and 1 µm) were internalised more efficiently in T cells. We, therefore, decided to include 100 nm nanoparticles in our panel and examined the effects on drug payload capability and delivery efficiency using a functional assay read-out. Therefore, in this study, we focused on the effects of encapsulating the HDACi RMD into PMA_{SH} 100 nm and 400 nm particles compared to free RMD. Furthermore, we assessed their potency in stimulating the expression of latent HIV and cytotoxicity using two latently infected cell lines (J-Lat A2 and J-Lat 10.6 T cells).

To construct PMA_{SH} loaded RMD particles, we employed the MS sphere templating approach (Figure 4.1). Mesoporous silica (MS) particles are an attractive templating system for high loading capability, adaptability, and physical protection to the cargo. The unique MS structure facilitates effective loading and delivery of hydrophobic drugs because of its tunable particle size, porosity and controlled release of the drugs (492). In addition, the pores within the MS serves as a reservoir and entrap loaded

hydrophobic drug molecules and release them when particles are intracellularly localised.

The RMD loaded MS particles were prepared by a modified encapsulation method, as previously reported by Wang et al. (492). To visually confirm the successful loading of hydrophobic drugs, the hydrophobic dye 1,1' -dioctadecyl-3,3,3',3' -tetramethindoocarbocyanine perchlorate (DiI) was first encapsulated into MS particles in parallel. In brief, 5 mg of 100 nm and 400 nm MS particles were co-dissolved separately into a solution of RMD, DiI dye or vehicle control dimethyl sulfoxide (DMSO) for six hours (Figure 4.1-i). Then, the suspension of MS particles loaded with RMD and DiI were centrifugated to collect free RMD for HPLC analysis of drug loading and encapsulation efficiency (DL wt % and EE wt %) and to remove free DiI. The dried loaded MS particles were coated subsequently with four layers of polyvinylpyrrolidone (PVPON) and thiolated poly (methacrylic) acid (PMA_{SH}) to form stable disulphide cross-linked PMA_{SH} loaded particles (Figure 4.1-ii) (detailed PMA_{SH} particles synthesis is presented in Chapters 2 and 3). We used confocal microscopy to visualise DiI loaded particles to demonstrate successful loading, as shown in Figure 4.1-iii. Subsequently, the RMD loaded PMA_{SH} particle shells were fluorescently labelled with Alexa Flour-Maleimide 647 (AF647) by conjugation with thiol residues on PMA_{SH} (Figure 4.1- iv). Finally, the disulphide bonded PMA_{SH} particles were degraded and released their payload through intracellular reductive enzymes (glutathione GSH) by cleavage of disulphide bonds after particle internalisation (Figure 4.1-v).

After successfully synthesising PMA_{SH} 100 nm and 400 nm RMD loaded particles, we next compared them to unloaded particles and explored the characteristics of particle size, polydispersity index (PDI) and surface charge (Table 4.1, Figure 4.2 A-E). To measure the size distribution of PMA_{SH} loaded particles, the nanoparticles tracking (NTA) technique was used for 100 nm RMDLNPs, and dynamic light scattering (DLS) was used for 400 nm RMDLNPs (Figure 4.2 A-B). NTA provides a precise size distribution and concentration profiles for small particles (<200 nm), overcoming inherent disadvantages in other optical techniques such as DLS. Both PMA_{SH} 100 nm and 400 nm RMDLNPs showed a distributed size

of particles with diameters of 123 nm and 426 nm, respectively. The PDI was 0.2 (Table 4.1, Figure 4.2 C).

Of note, we observed that PMA_{SH} 400 nm RMDLNPs tended to show minor aggregation. The particle aggregation was likely caused by the presence of residual hydrophobic RMD on the outer surface of the MS. This particle aggregation did not affect the overall particle size distribution and behaviour with brief sonication before polymer layering. Furthermore, the particle size distribution of RMDLNP compared to unloaded particles was not significantly different. In terms of surface charge, the Zeta potential of all particles was measured using the micro electrophoresis technique (Figure 4.2 D-E). All particles exhibited a negative surface charge approximately between -31 mV and -38 mV (Figure 4.2). However, we observed a slight shift in 100 nm RMDLNPs compared to unloaded particles (from -31 mV to -37 mV) (Figure 4.2). Both size and zeta potential data suggested the proper and successful construction of RMDLNPs.

Further characterisation was carried out to quantify drug loading (DL wt %) and verify encapsulation efficiency (EE %) in PMA_{SH} 100 nm and 400 nm RMDLNP. We used high-performance liquid chromatography (HPLC) using a previously reported method (492). An initial 10 weight % (wt %) was noted, following the input of the hydrophobic drug RMD in 100 nm and 400 nm MS particles the DL wt % of 0.014 and 1.7 respectively (Table 4. 1, Figure 4.3). EE % of RMD was 0.14 % and 17 % in 100 nm and 400 nm MS, respectively (Table 4.1). This was similar to previous reports using other hydrophobic drugs, such as Thiocoraline encapsulated in 400 nm MS (492). However, the EE % in 100 nm MS compared to 400 nm MS particles was lower because the size of the pores of 100 nm MS was smaller (range of 5-15 nm) compared to 400 nm (range of 10-40 nm) as previously reported by Yutiam Ma et al. (493). Therefore, the larger pores in the 400 nm MS enable higher payload capacity, an essential property for using nanoparticle drug delivery systems.

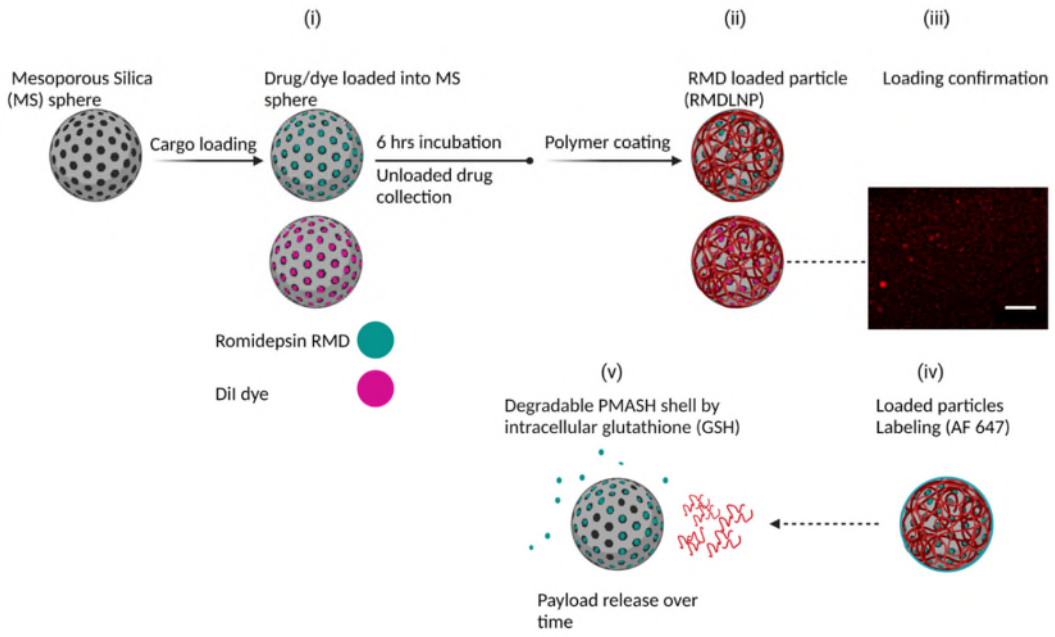

Figure 4.1 Schematic illustration of the HDACi romidepsin (RMD) encapsulation into PMA_{SH} particles via mesoporous silica (MS).

Physical encapsulation of RMD in 100 nm and 400 nm MS spheres. (i) Drug molecules and 1,1' -dioctadecyl-3,3,3',3' -tetramethindoocarbocyanine perchlorate (DiI) dye loading; encapsulation of RMD and DiI dye (positive control for loading hydrophobic drugs) into 100 nm and 400 nm MS sphere supraparticles (493, 503) with pore diameter size range from 5-15 nm and 10-40 nm respectively(503); (ii) Layer-by-Layer (Lb-L) assembly of multilayer PMA_{SH} shell on the surface of the loaded MS particles (RMDLNP). Characterisation of loading dye into a particle (iii) Representative confocal image demonstrates loaded dye into a PMA_{SH} 400 nm particle. (iv) RMDLNPs were labelled with Alexa fluor 647 (AF 647) for detection. (v) Payload was released when particles were exposed to intracellular Glutathione (GSH), a natural reducing agent. Scale bar 10 μm.

Table 4.1 Physical properties of RMDLNP formulations. EE, encapsulation efficiency; n.d. not determined

Particle[a]	Size (d.nm) [b]	PDI[c]	Zeta potential (mV)[c]	Drug input (wt %)	Drug loading (wt %)[d]	EE (%)[e]	Time to release 50% (hours)	NP conc. (mg/mL)	Loaded RMD conc. (µg/mL)
PMA_{SH} 100 nm RMDLNP	123 ± 5	n.d.	-31	10	0.014	0.14	n.d	5	7
PMA_{SH} 100 nm Unloaded	119 ± 2	n.d.	-37						
PMA_{SH} 400 nm RMDLNP	426 ± 9	0.2 ± 0.10	-38	10	1.7	17	24	5	85
PMA_{SH} 400 nm Unloaded	428 ± 3	0.08 ± 0.01	-38						

a: Samples were diluted (1:1000) in MilliQ water and assessed for size, polydispersity index (PDI) independent measurement, zeta potential and encapsulation efficiency (EE). For at least three batches assessed independently. The mean or mean ±SEM is shown; **b:** Size of particles is shown as the mean ± standard error of the mean (SEM; N ≥ 3); **c:** PDI-polydispersity index independent; **d:** Data represent the mean of two independently formulated batches; **e:** EE is the ratio of the actual loaded drug (wt %) to the drug input (wt %) expressed as a percentage.

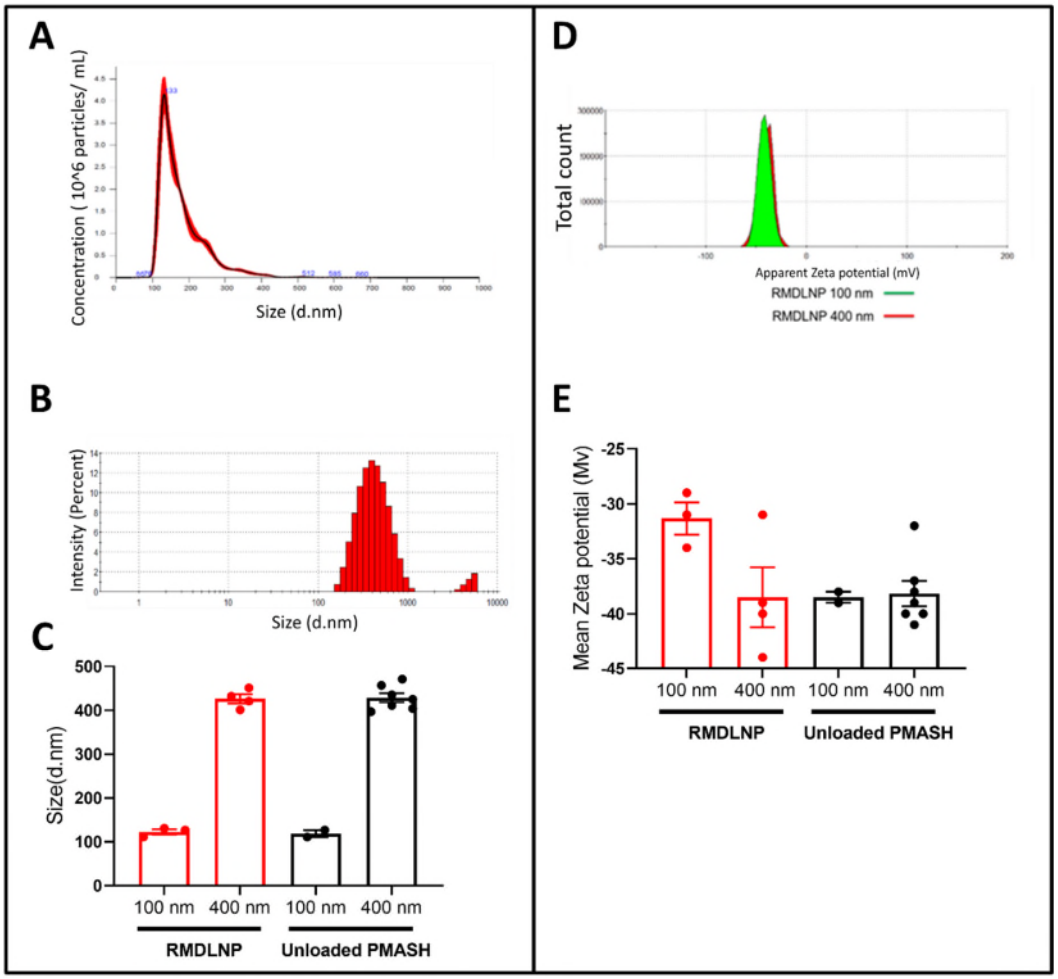

Figure 4.2 Characterisation of size and surface charge after sequential layering of romidepsin loaded PMA$_{SH}$ 100 nm and 400 nm RMDLNP.

A) Representative graphic of the size distribution of monodispersed 100 nm RMDLNP using nanoparticle tracking analysis NTA (Particles ≤ 100 nm). The red curve represents the standard deviation obtained from multiple measurements. The NTA measurement showed a mean nanoparticle size of 133 nm. B) Histogram of the size distribution of 400 nm RMDLNP using dynamic light scattering (DLS). DLS showed a mean particle size distribution of 438 nm. C) Size characterisation of unloaded PMA$_{SH}$ 100 nm and 400 nm and RMDLNP showing drug loading did not impact the size of the loaded particles. D) Histogram representing the size measurement of 100 nm and 400 nm RMDLNP. E) Zeta potential corresponding to PMA$_{SH}$ 100 nm and 400 nm RMDLNP were obtained by micro electrophoresis technique confirming negative surface charge of particles. For all column graphs, the mean ± standard error of the mean from two (100 nm particles)

and four (400 nm particles) independent formulated batches (SEM; N ≥ 4) is shown.

4.2.2 Romidepsin release study from PMA_{SH} particles

The PMA_{SH} particles are stabilised via disulphide linkages that are present on the outer shell (490). One significant advantage of the PMA_{SH} particles system is that particles are well stabilised in oxidative environments (such as the bloodstream), and particle degradation occurs at reductive conditions close to those within the live cells (487, 489). Intracellular degradation of particles occurs through the cleavage of the disulphide bond by the natural presence of the reductive enzyme glutathione (GSH), which leads to the release of cargo intracellularly (Figure 4.1 V) (607). RMDLNP were dissolved in phosphate buffer saline (PBS) solution in the presence or absence of a similar physiological concentration of GSH (5 mM). Figure 3 illustrates the RMD release kinetics from the 400 nm PMA_{SH} particles in a reductive environment. To quantify the released drug from particles, we employed HPLC (Figure 4.3 A). In the absence of GSH, we found negligible drug release from 400 nm PMA_{SH} particles [0.7 %] after 3 hours, indicating the high stability of PMA_{SH} particles and no drug leakage from the mesoporous silica (Figure 4.3 B). In contrast, in the presence of 5 mM GSH, 2.1 % of RMD were released from 400 nm PMA_{SH} particles within the initial first hour, and the amount of released drug was double after 3 hours [4.2 %] (Figure 4.3 B).

Interestingly, 5 % of the encapsulated drug was released at 24 hours, indicating a controlled and slow burst-release profile of the PMA_{SH} particle system. We did not observe drug release beyond the first 24 hours and up to 96 hours (Figure 4.3 B). This may have been caused by the hydrophobic nature of RMD, which may have required a longer time to detach from the pores and be released into the cell.

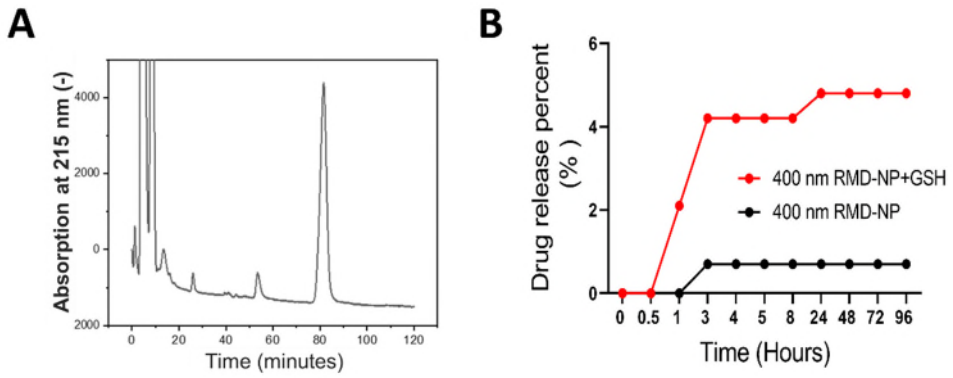

Figure 4.3 The cumulative release profile of romidepsin from 400 nm PMA_{SH} particles in the presence of a glutathione (GSH) reductive environment and 37 ◦C.

A) representative chromatogram using High-performance liquid chromatography (HPLC) of 400 nm RMDLNP was obtained four days after starting the romidepsin release experiment. Before the HPLC run, the sample was diluted twice and spiked with internal standard (IS) at 50 µg/mL. The peaks correspond to glutathione (~ 5 min.), romidepsin (~ 50 min), and IS (~ 80 min). B) The percentage of drugs released was measured by HPLC. The cumulative release percentage of RMD as a free drug in the presence of GSH reductive environment (red) and in the absence of GSH (PBS solution) (black). All data from one experiment (n=1).

4.2.3 Efficacy of RMD loaded PMA_{SH} 100 nm and 400 nm RMDLNPs on reactivation of HIV latency in the J-Lat A2 cell line

To investigate the potency and toxicity profile of RMD loaded PMA_{SH} 100 nm and 400 nm RMDLNPs and RMD free drug on the activation of the HIV-LTR, we used the latent cell line model J-Lat A2. The J-Lat A2 cells line contains a single integrated copy of the HIV LTR driving the expression of the viral Tat- and green fluorescent protein (GFP) genes. Translation of GFP is provided by an internal ribosomal entry site (IRES) leading to LTR-Tat-IRES-GFP (249). Given that GFP expression is under the control of the HIV LTR, activation of the LTR can be quantified in GFP^+ cells using flow cytometry. Additionally, we simultaneously assessed toxicity by Propidium Iodide (live/dead staining, PI) staining. PI live/dead staining was selected as we could not use commonly used fixative amine-reactive live/dead dyes

because PMA_{SH} particles shells contain free thiol groups (490). As a result, an amine-reactive dye will stain the PMA_{SH} particles, resulting in false-positive dead cells.

J-Lat A2 cells were exposed to RMDLNPs (400 and 100 nm in diameter) and the reactivation potency and toxicity profile compared to free RMD. RMD free drug formulations were chosen to represent the minimal and maximal matched dose encapsulated in RMDLNPs formulations (Table 4.1). There is usually a trade-off between potency and toxicity with free RMD, which was previously reported as toxic at a concentration greater than 20 nM (376, 434, 608, 609). We used a combination of phorbol 12-myristate 13-acetate (PMA) and the calcium ionophore ionomycin (Iono) as a positive control, which robustly activates the LTR in this cell line (595). Finally, to determine whether RMD leaked from the RMDLNPs prior to intracellular delivery, we incubated RMDLNPs in cell culture media for ~ 2 days and then centrifuged the RMDLNPs suspension and incubated fresh J-Lat A2 cells with the supernatant (sup RMDLNP).

The RMDLNPs, free drug and controls were incubated in two conditions: (a) continuous exposure for 48- and 72- hours (continuous- treatment) or (b) for 4 hours followed by a washing step and media replacement, followed by 48 hours and 72 hours incubation (pulse- treatment) as previously reported (369) (Figure 4.4 A). We proposed 48- and 72-hours hours treatment to allow time for particles to engage with cells, internalize, and release their cargo into the cytosol resulting in reactivating HIV LTR and the lag time. We proposed 48- and 72-hours hours treatment to allow time for particles to engage with cells, internalize, and release its cargo into the cytosol resulting in reactivating HIV LTR". In addition we choose the 4 hours exposure time because the terminal half-life of RMD *in vivo* is approximately 3 hours (376, 610, 611). The harvested cells were stained with PI and analysed by flow cytometry immediately. For the flow analysis, cells were gated on the forward scatter area (FSC-A), and side scatter area (SSC-A) to locate J-Lat cells. We then gated on forward scatter Height (FSC-H) versus forward scatter area (FSC-A) to exclude doublets. Next, cells were gated for PI and forward scattered area (FSC-A) to exclude dead cells (PI^+). Finally, live cells

(PI^-, %viability) were gated versus GFP to determine PI^-GFP^+ populations (Figure 4.4 B).

In the pulse-treated cells, as predicted, after 48 hours, the RMDLNPs did not show induction of GFP expression compared to DMSO (Figure 4.5 A). This is likely because RMDLNPs required more than 4 hours to internalise efficiently in T cells. We did not observe an increase in GFP expression at any concentration using 100 nm RMLNPs or supernatant from either the 400 nm or 100 nm particles. In contrast, free RMD showed a dose-dependent effect on potency and toxicity. Treatment with 2.5 and 10 nM resulted in over 45 % and 80 % GFP+ cells [p = 0.0202, and 0.0025 unpaired t test] respectively compared to DMSO. (Figure 4.5 A). In cells treated with both RMD 2.5 nM and 10 nm, we observed viability of 77 % and 44 % [p = 0.1567 and 0.0217, unpaired t test], respectively compared to DMSO (Figure 4.5 B). This data is consistent with other studies demonstrating that free RMD is strongly linked to toxicity *in vitro* (434, 609, 612). Using the pulse treatment, at 72 hours, we observed a small increase of GFP^+ cells [12 %] in cells treated with PMA_{SH} 400 nm RMDLNPs compared to DMSO (Figure 4.5C). This delayed increase in GFP at the later time point suggested slow drug release from these particles. Cell viability was decreased compared to DMSO treated cells (Figure 4.5 C). In cells treated with 2.5 nM and 10 nM RMD, we observed an increase in GFP^+ cells of 71 % and 86 % [p = 0.0002 ,0.0001, unpaired t test], respectively compared to DMSO (Figure 4.5 C). A similar relationship between efficacy and cytotoxicity was observed for cells treated with free RMD (Figure 4.5 C). These observations of the accumulated effect of cell toxicity align with the effect of continuous exposure of RMD *in vitro* reported by Jones et al. and Zhao et al. (376, 434).

In sharp contrast, following continuous exposure for 48 h of 400 nm RMDLNPs to cells at the highest ratio (particle: cell ratio of 800:1), we observed significant GFP expression, reaching 70 % [p = 0.0002, unpaired t test compared to DMSO] (Figure 4.6 A). This high response rate was likely due to the longer time for exposure of particles to cells and slower release of encapsulated RMD from silica pores. Cell viability was reduced by the potent activation in cells treated with 400 nm RMDLNPs (Figure 4.6 B). Cells

treated with free RMD at 10 nM compared to 2.5 nM and DMSO showed increased GFP expression following 48 and 72 hours continues-treatment (Figure 4.6 A and C). As expected, a high cytotoxicity effect was observed after 72 hours of continuous treatment (Figure 4.6 B and D), consistent with other studies that reported RMD EC50 of 4.5 ± 1.0 nM (369). Interestingly, at a concentration of 400: and 800:1 particle: cells, of 400 RMDLNPs, we observed an increase of GFP expression, reaching mean values of 62 % and 22 % GFP^+ cells [p = 0.0098, p = 0.0096 unpaired t test], respectively compared to DMSO (Figure 4.6 C).

After 72 hours of continuous treatment, 100 nm RMDLNPs induced GFP expression in 18 % of cells (Figure 4.6 C). The reduced potency of 100 nm RMDLNP is likely due to a reduced capacity to encapsulate a high payload of RMD due to the smaller pore size. This interpretation is supported by our earlier reports of lower encapsulation efficiency and loading capacity in 100 nm particles compared to 400 nm particles (Table 4.1). A similar relationship between efficacy and cytotoxicity was observed for cells treated with RMDLNPs (Figure 4.6 D).

In conclusion, these data demonstrate that, for continuous treatment of J-Lat A2, 400 nm RMDLNP formulation showed equivalent potency of activation of the LTR, but vastly reduced toxicity compared to free RMD.

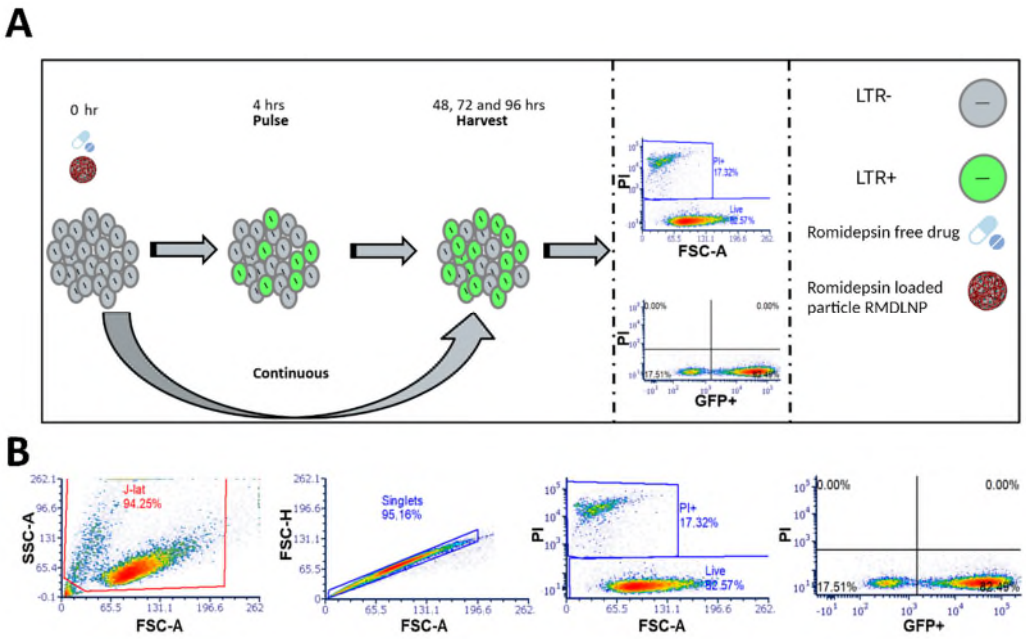

Figure 4.4 Efficacy of RMD loaded PMA_{SH} 100 nm and 400 nm RMDLNPs to activate the HIV-LTR in the J-Lat A2 cell line.

A) Schematic illustration of the method used. In brief, J-Lat A2 cells were treated (using pulsed or continuous treatment) with either free RMD (2.5 nM and 10 nM) or PMA_{SH} RMDLNPs (100 nm and 400 nm) for 24 hours or 72 hours. B) Toxicity and expression of GFP were quantified using flow cytometry. Representative flow cytometry plots and gating strategy for PI- (live) and GFP^+ (activated) is shown.

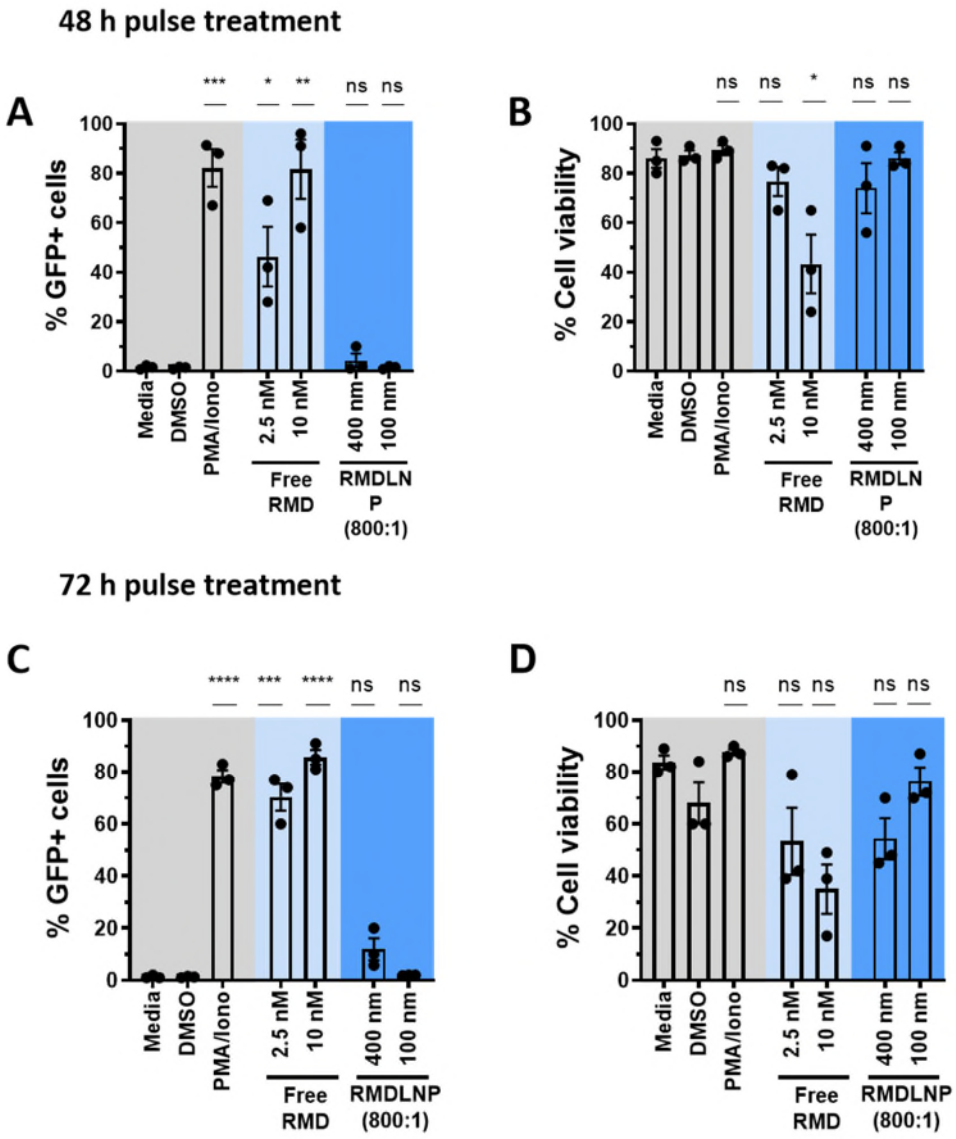

Figure 4.5 PMA_{SH} 100 nm and 400 nm RMDLNPs administered as a pulse did not increase LTR activation in J-Lat A2 cells.

A) Percentage of GFP^+ cells and B) viability from cells treated with free RMD formulations (2.5 nM or 10 nM) and RMD formulated PMA_{SH} particles RMDLNP (100 nm and 400 nm) for 48 hours. C) a percentage of GFP^+ cells and D) viability using the same conditions but after 72 hours of treatment. All data are shown as the mean ± standard error of the mean from three independent experiments (SEM; N = 3). All P values were determined using two-tailed, unpaired t-tests: *P<0.05, **P<0.001, ***P<0.0005 and ****P<0.0001.

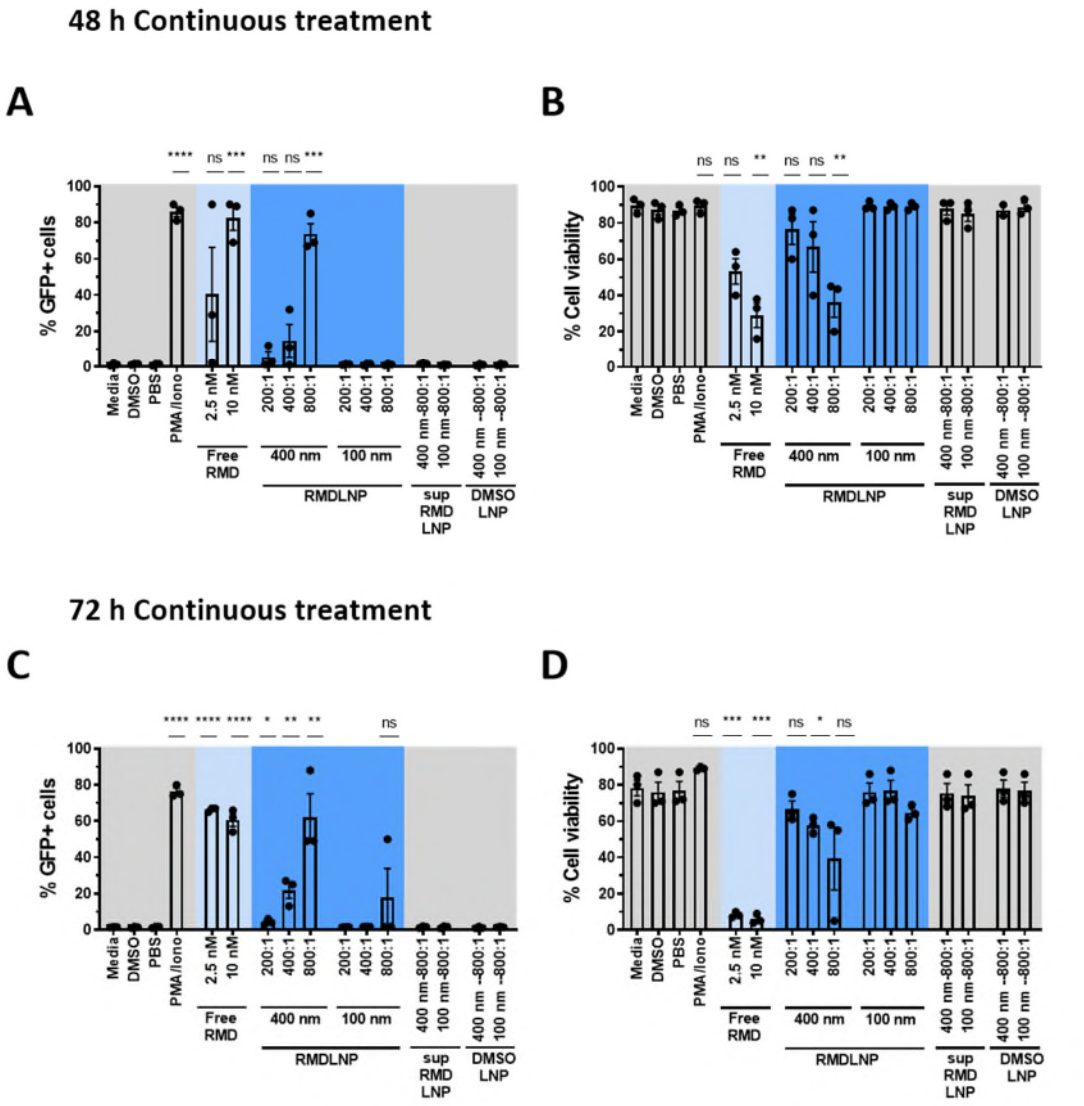

Figure 4.6 PMA_{SH} 100 nm and 400 nm RMDLNPs administered continuously potently increased LTR activation but with no toxicity in J-Lat A2 cells.

A) Percentage of GFP^+ cells and B) viability from cells treated with free RMD formulations (2.5 nM or 10 nM) and RMD formulated PMA_{SH} particles RMDLNP (100 nm and 400 nm) for 48 hours. C) a percentage of GFP^+ cells and D) viability using the same conditions but after 72 hours of treatment. All data are shown as the mean ± standard error of the mean from three independent experiments (SEM; N = 3). All P values were determined using two-tailed, unpaired T-test: *P<0.05, **P<0.001, ***P<0.0005 and ****P<0.0001.

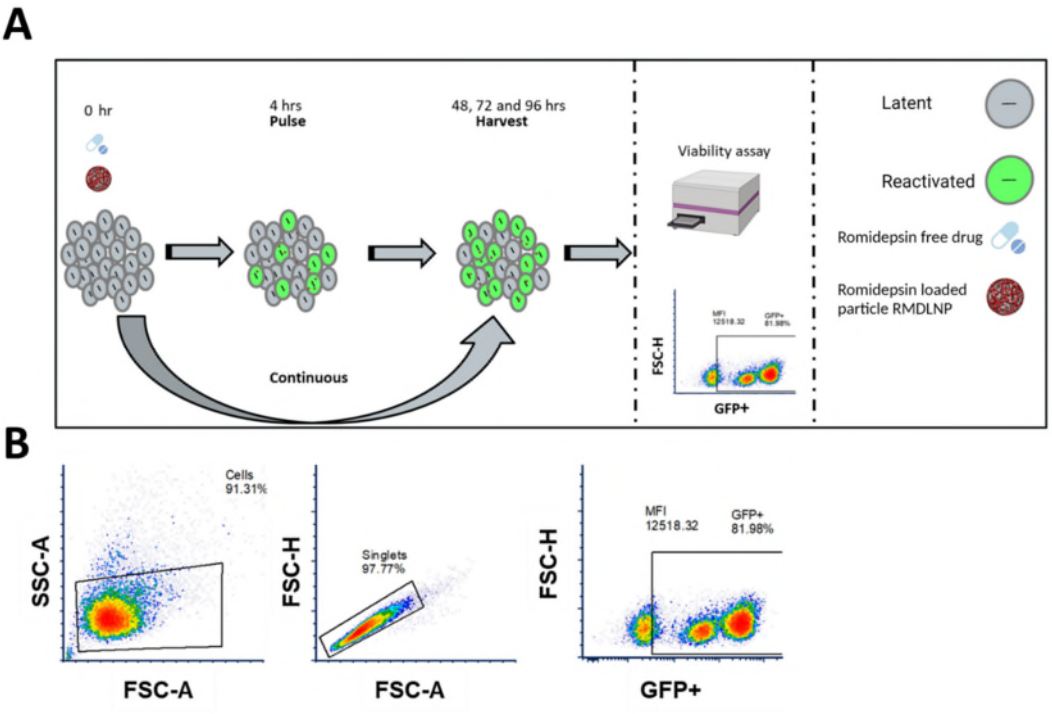

Figure 4.7 Effect of RMD free drug and PMA$_{SH}$ RMDLNPs on activation of the LTR in J-Lat 10.6 cells.

A) Schematic illustration of the method used. In brief, J-Lat A2 cells were pulse-treated with free RMD (2.5 nM and 10 nM) for 4 hours, and cells were washed and then cultured for 48, 72 and 96 hours. In separate experiments, free RMD formulation (2.5 nM and 10 nM) or PMA$_{SH}$ RMDLNPs (100 nm and 400 nm) were incubated continuously for 24 hours or 72 hours. Cell viability was measured using a cell titre glow luciferase-based assay B) Representative gating strategy for GFP$^+$ cells is shown.

4.2.4 RMD loaded PMA$_{SH}$ 400 nm particles RMDLNP reactivate HIV latency with reduced toxicity in J-Lat 10.6 cells

Next, to examine whether RMDLNPs can stimulate HIV latency beyond the minimal promoter system (i.e., J-Lat A2 T cells), we utilised the J-Lat 10.6 cell line. The J-Lat 10.6 T cells contain a stably integrated full-length HIV provirus (10.6 strain) where green fluorescent protein (GFP) replaces the *Nef* coding sequence and a frameshift in *env* that express GFP upon activation of the HIV LTR (249, 613, 614). The percentage of GFP$^+$ cells was measured by flow cytometry and used to assess the potency of free RMD and RMDLNPs (i.e., PMA$_{SH}$ 100 nm and 400 nm). These experiments

were required to be performed in physical containment level 3 (PC3) laboratories which necessitated the use of paraformaldehyde to fix cells, thus precluding the use of live/dead PI staining. To this end, the cytotoxicity of the compounds was determined by monitoring metabolic activity based on the quantification of present ATP. In this model of latent infection, we mimicked similar experimental settings and conditions we used in the J-Lats A2 cells, but we introduced additional time points (i.e., 96 hours) to investigate the slow-release kinetics of RMD from RMDLNPs. To minimise the cytotoxic effect of free RMD in J-Lat T cells, we used a 4-hour pulse treatment with free RMD, followed by extended cell culture for 48, 72 and 96 hours (h) (Figure 4.7 A). Of note, we did not perform pulse treatment with RMDLNPs as we previously demonstrated that particles required a longer time of exposure (longer than 4 hours of exposure to cells) to be able to localise intracellularly and release the encapsulated drug (Figure 4.5 A and C). To quantify potency, samples were harvested, and GFP expression was analysed by flow cytometry. As previously, we gated on FSC-A and SSC-A to identify live J-Lat cells, then gated on FSC-H versus FSC-A to exclude doublet cells. Finally, we quantified the proportion of live cells expressing GFP (Figure 4.7 B).

Following a 4-hours pulse of free RMD free formulation treated cells, at 48 hours, we observed only modest reactivation of HIV with the highest concentration of 10 nM (mean = 8.9 % GFP^+ cells) [p = 0.0028, compared to DMSO, unpaired t test]. In contrast, the positive control of PMA/Iono increased GFP^+ cells with a mean value of 83.7 % [p = 0.0001 unpaired t-test, compared to DMSO] (Figure 4.8 A, left). When cytotoxicity was determined under identical conditions, all tested compounds showed no toxic effect other than DMSO vehicle negative control (Figure 4.8 A, right). In the extended culture of 72 hours and 96 hours-pulse treated cells, we observed a slight decrease of GFP^+ cells (mean = 6 % at 72 h and 5.4 % at 96 h) in cells treated with free RMD (10 nM) compared to the 48 hours-pulse treated cells (Figure 4.8 B and C, left). GFP expression in cells treated with the positive control PMA/Iono induced an increase in GFP+ cells, which plateau at 72 hours, mean = 83.75 %, [p = 0.0001 unpaired t test] (Figure 4.8 B, left).

Cell viability of 400 nm RMDLNPs treated cells remained similar to DMSO negative control cells (Figure 4.8 C and D, right). However, we observed a slight increase in ATP activity in cells treated with the PMA/Iono positive control. We speculated this could have resulted from the proliferation of cells induced by PMA/Iono (615, 616). Pulsed treatment with free RMD induced a lower frequency of GFP^+ cells.

Next, we assessed the latency reversal and toxicity of free RMD and RMDLNPs following continuous treatment of J-Lat 10.6 cells. Interestingly, 400 nm RMDLNPs induced a dose-response reactivation of HIV latency in cells treated with 200:1, 400:1 and 800:1 particles to cells, with 11.75 %, 29 % and 53 % GFP^+ cells observed respectively, [p = 0.0241, 0.0363 and 0.0013 unpaired t-test compared to DMSO treated cells] (Figure 4.9 A, left). Interestingly, with the 400 nm RMDLNP at a ratio of 800 : 1 compared to 2.5 nM and 10 nM free RMD, we showed significantly higher potency in reactivation of HIV latency, with a mean value 53 %, 16 % and 22 % GFP^+ cells, [p = 0.0065 and 0.253 unpaired t test] (Figure 4.9 A, left).

Importantly, the cytotoxicity effect of 400 nm RMDLNPs formulation (800 : 1) were significantly lower, [p = 0.0041 and 0.0001 unpaired t test], compared to 2.5 nM and 10 nM respectively (Figure 4. 9 A, right). Cells treated with 400 nm RMDLNPs did not show a decrease in viability over time (48, 72 and 96 hours), while the lowest concentration RMD free drug formulation (2.5 nM) showed a decrease in cell viability at 48, 72 and 96 hours (55 %, 15 % and 6 % respectively, [p = 0.011, $p<0.001$ and $p<0.001$ respectively, unpaired t test] over time compared to the DMSO treated cells (Figure 4.9 A, B, and C left).

We also quantified the change in GFP expression over time in J-Lat 10.6 T cells for 96 hours. We observed that GFP expression for PMA/Iono, free RMD and RMDLNPs reached a maximum or plateau at 48 hours of drug exposure (Figure 4.9 A, left). The positive control PMA/Iono induced expression of GFP to a mean value of 82 %, [$p<0.001$ unpaired t test], followed by 400 nm RMDLNP at a ratio of 800: 1 to a mean value of 53 % of GFP^+ cells [p = 0.0013, unpaired t test] (Figure 4.9 A, left). The 400 nm RMDLNPs induced a concentration-dependent expression of GFP ranging from 6 % to 53 % of cells (ratio of particle: cell, 200:1, 400:1 and 800:1)

(Figure 4.9 A-C). After 48, 72 and 96 hours, in cells treated with free RMD at 10 nM, we observed a slight increase in GFP^+ cells with a mean value of 22 %, 25 % and 29 %, respectively (Figure 4.9, A, B and C, right).
Overall, these data demonstrated the ability of RMD loaded PMA_{SH} 400 nm particles RMDLNPs to induce greater reactivation of HIV latency while avoiding toxicity in J-Lat 10.6 cells.

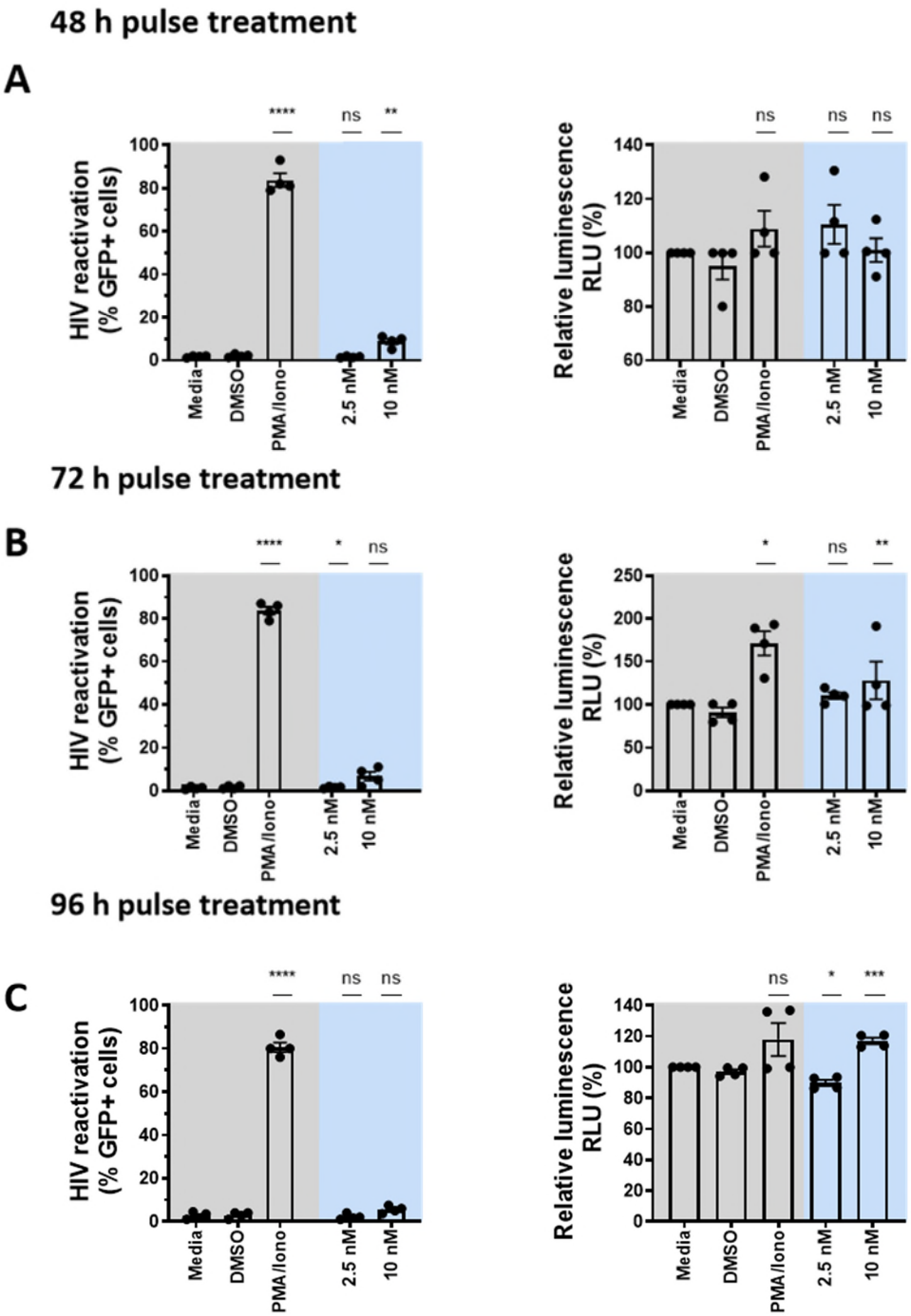

Figure 4.8 Free RMD induced modest activation of HIV latency from J-Lat 10.6 cells.

A) GFP expression as a surrogate for HIV reactivation and cell viability is shown in J-Lat 10.6 cells in the presence of free RMD (2.5 nM and 10 nM) pulsed for 4 hours and then incubated for 48; B) 72 and C) 96 hours**.** All data are shown as the mean ± standard error of the mean from three independent experiments (SEM; N = 3). All P values were determined using two-tailed, unpaired T-test: *P<0.05, **P<0.001, ***P<0.0005 and ****P<0.0001.

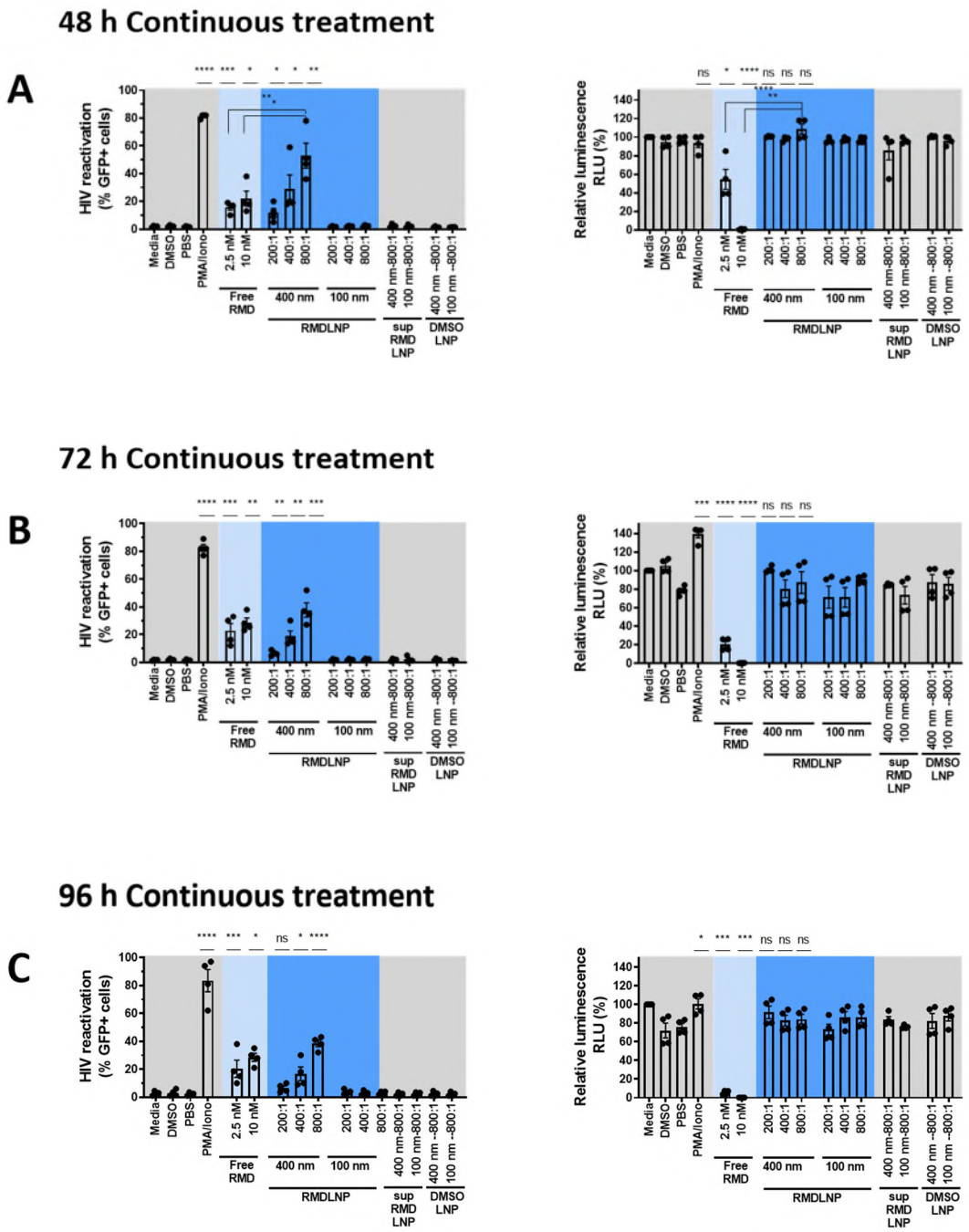

Figure 4.9 PMA_{SH} 400 nm RMDLNPs enhanced latent HIV reactivation and reduced cytotoxicity in JLat 10.6 cells.

A) Free RMD or PMA_{SH} 100 nm and 400 nm RMDLNPs were incubated with J-Lat 10.6 cells, and GFP expression as a surrogate for HIV reactivation or cell viability was quantified after 48; B) 72, and C) 96 hours. All data are shown as the mean ± standard error of the mean (SEM; N = 4). All P values were determined using unpaired two-tailed, unpaired T test: *P<0.05, **P<0.001, ***P<0.0005 and ****P<0.0001.

4.3 DISCUSSION

A major obstacle to eliminating latently infected cells through the shock and kill strategy is balancing LRA potency and toxicity. Besides a cytotoxic effect on $CD4^+$ T cells, several LRAs (e.g. the HDACi RMD) showed cytotoxicity on HIV-specific $CD8^+$ T cells resulting in exhaustion and impaired function (374, 376, 611, 617). Ultimately, this is not acceptable given that an efficient HIV-specific immune response is also needed to eliminate infected cells. Nanoparticles have shown great promise in successfully delivering pharmacological therapeutics that target endogenous immune cells while limiting exposure of the drug systemically (410, 416, 417, 455, 597, 618). Here we demonstrated that delivery of RMD by nanoparticles could not only enhance its potency in reversing latency but can also dramatically reduce toxicity in a latently infected cell line. Whether these findings can be translated to primary cells remains to be determined.

We successfully encapsulated the HDACi RMD, a drug of limited solubility (458), into 100 nm and 400 nm MS particles, then formulated multilayer PMA_{SH} RMD loaded particles (PMA_{SH} 100 nm and 400 nm RMDLNP). We showed that RMD loaded PMA_{SH} particles (400 nm RMDLNPs) can sufficiently reactivate HIV gene expression in latently infected cell lines (J-Lat A2 and J-Lat 10.6 T cells) without a significant drop in cell viability. First, this work is potentially relevant to strategies to encapsulate other hydrophobic drugs. Second, we did not observe an effect when cells were pulse-treated with 400 nm RMDLNPs. We propose that 4 hours was insufficient for particles to internalise, degrade and release their cargo in J-Lat A2 T cells. Future work should include an assessment of the internalisation kinetics of RMDLNP into T cells. Several studies have reported the interaction of unloaded and PMA_{SH} particles with cells over time (453, 492, 619). However, these studies were either limited to quantification of association (not internalisation) or using a specific cell type (Hela cells and phagocytic cells), which are different from T cells, which are non-phagocytic cells.

When we continuously exposed 400nm RMDLNPs and free RMD to J-Lat A2 cells, both formulations activated LTR expression to similar levels seen with the positive control PMA/Iono. However, the cytotoxicity of these

formulations was moderate in comparison to DMSO treated cells. These findings are in agreement with a recent study that examined RMD combined with negatively charged dendrimer nanoparticles and the impact on J89GFP T cells after 48 hours treatment (608). Although we only assessed these formulations in cell lines, it is important to note that we previously investigated the toxicity of unloaded PMA_{SH} particles in primary T cells and found minimal toxicity after 24 and 48 hours of treatment, except for 800 nm PMA_{SH}-PLL particles (Chapter 3). Clinical translatability will be different as these RMD loaded particles must be targeted to $CD4^+$ T cells which will adapt different association kinetics. In addition, our *in vitro* experiment design cannot predict the association kinetics with T cells *in vivo.*

Future work will need to prioritise the assessment of these novel reagents in primary T cells.

Using 400 nm RMDLNP, we were able to uncouple the potency of HIV reactivation and cytotoxicity in the J-Lat 10.6 cell line. There may be several potential explanations for this finding, extrapolating from previous work using different cells (mainly cancer cell lines) and nanoparticle systems. First, RMD is a small prodrug molecule (MW = 540.7) and is activated inside the cell by glutathione (GSH) (368). This characteristic can facilitate cell uptake by simple diffusion (73, 74); therefore, RMD cytotoxicity is dose-dependent (370, 593, 612, 620). In contrast, when RMD is encapsulated into PMA_{SH} particles, RMDLNPs, energy-dependent cell internalisation is needed while the drug is within the MS. This will prevent accumulative exposure of the drug intracellularly. Therefore, the sustained and slow drug release kinetic property of PMA_{SH} particles (492, 621) probably contributes to the reduced cytotoxic effect of RMD, compared to free RMD, where cytotoxicity increased over time. Second, free RMD is transported intracellularly via an influx transporter, the organic anion transporter, OATP2 and OATP3 and clearance of intracellular RMD (Efflux) by the permeability glycoprotein (p-glycoprotein) (593, 622, 623). In contrast, RMDLNPs formulation, to the best of our knowledge, most likely undergoes endocytosis, although the exact pathway of uptake of PMA_{SH} particles in T cells remains unknown. However, given the size of these 400 nm particles, internalisation is likely to occur through non-specific macro-pinocytosis

(416, 440, 534, 624). Third, the intracellular trafficking of free RMD is distinct from PMA_{SH} RMDLNPs. Intracellular trafficking of free RMD is believed to occur via p-glycoprotein, but the exact mechanism of cellular entry remains poorly defined (368). In contrast, PMA_{SH} RMDLNP is believed to traffic through the endosomal pathway, then accumulate in the cytosol, where the release of the encapsulated RMD occurs (490, 492). Off note, endosomal escape strategies have been utilized in increasing therapeutic efficiency. In particular, if nanoparticle or loaded cargo are entrapped in acidic endosomal compartments, degraded in lysosomes or recycled back to the cell membrane, the therapeutic can be rendered completely ineffective (625, 626). Manipulation of the host cell biology, using small molecules for example, or the design of more effective delivery systems that can achieve endosomal escape represents an opportunity for boosting endosomal escape and delivery efficiency (500, 626, 627). Finally, prior studies have shown that RMD toxicity is highly dependent on mitochondrial engagement and activation of the intrinsic apoptosis pathway (366, 628, 629). It is possible that internalised RMDLNPs release RMD in a different cellular compartment, bypassing the mitochondria-mediated apoptosis pathway.

Further studies are necessary to investigate the molecular mechanism involved in the intracellular trafficking of RMDLNPs and the location of the release of RMD within cellular compartments. This could potentially be done by labelling the RMD with a fluorochrome and examining intracellular target engagement and resident time of labelled RMD (630, 631). Additionally, assessing mitochondrial activity in the presence of both formulations could pave the way to understand the molecular mechanism of action.

We also observed different GFP expression (activation) and cytotoxicity patterns between J-Lat A2 T cells and J-Lat 10.6 T cells when treated with free RMD and RMDLNPs formulations. Although both cell lines are derived from Jurkat cells, these cell lines may have different sensitivity to the HDACi RMD. There may be several explanations for this variation. First, both cell lines are distinct clones with the LTR integrated at different sites. J-Lat A2 cells harbour a minimal HIV minigenome feedback construct containing LTR-Tat-IRES-GFP virus (similar to H2 and A10 clone), while J-Lat 10.6 cells harbour the full-length HIV (HIV-R7-E^{-}GFP) construct. Following

reactivation of the J-Lat A2 clone, only part of the HIV (Tat) activates the HIV LTR promoter and subsequently drives GFP expression. Whereas the J-Lat 10.6 clone contains full-length HIV that is heavily repressed by DNA methylation (249, 632, 633). Second, provirus integration in latently infected cells usually occurs at the site of heterochromatin (249). Thus different integration sites in latently infected cell lines (J-Lat A2 and 10.6 clones) will have different surrounding chromatin structures and could also account for the difference in activation observed with RMD (179, 634). Finally and importantly, these differential effects on HIV activation of epigenetic transcription may not be surprising since the chromatin structure of the LTR can differ for the proviruses integrated into one cell line or another (137, 635, 636).

Although we have made an exciting discovery using PMA_{SH} particles to uncouple potency and toxicity, an important caveat in this study is that we did not evaluate primary T cells or $CD4^+$ T cells from people living with HIV (PLWH) *ex vivo* (322, 637, 638). In PLWH on ART, the frequency of latently infected $CD4^+$ T cells in blood is low, and only a small fraction of latently infected $CD4^+$ T cells contain intact replication-competent provirus (97). Furthermore, the virus will be integrated into a range of locations and with different epigenetic environments. However, we showed that in two diverse cell lines, 400 nm RMDLNPs could reverse HIV latency with reduced cytotoxicity. Further studies will be needed to investigate the potential effect of these particles in reversing latency in $CD4^+$T cells from PLWH *ex vivo*.

4.4 CONCLUSION

In summary, we showed in two models of HIV latency that PMA_{SH} 400 nm RMDLNP particles compared to free RMD induced more potent reactivation of the LTR with reduced toxicity. However, although our results are promising, the mechanism of our RMDLNPs reactivation and the use of more physiological models such as latently infected primary cells or *in vivo* models should be studied. Finally, these data illustrate the potential use of nano-engineered drug delivery systems to enhance latency reversal strategies.

5 Nanoparticles delivery of 5`triphosphate RNA to tackle HIV latency

5.1 INTRODUCTION

One strategy toward eliminating HIV latency is the activation of HIV viral production by latency reversal agents (LRAs) to induce virus-mediated cytolysis or clearance through immune recognition in the presence of ART (often called "shock and kill") (272, 312). However, although there is evidence of latency reversal in clinical trials of LRA, no studies in people with HIV have yet shown a decrease in the reservoir (61, 375, 587). Therefore, more potent and less toxic LRAs are still needed and almost certainly need to be combined with immunotherapeutic agents or pro-apoptotic drugs (95, 588, 639–642).

Innate immune responses have been appreciated to play an essential role in the pathogenesis of HIV infection and shaping the adaptive immune response (313, 643–646). Innate immune signalling pathways are activated by pattern recognition receptors (PRRs) and can be exploited to treat viral infection (313, 647, 648). Recently, Gayo et al. have demonstrated that exposure of conventional dendritic cells (cDCs) from elite controlers (EC) to HIV infection effectively mounted cell-intrinsic type I interferon (IFN) secretion and enhanced HIV-specific $CD8^+$ T cells responses (649). Retinoic acid-inducible gene I (RIG-I) is a cytosolic DexD/H box RNA helicase and belongs to the PRR family (650–653) that can sense cytoplasmatic 5` triphosphorylated double-stranded RNA (ds RNA). Upon recognising pathogenic RNA, RIG-I induces a signalling cascade leading to phosphorylation of IFN regulatory factors 3 and 7 (IRF3/7) and induction of a type I IFN dominated antiviral response (648, 654). These responses can also lead to apoptosis (655, 656).

Following virus attachment and entry into the cell, the HIV genome consisting of two identical copies of positive-strand ssRNA is placed into the cell cytoplasm along with the viral capsid. During reverse transcription, RIG-I senses both monomeric and dimeric forms of HIV dsRNA (657, 658). However, HIV infection evades RIG-I signalling by sequestration and degradation (658), resulting in lower RIG-I protein expression levels in $CD4^+$ T cells compared to healthy individuals from people living with HIV (659). In addition, HIV infection has developed strategies to circumvent immune surveillance and manipulates antiviral immune response (660, 661). Following the HIV replication cycle, abortive HIV RNA, which contains a 5'cap structure and a polyadenylated (poly-A) tail that is released following transcription and translation of provirus, is a poor pathogen-associated molecular pattern (PAMP) for RIG-I recognition (646, 657, 662).

Synthetic RIG-I agonist ligand is a 5'triphosphate double-strand RNA (3p dsRNA) (3p dsRNA, 21 nucleotides (nt) base pair RNA stretch) that was generated by in vitro transcription reaction (IVT) (516, 650). RIG-I agonists could potentially act as latency reversal agents through activation of p300 acetyltransferase and the non-canonical NF-kB pathway, which could lead to the stimulation of HIV transcription and promote apoptosis of reactivated cells through the induction of type I IFN (663, 664). Despite RIG-I agonists promising latency reversal and antiviral activities, its efficacy in activating antiviral innate immunity, its activity is hindered by its poor delivery to target cells (136). Several barriers include serum nuclease degradation and poor delivery of highly hydrophilic dsRNA through membranes into the cytosol, where RIG-I is localized (665, 666).

One major challenge for delivering nucleic acid to $CD4^+$ T cells is the fact that $CD4^+$ T-cells are not phagocytic. Soft glycogen nanoparticles (NP) are a promising delivery system capable of efficiently encapsulating nucleic acids (418, 498). The advantages of soft glycogen NP over other synthetic and natural polymers are their tunable size, degradability, and lack of toxicity at high concentrations (418). Glycogen NP can be synthesised from different biological sources such as bovine liver (BG), rabbit liver (RG) and oysters (OG) (482, 497). The hyperbranched BG glycogen NPs are a favourable non-viral gene delivery system because they have endo-

lysosomolytic properties allowing for cytosolic localisation and endosomal escape. Second, they can deliver multiple copies of oligonucleotides and finally, they have reduced cytotoxicity (418, 499, 500).

Our aim in the chapter was to develop a novel strategy for delivering a RIG-I agonist into a T cell. We used ethylenediamine BG_{EDA} NP to deliver 5' triphosphate double-stranded RNA (3p dsRNA) to T cells. We evaluated RIG-I activity by quantifying interferon stimulating genes (ISG) and the secretion of type I IFN and NF-κB activation in THP-1 cell line, primary $CD4^+$ T cells and human peripheral blood mononuclear cells (PBMC). Finally, we assessed the effects of this RIG-I agonist on the induction of HIV expression in latently infected J-Lat A2 cell lines.

5.2 RESULTS

5.2.1 Synthesis of the cationic bovine glycogen (BG) nanoparticle (NP) RIG-I agonist for *in vitro* delivery

To deliver a synthetic RIG-I agonist (RIG-I A) to T cells, we first evaluated the ability of BG NP to form a stable complex with 3p dsRNA, a previously described method (418). We used dsRNA (21 nt in length) (5'OH-RNA) as a negative control ligand (Ctr ligand) because this construct lacks a triphosphate group, as previously reported (516, 667). BG NPs were synthesised as previously described (418). To construct BG NP/RIG-I A and BG NP/Ctr ligand complexes, we used the positively charged ethylenediamine modified BG (BG_{EDA}) NP to facilitate electrostatic interaction with 3p-dsRNA (418). Throughout this study, we will represent 5'-3p dsRNA' as RIG-I A and 'dsRNA, 5'OH-RNA' as Ctr (control) ligand for ease of terminology.

The cationic BG particles were incubated with the synthetic RIG-I A or the Ctr ligand for 15 minutes, allowed to equilibrate and form an electrostatic interaction between the NP and nucleic acid (Figure 5.1 A). To deliver BG_{EDA} 3p/dsRNA into T cells, fine control over the complexations is necessary because rapid aggregation can be driven by the electrostatic interaction between the attached BG_{EDA} and dsRNA molecule complex. To determine the optimal ratio needed to fully complex dsRNA and BG_{EDA} NP, we used a different ratio as a weight per weight ratio (W/W) of the anionic charged

dsRNA and cationic charged BG_{EDA} NPs. Formation of the BG_{EDA}-RIG-I A and BG_{EDA}-Ctr ligand complexes was assessed by agarose gel electrophoresis. Retardation of migration was examined at escalating ratios of BG_{EDA} to 3p-dsRNA and using naked dsRNA and BG_{EDA} as a negative control indicating unbound dsRNA.

As shown in (Figure 5.1 B), the migration of 3pdsRNA was completely retarded at W/W ratios of 4:1 BG_{EDA}-RIG-I A and BG_{EDA}-Ctr ligand. Complete NP and dsRNA complexation was achieved for both BG_{EDA}-RIG-I A and BG_{EDA}-Ctr ligand at a ratio of 5:1 and 6:1, respectively (Figure 5.1 B). This result is consistent with previous results from Wojnilowicz et al., who used BG_{EDA} NP conjugated with siRNA (418). Considering that one molecule of BG_{EDA} can bind five molecules of dsRNA (418), we concluded that ratios from 6:1 would be optimal for subsequent investigations.

We further characterised the size and surface charge of BG_{EDA} NP alone, BG_{EDA}-RIG-I A and BG_{EDA}-Ctr ligand constructs (ratio 6:1) using DLS (size) and micro electrophoresis (surface charge) techniques. As expected, BG NP alone showed a mean hydrodynamic diameter of 12 nm (polydispersity index, PDI of 0.126), while BG_{EDA}-RIG-I A and BG_{EDA}-Ctr ligand showed an increase in size with a mean hydrodynamic diameter of 20 nm (PDI of 0.196) and 17 nm (PDI of 0.247), respectively (Table 5.1) (Figure 5.2 A). The increase in size observed in BG_{EDA}-RIG-I A and BG_{EDA}-Ctr ligand further confirmed the complexation and, importantly, indicated no aggregation. Although we did not observe aggregation at the higher w/w ratio tested (6:1), Wojnilowicz et al. observed a dramatic increase in size (800 nm-900 nm) when BG_{EDA} NPs were mixed with siRNA at a higher w/w ratio (7:1) (418). Aggregation was most likely induced by free BG_{EDA} NPs. In addition to size, zeta potential (Ƶ) measurement of BG_{EDA} (naked particles) decreased from +19mV to slightly positive values of +7 and +6 at BG_{EDA}-RIG-I A and BG_{EDA}-Ctr ligand, respectively (Figure 5.2 B, Table 5.1), indicating the complexation of dsRNA to BG_{EDA} NP was due to the electrostatic interaction between cationic BG_{EDA} NP and anionic 3p/dsRNA.

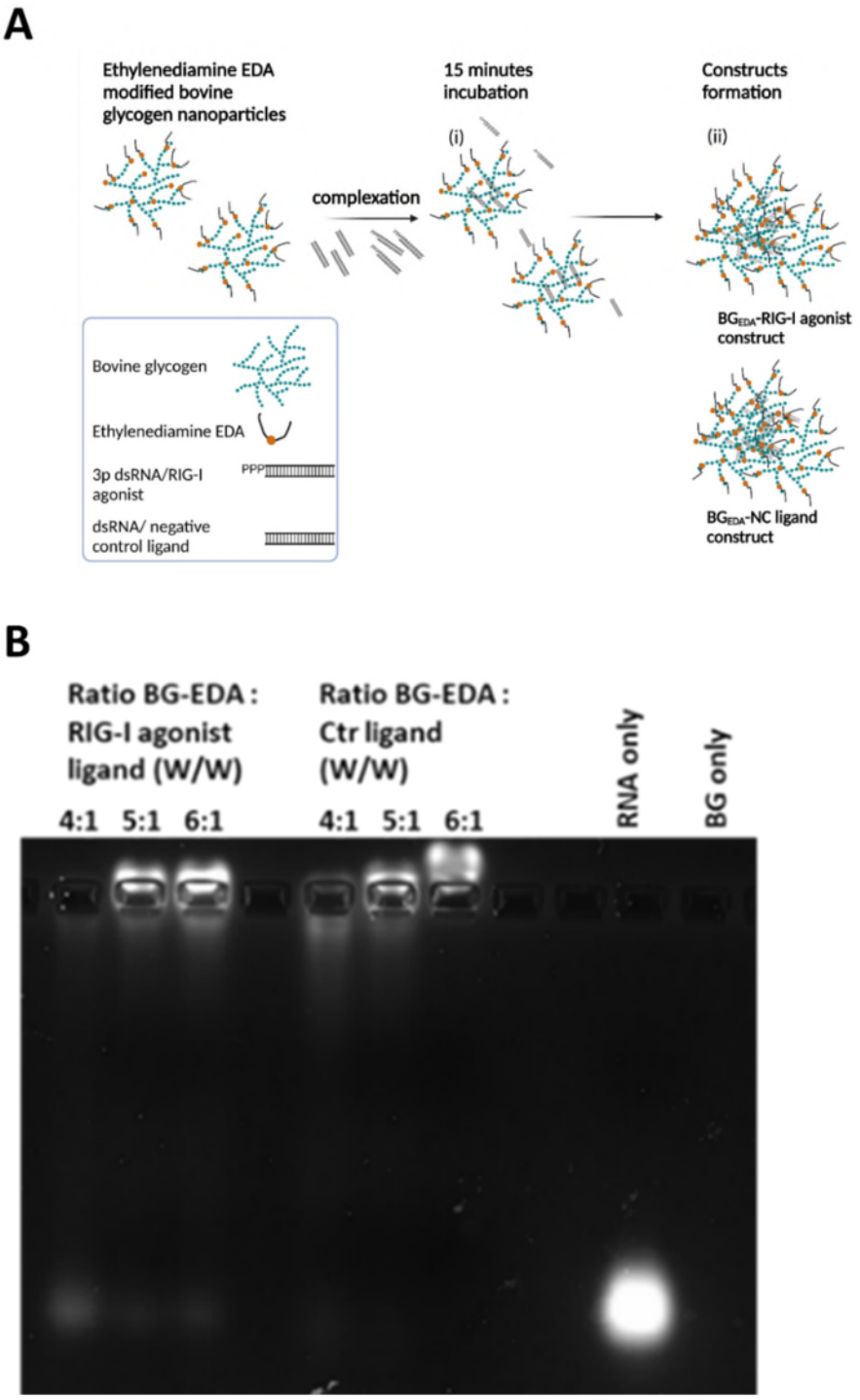

Figure 5.1 Complexation of ethylenediamine modified bovine glycogen-3p-dsRNA (RIG-I agonist)/dsRNA (Ctr ligand) constructs.

A) Schematic of glycogen/3p-dsRNA and dsRNA formation, (i) mixing of 3p-dsRNA with bovine glycogen nanoparticles (BG NP) at the optimised w/w ratio; (ii) formation of glycogen-3p/dsRNA constructs with controlled size and surface charge. Green circles in the glycogen structure indicate amino functionalities. B) Agarose gel electrophoresis used to evaluate the degree

of nucleic acid complexation formed at 5:1 AND 6:1, particle-to-3p-dsRNA w/w ratios: BG_{EDA}-3p-dsRNA (RIG-I agonist) and BG_{EDA}-dsRNA (Ctr ligand). Schematic (A) adapted from Wojnilowicz et al. (418).

Table 5.1 Physicochemical properties (size and zeta-potential) of ethylenediamine (EDA) modified glycogen nanoparticles from bovine liver BG_{EDA}, BG_{EDA}-RIG-I A and BG_{EDA}-Ctr ligand.

Particle/Construct	Size (d.nm)	PDI	Zeta potential (mV)	EDA modification (%)
BG_{EDA}	12 ± 6	0.126	19.5 ±5	15.5
BG_{EDA}-RIG-I A	20 ± 10	0.196	7 ±2	15.5
BG_{EDA}-Ctr ligand	17 ± 10	0.247	6 ±3	15.5

Hydrodynamic diameter determined by dynamic light scattering (DLS); zeta potential determined by micro electrophoresis; PDI = polydispersity index. Data represent mean ± standard deviation (SD) from two independently formulated batches and three independent measurements of each batch.

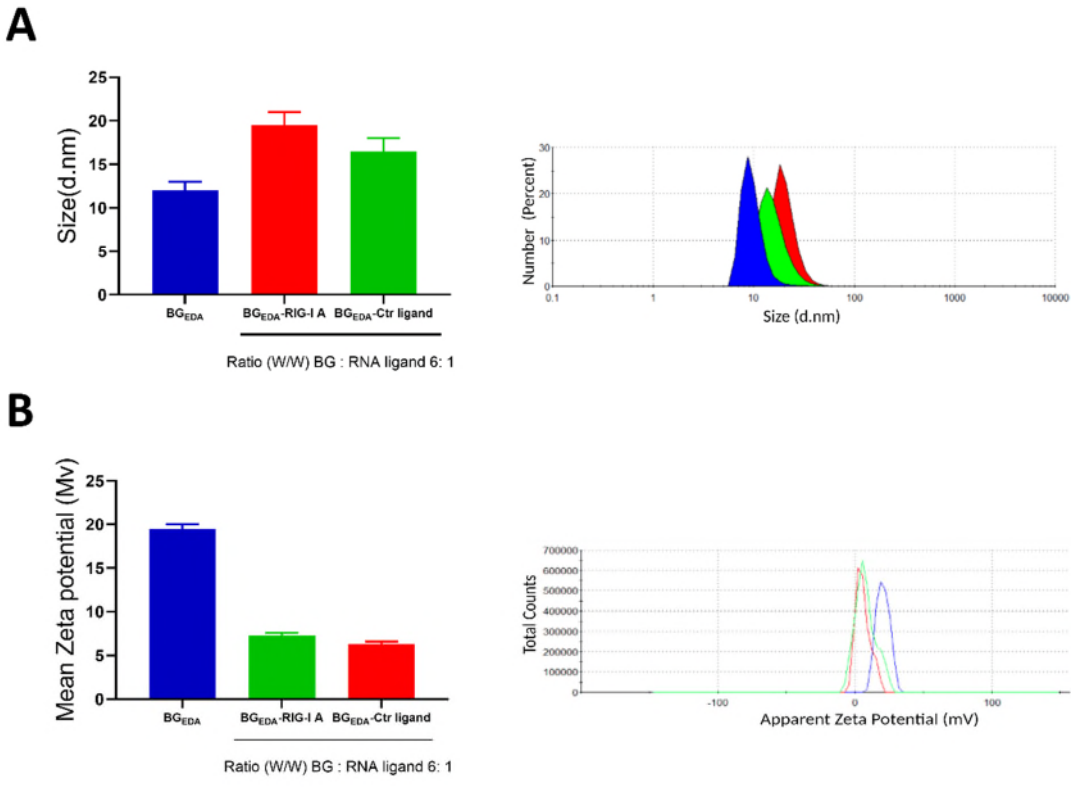

Figure 5.2 Characterisation of size and surface charge of nanoengineered BG_{EDA}-RIG-I agonist and BG_{EDA}-Ctr ligand constructs. A) Column graph showing hydrodynamic diameter measurement of BG_{EDA} (Blue), BG_{EDA}-RIG-I agonist complex (BG_{EDA}-RIG-I A, Green), and BG_{EDA}-control ligand complex (BG_{EDA}-Ctr ligand, Red) constructs at determined 6:1 w/w ratio (left) and a representative graph of dynamic light scattering (DLS) showing the size of the NP (right). B) The zeta-potential of BG_{EDA}, BG_{EDA}-RIG-I agonist, and BG_{EDA}-Ctr ligand constructs at determined 6:1 w/w ratio (left) and a representative graph of microelectrophoresis showing the zeta measurement of each construct. All column graphs are presented as the mean ± standard deviation (SD) of two independently formulated batches and three independent measurements.

5.2.2 Endosomolytic BG_{EDA} loaded RIG-I agonists trigger the IFN I and NF-*κ*B pathways in the undifferentiated THP-1 monocyte dual reporter cell line

Synthetic RIG-I agonist ligands have been shown to trigger the release of type I IFN in T cells mediated by interferon regulatory factor 3/7/9 (IRF3/7/9) and the activation of interferon-stimulated genes (ISGs) and NF-*κ*B signalling (133, 668–670). We first investigated the delivery and activity of BG_{EDA}-RIG-I A and BG_{EDA}-Ctr ligand in the THP-1 monocyte dual reporter cell line. THP-1 cell line is a monocytic cell line that contains an integrated copy of a secreted luciferase (Lucia) gene reporter driven by the expression of interferon stimulating genes 54 (ISG54), a known target gene of the transcriptional factor for IRF9; and an NF-κB inducible secreted alkaline phosphate (SEAP) (Figure 5.3 A) (507). BG_{EDA} NPs conjugated with RIG-IA (BG_{EDA}- RIG-I A) were used to examine RIG-I agonist dependent expression of type 1 interferon (IFN I) (ISG54-Luci) and NF-κB signalling (NF-κB-SEAP) (Figure 5.3 A). Additionally, we used Lipofectamine 2000 transfection (a commercial lipid-based transfection agent used primarily for *in vitro* nucleic acid transfections) as a positive control. To test the inducibility of ISG54-luciferase in THP-1 dual cells, we titrated recombinant human interferon-alpha subtype (rhIFN-α) on THP-1 cells. The rhIFN-α

subtype is classified as an intermediate/strong ISG54 (IFN I) inducer (671, 672).

In the classical model of IFN I activation, rhIFN-α first binds to the interferon-alpha and beta receptor subunit 1 IFNAR1 and IFNAR2 receptors to form a high-affinity ternary complex that induces a signalling cascade initiated through the activation of Janus kinase 1 (Jak1) and tyrosine kinase 2 (Tyk2) followed by phosphorylation and recruitment of signal transducer and activator of transcription 1 and 2 (STAT1) and (STAT2) transcription factors (673, 674). STAT1 and STAT2 subsequently trimerise with IRF9 to form the transcription factor interferon-stimulated growth factor-3 (ISGF3) complex. Once this complex is formed, ISGF3 translocates to the nucleus and binds to interferon-stimulated response elements (ISREs), resulting in the activation of ISGs (671, 675, 676). In THP-1 cells treated with rhIFN-α, we observed an increase in ISG54-Luci activity at increased concentrations post 24 hours and 48 hours (Figure 5.3 B), confirming the biological potency of rhIFN-α in inducing IFN I in THP-1 cells.

Next, THP-1 cells were challenged with (500 ng/mL) BG_{EDA}-RIG-I A, BG_{EDA}-Ctr ligand or an equal amount of RIG-I A and ctr ligand transfected with lipofectamine 2000. Additionally, to validate the importance of BG_{EDA} NP delivery to enhance RIG-I agonist activity, free RIG-I A, Ctr ligand and BG_{EDA} NP were used as controls. Induction of ISG54-Luci and NF-κB-SEAP were analysed post 24 hours and 48 hours post-treatment. Free RIG-I A or Ctr ligand (that was not conjugated with NP or Lipofectamine) or BG_{EDA} did not induce expression of ISG54-Luci compared to untreated cells after 24 hours and 48 h incubation (Figure 5.4 A-D). This result is potentially consistent with poor cytosolic bioavailability. Transfection of RIG-I A by lipofectamine induced potent ISG54-Luci activity at both 24 hours and 48 hours compared to untreated cells (mean fold change induction after 24 hours and 48 hours was 152 and 22 respectively) (Figure 5.4 A-D). In contrast, modest activity was observed in lipofectamine-Ctr ligand transfected cells (mean fold change induction after 24 hours and 48 hours was 5 and 6 respectively) (Figure 5.4 A-D).

BG_{EDA} NP delivery of RIG-I A (BG_{EDA}-RIG-I A) show enhanced ISG54-Luci induction in THP-1 cells compared to untreated cells (mean fold change

after 24 hours and 48 hours was 45 and 8-fold respectively) (Figure 5.4 A-B). Additionally, no activity was observed in cells treated with BG_{EDA}-Ctr ligand compared to untreated cells (mean fold change induction post 24 hours and 48 hours was 1.1 and 2.1 respectively) (Figure 5.4 C-D), confirming that 5' triphosphate specifically activated RIG-I signalling (650). We did observe some non-specific activity in cells transfected with lipofectamine and the Ctrl as well as BG_{EDA}-Ctr ligand (mean fold change compared to untreated cells was 2.3 and 2.1 respectively), suggesting that dsRNA can also bind and stimulate RIG-I *in vitro* (650, 651, 677–679).

It is well documented that RIG-I activation also stimulates the non-canonical NF-κB pathway (645, 680). In cells treated with free RIG-I A, Ctr ligand or BG_{EDA}, we observed a modest increase in induction of NF-κB-SEAP compared to untreated cells (mean fold change increase after 24 hours was 6.6 and 5.2 respectively and after 48 hours was 2.2, 1.2 and 3.3 respectively) (Figure 5.5 A-D). In addition, transfection of RIG-I A by lipofectamine induced non-specific NF-κB-SEAP activity compared to untreated controls (mean fold change at 24 hours and 48 hours was 13.8 and 9.4 respectively) (Figure 5.5 A-D). A modest increase was also seen at 24 hours only with transfection of Ctrl by lipofectamine (mean fold increase at 24 hours and 48 hours was 1.2 and 1 respectively) (Figure 5.5 A-D). Schlee et al. and Schmidt et al. reported that double-stranded RNA molecules that do not possess a 5′-triphosphate end might exhibit very low and uncontrolled RIG-I stimulation (653, 681). Indeed, the presence of 5' triphosphate end in RIG-I A supports the interaction of the dsRNA lysine residues in the RNA binding cleft of the C-terminal domain of RIG-I (668, 682, 683).

Delivery of BG_{EDA}-RIG-I A in THP-1 cells showed increased production of NF-κB in THP-1 cells compared to untreated cells (mean fold increase at 24 hours and 48 hours was 7.6 and 11 respectively) (Figure 5.5 A-B). Extended incubation of BG_{EDA}-RIG-I A to 48 hours resulted in comparable NF-κB induction over the delivery of RIG-I A with Lipofectamine (Figure 5.5 C-D).

In summary, these data showed that delivery of RIG-I A either via BG_{EDA} or lipofectamine to THP-1 dual cell reporter enhanced ISG54-Luci and NF-κB-SEAP activity compared to a Ctr ligand. Importantly, these data

demonstrated the capacity of BG_{EDA}-RIG-I A to stimulate RIG-I activation and subsequently stimulate IFN I and NF-κB pathways in the THP-1 dual monocyte cells.

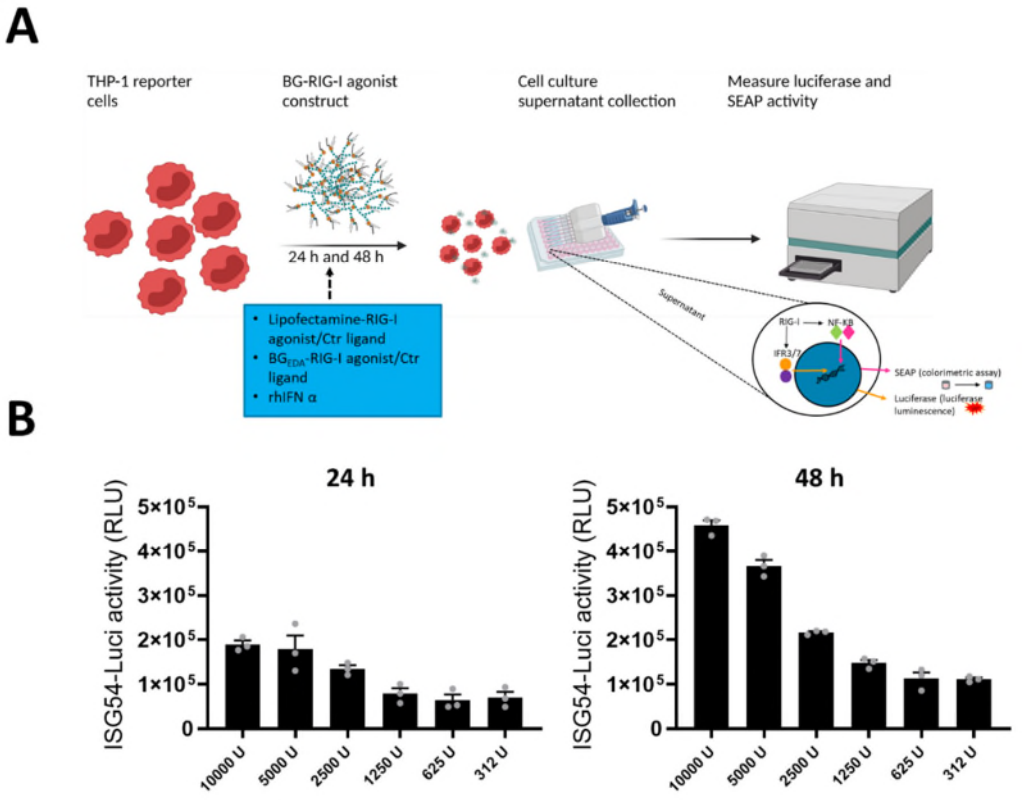

Figure 5.3 Evaluation of the activity of BG_{EDA}-RIG-I A in undifferentiated THP-1 dual reporter cell line.

A) Schematic representation of the methods used. In brief, the THP-1 dual reporter cell line was treated with BG_{EDA}-RIG-I A and BG_{EDA}-Ctr ligand and interferon-stimulated gene (ISGs) and nuclear factor-κB (NF-κB) were quantified in the supernatant. THP1-Dual cells were incubated with increasing concentrations of recombinant human IFN-α (rhIFN- α) (U/mL), and after 24 hours B) and C) 48 hours. ISG activation was assessed by measuring Lucia luciferase activity (ISG54-Luci) in the supernatant. All data are presented as column graphs, and the means of biological duplicates ± standard error of the mean is shown from three independent experiments (SEM; N = 3).

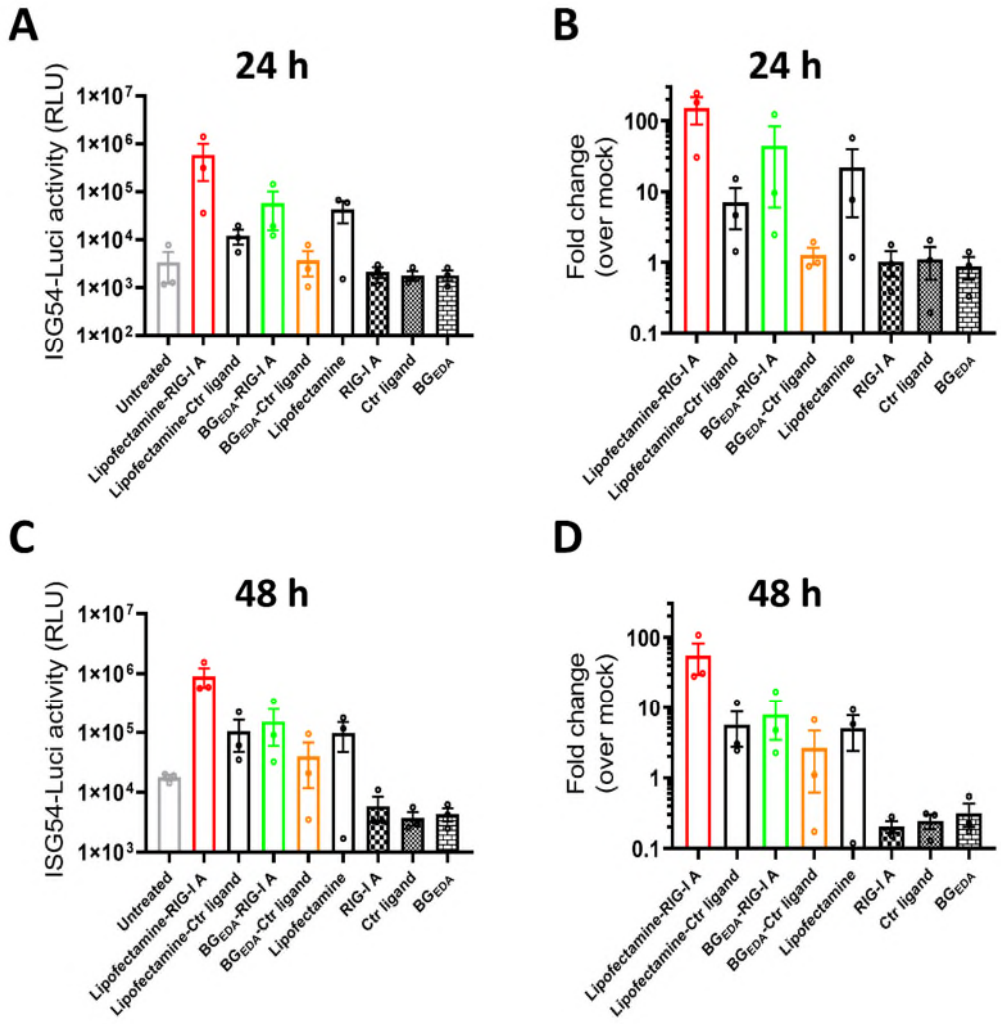

Figure 5.4 BG_{EDA} delivery of a RIG-I agonist-induced ISG54 in an undifferentiated THP-1 cell line.

Undifferentiated THP-1 dual cells were incubated with BG_{EDA}-RIG-I A (500 ng/mL), BG_{EDA}-Ctr ligand (500 ng/mL), lipofectamine-RIG-I A (500 ng/mL), or lipofectamine-Ctr ligand (500 ng/mL). ISG54 activation was assessed by measuring the levels of secreted Lucia luciferase in the supernatant after 24 hours (h), A) or 48 hours, C). The fold change of ISG54 was calculated in relation to the respective mock sample of each experiment after 24 hours, B) or 48 hours, D). The levels of Lucia luciferase were determined by measuring the relative light units (RLU) in a luminometer. Three independent experiments were performed. All data are shown as column graphs, and the mean ± standard error of the mean is shown from three independent experiments (SEM; N = 3). Due to the high differences in the overall induction values achieved in the three experiments (biological

variation), only the means of biological duplicates ± SEM is shown. Comparisons were performed using two-tailed unpaired t-tests, no comparisons were significant [p values were found > 0.05].

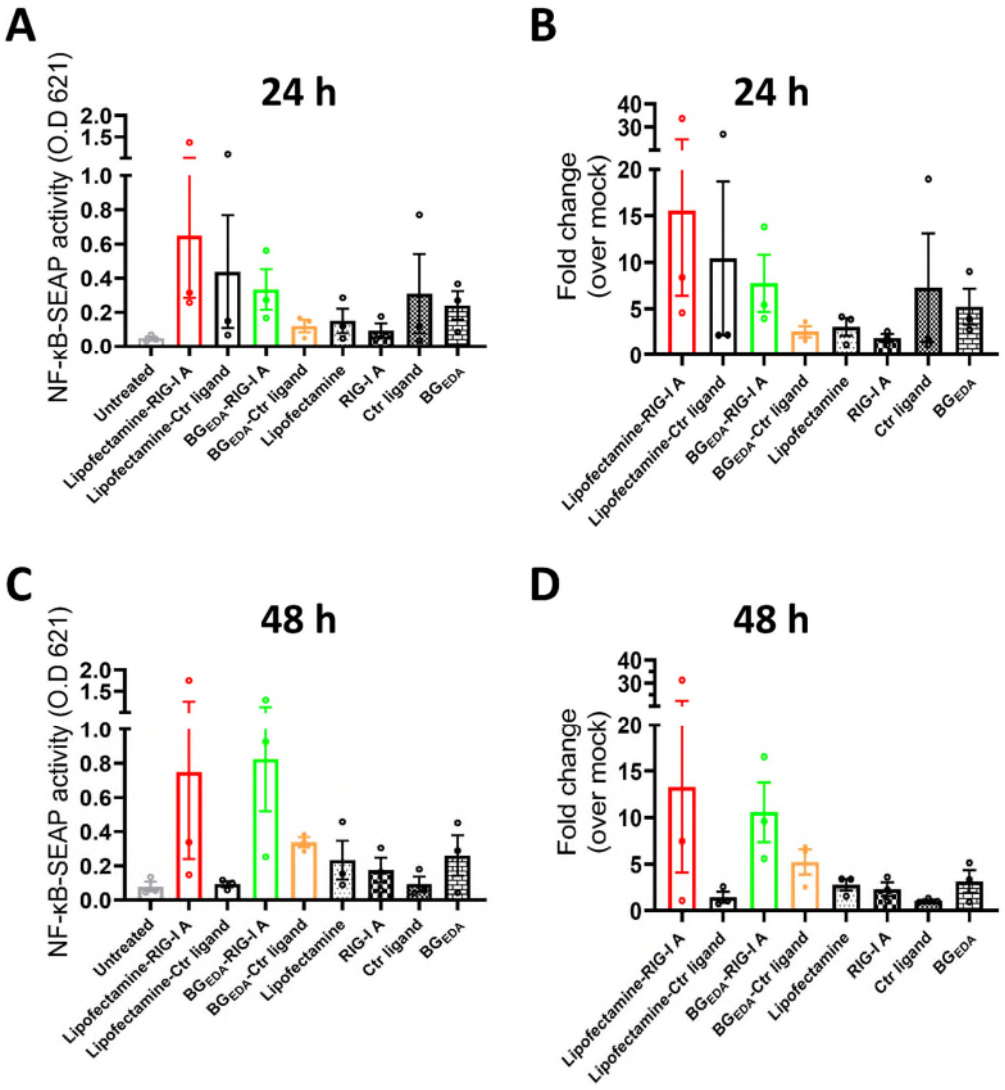

Figure 5.5 BG_{EDA} delivery of RIG-I agonist triggers NF-κB signalling in an undifferentiated THP-1 cell line.

Undifferentiated THP-1 dual cells were stimulated with BG_{EDA}-RIG-I A (500 ng/mL), BG_{EDA}-Ctr ligand (500 ng/mL), lipofectamine-RIG-I A (500 ng/mL), or lipofectamine-Ctr ligand (500 ng/mL). A) Post 24 hours (h) treatment, NF-κB activation was quantified as the levels of secreted embryonic alkaline phosphate (SEAP) in the supernatant after 24 hours, A) or 48 hours, C). The fold change of SEAP was calculated in relation to the respective mock sample of each experiment after 24 hours, B) or 48 hours, D). The levels of

SEAP were determined by reading the optical density (O.D) at 619 nm. Three independent experiments were performed. All data are presented as a column graph, and the means of biological duplicates ± standard error of the mean is shown from three independent experiments (SEM; N = 3). Due to the high differences in the overall induction values achieved in the three experiments (biological variation), only the means of biological duplicates ± SEM is shown. Comparisons were performed using a two-tailed unpaired t-test, no comparisons were significant [p values were found > 0.05].

5.2.3 BG_{EDA} NP delivery of RIG-I agonist triggers IFN-α in activated primary $CD4^+$ T cells and human peripheral blood mononuclear cells (PBMCs)

Next, we investigated the potential to leverage BG_{EDA} NP for RIG-I A delivery to primary $CD4^+$ T cells and PBMC. First, we evaluated the ability of BG_{EDA}-RIG-I A to enhance bioactive IFN-α secretion in activated primary $CD4^+$ T cells and PBMC. Primary $CD4^+$ T cells were activated for 2 days, then PBMC and primary $CD4^+$ T cells were incubated with BG_{EDA}-RIG-I A, BG_{EDA}-Ctr ligand or infected with Sendai virus as a positive control (Figure 5.6 A). Sendai virus is well characterized as a potent inducer of RIG-I activation and IFN I production upon infection (160, 684, 685). To measure bioactive IFN-α activity, supernatants were harvested at day 1 and day 3 post-treatment, and the supernatant was incubated with the HEK-Blue reporter cells (IFN-α/β reporter cell line) (686, 687) and the colour quantified by SEAP activity (Figure 5.6 A).

The IFN-α/β reporter HEK 293 cell line (HEK-Blue) was generated by the stable introduction of genes (STAT2 and IRF9) that respond to IFN I into the human embryonic kidney (HEK) 293 cells. This IFN I response demonstrates an active IFN I signalling pathway, where the other five interferon receptor signalling genes (IFNAR1, IFNAR2, JAK1, TYK2 and STAT2) are naturally expressed (688). Stimulation of HEK-Blue cells with rhIFN-α stimulated the ISG54 pathway and subsequently induced the secretion of SEAP. Therefore, to validate the inducibility of ISG54-SEAP in HEK-Blue cells, we titrated rhIFN-α on these cells and assessed activity after 24 hours (Figure 5.6 B) (688). It has been previously demonstrated

that RIG-I overexpression in HEK-Blue cells is essential for producing IFNs following RIG-I agonist stimulation (689). In this notion, to confirm that the IFN promoter activity in HEK blue cells was due to IFNs produced from targeted cells (i.e., $CD4^+$ T cells and PBMC) and not from stimulus applied to the targeted cells, we challenged HEK blue cells with different stimuli, including, SeV, BG_{EDA}-RIG-I A and BG_{EDA}-Ctr ligand and IFN-α-SEAP activity were analysed. The data show that SeV, RIG-A, and Ctrl conjugated NP did not activate the IFN promotor in HEK blue cells (Figure 5.6 C). Thus, this data indicates that if we see an IFN-I upregulation, it can only be produced from the targeted cells exposed to the stimulus and not the stimulus itself.

Unconjugated ligands, RIG-I A or Ctr ligand, not bound to NP or naked BG_{EDA} did not induce IFN-α-SEAP in $CD4^+$ T cells compared to untreated cells post day 1 and day 3 treatment (Figure 5.7 A-B). Interestingly, delivery of BG_{EDA}-RIG-I A enhanced IFN-α-SEAP production in $CD4^+$ T cells post day 1 day 3 post-treatment compared to untreated cells (mean fold change enhancement at days 1, and 3 was 6.4 and 24 respectively, [$p = 0.211$, $p < 0.001$, respectively, unpaired t test] (Figure 5.7 A-B). In addition, we observed a significant increase in IFN-α-SEAP production in cells treated with BG_{EDA}-RIG-I A at day 3 post-treatment compared to day 1 [$p = 0.025$, unpaired t test] (Figure 5.7 A-B). In contrast, the BG_{EDA}-Ctr ligand (dsRNA lacking a 5'-triphosphate modification) did not induce expression at either day 1 or day 3 (Figure 5.7 A-B). These findings again demonstrate the importance of the 5'-triphosphate end of dsRNA for RIG-I activation (650, 681). Furthermore, we observed a significant enhancement in IFN-α-SEAP production in cells treated with BG_{EDA}-RIG-I A compared to BG_{EDA}-Ctr ligand at day 3 post-treatment [$p = 0.0021$, unpaired t test] (Figure 5.7 A-B), which was not observed with free RIG-I-A.

Next, we wanted to examine whether the stimulation of human PBMC with BG_{EDA}-RIG-I A can induce IFN-α production. Results were largely similar to those obtained in activated $CD4^+$ T cells. At day 1 post-treatment, BG_{EDA}-RIG-I A activation enhanced IFN-α-SEAP production compared to untreated cells (mean fold increase = 4.9) (Figure 5.7 C-D). In addition, we observed some non-specific IFN-α-SEAP activity in cells treated with BG_{EDA}-Ctr ligand

(Figure 5.7 C-D). Interestingly, in cells treated with BG_{EDA}-RIG-I A, we observed an increase in IFN-α-SEAP production on day 3 compared to day 1 (4.2-fold change increase, [p = 0.0230, unpaired t test] (Figure 5.7 C-D), suggesting some accumulation of the 3p-dsRNA which would be released from BG_{EDA} NP over time. Alternatively, this may be due to an effect on bystander immune cells other than T cells (PBMC). This alteration in the induction of IFN-α in BG_{EDA}-RIG-I A could lead to another hypothesis that the up-regulation ISG54 signalling pathway was strongly dependent upon bystander PBMC as isolated $CD4^+$ T cells were moderately sensitive to this modulation. Alternatively, non-specific uptake of BG_{EDA}-Ctr ligand by monocytes and plasmacytoid dendritic cells (pDCs) amplified the induction of IFN-α in BG_{EDA}-Ctr ligand treated cells (690).

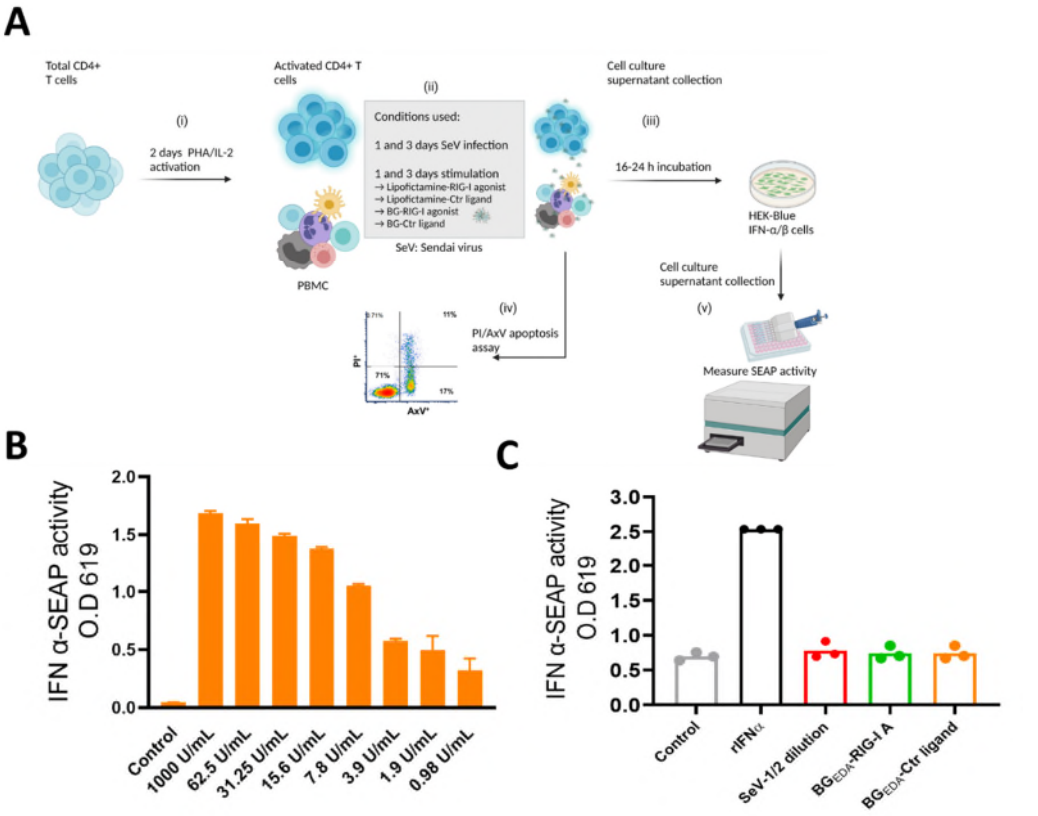

Figure 5.6 Evaluation of the activity of BG_{EDA}-RIG-I A in primary CD4+ T cells and human Peripheral blood mononuclear cells (PBMC) using HEK-Blue IFN-α /β assay.

A) Schematic representation of the method used. In brief, activated $CD4^+$ T cells and human PBMC were incubated with either BG_{EDA}-RIG-I A or BG_{EDA}-

Ctr ligand for 1 and 3 days. After 24 hours, the type I IFN-SEAP reporter was quantified in the supernatant, and cell viability and apoptosis were quantified by flow cytometry using antibodies to annexin-V (AxV) and propidium iodide (PI). B) IFNα-SEAP production following titration of rhIFN-α in HEK-Blue cells and measurement after 16-24 hours. Data are presented as a column graph, and the means of biological duplicates ± standard error of the mean is shown from three independent experiments (SEM; N = 3). C) response of HEK-Blue IFN-α /β cells to direct treatment with rhIFN-α, SeV**,** BG_{EDA}-RIG-I A and BG_{EDA}-Ctr ligand. Data are presented as a column graph, and the means of biological duplicates are shown from one experiment (N = 1).

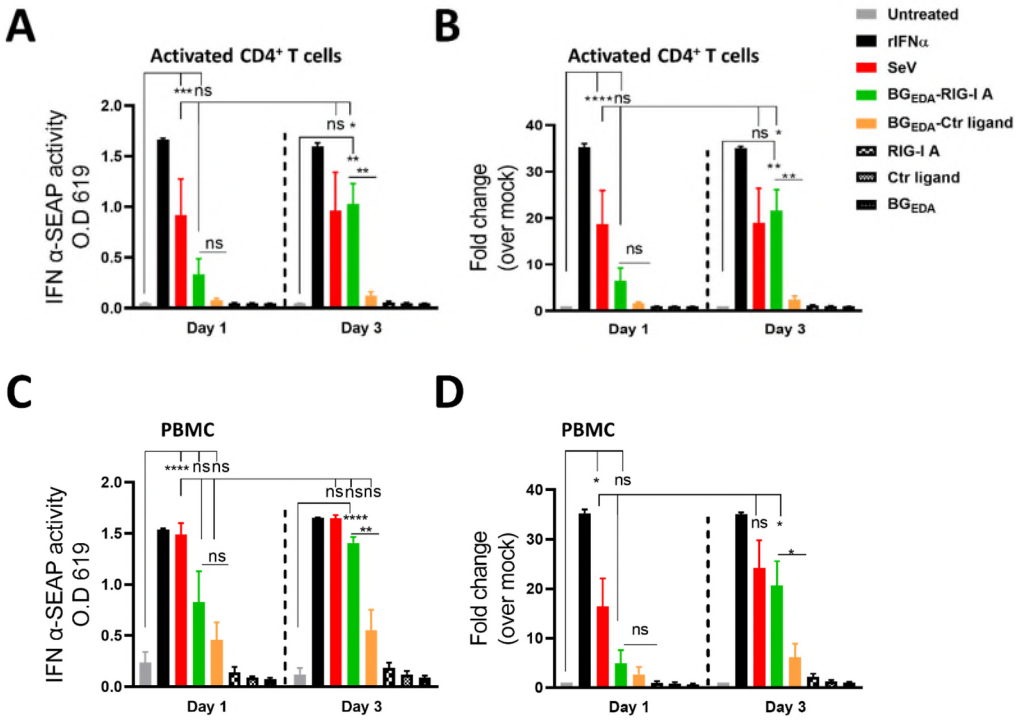

Figure 5.7 BG_{EDA} delivery of a RIG-I agonist induces IFN-α gene expression in primary CD4+ T cells and human PBMC.

A) Levels of secreted IFN-α were measured using the HEK-Blue SEAP assay after- 1 and 3-days treatment of activated $CD4^+$ T cells with the indicated formulation. B) Fold change induction of IFN-α-SEAP in primary $CD4^+$ T cells. C) Levels of secreted IFN-α were measured using HEK-Blue SEAP assay after 1- and 3-days treatment of PBMC with the indicated formulation. D) Fold change induction of IFN-α-SEAP in PBMC. All data are

presented as a column graph, and the means of biological duplicates ± standard error of the mean is shown from five independent experiments (SEM; N = 5). All P values were determined using two-tailed, unpaired T test: *P<0.05, **P<0.001, ***P<0.0005 and ****P<0.0001.

5.2.4 NP delivery of RIG-I A did not trigger cell death in primary CD4$^+$ T cells

We next hypothesized that transcriptional activation of type I IFN will increase cellular apoptosis in BG_{EDA}-RIG-I A treated cells given prior reports (670, 691). To confirm this, we quantified apoptosis (percentage of annexin$^+$ V cells (% AxV$^+$, early apoptosis) and propidium iodide cells (% PI$^+$ late apoptosis) in activated CD4$^+$ T cells treated with SeV, BG_{EDA}-RIG-I A or BG_{EDA}-Ctr ligand using flow cytometry (Figure 5.6 A). Where induction of IFN-α was observed, we found that BG_{EDA}-RIG-I A or BG_{EDA}-Ctr ligand did not induce early apoptotic cells (% AxV$^+$/PI$^-$) or late apoptotic cells (% AxV$^+$/PI$^+$) after one and three days of treatment compared to the control (Figure 5.8 A-B). However, in cells treated with SeV, we observed an increase in early apoptotic and late apoptotic cells (AxV$^+$/PI$^-$ and AxV$^+$/PI$^+$) compared to the control (Figure 5.8 A-B). Previous reports have shown that activation of RIG-I signalling induced preferential apoptosis in several cancer cells, while antigen-presenting cells are more resistant to RIG-I-mediated apoptosis (692–695).

Collectively, these data demonstrate that BG_{EDA} NP delivery of synthetic RIG-I A can induce the production of type I IFN (ISG54) and NF-κB in THP-1 cells and IFN-α in primary CD4$^+$ T cells and human PBMC but did not elicit cell death in primary CD4$^+$ T cells.

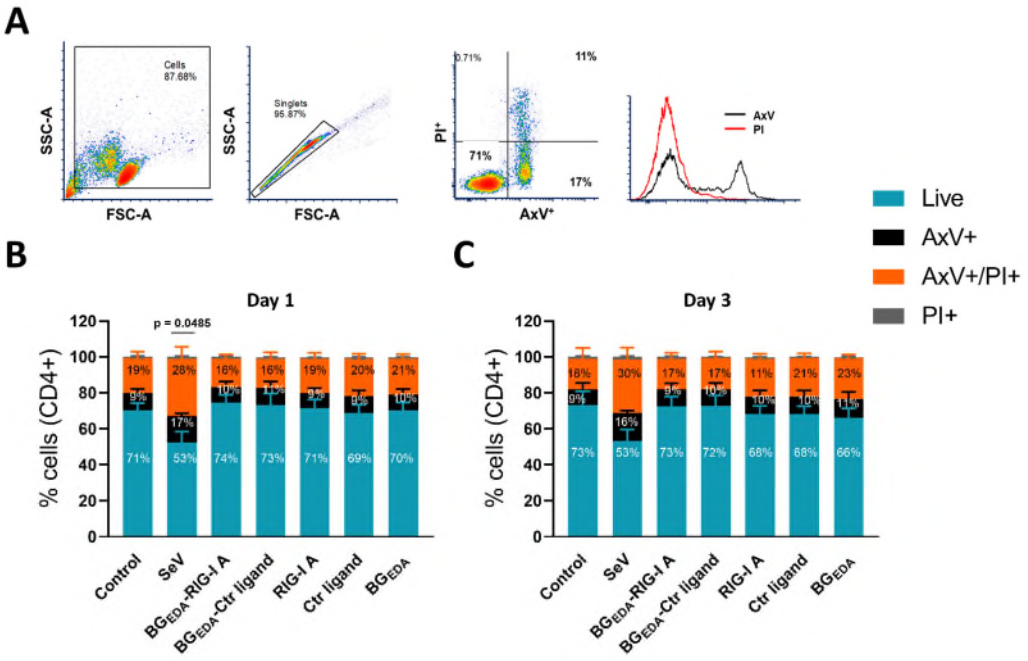

Figure 5.8 BG_{EDA} delivery of RIG-I agonist did not induce cell death in activated $CD4^+$ T cells.

A) Representative flow cytometry dot plots and analysis of cell viability and apoptosis in $CD4^+$ T-cells using annexin-V (AxV) and propidium iodide (PI) staining after treatment with indicated formulation for B) one day (Day 1) and C) three days (Day 3). Early and late apoptotic cell populations was evaluated by annexin V (AxV) and Propidium iodide (PI) staining, respectively. Numbers indicate the percentage (%) of each cell population expressing the relevant marker. All data are presented as stacked column graphs, and the means of technical replicates ± standard error of the mean is shown from three independent experiments (SEM; N = 5). Comparisons were performed using a two-tailed unpaired t-test; no comparisons were significant, i.e., all p values were > 0.05, except day 1 SeV treated cell [p values were found > 0.0485].

5.2.5 BG_{EDA}-RIG-I A induces HIV latency reactivation *in vitro* without affecting cell death in the J-Lat A2 cell line

Since we observed that delivery of BG_{EDA}-RIG-I A can stimulate and activate type I IFN and NF-κB pathways in THP-1 derived monocyte cells, we hypothesised that BG_{EDA}-RIG-I A could also reverse HIV latency and may also potentially promote immunogenic clearance of latently infected cells

through the associated-cellular response to 3p-dsRNA via induction of NF-κB and type I IFN. Therefore, we investigated the effects of BG_{EDA}-RIG-I A to reverse HIV latency and induce cell death in the J-Lat A2 T cell line. The J-Lat A2 harbours a single integrated provirus that consists of the HIV promoter LTR driving the expression of a cassette consisting of the viral Tat-gene and green fluorescent protein (GFP) (249). Given that GFP expression is under the control of the HIV LTR, activation of the LTR can be quantified by the expression of GFP. Cell death was quantified by staining with PI and using flow cytometry. Briefly, J-Lat A2 cells were treated for 48 hours with 20 nM BG_{EDA}-RIG-I A or BG_{EDA}-Ctr ligand, phosphate buffer saline (PBS, vehicle control) or a combination of phorbol 12-myristate 13-acetate (PMA) and the calcium ionophore ionomycin (Iono) as positive control stimulus (PMA/Iono). The harvested cells were stained with propidium iodide (PI, viability staining), and both PI and GFP were quantified by flow cytometry. For the flow analysis strategy, cells were gated on forward scatter area (FSC-A) against side scatter area (SSC-A) to locate J-Lat cells, then forward scatter Height (FSC-H) versus forward scatter area (FSC-A) to exclude doublets. Next, cells were gated for PI and forward scattered area (FSC-A) to exclude dead cells (PI^+). Finally, live cells (PI^-, % viability) were gated versus GFP to determine GFP^+ populations (Figure 5.9 A).

Interestingly, in this model, BG_{EDA}-RIG-I A compared to PBS- or BBG_{EDA}-Ctr ligand treated cells activated HIV expression. However, we did not observe a change in viability between different treatments (Figure 5.9 B). The effect of BG_{EDA}-RIG-I A on J-Lat A2 cells was modest (an increase of 7 % GFP^+ cells) compared to the positive control PMA/Iono (an increase of 80% of GFP^+ cells). Importantly, naked RIG-I A, Ctr ligand or BG_{EDA} alone did not show reactivation activity compared to PBS control (Figure 5.8 B). These results indicate that BG_{EDA}-RIG-I A at the concentration used showed modest activation of HIV latency in the J-Lat A 2 T cell line.

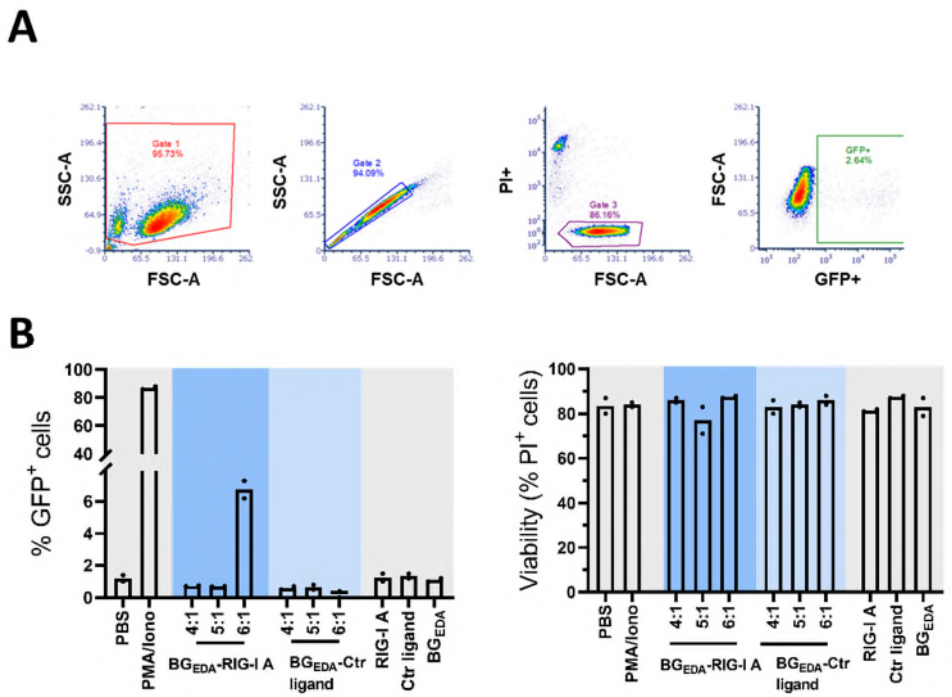

Figure 5.9 BG_{EDA}-RIG-I A can modestly activate the HIV-LTR in the J-Lat A2 T cell line.

A) Representative flow cytometry plots of gating strategy for PI- population (Live) and activated cells for GFP+ cells. B) The proportion of GFP+-positive cells in the viable cell population (left) and the proportion of viable cells based on propidium iodide staining (right). All data are presented as a column graph, and the means of technical duplicates are shown from one experiment (N=1).

5.3 DISCUSSION

Although several of the currently available LRAs can activate HIV transcription in people with HIV on ART in vivo, none are able to reduce the HIV reservoir (61, 696–699). New classes of immunomodulatory LRAs have been explored recently as innate immune agonists. These include TLR7 and TLR9 agonists (393, 400, 401). However, RIG-I agonists could also potentially play a role. The RIG-I ligand targets the cytosolic pattern recognition receptor (PPR) RIG-I-like helicases (RLH) (403, 587, 663, 700). RNA therapeutics targeting the immunoreceptor RIG-I have been explored extensively in oncology as an anti-cancer therapy to stimulate the induction of an antiviral response program through the production of type I IFN and

NF-κB (680, 701–706). However, delivering RNA as a RIG-I agonist in T cells is challenging because of biological barriers, including the negative charge of RNA, nuclease degradation, and poor intracellular bioavailability (418, 707–709). While there has been extensive work for developing non-viral carriers for RNA based therapy, including lipid-based nanoparticles, polyplexes and polymer-based particles, to name a few, there has been a minimal investigation into a delivery system that could specifically target T cells (416, 710, 711). In addition, there have only been limited studies exploring delivery systems for an RNA RIG-I agonist ligand that have utilised commercial *in vitro* lipid-based transfection agents or polyethyleneimine (PEI). However, neither of these approaches are specifically optimised for delivery of 3p-dsRNA delivery nor targeted to T cells (695, 712–716). While RIG-I agonists have been developed to treat malignancies, they are now being considered potential LRA and immunotherapeutic interventions to reactivate HIV latency from $CD4^+$ T cells from PLWH *ex vivo* while also creating an immunostimulatory milieu that induces preferential apoptosis in latently infected cells (133, 403, 404, 664, 700).

RIG-I agonist (RIG-I A) conjugated with functionalised bovine glycogen (BG_{EDA}-RIG-I A) NP induced ISG54 and NF-κB in THP-1 derived monocyte dual reporter cell lines. Additionally, we also observed secretion of IFN-α in primary $CD4^+$ T cells and PBMC treated with BG_{EDA}-RIG-I A.

Interestingly, BG_{EDA}-RIG-I A also reactivated HIV latency in the J-Lat A 2 cell line. It is well-documented that the IFN I and innate immune NF-κB signalling pathway share many areas of cross-regulation and expression (668, 717). In addition, it was found that RIG-I can activate the NF-κB signalling pathway during respiratory syncytial virus (RSV) infection via the upstream canonical IkBa- NF-κB pathway (718, 719). Accordingly, evidence supports the hypothesis that BG_{EDA}-RIG-I A acts by enhancing the RIG-I signalling cascades in J-Lat A2 cells, which subsequently induced both IFN I and canonical NF-κB pathway, resulting in driving HIV expression. However, this hypothesis must be addressed and investigated in future experiments. In addition, further studies are needed to dissect whether IFN pathway I or NF-κB signalling mediated HIV transcription in J-Lat A2 cells.

Recently Indra Sarabia et al., showed RIG-I agonist can reactivate HIV latency in J-Lat cells through the full length MAVS (405). Prior interest in the role of RIG-I agonists and HIV latency reversal has focused on the small molecule acitretin, an FDA approved drug for the management of psoriasis, with mixed results. In 2016, Li et al. showed that acitretin in the latently infected TZM-bl cell line or primary $CD4^+$ T cells from PLWH on ART induced RIG-I expression and increased HIV transcription, but also RIG-I signalling selectively induced IFN-mediated apoptosis of HIV-positive cells (133). In contrast, Garcia-Vidal et al. and Palermo et al. found that acitretin mediated stimulation of RIG-I expression but failed to induce potent HIV reactivation and lacked selective cell death of HIV- positive cells in the latently infected J-Lat T cell line or primary $CD4^+$ T cells from PLWH on ART (403, 404). The discrepancies between acitretin efficacy and outcome obtained from those two studies may be attributed to differences in cells and virus strains used. Despite the initial reports of acitretin in 2016, it is interesting that this work has never been repeated or confirmed by another group. Our findings are consistent with Garcia-Vidal et al. and Palermo et al., where we showed in a J-Lat cell line only modest latency reversal and no selective cell death. One explanation for this outcome is that RIG-I agonist treatment of the J-Lat cell line exhibited no or little expression of IFN-α and RIG-I, respectively (155).

Interestingly, low or no expression of RIG-I was observed across multiple HIV infected cell lines, including U1, ACH2 and 8E5 (155), suggesting that these cell lines might not be a suitable model for investigating RIG-I activity. While many PRRs share common signalling molecules, the resultant innate immune response's molecular phenotype (e.g., cytokine profile) can vary significantly between PRRs (663, 720). Interestingly, a combination of a similar innate immune agonist (cGAS-STING agonist) with the HDACi resminostat amplified viral reactivation and induced specific death of HIV-infected cells in the J-Lat T cell line and ACH2 cells (404). However, this magnitude of HIV reactivation and death of latently infected cells was not observed using cells from PWH on ART *ex vivo*. Importantly, these studies highlighted the therapeutic potential in synergising innate immune agonists with other LRA classes (e.g., HDACi). Another approach could be

combining a RIG-I agonist with other immunotherapeutic modalities such as PD-1 immune checkpoint blockade (ICB), reinvigorating T cell effector function and cytotoxic activity (407, 408). In addition, we and others have shown that anti-PD1 and other ICBs can also reverse HIV latency (107, 721, 722).

Although further work is needed to determine if the type 1 IFN pathway or NF-κB or both are driving latency reversal, we believe that induction of IFN might be playing a role here. Supporting this hypothesis, others have shown that the amount of IFN I induced by cytosolic PPR agonists correlates with the level of HIV reactivation using either a TLR7 agonist in non-human primates and acitretin in patient cells *ex vivo* respectively, of latently infected cells *in vivo* (393, 396, 723). In addition, Another potential mechanism by which TLR-7 agonists can reactivate latent HIV is through the induction of TNFα (723). Our laboratory has also shown that type I interferons (specifically rhIFN-α) can inhibit the establishment of latency *in vitro* but also reversed HIV latency in $CD4^+$ T cells from PLWH on ART *ex vivo* through phosphorylation of STAT5 (724). Taken together, an RNA RIG-I agonist alone or in combination with other LRAs could be a potential LRA candidate that works on multiple pathways to reactivate HIV latency. Further work is still needed to determine if an RNA RIG-I agonist can also mediate the selective killing of latently infected cells.

We also demonstrated that BG_{EDA}-RIG-I A can trigger RIG-I signalling and downstream immunostimulatory effects (Type I IFN, ISGs and NF-κB) in the THP-1 cell line activated primary $CD4^+$ T cells and PBMC. Importantly BG_{EDA}-RIG-I A delivery in activated primary $CD4^+$ T induced the secretion of IFN-α/ß, but BG_{EDA}-Ctr ligand did not induce activity. To the best of our knowledge, this is the first-time delivery of 3p-dsRNA using a nanoparticles-based delivery system that has been reported in primary $CD4^+$ T cells and PBMC.

Despite our exciting and novel findings, these experiments have a number of potential limitations. First, further experiments will be required to confirm whether BG_{EDA}-RIG-I A can indeed reverse HIV latency. We have only performed this experiment once. Other HIV latency models need to be explored, including $CD4^+$ T cells or monocytes from PLWH on suppressive

ART, which may have different susceptibility to BG_{EDA}-RIG-I A. Second, the impact of RIG-I induction on IFN I or NF-κB on the HIV LTR needs to be explored. One way to pin down this mechanism would be to knock out various proteins of the RIG-I signalling pathway and determine latency reversal potential by BG_{EDA}-RIG-I A. Alternatively, through inhibiting IFN I or NF-κB signalling.

In addition, whether RIG-I activation induces T cell activation remains unknown. We were also unable to determine the level of binding and internalisation of BG_{EDA} particles with T cells. This was due the limit of detection of small size nanoparticles (≤ 100 nm) which renders particles undisguisable from background using conventional flow cytometry or confocal microscopy (725). However, given the significant biological effects that we observed, we suspect there was some degree of binding and internalisation. Additional work will be required to quantify the interaction of BG_{EDA} and BG_{EDA}-RIG-I A with T cells using flow cytometry and confocal microscopy. In addition, whether BG_{EDA} could elicit an immune response *in vitro* or *in vivo* and the potential to develop nanoparticles-specific antibodies remains unknown. Consequently this will result in accelerated clearance of nanoparticles by phagocytic immune cells and contributes to the change in the pharmacokinetic profile of subsequent doses of BG_{EDA}. Therefore, it is crucial to evaluate the undesirable immunostimulatory potential effects of BG_{EDA} and the subsequent formation of BG_{EDA} antibodies. Finally, we did not evaluate the capacity of BG_{EDA}-RIG-I A to enhance the RIG-I signalling pathway by quantification of RIG-I protein expression.

5.4 CONCLUSION

In summary, this study demonstrated for the first time that BG nanoparticles can efficiently deliver an RNA RIG-I agonist, 3p-dsRNA, to primary $CD4^+$ T cells. Additionally, this novel complex could potentially reverse HIV latency, but further experiments will be needed with different models of HIV latency and using the BG-RIG-I-A alone and in combination with other LRAs.

6 Integrated Discussion

6.1 SUMMARY OF WORK OUTLINED IN THIS THESIS

Antiretroviral therapy (ART) effectively suppresses HIV replication in people living with HIV (PLWH), but treatment is lifelong. The persistence of a reservoir of long-lived and proliferating latently infected resting $CD4^+$ T cells that carry replication-competent provirus is a significant challenge in achieving a cure for HIV infection (74, 79, 80, 586). These latently infected cells contain a transcriptionally silent provirus that can evade ART and resist immune-mediated clearance. One strategy toward eliminating HIV latency is the activation of HIV viral production by latency reversal agents (LRAs) in the presence of ART to induce virus-mediated cytolysis or clearance through immune recognition (often called “shock and kill”) (272, 312).

Several pharmacological and immunotherapeutic compounds that harbour LRA activity, including epigenetic regulators (for example, the histone deacetylase inhibitor romidepsin, RMD) and pattern recognition receptors(PPRs) agonists (for example, toll-like receptors (TLR), TLR2, TLR7 and TLR9,) are now being extensively explored clinically as therapeutics to eliminate latency and purge the HIV latent reservoir (323, 393, 663, 723, 726). While RMD and RIG-I A are promising classes of LRA, to date, these compounds have not shown clear success in reducing the reservoir, potentially due to limited potency, cytotoxicity profile and/or inadequate delivery to latently infected $CD4^+$ T cells (61, 133, 375, 403, 588, 727, 728). Thus, there is a need for safe and effective delivery strategies for LRA compounds to specifically target latently infected T cells.

One approach to address this limitation is using nano-engineered particle delivery systems loaded with LRA, which possess several advantages over more traditional drug delivery methods (410, 565, 596). Nano-engineered particles-based drug delivery of LRAs to T cells can potentially protect the encapsulated cargo from degradation, increase drug solubility and bioavailability, and enhance intercellular delivery (416, 597–599). Several

studies have utilised nano-engineered carriers to improve the delivery of different classes of LRAs with substantially reduced therapeutic related toxicity (417, 458, 600). However, safe delivery of particles remains a major technological challenge, primarily due to the non-phagocytic nature of T cells.

In this thesis, we outlined the importance of nano-engineered drug delivery systems to deliver small hydrophobic molecules and nucleic acid-based therapeutics to T cells. To do so, we designed specific nano-engineered particles solutions to deliver both RMD and RNA RIG-I A into T cells. Due to the different requirements for hydrophobic drug and nucleic acid therapeutics delivery, we required two different solutions. First, we utilised the PMA_{SH} particle drug delivery platform to encapsulate and deliver the hydrophobic RMD (RMD-NPs). We demonstrated that this delivery mechanism enhances the potency of reactivation of HIV latency and also reduces cytotoxicity in cell line models of HIV latency. Second, we utilised the endosomatic ethylenediamine (EDA) functionalised bovine glycogen-based nanoparticles (BG_{EDA} NP) to deliver RNA RIG-I agonist and demonstrated that this approach directly stimulated the innate immune system and also activated HIV latency *in vitro*.

Collectively, these results have demonstrated proof-of-principal that nano-engineered particles can provide a drug delivery platform for hydrophobic LRA, immunomodulators, and oligonucleotide compounds and could provide a foundation for future novel HIV latency purging strategies. We propose that future directions should include targeting PMA_{SH} RMD- and BG_{EDA}-RIG-I agonist NP specifically to $CD4^+$ T cells, investigating the potential synergism of RMD- and BG_{EDA}-RIG-I agonist NP to boost HIV transcription and killing of HIV-infected cells and evaluating the biodistribution of these particles *in vivo.*

6.1.1 Determination of optimal factors for nanoparticles uptake by $CD4^+$ T cells for the elimination of HIV latency

6.1.2 Size and surface charge matter

Fundamental knowledge on the best nano-engineered particle design (size and surface charge) for drug delivery to T cells is lacking. In tandem, to help

gain such fundamental knowledge, a reliable assay that can quantify and compare the association (binding and uptake) of different particle designs with T cells is also needed.

T cells are susceptible to many diseases, including blood cancers (e.g., acute lymphoblastic leukemia and T cell Lymphoma) and viral infections (e.g. HIV and HTLV-1), making them an important target for therapeutics (312, 431–433). In the context of HIV infection, the experimental LRAs have been shown to induce HIV gene expression in latently infected T cells (312). However, the efficacy of LRAs is impaired by the systematic toxicity induced by the non-specific activity of these compounds (375, 434). Nano-engineered particles-based delivery of LRAs to T cells may circumvent these unwanted effects. However, safe delivery of particles and encapsulated cargo remains a major technological challenge, primarily due to the non-phagocytic nature of $CD4^+$ T cells.

The negatively charged plasma membrane surrounding a living cell forms a boundary between the cytosolic and external microenvironment and provides structural support to the cell (423, 435). Non-phagocytic T cells strictly control charged molecule intake from the extracellular environment (423). Small soluble molecules with a molecular weight below 1 KDa (e.g. medical drugs) pass quickly through passive diffusion, whereas larger molecules (> 1 KDa) require energy-dependent or membrane modelling to cross the cell membrane (438, 557). Micropinocytosis is an intracellular uptake mechanism used by T cells for particles > 200 nm that relies on membrane ruffling and results from actin polymerisation (439, 440). Another uptake mechanism in T cells that has played an essential role in receptor-mediated endocytosis is clathrin-dependent endocytosis, where smaller molecules < 200 nm use this pathway for cellular uptake (442, 443). Therefore, the surface charge of particles is another critical parameter that influences particles uptake and may have a dominant effect over nanoparticles size (445, 446). Studying the fundamental influence of nanoparticles physiochemical properties (size and surface charge) in interaction with T cells is critical for developing an efficient, smart-drug delivery nanoparticle system. Importantly, we found that nanoparticle size

and surface charge are two critical parameters for determining intracellular uptake.

We showed that negatively charged PMA_{SH} more readily associated with T cells compared to neutral PMA_{SH}-PEG and positively charged PMA_{SH}-PLL. Further, smaller and negatively charged particles (400 nm) were preferentially internalised in T cells compared to larger particles. With respect to size, 40 nm BG_{EDA}-RIG-I A nanoparticles triggered RIG-I signalling and downstream immunostimulatory effects (Type I IFN and NF-κB) in T cells. These biological effects, we assumed, are the result of efficient internalization of BG_{EDA}-RIG-I A into T cells. Overall, these results suggest that particle size and surface charge play an essential role in interaction with T cells. An important caveat is that PMA_{SH} and glycogen nanoparticles delivery systems are two different platforms; each system offers several opportunities to address the limitations such as poor aqueous solubility and low bioavailability of hydrophobic and nucleic acid-based therapeutics. However, we argue that connecting the right therapeutic candidate to the right platform is crucial for nanomedicine design. In addition, nanoparticle delivery platforms differ in their ability to carry large payloads and their interactions with immune cells, allowing for the appropriate selection of carriers to treat patient-specific disease conditions. Particles may acquire different identities when interacting with biological fluids such as blood and cell culture media. In biological fluids, the surface charge may change drastically by the adsorption of biomolecules, including protein abundance and other plasma components, to form the protein corona (449–453). This new biological identity of nanoparticles can significantly alter the behaviour and fate of their interaction with cells. In addition, material composition and surface charge can negatively affect nanoparticles fate by provoking the immune system to launch an attack on nanoparticles (449, 729). Therefore, we extended this study by investigating the influence of surface charge in nanoparticles interaction with immune cells in human whole blood and PBMC. In addition, as PMA_{SH} particles drug delivery systems progress towards clinical use as a nanocarrier for LRA delivery, the ability to engineer PMA_{SH} particles with defined biological properties is essential. Again, we described the charge as a fundamental

physiochemical property of functionalised PMA_{SH} particles (PMA_{SH}-PEG and PMA_{SH}-PLL) that dictates their interaction with distinct primary cell subsets in human whole blood and PBMC. In contrast to association results from monoculture $CD4^+$ T cells, 400 nm PMA_{SH}-PEG and PMA_{SH}-PLL demonstrated increased association with T cells in a mixed culture of human whole blood and PBMC.

Ultimately, the goal of any drug delivery system is to provide the therapeutic amount of drug to the specific organ or cell in the body to promptly achieve and maintain the desired drug concentration (730). A significant advance in nanocarrier drug delivery using a nanoscale mesoporous particle system is their ability to efficiently encapsulate different therapeutic payloads due to their tunable mesopore size. Thus, in addition to particle size, pore morphology and size are other factors in designing an efficient drug reservoir for both the accessibility of in-coming hydrophobic drugs into mesoporous silica (MS) particles and the release of already-loaded drugs (731, 732). Ideally, the pore size should be larger than the in-coming drug molecules to host the drug inside the pore space for drug loading. For example, Fujiwara et al. demonstrated that MS pore size was crucial for the encapsulation and release of DNA-based therapeutics (733). Jia et al. have investigated the encapsulation and release of the hydrophobic paclitaxel drug delivery system based on MS particles with a pore size range from 3 - 10 nm. They have found that the larger the pore size, the higher drug loading content, the faster release rate and the higher *in vitro* anti-cancer activity (734–736).

Given the advantages of smaller particle size in uptake, we hypothesised that 100 nm PMA_{SH} particles would perform better compared to the larger sized particles. Interestingly, this turned out to not be the case. Drug content and encapsulation efficiency were higher in the 400 nm MS particles than 100 nm MS core. In addition, we did not observe reactivation activity in latently infected cells treated with 100 nm RMD loaded PMA_{SH} nanoparticles, whereas cells treated with 400 nm RMD loaded PMA_{SH} particles showed potent reactivation activity. These results are in line with other published reports about the influences of pore size on the *in vivo* activity of anti-cancer drugs (735–738). Although a high level of cellular

uptake is the prerequisite for intracellular drug delivery, high drug loading is also critical for efficient activity. Our data demonstrated that smaller particles (100 nm) might offer high cellular uptake but poor intracellular drug delivery due to the confinement effect of limited loading capacity within MS pores. In efforts to design an optimal particle delivery system for hydrophobic drugs, we suggest that the balance between particle size and appropriate pore size of MS particles is quite an essential subject to achieve for efficient drug delivery to T cells.

In summary, the smaller PMA_{SH} (400 nm) and BG_{EDA} particles enabled cargo delivery to T cells, suggesting that nanoparticles can be an effective vehicle to deliver hydrophobic drugs and nucleic acid to T cells. Although clearly, a balance must be struck between size for uptake and size for optimal drug loading. In addition, this knowledge can be used in the rational design of future nanomedicines that most safely and effectively deliver LRAs targeting latently infected $CD4^+$ T cells.

6.2 FUTUER WORK

6.2.1 Customisation of PMA_{SH} RMD-NP and BG_{EDA}-RIG-I A nanoparticles for targeted drug delivery

This thesis demonstrated that RMD or RNA RIG-I agonist delivery using PMA_{SH} 400 nm (RMD-NP) and BG_{EDA} particles (BG_{EDA}-RIG-I agonist) nanoformulations to latently infected T cells stimulated latent HIV gene expression with minimal toxicity. However, these remain non-specific particles with the likelihood of delivery to a range of non-T cell targets. Moving forward, the next major innovation will be to enable cell-specific targeting, with the expectation of further reductions in off-target effects and increased therapeutic efficiency.

The viral reservoir is usually defined as a cell type or anatomical site where replication-competent provirus can persist for a prolonged period in people living with HIV (PLWH) on suppressive ART (84). HIV persistence can be primarily found in various compartments, including the blood, lymphatic system (lymph nodes, gut-associated lymphoid tissues GALT), and central nervous system (CNS) (171, 189, 212). A minimally toxic approach to eliminate the HIV reservoir would be to target latently infected cells

selectively. To date, no preferential gene expression signature can be used to distinguish latently infected cells from their healthy counterparts nor cells harbouring replication-competent or defective provirus. However, published reports have been proposed that defective proviruses can produce viral proteins that can cause chronic immune activation, which may play a role in HIV pathogenesis (283, 739–741).

Although it remains challenging to identify and target all HIV reservoir cells, the ability of targeted nanocarriers to navigate and deliver LRA to sites enriched for latently infected cells could potentially increase their therapeutic index and enhance the potency of the shock and kill approach. Therefore, ultimately the beneficial attribute of nanoparticle drug delivery system is to alter biodistribution and pharmacokinetics (PK) and provide efficacy and accurate payload targeting HIV cellular and anatomical reservoirs. To this end, the underlying rationale for cloaking PMA_{SH} and BG_{EDA} particles with targeted molecules (active targeting) specifically to T cells or targeted organs is two-fold: (i) targeted PMA_{SH} particles increase efficacy accuracy and attain payload concentration in sheltered viral reservoirs through enhanced particles-cell interaction, and (ii) reduced off-target effects of loaded cargo. A vast number of cellular active targeting delivery strategies have been tested through the attachment of high-affinity ligands such as peptides, carbohydrates, aptamers, monoclonal antibodies, antibodies fragments or proteins on the surface of nanocarrier for specific homing and uptake by targeted cells (417, 742–749). However, target receptor efficacy may vary with the specificity of that receptor to the intended target population and affinity or avidity when linked to nanocarriers (750). In addition, the physicochemical properties of nanocarriers may also affect targeting. For example, Cao et al. have shown that neutral or positively charged lipid nanoparticles conjugated with anti-$CD4^+$ T antibody had a high level of non-specific binding to $CD4^+$ T cells compared to negatively charged particles, which hindered receptor-mediated targeting (746).

The most commonly chosen receptors to date are general lymphocyte T cell surface markers, i.e., CD3, CD4, CD7, and CD8 (456, 751–754) (extensively addressed in (416)). An alternative targeting strategy could be to use antibodies targeting other cellular markers that are enriched for

latently infected cells, including the immune checkpoint molecules, programmed death protein 1 (PD-1), or CD2 and CD30 (79, 197, 755–759). In particular, targeting RMD loaded particles to PD-1 high expressing cells could have multiple beneficial outcomes, including latency reversal due to RMD (370, 760) and PD-1 blockade (107). However, this strategy must be considered cautiously, as general targeting to all T cell subsets expressing PD-1 can result in dose-limiting toxicities (761, 762).

Several studies have shown that conjugating nanocarriers (loaded or unloaded) with an active T cell targeting molecule increases the particle-cell interaction with T cell populations in monoculture in the complex environment of a mixed population of primary human blood cells or *in vivo* compared to untargeted nanocarriers (526, 599, 746, 752, 763, 764). For example, Glass et al. showed selective targeting of caveosphere nanoparticles to CCR5 enhanced caveosphere internalisation by $CD4^+$ T cells compared to untargeted caveosphere nanoparticles in mixed cell culture (765).

In the context of HIV remission, targeting RMD loaded PMA_{SH} particles and BG_{EDA}-RIG-I A to blood circulating and tissue-resident $CD4^+$ T cells will enable specific delivery of cargo to sanctuary sites such as lymphoid tissues and lymphatic organs where vast numbers of latently infected $CD4^+$ T cells reside and are considered to be drug-free zones and safe havenfor HIV (84, 171, 204, 212, 416, 766–769). In a study targeting the latent reservoir in blood circulated $CD4^+$ T cells, Kovochich et al. utilised $CD4^+$ T cell-targeted polymer nanoparticles incorporating a potent protein kinase C agonist (PKC) (770), bryostatin and the HIV protease inhibitor, nelfinavir (771). Their bryostatin-nelfinavir nanoformulation selectively activated latently infected $CD4^+$ T cells in PBMC culture and inhibited viral spread (455). As we mentioned earlier, LRA loaded nanocarriers targeting lymph nodes, including secondary lymphatic tissues, is of interest in eradicating the HIV reservoir in remote sites. These targeted interventions would substantially reduce systematic related therapeutic toxicity and indeed achieve sufficient concentration at targeted sites. In addition, lymph nodes harbour a significant fraction of the total immune cells in the body, making this site of interest for targeted immunomodulatory therapy (171). Several

immunomodulatory interventions have been used to directly act on naïve T cells to modify the adaptive immune response by regulating their activation, function and differentiation upon antigen recognition (197, 416, 742, 772, 773).

Active targeting delivery to the lymph node paracortex compartment (T cell zone) can be achieved via intramuscular injection or via targeting of the peripheral node addressin (PNAd) on the capillary wall, followed by diffusion of the delivered nanocarrier into the lymph node mimicking the natural homing process of T cells into the lymph node (Extravasation) (742). Alternatively, smaller nanocarriers (10 nm - 100 nm in diameter) exit the blood circulation to the lymph nodes through the walls of high endothelial venules, owing to the low pressure inside the lymphatic vessel lumen (passive targeting) (465, 742, 774, 775). However, the nanocarriers must overcome physiological barriers before a subsequent uptake by the lymphatic system where the shape, size and surface charge of the nanocarrier matters (742, 776–778). In a study using PMA_{SH} capsules, Koker et al. showed that in the absence of antibody conjugation, polyethylene glycol (PEG) functionalised poly- (methacrylic acid) (PMA)-based nanoparticles efficiently targeted the T cell zone in the draining lymph nodes following subcutaneous administration (775). In another *in vivo* study using untargeted BG_{EDA}-siRNA and BG_{EDA}-PEG-siRNA, both nanoformulations showed high liver uptake and poor accumulation in the spleen following intravenous administration, suggesting that macrophages captured most particles (418). In a recent study, Cao et al. have shown conjugation of an anti-CD4-monoclonal antibody to negatively charged lipid-coated poly (lactic-co-glycolic acid) (PLGA) nanoparticles loaded with ingenol-3-angelate (Ing3A) selectively activated $CD4^+$ T cells from macaque PBMCs over untargeted nanoparticles. Overall, nanoparticles that are surface decorated with targeting ligand showed enhanced co-localisation with their targeted cells or site (456, 752, 779, 780).

In summary, targeting HIV reservoirs within blood circulating $CD4^+$ T cells and lymph node-resident T cells presents a major technological challenge in engineering a stealth nanoparticles system that can enhance

nanocarriers interaction with T cells and maintain higher affinity to surface decorated targeted ligands in the complex *in vivo* environment.

6.2.2 Combination, synergism, and scalable therapy using PMA_{SH} RMD-NP and BGEDA-RIG-I A nanocarriers to eliminate the total latent HIV reservoir

In the context of the shock and kill strategy, the inability of single LRAs to clear and reduce the latent HIV reservoir in clinical trials suggested that LRA monotherapy is not sufficient to reduce the latent reservoir (313, 375, 781, 782), with an estimated only 5 % of latently infected cells being activated (465). In addition, published studies showed that interval dosing of certain LRAs induced higher HIV expression, while sequential treatment rounds yielded new virions (326, 783, 784). Given that multiple cellular mechanisms suppress viral reactivation in latently infected cells and that transcriptional activity of cellular and tissue reservoirs is stochastic (158, 231, 781, 782, 785), it is unlikely that a single intervention will significantly impact the latent reservoir(158, 782). Therefore, the most effective way to reverse latency would be to hit distinct regulatory pathways involved in maintaining HIV latency using a combination of multiple mechanistic interventions. Several studies have demonstrated the effect of synergism using LRA combination therapy *ex vivo* (227, 338, 344, 458, 786, 787). Preclinical studies have shown the synergy of LRA combinations with several compounds working together to reactivate latent HIV reservoirs by maximising potency and minimising toxicity (227, 313, 609, 781, 788, 789). However, neurotoxicity has been reported in clinical trials when disulfiram combined with vorinostat, highlighting caution in using dual LRA therapies (790).

RIG-I agonists are postulated to involve the modulation of the nuclear factor-kB (NF-κB) and type I interferon (IFN I) signalling (668, 680), which stimulates HIV transcription and potentially arming the innate immune defence (133, 791). The HDACi RMD is an epigenetic regulator that targets class I HDACs (593) and has reversed latency *in vitro* and *in vivo* (362, 365, 375, 784). Given that loading RMD into PMA_{SH} particles showed effective delivery and reduced RMD cytotoxic effect, we hypothesise that combination with a RIG-I agonist could represent an excellent strategy to

amplify the induction of HIV expression and potentially selective elimination of the latent reservoir by boosting HIV specific $CD8^+$ T cells with strong effector function from naïve T cells through the induction of IFN I and pro-inflammatory cytokines.

HIV encodes a range of regulatory proteins with pro and anti-apoptotic qualities, including gp 120, Tat, Nef, Vpr, and HIV protease (590, 792). However, evidence suggests that latently infected cells are resistant to apoptosis (313, 639, 793). When HIV reactivation and replication occur, several HIV-encoded proteins such as HIV protease, Vpr, Nef and Tat downmodulate pro-apoptotic proteins (such as Bak, FasL, Bax, and caspase 8) or upregulate endogenous apoptosis inhibitory proteins (such as Bcl-2, c-FLIP and caspase 10) (590, 591, 792, 794–797); this shift in apoptotic balance enables an HIV-infected cell to survive and actively produce more virions (313). Presumably, the fact that the expression of these viral proteins may indeed enhance cell survivability (for example, upregulation of Bcl-2 expression), or the latently infected cells naturally have a high level of Bcl-2 may contribute to allowing the reservoir to persist following reactivation. In this regard, we argue this could well be responsible for the inability of LRAs to eliminate the latently infected cells. Therefore, we suggest that innate immune-boosting strategies could be used simultaneously with LRA to support LRA function by stimulating the pro-apoptotic pathways and improving the killing of latently infected cells. In particular, modulation of several elements of the apoptosis regulatory network, including the pro-apoptotic proteins Caspase 8 and Bcl-2-associated X protein (Bax) and the anti-apoptotic protein Bcl-2.

Our approach would lend itself well to this two-step strategy that can lead to reactivation and killing HIV infected cells by combining the potential of epigenetic reprogramming (RMD) and stimulation of innate immunity (RIG-I agonist). The rationale for adding RIG-I agonist is two-fold: (i) an additive effect of HIV proviral reactivation following chromatin relaxation driven in an NF-κB- dependent fashion (ii) drive reactivated cells to apoptosis either by induction of viral pro-apoptotic proteins, sensing the produced HIV RNA resulting in an IFN I mediated antiviral response and priming the infected cells to be on the precipice of apoptosis. The first step, adding RMD, leads

to a more ‘open’ chromatin conformation, favouring transcription factor binding and gene transcription and subsequently reactivating HIV proviral expression, viral pro-apoptotic proteins, and HIV RNA. In the second step, we add the RIG-I agonist to amplify the magnitude of latency reversal and induce cell death. It is worthy to note, the combination of the HDACi related compound LAQ824 with RIG-I agonist decreased mitochondria membrane permeability, leading to an increase in the production of reactive oxygen species (ROS), activation of caspase cascade and degradation of Bcl-2 anti-apoptotic protein in melanoma cells (798), suggesting this combination could also improve the shock and kill strategy.

Thus, we propose that the HDACi RMD paired with the immunostimulatory RIG-I agonist could lead to synergistic reactivation and preferential killing of HIV-infected cells.

6.2.3 The importance of animal studies for the development of LRA nanocarriers to eliminate HIV latency

Nanoparticle drug delivery platforms have emerged as suitable carriers to overcome the pharmacokinetic limitations associated with free drug formulations. Although nanoparticles are emerging as a powerful strategy to deliver cargo *in vitro* and *ex vivo*, substantial challenges are still present that can severely limit site-specific *in vivo* bioavailability. The assessment of bio-nano interaction *in vitro* and *ex vivo* can provide some information on how nanoparticles interact in the complex biological microenvironment.

Animal studies are essential for the development of therapeutics before being approved for human use. Such models usually involve small animals with mice and rat models most commonly used for biodistribution and efficacy and safety studies. Therefore, the use of animal models must be explored to facilitate the understanding of biological barriers, *in vivo* behaviour of nanoparticles, drug release kinetics, potency and lymphatic uptake following systematic administration. In addition, it is well established that a portion of blood circulating nanoparticles are non-specifically taken up by monocytes, dendritic cells, and liver-resident macrophages (Kupffer cells) (799–801). As we discussed earlier, tuning innovative design features such as size, surface charge and targeted molecules within the nanocarriers

for proper negotiation of nanocarrier-cell interaction will help provide details for future efforts in the rational design of T cell-targeted nanoparticle drug delivery systems.

The ultimate goal of HIV research is to design a strategy to eliminate the latent reservoir to achieve a cure for HIV. Given that lymph nodes and gut-associated lymphoid tissues play a crucial role in HIV persistence (207, 212), *in vitro* studies may not represent the complex environment and the nature of interactions between immune cells in *vivo*. In addition, the inconsistency in multiple HIV latency model systems and *ex vivo* studies could yield misleading outcomes (232). Therefore, *in vivo* model systems may reflect a robust model to characterise HIV persistence and further evaluate LRA nanoformulations for eliminating the HIV latent reservoir. Furthermore, a small animal model can also provide insights into whether other parameters, such as sex and age, may be relevant biological variables (802, 803).

Several humanised mice models have been developed to study HIV replication and latency (418, 544, 804–807). Humanised mice are immunodeficient mice engrafted with human immune cells or tissues, allowing them to be infected with HIV (808, 809). In addition, mice models allow for investigating nanocarrier biosafety, biodistribution and residual accumulation in systemic host filtration organs (liver, spleen, lungs and kidney), which are essential parameters for proper risk assessment of nanocarriers in defining their therapeutic effects *in vivo* (810, 811). Thus, we propose that further research should be undertaken to study the biodynamic of PMA_{SH} RMDLNP and bovine glycogen BG_{EDA}-RIG-I agonist in uninfected and HIV-infected humanized mice with the goal to understand the impact on the latent reservoir.

6.2.4 Crossing of the physiological barrier by nanoparticles

One of the biggest challenges in nanoparticle drug delivery systems for clinical translation is crossing physiological and biological barriers, such as mucosal barriers and their impact on nanoparticle biodistribution and encapsulated drug delivery. Once administered, nanoparticle-based therapeutics should be in a concentration that achieves full efficacy with no

associated side effects. In this line, various nanoparticles drug delivery systems are being investigated for different routes of administration such as parenteral, including intravenous (IV) and intramuscular (IM), oral, topical or nasal routes (812). The vast majority of the investigations dealing with drug delivery applications of nanoparticles focus on the IM and IV administration, albeit the oral route is the preferred and the most widely used due to its non-invasive nature and patient compliance. Even with these clear advantages, the oral route presents some limitations in administering specific molecules, including inadequate intestinal absorption, poor stability to the aggressive gastrointestinal conditions or solubility issues (e.g., peptides, antibiotics).

The IM route achieves a direct administration of therapeutic agents deep into the muscle to obtain local or systematic effects (812). On the other hand, the IV route delivery is defined as an injection or infusion method of drug (nanocarrier-based drug) administration into the vein to achieve the systematic effect of the encapsulated drug. This route of administration is suitable for formulations that cannot be injected into muscles or absorbed by the gastrointestinal tract (813). The IV route provides a safe instantaneous response and complete encapsulated drugs bioavailability because of the direct exposure in the systematic circulation (814). Importantly, direct administration into a vein overcomes the issue of first-pass metabolism (815). However, most nanoparticles-based therapies administrated through the IV route displayed passive liver and kidney targeting (816). Transdermal nanoparticle drug delivery modes (TDDs) are being investigated to circumvent hepatic nanoparticle encapsulated drug accumulation (817–819). In addition, optimising the administration route can improve encapsulated drug pharmacodynamic and alter its fate and efficacy *in vivo*. For instance, IV administration of PLGA nanocarriers primarily accumulated in the liver and spleen, whereas when these nanocarriers are subcutaneously or intranodal administrated, they are highly accumulated in local lymph nodes (820). Furthermore, a targeted T cell zone in the lymph node paracortex compartment can be achieved via IM administration targeting PNAd on the capillary wall (742, 776). These alternate administration routes enable NPs to reach the lymphatic system prior to the systemic circulation, which could be beneficial in targeting the HIV reservoir

while eliminating the non-specific distribution of nanocarrier encapsulated LRA.

6.2.5 Suggestions for future work

In summary, we proposed these further experiments; targeted delivery of RMD-LNPs specifically to CD4+ T cells by conjugating targeting molecules such as CD2 and investigating the efficacy of RMD-LNPs in reversing HIV latency in latently infected CD4+ T cells from PLWH on ART. Finally, examine the potential synergism between RMD-LNPs and BG-EDA-RIG-I agonist.

6.3 CONCLUDING REMARKS

In conclusion, as progress toward creating a functional cure against HIV continues, we have optimised two solutions to encapsulate hydrophobic and nucleic acid therapeutics to target the latent HIV reservoir. We show that RMD loaded PMA_{SH} particles and bovine glycogen incorporated RIG-I agonist particles can effectively target T cells, deliver cargo, and reverse HIV latency in a range of cell line models. This thesis thus advances our understanding of the delivery of therapeutics to T cells and provides a novel new approach to further optimise the potency and selective delivery of LRAs to latently infected cells with the overall goal of eliminating the HIV reservoir.

This page has been left intentionally blank

Chapter 7: Bibliography

1. Gallo RC, Montagnier L. 2003. The Discovery of HIV as the Cause of AIDS. N Engl J Med 349:2283–2285.
2. Barre-Sinoussi F, Chermann J, Rey F, Nugeyre M, Chamaret S, Gruest J, Dauguet C, Axler-Blin C, Vezinet-Brun F, Rouzioux C, Rozenbaum W, Montagnier L. 1983. Isolation of a T-lymphotropic retrovirus from a patient at risk for acquired immune deficiency syndrome (AIDS). Science, 220:868–871.
3. GBD 2017 HIV collaborators. 2019. Global, regional, and national incidence, prevalence, and mortality of HIV, 1980-2017, and forecasts to 2030, for 195 countries and territories: a systematic analysis for the Global Burden of Diseases, Injuries, and Risk Factors Study 2017. lancet HIV 6:831–859.
4. 2021. Global HIV & AIDS statistics — Fact sheet | UNAIDS. UNIAIDS.
5. Stover J, Bollinger L, Izazola JA, Loures L, DeLay P, Ghys PD, Group FT modeling working. 2016. What is required to end the AIDS epidemic as a public health threat by 2030 The cost and impact of the fast-track approach. PLoS One 11:341–353.
6. Mizutani S, Boettiger D, Temin HM. 1970. A DNA-depenent DNA polymerase and a DNA endonuclease in virions of Rous sarcoma virus. Nature 228:424–427.
7. Haseltine WA. 1991. Molecular biology of the human immunodeficiency virus type 1. FASEB J 5:2349–2360.
8. Muesing MA, Smith DH, Cabradilla CD, Benton C V., Lasky LA, Capon DJ. 1985. Nucleic acid structure and expression of the human AIDS/lymphadenopathy retrovirus. Nature 313:450–458.
9. Bubeck D, Filman DJ, Cheng N, Steven AC, Hogle JM, Belnap DM. 2005. The Structure of the Poliovirus 135S Cell Entry Intermediate at 10-Angstrom Resolution Reveals the Location of an Externalized Polypeptide That Binds to Membranes. J Virol 79:7745–7755.

10. Turner BG, Summers MF. 1999. Structural biology of HIV. J Mol Biol 285:1–32.
11. Frankel AD, Young JAT. 1998. HIV-1: Fifteen Proteins and an RNA. Annu Rev Biochem 67:1–25.
12. Renga B, Francisci D, D'Amore C, Schiaroli E, Mencarelli A, Cipriani S, Baldelli F, Fiorucci S. 2012. The HIV Matrix Protein p17 Subverts Nuclear Receptors Expression and Induces a STAT1-Dependent Proinflammatory Phenotype in Monocytes. PLoS One 7:1-16.
13. German Advisory Committee Blood (Arbeitskreis Blut) S 'Assessment of PT by B. 2016. Human Immunodeficiency Virus (HIV). Transfus Med Hemother 43:203–222.
14. Sundquist WI, Krausslich H-G. 2012. HIV-1 Assembly, Budding, and Maturation. Cold Spring Harb Perspect Med 2:6924-6924.
15. Trentin B, Rebeyrotte N, Mamoun RZ. 1998. Human T-Cell Leukemia Virus Type 1 Reverse Transcriptase (RT) Originates from the pro andpol Open Reading Frames and Requires the Presence of RT-RNase H (RH) and RT-RH-Integrase Proteins for Its Activity. J Virol 72:6504–6510.
16. Doms RW, Trono D. 2000. The plasma membrane as a combat zone in the HIV battlefield. Genes Dev 14:2677–2688.
17. Sauter D, Unterweger D, Vogl M, Usmani SM, Heigele A, Kluge SF, Hermkes E, Moll M, Barker E, Peeters M, Learn GH, Bibollet-Ruche F, Fritz J V., Fackler OT, Hahn BH, Kirchhoff F. 2012. Human Tetherin Exerts Strong Selection Pressure on the HIV-1 Group N Vpu Protein. PLoS Pathog 8:1003–1093.
18. Levy JA. 1993. Pathogenesis of human immunodeficiency virus infection. Microbiol Rev. 57:183–289.
19. Emerman M, Malim MH. 1998. HIV-1 regulatory/accessory genes: keys to unraveling viral and host cell biology. Science. 280:1880–1884.
20. Temin HM. 1993. Retrovirus variation and reverse transcription: abnormal strand transfers result in retrovirus genetic variation. Proc Natl Acad Sci. 90:6900–6903.
21. Klaver B, Berkhout B. 1994. Comparison of 5'and 3'long terminal

repeat promoter function in human immunodeficiency virus. J Virol 68:3830–3840.

22. Jeeninga RE, Hoogenkamp M, Armand-Ugon M, de Baar M, Verhoef K, Berkhout B. 2000. Functional Differences between the Long Terminal Repeat Transcriptional Promoters of Human Immunodeficiency Virus Type 1 Subtypes A through G. J Virol 74:3740–3751.
23. Briggs JAG, Simon MN, Gross I, Kräusslich H-G, Fuller SD, Vogt VM, Johnson MC. 2004. The stoichiometry of Gag protein in HIV-1. Nat Struct Mol Biol 11:672-681.
24. Deeks SG, Overbaugh J, Phillips A, Buchbinder S. 2015. HIV infection. Nat Rev Dis Prim 1:153035–153054.
25. Wilen CB, Tilton JC, Doms RW. 2012. HIV: cell binding and entry. Cold Spring Harb Perspect Med 2:6866–6876.
26. Kwong PD, Wyatt R, Robinson J, Sweet RW, Sodroski J, Hendrickson WA. 1998. Structure of an HIV gp120 envelope glycoprotein in complex with the CD4 receptor and a neutralizing human antibody. Nature 393:648–659.
27. Dean M, Carrington M, Winkler C, Huttley GA, Smith MW, Allikmets R, Goedert JJ, Buchbinder SP, Vittinghoff E, Gomperts E, Donfield S, Vlahov D, Kaslow R, Saah A, Rinaldo C, Detels R, O'Brien SJ. 1996. Genetic restriction of HIV-1 infection and progression to AIDS by a deletion allele of the CKR5 structural gene. Hemophilia Growth and Development Study, Multicenter AIDS Cohort Study, Multicenter Hemophilia Cohort Study, San Francisco City Cohort, ALIVE . Science 273:1856–1862.
28. Stein BS, Gowda SD, Lifson JD, Penhallow RC, Bensch KG, Engleman EG. 1987. pH-independent HIV entry into CD4-positive T cells via virus envelope fusion to the plasma membrane. Cell 49:659–668.
29. Farnet CM, Haseltine WA. 1990. Integration of human immunodeficiency virus type 1 DNA in vitro. Proc Natl Acad Sci U S A 87:4164–4168.
30. Brown PO, Bowerman B, Varmus HE, Bishop JM. 1989. Retroviral

integration: structure of the initial covalent product and its precursor, and a role for the viral IN protein. Proc Natl Acad Sci U S A 86:2525–2529.

31. Fields BN, Knipe DM (David M, Howley PM. 2013. Fields virology 6:82–94.
32. Shan L, Yang H-C, Rabi SA, Bravo HC, Shroff NS, Irizarry RA, Zhang H, Margolick JB, Siliciano JD, Siliciano RF. 2011. Influence of host gene transcription level and orientation on HIV-1 latency in a primary-cell model. J Virol 85:5384–93.
33. Sherrill-Mix S, Lewinski MK, Famiglietti M, Bosque A, Malani N, Ocwieja KE, Berry CC, Looney D, Shan L, Agosto LM, Pace MJ, Siliciano RF, O'Doherty U, Guatelli J, Planelles V, Bushman FD. 2013. HIV latency and integration site placement in five cell-based models. Retrovirology 10:90-101.
34. Han Y, Lassen K, Monie D, Sedaghat AR, Shimoji S, Liu X, Pierson TC, Margolick JB, Siliciano RF, Siliciano JD. 2004. Resting CD4+ T cells from human immunodeficiency virus type 1 (HIV-1)-infected individuals carry integrated HIV-1 genomes within actively transcribed host genes. J Virol 78:6122–6133.
35. Roebuck KA, Saifuddin M. 1999. Regulation of HIV-1 Transcription. Gene Expr 8:67–78.
36. Perkins ND, Edwards NL, Duckett CS, Agranoff AB, Schmid RM, Nabel GJ. 1993. A cooperative interaction between NF-kappa B and Sp1 is required for HIV-1 enhancer activation. EMBO J 12:3551–8.
37. Alcamí J, Laín de Lera T, Folgueira L, Pedraza MA, Jacqué JM, Bachelerie F, Noriega AR, Hay RT, Harrich D, Gaynor RB. 1995. Absolute dependence on kappa B responsive elements for initiation and Tat-mediated amplification of HIV transcription in blood CD4 T lymphocytes. EMBO J. 14:1552–1560.
38. Pan X, Baldauf H-M, Keppler OT, Fackler OT. 2013. Restrictions to HIV-1 replication in resting CD4+ T lymphocytes. Cell Res. 23:876–885.
39. Jones KA, Kadonaga JT, Luciw PA, Tjian R. 1986. Activation of the AIDS retrovirus promoter by the cellular transcription factor, Sp1.

Science. 232:755–759.

40. Toohey MG, Jones KA. 1989. In vitro formation of short RNA polymerase II transcripts that terminate within the HIV-1 and HIV-2 promoter-proximal downstream regions. Genes Dev 3:265–282.
41. Kao S-Y, Calman AF, Luciw PA, Peterlin BM. 1987. Anti-termination of transcription within the long terminal repeat of HIV-1 by tat gene product. Nature. 330:489–493.
42. Mayhood T, Kaushik N, Pandey PK, Kashanchi F, Deng L, Pandey VN. 2000. Inhibition of Tat-mediated transactivation of HIV-1 LTR transcription by polyamide nucleic acid targeted to TAR hairpin element. Biochemistry. 39:11532–11539.
43. Fritz CC, Green MR. 1996. HIV Rev uses a conserved cellular protein export pathway for the nucleocytoplasmic transport of viral RNAs. Curr Biol 6:848–854.
44. Weinberger LS, Dar RD, Simpson ML. 2008. Transient-mediated fate determination in a transcriptional circuit of HIV. Nat Genet 40:466–470.
45. Purcell DF, Martin MA. 1993. Alternative splicing of human immunodeficiency virus type 1 mRNA modulates viral protein expression, replication, and infectivity. J Virol 67:6365–6378.
46. Stoltzfus CM. 2009. Chapter 1. Regulation of HIV-1 alternative RNA splicing and its role in virus replication. Adv Virus Res 74:1–40.
47. Sherpa C, Rausch JW, Le Grice SFJ, Hammarskjold M-L, Rekosh D. 2015. The HIV-1 Rev response element (RRE) adopts alternative conformations that promote different rates of virus replication. Nucleic Acids Res 43:4676–4686.
48. Furtado MR, Balachandran R, Gupta P, Wolinsky SM. 1991. Analysis of alternatively spliced human immunodeficiency virus type-1 mRNA species, one of which encodes a novel TAT-ENV fusion protein. Virology 185:258–270.
49. Karn J, Stoltzfus CM. 2012. Transcriptional and Posttranscriptional Regulation of HIV-1 Gene Expression. Cold Spring Harb Perspect Med 2:916–933.
50. Klotman ME, Kim S, Buchbinder A, DeRossi A, Baltimore D, Wong-

Staal F. 1991. Kinetics of expression of multiply spliced RNA in early human immunodeficiency virus type 1 infection of lymphocytes and monocytes. Proc Natl Acad Sci U S A 88:5011–5.

51. Stoltzfus C, Madsen J. 2005. Role of Viral Splicing Elements and Cellular RNA Binding Proteins in Regulation of HIV-1 Alternative RNA Splicing. Curr HIV Res 4:43–55.
52. Engelman A, Cherepanov P. 2012. The structural biology of HIV-1: mechanistic and therapeutic insights. Nat Rev Microbiol 10:279–90.
53. Freed EO. 2001. HIV-1 replication. Somat Cell Mol Genet 26:13–33.
54. Ray M, Logan R, Sterne JA, Hernandez-Diaz S, Robins JM, Sabin C, Bansi L, van Sighem A, de Wolf F, Costagliola D, Lanoy E, Bucher HC, von Wyl V, Esteve A, Casbona J, del Amo J, Moreno S, Justice A, Goulet J, Lodi S, Phillips A, Seng R, Meyer L, Perez-Hoyos S, Garcia de Olalla P, Hernan MA. 2010. The effect of combined antiretroviral therapy on the overall mortality of HIV-infected individuals. AIDS 24:123–137.
55. Mitsuya H, Yarchoan R, Broder S. 1990. Molecular Targets for AIDS Therapy. Science 249:1533–1544.
56. Arts EJ, Hazuda DJ. 2012. HIV-1 Antiretroviral Drug Therapy. Cold Spring Harb Perspect Med 2:7161–7161.
57. Margolis DA, Brinson CC, Smith GHR, de Vente J, Hagins DP, Eron JJ, Griffith SK, Clair MHS, Stevens MC, Williams PE, Ford SL, Stancil BS, Bomar MM, Hudson KJ, Smith KY, Spreen WR, LAI116482 Study Team. 2015. Cabotegravir plus rilpivirine, once a day, after induction with cabotegravir plus nucleoside reverse transcriptase inhibitors in antiretroviral-naive adults with HIV-1 infection (LATTE): a randomised, phase 2b, dose-ranging trial. Lancet Infect Dis 15:1145–1155.
58. Lee JH, Andrabi R, Su C-Y, Yasmeen A, Julien J-P, Kong L, Wu NC, McBride R, Sok D, Pauthner M, Cottrell CA, Nieusma T, Blattner C, Paulson JC, Klasse PJ, Wilson IA, Burton DR, Ward AB. 2017. A Broadly Neutralizing Antibody Targets the Dynamic HIV Envelope Trimer Apex via a Long, Rigidified, and Anionic β-Hairpin Structure. Immunity 46:690–701.

59. Davey RT, Bhat N, Yoder C, Chun T-WW, Metcalf JA, Dewar R, Natarajan V, Lempicki RA, Adelsberger JW, Miller KD, Davey Jr. RT, Bhat N, Yoder C, Chun T-WW, Metcalf JA, Dewar R, Natarajan V, Lempicki RA, Adelsberger JW, Miller KD, Kovacs JA, Polis MA, Walker RE, Falloon J, Masur H, Gee D, Baseler M, Dimitrov DS, Fauci AS, Lane HC, Davey RT, Bhat N, Yoder C, Chun T-WW, Metcalf JA, Dewar R, Natarajan V, Lempicki RA, Adelsberger JW, Miller KD. 1999. HIV-1 and T cell dynamics after interruption of highly active antiretroviral therapy (HAART) in patients with a history of sustained viral suppression. Proc Natl Acad Sci 96:15109–15114.
60. Freed EO. 1998. HIV-1 gag proteins: diverse functions in the virus life cycle. Virology 251:1–15.
61. Katlama C, Deeks SG, Autran B, Martinez-Picado J, van Lunzen J, Rouzioux C, Miller M, Vella S, Schmitz JE, Ahlers J, Richman DD, Sekaly RP. 2013. Barriers to a cure for HIV: new ways to target and eradicate HIV-1 reservoirs. Lancet 381:2109–2117.
62. Mannheimer S, Friedland G, Matts J, Child C, Chesney M. 2002. The Consistency of Adherence to Antiretroviral Therapy Predicts Biologic Outcomes for Human Immunodeficiency Virus–Infected Persons in Clinical Trials. Clin Infect Dis 34:1115–1121.
63. Perelson AS, Essunger P, Cao Y, Vesanen M, Hurley A, Saksela K, Markowitz M, Ho DD. 1997. Decay characteristics of HIV-1-infected compartments during combination therapy. Nature 387:188–191.
64. Dahl V, Josefsson L, Palmer S. 2010. HIV reservoirs, latency, and reactivation: prospects for eradication. Antiviral Res 85:286–94.
65. Rong L, Perelson AS. 2009. Modeling latently infected cell activation: viral and latent reservoir persistence, and viral blips in HIV-infected patients on potent therapy. PLoS Comput Biol 5:533–554.
66. Nettles RE. 2005. Intermittent HIV-1 Viremia (Blips) and Drug Resistance in Patients Receiving HAART. JAMA 293:817.
67. Maldarelli F, Palmer S, King MS, Wiegand A, Polis MA, Mican J, Kovacs JA, Davey RT, Rock-Kress D, Dewar R, Liu S, Metcalf JA, Rehm C, Brun SC, Hanna GJ, Kempf DJ, Coffin JM, Mellors JW. 2007. ART Suppresses Plasma HIV-1 RNA to a Stable Set Point

Predicted by Pretherapy Viremia. PLoS Pathog2007/04/07. 3:e46.

68. Siliciano JD, Siliciano RF. 2006. The latent reservoir for HIV-1 in resting CD4+ T cells: a barrier to cure. Curr Opin HIV AIDS1:121–128.
69. Chun TW, Stuyver L, Mizell SB, Ehler LA, Mican JA, Baseler M, Lloyd AL, Nowak MA, Fauci AS. 1997. Presence of an inducible HIV-1 latent reservoir during highly active antiretroviral therapy. Proc Natl Acad Sci U S A 94:13193–13197.
70. Chun T-W, Fauci AS. 2012. HIV reservoirs. AIDS 26:1261–1268.
71. Van Lint C, Bouchat S, Marcello A. 2013. HIV-1 transcription and latency: an update. Retrovirology 10:67-71.
72. Wei X, Ghosh SK, Taylor ME, Johnson VA, Emini EA, Deutsch P, Lifson JD, Bonhoeffer S, Nowak MA, Hahn BH, al. et. 1995. Viral dynamics in human immunodeficiency virus type 1 infection. Nature 373:117–122.
73. Finzi D, Blankson J, Siliciano JD, Margolick JB, Chadwick K, Pierson T, Smith K, Lisziewicz J, Lori F, Flexner C, Quinn TC, Chaisson RE, Rosenberg E, Walker B, Gange S, Gallant J, Siliciano RF. 1999. Latent infection of CD4+ T cells provides a mechanism for lifelong persistence of HIV-1, even in patients on effective combination therapy. Nat Med 5:512–517.
74. Siliciano JD, Kajdas J, Finzi D, Quinn TC, Chadwick K, Margolick JB, Kovacs C, Gange SJ, Siliciano RF. 2003. Long-term follow-up studies confirm the stability of the latent reservoir for HIV-1 in resting CD4+ T cells. Nat Med. 9:727–728.
75. Persaud D, Pierson T, Ruff C, Finzi D, Chadwick KR, Margolick JB, Ruff A, Hutton N, Ray S, Siliciano RF. 2000. A stable latent reservoir for HIV-1 in resting CD4+ T lymphocytes in infected children. J Clin Invest 105:995–1003.
76. Bosque A, Planelles V. 2009. Induction of HIV-1 latency and reactivation in primary memory CD4+ T cells. Blood 113:58–65.
77. Duverger A, Jones J, May J, Bibollet-Ruche F, Wagner FA, Cron RQ, Kutsch O. 2009. Determinants of the Establishment of Human Immunodeficiency Virus Type 1 Latency. J Virol 83:3078–3093.

78. Henrich TJ, Hanhauser E, Marty FM, Sirignano MN, Keating S, Lee T-H, Robles YP, Davis BT, Li JZ, Heisey A, Hill AL, Busch MP, Armand P, Soiffer RJ, Altfeld M, Kuritzkes DR. 2014. Antiretroviral-free HIV-1 remission and viral rebound after allogeneic stem cell transplantation: report of 2 cases. Ann Intern Med 161:319–327.
79. Chomont N, El-Far M, Ancuta P, Trautmann L, Procopio FA, Yassine-Diab B, Boucher G, Boulassel M-R, Ghattas G, Brenchley JM, Schacker TW, Hill BJ, Douek DC, Routy J-P, Haddad EK, Sékaly R-P. 2009. HIV reservoir size and persistence are driven by T cell survival and homeostatic proliferation. Nat Med 15:893–900.
80. Soriano-Sarabia N, Bateson RE, Dahl NP, Crooks AM, Kuruc JD, Margolis DM, Archin NM. 2014. Quantitation of Replication-Competent HIV-1 in Populations of Resting CD4 + T Cells. J Virol 88:14070–14077.
81. Josefsson L, Palmer S, Faria NR, Lemey P, Casazza J, Ambrozak D, Kearney M, Shao W, Kottilil S, Sneller M, Mellors J, Coffin JM, Maldarelli F. 2013. Single Cell Analysis of Lymph Node Tissue from HIV-1 Infected Patients Reveals that the Majority of CD4+ T-cells Contain One HIV-1 DNA Molecule. PLoS Pathog 9:1–16.
82. Khoury G, Anderson JL, Fromentin R, Hartogenesis W, Smith MZ, Bacchetti P, Hecht FM, Chomont N, Cameron PU, Deeks SG, Lewin SR. 2016. Persistence of integrated HIV DNA in CXCR3 + CCR6 + memory CD4R T cells in HIV-infected individuals on antiretroviral therapy. AIDS 30:1511–1520.
83. Khoury G, Fromentin R, Solomon A, Hartogensis W, Killian M, Hoh R, Somsouk M, Hunt PW, Girling V, Sinclair E, Bacchetti P, Anderson JL, Hecht FM, Deeks SG, Cameron PU, Chomont N, Lewin SR. 2017. Human immunodeficiency virus persistence and T-cell activation in blood, rectal, and lymph node tissue in human immunodeficiency virus-infected individuals receiving suppressive antiretroviral therapy. J Infect Dis 215:911–919.
84. Estes JD, Kityo C, Ssali F, Swainson L, Makamdop KN, Del Prete GQ, Deeks SG, Luciw PA, Chipman JG, Beilman GJ, Hoskuldsson T, Khoruts A, Anderson J, Deleage C, Jasurda J, Schmidt TE, Hafertepe

M, Callisto SP, Pearson H, Reimann T, Schuster J, Schoephoerster J, Southern P, Perkey K, Shang L, Wietgrefe SW, Fletcher C V, Lifson JD, Douek DC, McCune JM, Haase AT, Schacker TW. 2017. Defining total-body AIDS-virus burden with implications for curative strategies. Nat Med 23:1271–1276.

85. Buzon MJ, Sun H, Li C, Shaw A, Seiss K, Ouyang Z, Martin-Gayo E, Leng J, Henrich TJ, Li JZ, Pereyra F, Zurakowski R, Walker BD, Rosenberg ES, Yu XG, Lichterfeld M. 2014. HIV-1 persistence in CD4+ T cells with stem cell-like properties. Nat Med2014/01/15. 20:139–142.
86. Roche M, Tumpach C, Symons J, Gartner M, Anderson JL, Khoury G, Cashin K, Cameron PU, Churchill MJ, Deeks SG, Gorry PR, Lewin SR. 2020. CXCR4-Using HIV Strains Predominate in Naive and Central Memory CD4+ T Cells in People Living with HIV on Antiretroviral Therapy: Implications for How Latency Is Established and Maintained. J Virol 94:1736-1745.
87. Chun TW, Engel D, Berrey MM, Shea T, Corey L, Fauci AS. 1998. Early establishment of a pool of latently infected, resting CD4(+) T cells during primary HIV-1 infection. Proc Natl Acad Sci U S A 95:8869–8873.
88. Persaud D, Gay H, Ziemniak C, Chen YH, Piatak Jr. M, Chun TW, Strain M, Richman D, Luzuriaga K. 2013. Absence of detectable HIV-1 viremia after treatment cessation in an infant. N Engl J Med 369:1828–1835.
89. Josefsson L, von Stockenstrom S, Faria NR, Sinclair E, Bacchetti P, Killian M, Epling L, Tan A, Ho T, Lemey P, Shao W, Hunt PW, Somsouk M, Wylie W, Douek DC, Loeb L, Custer J, Hoh R, Poole L, Deeks SG, Hecht F, Palmer S. 2013. The HIV-1 reservoir in eight patients on long-term suppressive antiretroviral therapy is stable with few genetic changes over time. Proc Natl Acad Sci 110:4987–4996.
90. Ananworanich J, Chomont N, Eller LA, Kroon E, Tovanabutra S, Bose M, Nau M, Fletcher JLK, Tipsuk S, Vandergeeten C, O'Connell RJ, Pinyakorn S, Michael N, Phanuphak N, Robb ML. 2016. HIV DNA Set Point is Rapidly Established in Acute HIV Infection and Dramatically

Reduced by Early ART. EBioMedicine 11:68–72.

91. Finzi D, Hermankova M, Pierson T, Carruth LM, Buck C, Chaisson RE, Quinn TC, Chadwick K, Margolick J, Brookmeyer R, Gallant J, Markowitz M, Ho DD, Richman DD, Siliciano RF. 1997. Identification of a reservoir for HIV-1 in patients on highly active antiretroviral therapy. Science 278:1295–1300.
92. Archin NM, Cheema M, Parker D, Wiegand A, Bosch RJ, Coffin JM, Eron J, Cohen M, Margolis DM. 2010. Antiretroviral intensification and valproic acid lack sustained effect on residual HIV-1 viremia or resting CD4+ cell infection. PLoS One 5:1–16.
93. Wong JK, Hezareh M, Günthard HF, Havlir D V., Ignacio CC, Spina CA, Richman DD. 1997. Recovery of replication-competent HIV despite prolonged suppression of plasma viremia. Science 278:1291–1295.
94. Hiener B, Horsburgh BA, Eden JS, Barton K, Schlub TE, Lee E, von Stockenstrom S, Odevall L, Milush JM, Liegler T, Sinclair E, Hoh R, Boritz EA, Douek D, Fromentin R, Chomont N, Deeks SG, Hecht FM, Palmer S. 2017. Identification of Genetically Intact HIV-1 Proviruses in Specific CD4+ T Cells from Effectively Treated Participants. Cell Rep 21:813–822.
95. Eriksson S, Graf EH, Dahl V, Strain MC, Yukl SA, Lysenko ES, Bosch RJ, Lai J, Chioma S, Emad F, Abdel-Mohsen M, Hoh R, Hecht F, Hunt P, Somsouk M, Wong J, Johnston R, Siliciano RF, Richman DD, O'Doherty U, Palmer S, Deeks SG, Siliciano JD. 2013. Comparative analysis of measures of viral reservoirs in HIV-1 eradication studies. PLoS Pathog 9:1-22.
96. Chun TW, Finzi D, Margolick J, Chadwick K, Schwartz D, Siliciano RF. 1995. In vivo fate of HIV-1-infected T cells: Quantitative analysis of the transition to stable latency. Nat Med 1:1284–1290.
97. Ho Y-C, Shan L, Hosmane NN, Wang J, Laskey SB, Rosenbloom DIS, Lai J, Blankson JN, Siliciano JD, Siliciano RF. 2013. Replication-competent noninduced proviruses in the latent reservoir increase barrier to HIV-1 cure. Cell 155:540–51.
98. Archin NM, Sung JM, Garrido C, Soriano-Sarabia N, Margolis DM.

2014. Eradicating HIV-1 infection: seeking to clear a persistent pathogen. Nat Rev Microbiol 12:750–764.

99. Swiggard WJ, Baytop C, Yu JJ, Dai J, Li C, Schretzenmair R, Theodosopoulos T, O'Doherty U. 2005. Human immunodeficiency virus type 1 can establish latent infection in resting CD4+ T cells in the absence of activating stimuli. J Virol 79:14179–14188.
100. Unutmaz D, KewalRamani VN, Marmon S, Littman DR. 1999. Cytokine signals are sufficient for HIV-1 infection of resting human T lymphocytes. J Exp Med 189:1735–1746.
101. Saleh S, Solomon A, Wightman F, Xhilaga M, Cameron PU, Lewin SR. 2007. CCR7 ligands CCL19 and CCL21 increase permissiveness of resting memory CD4+ T cells to HIV-1 infection: a novel model of HIV-1 latency. Blood 110:4161–4.
102. Zhang L, Ramratnam B, Tenner-Racz K, He Y, Vesanen M, Lewin S, Talal A, Racz P, Perelson AS, Korber BT, Markowitz M, Guo Y, Duran M, Hurley A, Tsay J, Huang Y-C, Wang C-C, Ho DD. 1999. Quantifying Residual HIV-1 Replication in Patients Receiving Combination Antiretroviral Therapy. N Engl J Med 340:1605–1613.
103. Zhang Z-Q, Schuler T, Zupancic M, Wietgrefe S, Staskus KA, Reimann KA, Reinhart TA, Rogan M, Cavert W, Miller CJ. 1999. Sexual transmission and propagation of SIV and HIV in resting and activated CD4+ T cells. Science 286:1353–1357.
104. Musey LK, Krieger JN, Hughes JP, Schacker TW, Corey L, McElrath MJ. 1999. Early and persistent human immunodeficiency virus type 1 (HIV-1)—specific T helper dysfunction in blood and lymph nodes following acute HIV-1 infection. J Infect Dis 180:278–284.
105. Eckstein DA, Penn ML, Korin YD, Scripture-Adams DD, Zack JA, Kreisberg JF, Roederer M, Sherman MP, Chin PS, Goldsmith MA. 2001. HIV-1 actively replicates in naive CD4(+) T cells residing within human lymphoid tissues. Immunity 15:671–682.
106. Lewin SR, Evans VA, Elliott JH, Spire B, Chomont N. 2011. Finding a cure for HIV: will it ever be achievable. J Int AIDS Soc 14:4–14.
107. Fromentin R, DaFonseca S, Costiniuk CT, El-Far M, Procopio FA, Hecht FM, Hoh R, Deeks SG, Hazuda DJ, Lewin SR, Routy J-PP,

Sékaly R-PP, Chomont N. 2019. PD-1 blockade potentiates HIV latency reversal ex vivo in CD4 + T cells from ART-suppressed individuals. Nat Commun 10:1–7.

108. Evans VA, Van Der Sluis RM, Solomon A, Dantanarayana A, McNeil C, Garsia R, Palmer S, Fromentin R, Chomont N, Sékaly RP, Cameron PU, Lewin SR. 2018. Programmed cell death-1 contributes to the establishment and maintenance of HIV-1 latency. AIDS 32:1491–1497.
109. Zack JA, Arrigo SJ, Weitsman SR, Go AS, Haislip A, Chen ISYY. 1990. HIV-1 entry into quiescent primary lymphocytes: Molecular analysis reveals a labile, latent viral structure. Cell 61:213–222.
110. Agosto LM, Herring MB, Mothes W, Henderson AJ. 2018. HIV-1-Infected CD4+ T Cells Facilitate Latent Infection of Resting CD4+ T Cells through Cell-Cell Contact. Cell Rep 24:2088–2100.
111. Stevenson M, Stanwick TL, Dempsey MP, Lamonica CA. 1990. HIV-1 replication is controlled at the level of T cell activation and proviral integration. EMBO J 9:1551–1560.
112. Baldauf HM, Pan X, Erikson E, Schmidt S, Daddacha W, Burggraf M, Schenkova K, Ambiel I, Wabnitz G, Gramberg T, Panitz S, Flory E, Landau NR, Sertel S, Rutsch F, Lasitschka F, Kim B, König R, Fackler OT, Keppler OT. 2012. SAMHD1 restricts HIV-1 infection in resting CD4 + T cells. Nat Med 18:1682–1687.
113. Emiliani S, Fischle W, Ott M, Van Lint C, Amella CA, Verdin E. 1998. Mutations in the tat gene are responsible for human immunodeficiency virus type 1 postintegration latency in the U1 cell line. J Virol 72:1666–1670.
114. Emiliani S, Van Lint C, Fischle W, Paras P, Ott M, Brady J, Verdin E. 1996. A point mutation in the HIV-1 Tat responsive element is associated with postintegration latency. Proc Natl Acad Sci U S A1996/06/25. 93:6377–6381.
115. Lenasi T, Contreras X, Peterlin BM, T L, X C, BM P. 2008. Transcriptional interference antagonizes proviral gene expression to promote HIV latency. Cell Host Microbe2008/08/12. 4:123–133.
116. Greger IH, Demarchi F, Giacca M, Proudfoot NJ. 1998.

Transcriptional interference perturbs the binding of Sp1 to the HIV-1 promoter. Nucleic Acids Res 26:1294–1301.

117. Ashe MP, Griffin P, James W, Proudfoot NJ. 1995. Poly(A) site selection in the HIV-1 provirus: inhibition of promoter-proximal polyadenylation by the downstream major splice donor site. Genes Dev 9:3008–25.
118. Kauder SE, Bosque A, Lindqvist A, Planelles V, Verdin E. 2009. Epigenetic regulation of HIV-1 latency by cytosine methylation. PLoS Pathog 5:49–55.
119. Mbonye U, Karn J. 2014. Transcriptional control of HIV latency: Cellular signaling pathways, epigenetics, happenstance and the hope for a cure. Virology 454–455:328–339.
120. Zhang Z, Klatt A, Gilmour DS, Henderson AJ. 2007. Negative Elongation Factor NELF Represses Human Immunodeficiency Virus Transcription by Pausing the RNA Polymerase II Complex. J Biol Chem 282:16981–16988.
121. Jadlowsky JK, Wong JY, Graham AC, Dobrowolski C, Devor RL, Adams MD, Fujinaga K, Karn J. 2014. Negative Elongation Factor Is Required for the Maintenance of Proviral Latency but Does Not Induce Promoter-Proximal Pausing of RNA Polymerase II on the HIV Long Terminal Repeat. Mol Cell Biol 34:1911–1928.
122. Williams SAF, Greene WC. 2005. Host factors regulating post-integration latency of HIV. Trends Microbiol2005/04/09. 13:137–139.
123. Lassen KG, Ramyar KX, Bailey JR, Zhou Y, Siliciano RF. 2006. Nuclear retention of multiply spliced HIV-1 RNA in resting CD4+ T cells. PLoS Pathog 2:68–82.
124. Zhang H. 2009. Reversal of HIV-1 latency with anti-microRNA inhibitors. Int J Biochem Cell Biol 41:451–454.
125. Cameron PU, Saleh S, Sallmann G, Solomon A, Wightman F, Evans VA, Boucher G, Haddad EK, Sekaly RP, Harman AN, Anderson JL, Jones KL, Mak J, Cunningham AL, Jaworowski A, Lewin SR. 2010. Establishment of HIV-1 latency in resting CD4+ T cells depends on chemokine-induced changes in the actin cytoskeleton. Proc Natl Acad Sci U S A 107:16934–16939.

126. Saleh S, Wightman F, Ramanayake S, Alexander M, Kumar N, Khoury G, Pereira C, Purcell D, Cameron PU, Lewin SR. 2011. Expression and reactivation of HIV in a chemokine induced model of HIV latency in primary resting CD4+ T cells. Retrovirology 8:80–96.
127. Coiras M, Bermejo M, Descours B, Mateos E, García-Pérez J, López-Huertas MR, Lederman MM, Benkirane M, Alcamí J. 2016. IL-7 Induces SAMHD1 Phosphorylation in CD4+ T Lymphocytes, Improving Early Steps of HIV-1 Life Cycle. Cell Rep 14:2100–2107.
128. Manganaro L, Hong P, Hernandez MM, Argyle D, Mulder LCF, Potla U, Diaz-Griffero F, Lee B, Fernandez-Sesma A, Simon V. 2018. IL-15 regulates susceptibility of CD4 + T cells to HIV infection. Proc Natl Acad Sci U S A 115:9659–9667.
129. Evans VA, Kumar N, Filali A, Procopio FA, Yegorov O, Goulet J-PP, Saleh S, Haddad EK, da Fonseca Pereira C, Ellenberg PC, Sekaly R-PP, Cameron PU, Lewin SR, Pereira C da F, Ellenberg PC, Sekaly R-PP, Cameron PU, Lewin SR. 2013. Myeloid Dendritic Cells Induce HIV-1 Latency in Non-proliferating CD4+ T Cells. PLoS Pathog 9:1–14.
130. Kumar NA, Cheong K, Powell DR, da Fonseca Pereira C, Anderson J, Evans VA, Lewin SR, Cameron PU. 2015. The role of antigen presenting cells in the induction of HIV-1 latency in resting CD4(+) T-cells. Retrovirology 12:76–89.
131. Anderson JL, Mota TM, Evans VA, Kumar N, Rezaei SD, Cheong K, Solomon A, Wightman F, Cameron PU, Lewin SR. 2016. Understanding factors that modulate the establishment of HIV latency in resting CD4+ T-Cells in vitro. PLoS One 11:1–14.
132. Dufour C, Gantner P, Fromentin R, Chomont N. 2020. The multifaceted nature of HIV latency. J Clin Invest. American Society for Clinical Investigation 3:1-14.
133. Li P, Kaiser P, Lampiris HW, Kim P, Yukl SA, Havlir D V, Greene WC, Wong JK. 2016. Stimulating the RIG-I pathway to kill cells in the latent HIV reservoir following viral reactivation. Nat Med 22:807–811.
134. Schröder ARW, Shinn P, Chen H, Berry C, Ecker JR, Bushman F. 2002. HIV-1 Integration in the Human Genome Favors Active Genes

and Local Hotspots. Cell 110:521–529.

135. Gallastegui E, Millán-Zambrano G, Terme J-M, Chávez S, Jordan A. 2011. Chromatin Reassembly Factors Are Involved in Transcriptional Interference Promoting HIV Latency. J Virol 85:3187–3202.
136. Ruelas DS, Greene WC. 2013. An integrated overview of HIV-1 latency. Cell 155:519–29.
137. Lewinski MK, Bisgrove D, Shinn P, Chen H, Hoffmann C, Hannenhalli S, Verdin E, Berry CC, Ecker JR, Bushman FD. 2005. Genome-wide analysis of chromosomal features repressing human immunodeficiency virus transcription. J Virol2005/05/14. 79:6610–9.
138. Hu WY, Bushman FD, Siva AC. 2004. RNA interference against retroviruses. Virus Res 102:59–64.
139. ter Brake O, Konstantinova P, Ceylan M, Berkhout B. 2006. Silencing of HIV-1 with RNA Interference: a Multiple shRNA Approach. Mol Ther 14:883–892.
140. Kim YK, Mbonye U, Hokello J, Karn J. 2011. T-cell receptor signaling enhances transcriptional elongation from latent HIV proviruses by activating P-TEFb through an ERK-dependent pathway. J Mol Biol 410:896–916.
141. Kinoshita S, Chen BK, Kaneshima H, Nolan GP. 1998. Host control of HIV-1 parasitism in T cells by the nuclear factor of activated T cells. Cell 95:595–604.
142. Sierra S, Kupfer B, Kaiser R. 2005. Basics of the virology of HIV-1 and its replication. J Clin Virol. J Clin Virol 4:22-34
143. Van Lint C, Emiliani S, Ott M, Verdin E. 1996. Transcriptional activation and chromatin remodeling of the HIV-1 promoter in response to histone acetylation. EMBO J 15:1112–1120.
144. Coull JJ, Romerio F, Sun J-M, Volker JL, Galvin KM, Davie JR, Shi Y, Hansen U, Margolis DM. 2000. The Human Factors YY1 and LSF Repress the Human Immunodeficiency Virus Type 1 Long Terminal Repeat via Recruitment of Histone Deacetylase 1. J Virol 74:6790–6799.
145. Tyagi M, Pearson RJ, Karn J. 2010. Establishment of HIV latency in primary CD4+ cells is due to epigenetic transcriptional silencing and

P-TEFb restriction. J Virol 84:6425–37.

146. Bieniasz PD, Grdina TA, Bogerd HP, Cullen BR. 1999. Recruitment of cyclin T1/P-TEFb to an HIV type 1 long terminal repeat promoter proximal RNA target is both necessary and sufficient for full activation of transcription. Proc Natl Acad Sci U S A 96:7791–7796.
147. D'Orso I, Jang GM, Pastuszak AW, Faust TB, Quezada E, Booth DS, Frankel AD. 2012. Transition Step during Assembly of HIV Tat:P-TEFb Transcription Complexes and Transfer to TAR RNA. Mol Cell Biol 32:4780–4793.
148. Chiang K, Sung T-LT-L, Rice AP. 2012. Regulation of cyclin T1 and HIV-1 Replication by microRNAs in resting CD4+ T lymphocytes. J Virol 86:3244–3252.
149. Hoque M, Shamanna RA, Guan D, Pe'ery T, Mathews MB. 2011. HIV-1 replication and latency are regulated by translational control of cyclin T1. J Mol Biol 410:917–932.
150. Ramakrishnan R, Dow EC, Rice AP. 2009. Characterization of Cdk9 T-loop phosphorylation in resting and activated CD4 + T lymphocytes. J Leukoc Biol 86:1345–1350.
151. Budhiraja S, Ramakrishnan R, Rice AP. 2012. Phosphatase PPM1A negatively regulates P-TEFb function in resting CD4T+ T cells and inhibits HIV-1 gene expression. Retrovirology 9:1–10.
152. Budhiraja S, Famiglietti M, Bosque A, Planelles V, Rice AP. 2013. Cyclin T1 and CDK9 T-Loop Phosphorylation Are Downregulated during Establishment of HIV-1 Latency in Primary Resting Memory CD4 + T Cells. J Virol 87:1211–1220.
153. Yang Z, Zhu Q, Luo K, Zhou Q. 2001. The 7SK small nuclear RNA inhibits the CDK9/cyclin T1 kinase to control transcription. Nature 414:317–322.
154. Sung TL, Rice AP. 2006. Effects of prostratin on Cyclin TI/P-TEFb function and the gene expression profile in primary resting CD4+ T cells. Retrovirology 3:1–14.
155. Telwatte S, Morón-López S, Aran D, Kim P, Hsieh C, Joshi S, Montano M, Greene WC, Butte AJ, Wong JK, Yukl SA. 2019. Heterogeneity in HIV and cellular transcription profiles in cell line

models of latent and productive infection: implications for HIV latency. Retrovirology 16:32–49.

156. Sun B, Yang R, Mallardo M. 2016. Roles of microRNAs in HIV-1 Replication and Latency. MicroRNA 5:120–123.
157. Detsika MG, Psarris A, Paraskevis D. 2012. MicroRNAs and HIV latency: a complex and promising relationship. AIDS Rev 14:188–194.
158. Deeks SG, Lewin SR, Ross AL, Ananworanich J, Benkirane M, Cannon P, Chomont N, Douek D, Lifson JD, Lo Y-R, Kuritzkes D, Margolis D, Mellors J, Persaud D, Tucker JD, Barre-Sinoussi F, International AIDS Society Towards a Cure Working Group, Alter G, Auerbach J, Autran B, Barouch DH, Behrens G, Cavazzana M, Chen Z, Cohen ÉA, Corbelli GM, Eholié S, Eyal N, Fidler S, Garcia L, Grossman C, Henderson G, Henrich TJ, Jefferys R, Kiem H-P, McCune J, Moodley K, Newman PA, Nijhuis M, Nsubuga MS, Ott M, Palmer S, Richman D, Saez-Cirion A, Sharp M, Siliciano J, Silvestri G, Singh J, Spire B, Taylor J, Tolstrup M, Valente S, van Lunzen J, Walensky R, Wilson I, Zack J. 2016. International AIDS Society global scientific strategy: towards an HIV cure 2016. Nat Med 22:839–850.
159. Blauvelt A, Asada H, Saville MW, Klaus-Kovtun V, Altman DJ, Yarchoan R, Katz SI. 1997. Productive infection of dendritic cells by HIV-1 and their ability to capture virus are mediated through separate pathways. J Clin Invest 100:2043–2053.
160. Rehwinkel J, Tan CP, Goubau D, Schulz O, Pichlmair A, Bier K, Robb N, Vreede F, Barclay W, Fodor E, Reis e Sousa C. 2010. RIG-I Detects Viral Genomic RNA during Negative-Strand RNA Virus Infection. Cell 140:397–408.
161. Perelson AS, Neumann AU, Markowitz M, Leonard JM, Ho DD. 1996. HIV-1 dynamics in vivo: virion clearance rate, infected cell life-span, and viral generation time. Science (80-)1996/03/15. 271:1582–1586.
162. Murray AJ, Kwon KJ, Farber DL, Siliciano RF. 2016. The Latent Reservoir for HIV-1: How Immunologic Memory and Clonal Expansion Contribute to HIV-1 Persistence. J Immunol 197:407–417.
163. Kent SJ, Reece JC, Petravic J, Martyushev A, Kramski M, De Rose

R, Cooper DA, Kelleher AD, Emery S, Cameron PU, Lewin SR, Davenport MP. 2013. The search for an HIV cure: tackling latent infection. Lancet Infect Dis 13:614–621.

164. Blankson JN, Persaud D, Siliciano RF. 2002. The challenge of viral reservoirs in hiv-1 infection. Annu Rev Med 53:557–593.
165. Wightman F, Solomon A, Khoury G, Green JA, Gray L, Gorry PR, Ho YS, Saksena NK, Hoy J, Crowe SM, Cameron PU, Lewin SR. 2010. Both CD31 + and CD31 − Naive CD4 + T Cells Are Persistent HIV Type 1–Infected Reservoirs in Individuals Receiving Antiretroviral Therapy. J Infect DiS 202:1738–1748.
166. Khoury G, Rajasuriar R, Cameron PU, Lewin SR. 2011. The role of naive T-cells in HIV-1 pathogenesis: an emerging key player. Clin Immunol 141:253–267.
167. Gubser C, Pitman MC, Lewin SR. 2019. CD4+ T cell signatures in HIV infection. Nat Immunol 20:948–950.
168. Sun H, Kim D, Li X, Kiselinova M, Ouyang Z, Vandekerckhove L, Shang H, Rosenberg ES, Yu XG, Lichterfeld M. 2015. Th1/17 Polarization of CD4 T Cells Supports HIV-1 Persistence during Antiretroviral Therapy. J Virol 89:11284–93.
169. Soriano-Sarabia N, Archin NM, Bateson R, Dahl NP, Crooks AM, Kuruc JD, Garrido C, Margolis DM. 2015. Peripheral Vγ9Vδ2 T Cells Are a Novel Reservoir of Latent HIV Infection. PLoS Pathog 11:11284–93.
170. Tran T-A, de Goër de Herve M-G, Hendel-Chavez H, Dembele B, Le Névot E, Abbed K, Pallier C, Goujard C, Gasnault J, Delfraissy J-F, Balazuc A-M, Taoufik Y. 2008. Resting regulatory CD4 T cells: a site of HIV persistence in patients on long-term effective antiretroviral therapy. PLoS One 3:3305.
171. Lorenzo-Redondo R, Fryer HR, Bedford T, Kim E-YY, Archer J, Kosakovsky Pond SL, Chung Y-SS, Penugonda S, Chipman JG, Fletcher C V., Schacker TW, Malim MH, Rambaut A, Haase AT, McLean AR, Wolinsky SM. 2016. Persistent HIV-1 replication maintains the tissue reservoir during therapy. Nature 530:51–56.
172. Wong JK, Yukl SA. 2016. Tissue reservoirs of HIV. Curr Opin HIV

AIDS 11:362–369.

173. Chun T-WW, Carruth L, Finzi D, Shen X, DiGiuseppe JA, Taylor H, Hermankova M, Chadwick K, Margolick J, Quinn TC, Kuo Y-HH, Brookmeyer R, Zeiger MA, Barditch-Crovo P, Siliciano RF. 1997. Quantification of latent tissue reservoirs and total body viral load in HIV-1 infection. Nature 387:183–8.
174. Massanella M, Richman DD. 2016. Measuring the latent reservoir in vivo. J Clin Invest 126:464–472.
175. Sathaliyawala T, Kubota M, Yudanin N, Turner D, Camp P, Thome JJ, Bickham KL, Lerner H, Goldstein M, Sykes M, Kato T, Farber DL. 2013. Distribution and compartmentalization of human circulating and tissue-resident memory T cell subsets. Immunity 38:187–197.
176. Murray JM, Zaunders J, Emery S, Cooper DA, Hey-Nguyen WJ, Koelsch KK, Kelleher AD. 2017. HIV dynamics linked to memory CD4+ T cell homeostasis. PLoS One 12:12–26.
177. Wang Z, Gurule EE, Brennan TP, Gerold JM, Kwon KJ, Hosmane NN, Kumar MR, Beg SA, Capoferri AA, Ray SC, Ho YC, Hill AL, Siliciano JD, Siliciano RF. 2018. Expanded cellular clones carrying replication-competent HIV-1 persist, wax, and wane. Proc Natl Acad Sci U S A 115:2575–2584.
178. Cohn LB, Silva IT, Oliveira TY, Rosales RA, Parrish EH, Learn GH, Hahn BH, Czartoski JL, McElrath MJ, Lehmann C, Klein F, Caskey M, Walker BD, Siliciano JD, Siliciano RF, Jankovic M, Nussenzweig MC. 2015. HIV-1 integration landscape during latent and active infection. Cell 160:420–432.
179. Symons J, Chopra A, Malantinkova E, Spiegelaere W De, Leary S, Cooper D, Abana CO, Rhodes A, Rezaei SD, Vandekerckhove L, Mallal S, Lewin SR, Cameron PU, Malatinkova E, De Spiegelaere W, Leary S, Cooper D, Abana CO, Rhodes A, Rezaei SD, Vandekerckhove L, Mallal S, Lewin SR, Cameron PU. 2017. HIV integration sites in latently infected cell lines: evidence of ongoing replication. Retrovirology 14:1–10.
180. Maldarelli F, Wu X, Su L, Simonetti FR, Shao W, Hill S, Spindler J, Ferris AL, Mellors JW, Kearney MF, Coffin JM, Hughes SH. 2014. HIV

latency. Specific HIV integration sites are linked to clonal expansion and persistence of infected cells. Science 345:179–183.

181. Wagner TA, McLaughlin S, Garg K, Cheung CYKK, Larsen BB, Styrchak S, Huang HC, Edlefsen PT, Mullins JI, Frenkel LM. 2014. Proliferation of cells with HIV integrated into cancer genes contributes to persistent infection. Science 345:570–573.
182. Lugli E, Dominguez MH, Gattinoni L, Chattopadhyay PK, Bolton DL, Song K, Klatt NR, Brenchley JM, Vaccari M, Gostick E, Price DA, Waldmann TA, Restifo NP, Franchini G, Roederer M. 2013. Superior T memory stem cell persistence supports long-lived T cell memory. J Clin Invest 123:594–599.
183. Liu R, Simonetti FR, Ho Y-C. 2020. The forces driving clonal expansion of the HIV-1 latent reservoir. Virol J 17:1–13.
184. Bacchus-Souffan C, Fitch M, Symons J, Abdel-Mohsen M, Reeves DB, Hoh R, Stone M, Hiatt J, Kim P, Chopra A, Ahn H, York VA, Cameron DL, Hecht FM, Martin JN, Yukl SA, Mallal S, Cameron PU, Deeks SG, Schiffer JT, Lewin SR, Hellerstein MK, McCune JM, Hunt PW. 2021. Relationship between CD4 T cell turnover, cellular differentiation and HIV persistence during ART. PLoS Pathog 17:1–16.
185. Honeycutt JB, Thayer WO, Baker CE, Ribeiro RM, Lada SM, Cao Y, Cleary RA, Hudgens MG, Richman DD, Victor Garcia J. 2017. HIV persistence in tissue macrophages of humanized myeloid-only mice during antiretroviral therapy. Nat Med 23:638–643.
186. Baxter AE, Russell RA, Duncan CJ, Moore MD, Willberg CB, Pablos JL, Finzi A, Kaufmann DE, Ochsenbauer C, Kappes JC, Groot F, Sattentau QJ. 2014. Macrophage infection via selective capture of HIV-1-infected CD4+ T cells. Cell Host Microbe 16:711–721.
187. Gray L, Roche M, Churchill MJ, Sterjovski J, Ellett A, Poumbourios P, Sheffief S, Wang B, Saksena N, Purcell DFJ, Wesselingh S, Cunningham AL, Brew BJ, Gabuzda D, Gorry PR. 2009. Tissue-Specific Sequence Alterations in the Human Immunodeficiency Virus Type 1 Envelope Favoring CCR5 Usage Contribute to Persistence of Dual-Tropic Virus in the Brain. J Virol 83:5430–5441.

188. Churchill MJ, Deeks SG, Margolis DM, Siliciano RF, Swanstrom R. 2016. HIV reservoirs: what, where and how to target them. Nat Rev Microbiol 14:55–60.
189. Lamers SL, Rose R, Maidji E, Agsalda-Garcia M, Nolan DJ, Fogel GB, Salemi M, Garcia DL, Bracci P, Yong W, Commins D, Said J, Khanlou N, Hinkin CH, Sueiras MV, Mathisen G, Donovan S, Shiramizu B, Stoddart CA, McGrath MS, Singer EJ. 2016. HIV DNA Is Frequently Present within Pathologic Tissues Evaluated at Autopsy from Combined Antiretroviral Therapy-Treated Patients with Undetectable Viral Loads. J Virol 90:8968–8983.
190. Gray LR, Roche M, Flynn JK, Wesselingh SL, Gorry PR, Churchill MJ. 2014. Is the central nervous system a reservoir of HIV-1 Curr Opin HIV AIDS 9:552–558.
191. Zalar A, Figueroa MI, Ruibal-Ares B, Baré P, Cahn P, de Bracco MM de E, Belmonte L. 2010. Macrophage HIV-1 infection in duodenal tissue of patients on long term HAART. Antiviral Res 87:269–271.
192. Yona S, Kim K-W, Wolf Y, Mildner A, Varol D, Breker M, Strauss-Ayali D, Viukov S, Guilliams M, Misharin A, Hume DA, Perlman H, Malissen B, Zelzer E, Jung S. 2013. Fate mapping reveals origins and dynamics of monocytes and tissue macrophages under homeostasis. Immunity 38:79–91.
193. Lambotte O, Taoufik Y, de Goer MG, Wallon C, Goujard C, Delfraissy JF. 2000. Detection of infectious HIV in circulating monocytes from patients on prolonged highly active antiretroviral therapy. J Acquir Immune Defic Syndr 23:114–119.
194. Martin CJ, Peters KN, Behar SM. 2014. Macrophages clean up: efferocytosis and microbial control. Curr Opin Microbiol 17:17–23.
195. Grouard G, Clark EA. 1997. Role of dendritic and follicular dendritic cells in HIV infection and pathogenesis. Curr Opin Immunol 9:563–567.
196. Burton G. 2002. Follicular dendritic cell contributions to HIV pathogenesis. Semin Immunol 14:275–284.
197. Banga R, Procopio FA, Noto A, Pollakis G, Cavassini M, Ohmiti K, Corpataux J-MM, De Leval L, Pantaleo G, Perreau M. 2016. PD-1+

and follicular helper T cells are responsible for persistent HIV-1 transcription in treated aviremic individuals. Nat Med 22:754–761.

198. Perreau M, Savoye A-LL, De Crignis E, Corpataux J-M, Cubas R, Haddad EK, De Leval L, Graziosi C, Pantaleo G, Jean-Marc Corpataux, Cubas R, Haddad EK, De Leval L, Graziosi C, Pantaleo G. 2013. Follicular helper T cells serve as the major CD4 T cell compartment for HIV-1 infection, replication, and production. J Exp Med 210:143–156.
199. Smith BA, Gartner S, Liu Y, Perelson AS, Stilianakis NI, Keele BF, Kerkering TM, Ferreira-Gonzalez A, Szakal AK, Tew JG. 2001. Persistence of infectious HIV on follicular dendritic cells. J Immunol 166:690–696.
200. Otero M, Nunnari G, Leto D, Sullivan J, Wang F-X, Frank I, Xu Y, Patel C, Dornadula G, Kulkosky J. 2003. Peripheral blood dendritic cells are not a major reservoir for HIV type 1 in infected individuals on virally suppressive HAART. AIDS Res Hum Retroviruses 19:1097–1103.
201. Westermann J, Pabst R. 1992. Distribution of lymphocyte subsets and natural killer cells in the human body. Clin Investig 70:539–544.
202. Di Mascio M, Paik CH, Carrasquillo JA, Maeng JS, Jang BS, In SS, Srinivasula S, Byrum R, Neria A, Kopp W, Catalfamo M, Nishimura Y, Reimann K, Martin M, Lane HC. 2009. Noninvasive in vivo imaging of CD4 cells in simian-human immunodeficiency virus (SHIV)-infected nonhuman primates. Blood 114:328–337.
203. Lampinen TM, Critchlow CW, Kuypers JM, Hurt CS, Nelson PJ, Hawes SE, Coombs RW, Holmes KK, Kiviat NB. 2000. Association of antiretroviral therapy with detection of HIV-1 RNA and DNA in the anorectal mucosa of homosexual men. AIDS 14:69–75.
204. Pantaleo G, Graziosi C, Butini L, Pizzo PA, Schnittman SM, Kotler DP, Fauci AS. 1991. Lymphoid organs function as major reservoirs for human immunodeficiency virus. Proc Natl Acad Sci U S A 88:9838–9842.
205. Pantaleo G, Graziosi C, Demarest JF, Cohen OJ, Vaccarezza M, Gantt K, Muro-Cacho C, Fauci AS. 1994. Role of lymphoid organs in

the pathogenesis of human immunodeficiency virus (HIV) infection. Immunol Rev 140:105–130.

206. McManus WR, Bale MJ, Spindler J, Wiegand A, Musick A, Patro SC, Sobolewski MD, Musick VK, Anderson EM, Cyktor JC, Halvas EK, Shao W, Wells D, Wu X, Keele BF, Milush JM, Hoh R, Mellors JW, Hughes SH, Deeks SG, Coffin JM, Kearney MF. 2019. HIV-1 in lymph nodes is maintained by cellular proliferation during antiretroviral therapy. J Clin Invest 129:4629–4642.
207. Boritz EA, Darko S, Swaszek L, Wolf G, Wells D, Wu X, Henry AR, Laboune F, Hu J, Ambrozak D, Hughes MS, Hoh R, Casazza JP, Vostal A, Bunis D, Nganou-Makamdop K, Lee JS, Migueles SA, Koup RA, Connors M, Moir S, Schacker T, Maldarelli F, Hughes SH, Deeks SG, Douek DC. 2016. Multiple Origins of Virus Persistence during Natural Control of HIV Infection. Cell 166:1004–1015.
208. Fukazawa Y, Lum R, Okoye AA, Park H, Matsuda K, Bae JY, Hagen SI, Shoemaker R, Deleage C, Lucero C, Morcock D, Swanson T, Legasse AW, Axthelm MK, Hesselgesser J, Geleziunas R, Hirsch VM, Edlefsen PT, Piatak M, Estes JD, Lifson JD, Picker LJ. 2015. B cell follicle sanctuary permits persistent productive simian immunodeficiency virus infection in elite controllers. Nat Med 21:132–139.
209. Veazey RS, DeMaria MA, Chalifoux L V., Shvetz DE, Pauley DR, Knight HL, Rosenzweig M, Johnson RP, Desrosiers RC, Lackner AA. 1998. Gastrointestinal tract as a major site of CD4+ T cell depletion and viral replication in SIV infection. Science 280:427–431.
210. Guadalupe M, Reay E, Sankaran S, Prindiville T, Flamm J, McNeil A, Dandekar S. 2003. Severe CD4 + T-Cell Depletion in Gut Lymphoid Tissue during Primary Human Immunodeficiency Virus Type 1 Infection and Substantial Delay in Restoration following Highly Active Antiretroviral Therapy. J Virol 77:11708–11717.
211. Mattapallil JJ, Douek DC, Hill B, Nishimura Y, Martin M, Roederer M. 2005. Massive infection and loss of memory CD4+ T cells in multiple tissues during acute SIV infection. Nature 434:1093–1097.
212. Chun TW, Nickle DC, Justement JS, Meyers JH, Roby G, Hallahan

CW, Kottilil S, Moir S, Mican JAM, Mullins JI, Ward DJ, Kovacs JA, Mannon PJ, Fauci AS. 2008. Persistence of HIV in gut-associated lymphoid tissue despite long-term antiretroviral therapy. J Infect Dis 197:714–720.

213. Yukl SA, Gianella S, Sinclair E, Epling L, Li Q, Duan L, Choi ALMM, Girling V, Ho T, Li P, Fujimoto K, Lampiris H, Hare CB, Pandori M, Haase AT, Günthard HF, Fischer M, Shergill AK, McQuaid K, Havlir D V., Wong JK. 2010. Differences in HIV burden and immune activation within the gut of HIV-positive patients receiving suppressive antiretroviral therapy. J Infect Dis 202:1553–1561.
214. Yukl SA, Sinclair E, Somsouk M, Hunt PW, Epling L, Killian M, Girling V, Li P, Havlir D V., Deeks SG, Wong JK, Hatano H. 2014. A comparison of methods for measuring rectal HIV levels suggests that HIV DNA resides in cells other than CD4+ T cells, including myeloid cells. AIDS 28:439–442.
215. Mowat AMI, Viney JL. 1997. The anatomical basis of intestinal immunity. Immunol Rev. Immunol Rev.
216. Kelley CF, Haaland RE, Patel P, Evans-Strickfaden T, Farshy C, Hanson D, Mayer K, Lennox JL, Brooks JT, Hart CE. 2011. HIV-1 RNA rectal shedding is reduced in Men with Low plasma HIV-1 RNA viral loads and is not enhanced by sexually transmitted bacterial infections of the rectum. J Infect Dis 204:761–767.
217. Anderson JL, Khoury G, Fromentin R, Solomon A, Chomont N, Sinclair E, Milush JM, Hartogensis W, Bacchetti P, Roche M, Tumpach C, Gartner M, Pitman MC, Epling CL, Hoh R, Hecht FM, Somsouk M, Cameron PU, Deeks SG, Lewin SR. 2020. Human Immunodeficiency Virus (HIV)-Infected CCR6+ Rectal CD4+ T Cells and HIV Persistence On Antiretroviral Therapy. J Infect Dis 221:744–755.
218. Guadalupe M, Sankaran S, George MD, Reay E, Verhoeven D, Shacklett BL, Flamm J, Wegelin J, Prindiville T, Dandekar S. 2006. Viral suppression and immune restoration in the gastrointestinal mucosa of human immunodeficiency virus type 1-infected patients initiating therapy during primary or chronic infection. J Virol 80:8236–

47.

219. van Marle G, Gill MJ, Kolodka D, McManus L, Grant T, Church DL. 2007. Compartmentalization of the gut viral reservoir in HIV-1 infected patients. Retrovirology 4:87–99.
220. Lerner P, Guadalupe M, Donovan R, Hung J, Flamm J, Prindiville T, Sankaran-Walters S, Syvanen M, Wong JK, George MD, Dandekar S. 2011. The Gut Mucosal Viral Reservoir in HIV-Infected Patients Is Not the Major Source of Rebound Plasma Viremia following Interruption of Highly Active Antiretroviral Therapy. J Virol 85:4772–4782.
221. Kramer-Hämmerle S, Rothenaigner I, Wolff H, Bell JE, Brack-Werner R. 2005. Cells of the central nervous system as targets and reservoirs of the human immunodeficiency virus. Virus Res 111:194–213.
222. Kumar A, Abbas W, Herbein G. 2014. HIV-1 latency in monocytes/macrophages. Viruses 6:1837–60.
223. Barton K, Winckelmann A, Palmer S. 2016. HIV-1 Reservoirs During Suppressive Therapy. Trends Microbiol2016/02/16. 24:345–355.
224. Richman DD, Margolis DM, Delaney M, Greene WC, Hazuda D, Pomerantz RJ. 2009. The challenge of finding a cure for HIV infection. Science Science.
225. Bruner KM, Murray AJ, Pollack RA, Soliman MG, Laskey SB, Capoferri AA, Lai J, Strain MC, Lada SM, Hoh R, Ho Y-CC, Richman DD, Deeks SG, Siliciano JD, Siliciano RF. 2016. Defective proviruses rapidly accumulate during acute HIV-1 infection. Nat Med 22:1043–9.
226. Marsden MD, Zack JA. 2010. Establishment and maintenance of HIV latency: Model systems and opportunities for intervention. Future Virol. NIH Public Access.
227. Darcis G, Kula A, Bouchat S, Fujinaga K, Corazza F, Ait-Ammar A, Delacourt N, Melard A, Kabeya K, Vanhulle C, Van Driessche B, Gatot J-S, Cherrier T, Pianowski LF, Gama L, Schwartz C, Vila J, Burny A, Clumeck N, Moutschen M, De Wit S, Peterlin BM, Rouzioux C, Rohr O, Van Lint C. 2015. An In-Depth Comparison of Latency-Reversing Agent Combinations in Various In Vitro and Ex Vivo HIV-1 Latency Models Identified Bryostatin-1+JQ1 and Ingenol-B+JQ1 to

Potently Reactivate Viral Gene Expression. PLoS Pathog 11:50–63.
228. Pace MJ, Agosto L, Graf EH, O'Doherty U. 2011. HIV reservoirs and latency models. Virology 411:344–354.
229. Whitney JB, Brad Jones R. 2018. In Vitro and In Vivo Models of HIV Latency, p. 241–263. *In* Advances in Experimental Medicine and Biology. Springer New York LLC. 22:1-12
230. Fujinaga K, Cary DC. 2020. Experimental Systems for Measuring HIV Latency and Reactivation. Viruses 12:1279–1296.
231. Coiras M, López-Huertas MR, Pérez-Olmeda M, Alcamí J. 2009. Understanding HIV-1 latency provides clues for the eradication of long-term reservoirs. Nat Rev Microbiol 7:798–812.
232. Spina CA, Anderson J, Archin NM, Bosque A, Chan J, Famiglietti M, Greene WC, Kashuba A, Lewin SR, Margolis DM, Mau M, Ruelas D, Saleh S, Shirakawa K, Siliciano RF, Singhania A, Soto PC, Terry VH, Verdin E, Woelk C, Wooden S, Xing S, Planelles V. 2013. An in-depth comparison of latent HIV-1 reactivation in multiple cell model systems and resting CD4+ T cells from aviremic patients. PLoS Pathog 9:100–116.
233. Chavez L, Calvanese V, Verdin E. 2015. HIV Latency Is Established Directly and Early in Both Resting and Activated Primary CD4 T Cells. PLoS Pathog 11:1004955.
234. Sahu GK, Lee K, Ji J, Braciale V, Baron S, Cloyd MW. 2006. A novel in vitro system to generate and study latently HIV-infected long-lived normal CD4+ T-lymphocytes. Virology 355:127–37.
235. Lassen KG, Hebbeler AM, Bhattacharyya D, Lobritz MA, Greene WC. 2012. A flexible model of HIV-1 latency permitting evaluation of many primary CD4 T-cell reservoirs. PLoS One 7:1–14.
236. Yang H-C, Xing S, Shan L, O'Connell K, Dinoso J, Shen A, Zhou Y, Shrum CK, Han Y, Liu JO, Zhang H, Margolick JB, Siliciano RF. 2009. Small-molecule screening using a human primary cell model of HIV latency identifies compounds that reverse latency without cellular activation. J Clin Invest 119:3473–86.
237. Brooks DG, Arlen PA, Gao L, Kitchen CMR, Zack JA. 2003. Identification of T cell-signaling pathways that stimulate latent HIV in

primary cells. Proc Natl Acad Sci U S A 100:12955–12960.

238. Chun TW, Engel D, Mizell SB, Ehler LA, Fauci AS. 1998. Induction of HIV-1 replication in latently infected CD4+ T cells using a combination of cytokines. J Exp Med 188:83–91.
239. Marini A, Harper JM, Romerio F. 2008. An in vitro system to model the establishment and reactivation of HIV-1 latency. J Immunol 181:7713–7720.
240. Kim M, Hosmane NN, Bullen CK, Capoferri A, Yang HC, Siliciano JD, Siliciano RF. 2014. A primary CD4+ T cell model of HIV-1 latency established after activation through the T cell receptor and subsequent return to quiescence. Nat Protoc 9:2755–2770.
241. Obrien MC, Ueno T, Jahan N, Zajac-Kaye M, Mitsuya H. 1995. HIV-1 expression induced by anticancer agents in latently HIV-1-infected ach2 cells. Biochem Biophys Res Commun 207:903–909.
242. Rasmussen TA, Søgaard OS, Brinkmann C, Wightman F, Lewin SR, Melchjorsen J, Dinarello C, Østergaard L, Tolstrup M. 2013. Comparison of HDAC inhibitors in clinical development: Effect on HIV production in latently infected cells and T-cell activation. Hum Vaccines Immunother 9:993–1001.
243. Doyon G, Zerbato J, Mellors JW, Sluis-Cremer N. 2013. Disulfiram reactivates latent HIV-1 expression through depletion of the phosphatase and tensin homolog. AIDS2012/06/29. 27:7–11.
244. Kutsch O, Wolschendorf F, Planelles V. 2012. Facts and Fiction: Cellular Models for High Throughput Screening for HIV-1 Reactivating Drugs. Curr HIV Res 9:568–578.
245. RF S, WC G, Siliciano RF, Greene WC. 2011. HIV Latency. Cold Spring Harb Perspect Med 1:7096–7096.
246. Folks TM, Clouse KA, Justement J, Rabson A, Duh E, Kehrl JH, Fauci AS. 1989. Tumor necrosis factor α induces expression of human immunodeficiency virus in a chronically infected T-cell clone. Proc Natl Acad Sci U S A 86:2365–2368.
247. Folks TM, Justement J, Kinter A, Dinarello CA, Fauci AS. 1987. Cytokine-induced expression of HIV-1 in a chronically infected promonocyte cell line. Science 238:800–802.

248. Kutsch O, Benveniste EN, Shaw GM, Levy DN. 2002. Direct and Quantitative Single-Cell Analysis of Human Immunodeficiency Virus Type 1 Reactivation from Latency. J Virol 76:8776–8786.
249. Jordan A, Bisgrove D, Verdin E. 2003. HIV reproducibly establishes a latent infection after acute infection of T cells in vitro. EMBO J 22:1868–77.
250. Hosmane NN, Kwon KJ, Bruner KM, Capoferri AA, Beg S, Rosenbloom DIS, Keele BF, Ho Y-CC, Siliciano JD, Siliciano RF. 2017. Proliferation of latently infected CD4+ T cells carrying replication-competent HIV-1: Potential role in latent reservoir dynamics. J Exp Med 214:959–972.
251. Bruner KM, Hosmane NN, Siliciano RF. 2015. Towards an HIV-1 cure: Measuring the latent reservoir. Trends Microbiol. Trends Microbiol 12:1520-1532
252. Boulassel MR, Chomont N, Pai NP, Gilmore N, Sékaly RP, Routy JP. 2012. CD4 T cell nadir independently predicts the magnitude of the HIV reservoir after prolonged suppressive antiretroviral therapy. J Clin Virol 53:29–32.
253. Yu JJ, Wu TL, Liszewski MK, Dai J, Swiggard WJ, Baytop C, Frank I, Levine BL, Yang W, Theodosopoulos T, O'Doherty U. 2008. A more precise HIV integration assay designed to detect small differences finds lower levels of integrated DNA in HAART treated patients. Virology 379:78–86.
254. Pinzone MR, O'Doherty U. 2018. Measuring integrated HIV DNA ex vivo and in vitro provides insights about how reservoirs are formed and maintained. Retrovirology. Retrovirology 35:1-13 .
255. Siliciano JD, Siliciano RF. 2018. Assays to Measure Latency, Reservoirs, and Reactivation, p. 23–41. *In* Current Topics in Microbiology and Immunology. Curr Top Microbiol Immunol 3:111-122 .
256. Liszewski MK, Yu JJ, O'Doherty U. 2009. Detecting HIV-1 integration by repetitive-sampling Alu-gag PCR. Methods. Methods.
257. Brady T, Kelly BJ, Male F, Roth S, Bailey A, Malani N, Gijsbers R, O'Doherty U, Bushman FD. 2013. Quantitation of HIV DNA

integration: Effects of differential integration site distributions on Alu-PCR assays. J Virol Methods 189:53–57.

258. Lee M, Kim WK, Kuroda MJ, Pal R, Chung HK. 2016. Development of real-time PCR for quantitation of simian immunodeficiency virus 2-LTR circles. J Med Primatol 45:215–221.
259. Malnati MS, Scarlatti G, Gatto F, Salvatori F, Cassina G, Rutigliano T, Volpi R, Lusso P. 2008. A universal real-time PCR assay for the quantification of group-M HIV-1 proviral load. Nat Protoc 3:1240–1248.
260. Rothenberger MK, Keele BF, Wietgrefe SW, Fletcher C V., Beilman GJ, Chipman JG, Khoruts A, Estes JD, Anderson J, Callisto SP, Schmidt TE, Thorkelson A, Reilly C, Perkey K, Reimann TG, Utay NS, Makamdop KN, Stevenson M, Douek DC, Haase AT, Schacker TW, Nganou Makamdop K, Stevenson M, Douek DC, Haase AT, Schacker TW. 2015. Large number of rebounding/founder HIV variants emerge from multifocal infection in lymphatic tissues after treatment interruption. Proc Natl Acad Sci 112:1126–1134.
261. Henrich TJ, Deeks SG, Pillai SK. 2017. Measuring the size of the latent human immunodeficiency virus reservoir: The present and future of evaluating eradication strategies. J Infect Dis. J Infect Dis 12:1-10 .
262. Bosman KJ, Wensing AMJ, Pijning AE, van Snippenberg WJ, van Ham PM, de Jong DMC, Hoepelman AIM, Nijhuis M. 2018. Development of sensitive ddPCR assays to reliably quantify the proviral DNA reservoir in all common circulating HIV subtypes and recombinant forms. J Int AIDS Soc 21:113–125.
263. Rutsaert S, Bosman K, Trypsteen W, Nijhuis M, Vandekerckhove L. 2018. Digital PCR as a tool to measure HIV persistence. Retrovirology. Retrovirology66:22-34 .
264. Strain MC, Lada SM, Luong T, Rought SE, Gianella S, Terry VH, Spina CA, Woelk CH, Richman DD. 2013. Highly Precise Measurement of HIV DNA by Droplet Digital PCR. PLoS One 8:55943–55957.
265. Martinez-Picado J, Zurakowski R, Buzón MJ, Stevenson M. 2018.

Episomal HIV-1 DNA and its relationship to other markers of HIV-1 persistence. Retrovirology. Retrovirology.

266. Deininger P. 2011. Alu elements: know the SINEs. Genome Biol 12:236–242.
267. O'Doherty U, Swiggard WJ, Jeyakumar D, McGain D, Malim MH. 2002. A Sensitive, Quantitative Assay for Human Immunodeficiency Virus Type 1 Integration. J Virol 76:10942–10950.
268. Lee GQ, Orlova-Fink N, Einkauf K, Chowdhury FZ, Sun X, Harrington S, Kuo H-HH, Hua S, Chen H-RR, Ouyang Z, Reddy K, Dong K, Ndung'U T, Walker BD, Rosenberg ES, Yu XG, Lichterfeld M, Ndung'u T, Walker BD, Rosenberg ES, Yu XG, Lichterfeld M. 2017. Clonal expansion of genome-intact HIV-1 in functionally polarized Th1 CD4+ T cells. J Clin Invest 127:2689–2696.
269. Symons J, Cameron PU, Lewin SR. 2018. HIV integration sites and implications for maintenance of the reservoir. Curr Opin HIV AIDS 13:152–159.
270. Patro SC, Brandt LD, Bale MJ, Halvas EK, Joseph KW, Shao W, Wu X, Guo S, Murrell B, Wiegand A, Spindler J, Raley C, Hautman C, Sobolewski M, Fennessey CM, Hu WS, Luke B, Hasson JM, Niyongabo A, Capoferri AA, Keele BF, Milush J, Hoh R, Deeks SG, Maldarelli F, Hughes SH, Coffin JM, Rausch JW, Mellors JW, Kearney MF. 2019. Combined HIV-1 sequence and integration site analysis informs viral dynamics and allows reconstruction of replicating viral ancestors. Proc Natl Acad Sci U S A 116:25891–25899.
271. Einkauf KB, Lee GQ, Gao C, Sharaf R, Sun X, Hua S, Chen SMY, Jiang C, Lian X, Chowdhury FZ, Rosenberg ES, Chun TW, Li JZ, Yu XG, Lichterfeld M. 2019. Intact HIV-1 proviruses accumulate at distinct chromosomal positions during prolonged antiretroviral therapy. J Clin Invest 129:988–998.
272. Archin NM, Liberty AL, Kashuba AD, Choudhary SK, Kuruc JD, Crooks AM, Parker DC, Anderson EM, Kearney MF, Strain MC, Richman DD, Hudgens MG, Bosch RJ, Coffin JM, Eron JJ, Hazuda DJ, Margolis DM. 2012. Administration of vorinostat disrupts HIV-1 latency in patients on antiretroviral therapy. Nature 487:482–485.

273. Pasternak AO, Adema KW, Bakker M, Jurriaans S, Berkhout B, Cornelissen M, Lukashov V V. 2008. Highly sensitive methods based on seminested real-time reverse transcription-PCR for quantitation of human immunodeficiency virus type 1 unspliced and multiply spliced RNA and proviral DNA. J Clin Microbiol 46:2206–2211.
274. Plantin J, Massanella M, Chomont N. 2018. Inducible HIV RNA transcription assays to measure HIV persistence: pros and cons of a compromise. Retrovirology 15:1–9.
275. Procopio FA, Fromentin R, Kulpa DA, Brehm JH, Bebin A-G, Strain MC, Richman DD, O'Doherty U, Palmer S, Hecht FM, Hoh R, Barnard RJO, Miller MD, Hazuda DJ, Deeks SG, Sékaly R-P, Chomont N. 2015. A Novel Assay to Measure the Magnitude of the Inducible Viral Reservoir in HIV-infected Individuals. EBioMedicine 2:874–83.
276. Yucha RW, Hobbs KS, Hanhauser E, Hogan LE, Nieves W, Ozen MO, Inci F, York V, Gibson EA, Thanh C, Shafiee H, El Assal R, Kiselinova M, Robles YP, Bae H, Leadabrand KS, Wang SQ, Deeks SG, Kuritzkes DR, Demirci U, Henrich TJ. 2017. High-throughput Characterization of HIV-1 Reservoir Reactivation Using a Single-Cell-in-Droplet PCR Assay. EBioMedicine 20:217–229.
277. Cillo AR, Sobolewski MD, Bosch RJ, Fyne E, Piatak M, Coffin JM, Mellors JW. 2014. Quantification of HIV-1 latency reversal in resting CD4+ T cells from patients on suppressive antiretroviral therapy. Proc Natl Acad Sci U S A 111:7078–7083.
278. Massanella M, Yek C, Lada SM, Nakazawa M, Shefa N, Huang K, Richman DD. 2018. Improved assays to measure and characterize the inducible HIV reservoir. EBioMedicine 36:113–121.
279. Bruner KM, Wang Z, Simonetti FR, Bender AM, Kwon KJ, Sengupta S, Fray EJ, Beg SA, Antar AAR, Jenike KM, Bertagnolli LN, Capoferri AA, Kufera JT, Timmons A, Nobles C, Gregg J, Wada N, Ho Y-CC, Zhang H, Margolick JB, Blankson JN, Deeks SG, Bushman FD, Siliciano JD, Laird GM, Siliciano RF. 2019. A quantitative approach for measuring the reservoir of latent HIV-1 proviruses. Nature2019/02/01. 566:120–125.
280. Gaebler C, Lorenzi JCC, Oliveira TY, Nogueira L, Ramos V, Lu C-L,

Pai JA, Mendoza P, Jankovic M, Caskey M, Nussenzweig MC. 2019. Combination of quadruplex qPCR and next-generation sequencing for qualitative and quantitative analysis of the HIV-1 latent reservoir. J Exp Med 216:2253–2264.

281. Peluso MJ, Bacchetti P, Ritter KD, Beg S, Lai J, Martin JN, Hunt PW, Henrich TJ, Siliciano JD, Siliciano RF, Laird GM, Deeks SG. 2020. Differential decay of intact and defective proviral DNA in HIV-1-infected individuals on suppressive antiretroviral therapy. JCI insight 5:132997.
282. Pollack RA, Jones RB, Pertea M, Bruner KM, Martin AR, Thomas AS, Capoferri AA, Beg SA, Huang SH, Karandish S, Hao H, Halper-Stromberg E, Yong PC, Kovacs C, Benko E, Siliciano RF, Ho YC. 2017. Defective HIV-1 Proviruses Are Expressed and Can Be Recognized by Cytotoxic T Lymphocytes, which Shape the Proviral Landscape. Cell Host Microbe 21:494–506.
283. Imamichi H, Dewar RL, Adelsberger JW, Rehm CA, O'Doherty U, Paxinos EE, Fauci AS, Lane HC, Imamichia H, Dewar RL, Adelsberger JW, Rehm CA, O'doherty U, Paxinos EE, Fauci AS, Lane HC. 2016. Defective HIV-1 proviruses produce novel proteincoding RNA species in HIV-infected patients on combination antiretroviral therapy. Proc Natl Acad Sci 113:8783–8788.
284. Laird GM, Eisele EE, Rabi SA, Lai J, Chioma S, Blankson JN, Siliciano JD, Siliciano RF. 2013. Rapid Quantification of the Latent Reservoir for HIV-1 Using a Viral Outgrowth Assay. PLoS Pathog 9:121–134.
285. Lewin SR, Rasmussen TA. 2020. Kick and kill for HIV latency. Lancet 395:844–846.
286. Knobel H, Domingo P, Suarez-Lozano I, Gutierrez F, Estrada V, Palacios R, Antela A, Blanco J-R, Fulladosa X, Refollo E, VACH Cohort. Rate of cardiovascular, renal and bone disease and their major risks factors in HIV-infected individuals on antiretroviral therapy in Spain. Enfermedades Infecc y Microbiol Clin 37:373–379.
287. Wang G, Zhao N, Berkhout B, Das AT. 2018. CRISPR-Cas based antiviral strategies against HIV-1. Virus Res 244:321–332.

288. Li L, Krymskaya L, Wang J, Henley J, Rao A, Cao L-F, Tran C-A, Torres-Coronado M, Gardner A, Gonzalez N, Kim K, Liu P-Q, Hofer U, Lopez E, Gregory PD, Liu Q, Holmes MC, Cannon PM, Zaia JA, DiGiusto DL. 2013. Genomic Editing of the HIV-1 Coreceptor CCR5 in Adult Hematopoietic Stem and Progenitor Cells Using Zinc Finger Nucleases. Mol Ther 21:1259–1269.
289. Tebas P, Stein D, Tang WW, Frank I, Wang SQ, Lee G, Spratt SK, Surosky RT, Giedlin MA, Nichol G, Holmes MC, Gregory PD, Ando DG, Kalos M, Collman RG, Binder-Scholl G, Plesa G, Hwang W-T, Levine BL, June CH. 2014. Gene Editing of CCR5 in Autologous CD4 T Cells of Persons Infected with HIV. N Engl J Med 370:901–910.
290. Xu L, Wang J, Liu Y, Xie L, Su B, Mou D, Wang L, Liu T, Wang X, Zhang B, Zhao L, Hu L, Ning H, Zhang Y, Deng K, Liu L, Lu X, Zhang T, Xu J, Li C, Wu H, Deng H, Chen H. 2019. CRISPR-Edited Stem Cells in a Patient with HIV and Acute Lymphocytic Leukemia. N Engl J Med 381:1240–1247.
291. Westby M, Lewis M, Whitcomb J, Youle M, Pozniak AL, James IT, Jenkins TM, Perros M, van der Ryst E. 2006. Emergence of CXCR4-using human immunodeficiency virus type 1 (HIV-1) variants in a minority of HIV-1-infected patients following treatment with the CCR5 antagonist maraviroc is from a pretreatment CXCR4-using virus reservoir. J Virol 80:4909–4920.
292. Cillo AR, Mellors JW. 2016. Which therapeutic strategy will achieve a cure for HIV-1? Curr Opin Virol2016/03/18. 18:14–19.
293. Spragg C, De Silva Feelixge H, Jerome KR. 2016. Cell and gene therapy strategies to eradicate HIV reservoirs. Curr Opin HIV AIDS 11:442–449.
294. Mediouni S, Chinthalapudi K, Ekka MK, Usui I, Jablonski JA, Clementz MA, Mousseau G, Nowak J, Macherla VR, Beverage JN, Esquenazi E, Baran P, de Vera IMS, Kojetin D, Loret EP, Nettles K, Maiti S, Izard T, Valente ST. 2019. Didehydro-cortistatin a inhibits HIV-1 by specifically binding to the unstructured basic region of tat. MBio 10:1–19.
295. Mousseau G, Clementz MA, Bakeman WN, Nagarsheth N, Cameron

M, Shi J, Baran P, Fromentin R, Chomont N, Valente ST. 2012. An Analog of the Natural Steroidal Alkaloid Cortistatin A Potently Suppresses Tat-Dependent HIV Transcription. Cell Host Microbe 12:97–108.

296. Mousseau G, Kessing CF, Fromentin R, Trautmann L, Chomont N, Valente ST. 2015. The tat inhibitor didehydro-cortistatin a prevents HIV-1 reactivation from latency. MBio 6:1–12.
297. Kessing CF, Nixon CC, Li C, Tsai P, Takata H, Mousseau G, Ho PT, Honeycutt JB, Fallahi M, Trautmann L, Garcia JV, Valente ST. 2017. In Vivo Suppression of HIV Rebound by Didehydro-Cortistatin A, a "Block-and-Lock" Strategy for HIV-1 Treatment. Cell Rep 21:600–611.
298. Wong RW, Lingwood CA, Ostrowski MA, Cabral T, Cochrane A. 2018. Cardiac glycoside/aglycones inhibit HIV-1 gene expression by a mechanism requiring MEK1/2-ERK1/2 signaling. Sci Rep 8:1–14.
299. Kyei GB, Meng S, Ramani R, Niu A, Lagisetti C, Webb TR, Ratner L. 2018. Splicing factor 3B subunit 1 interacts with HIV tat and plays a role in viral transcription and reactivation from latency. MBio 9:342–353.
300. Cheung PK, Horhant D, Bandy LE, Zamiri M, Rabea SM, Karagiosov SK, Matloobi M, McArthur S, Harrigan PR, Chabot B, Grierson DS. 2016. A Parallel Synthesis Approach to the Identification of Novel Diheteroarylamide-Based Compounds Blocking HIV Replication: Potential Inhibitors of HIV-1 Pre-mRNA Alternative Splicing. J Med Chem 59:1869–1879.
301. Sarracino A, Gharu L, Kula A, Pasternak AO, Avettand-Fenoel V, Rouzioux C, Bardina M, De Wit S, Benkirane M, Berkhout B, Van Lint C, Marcello A. 2018. Posttranscriptional Regulation of HIV-1 Gene Expression during Replication and Reactivation from Latency by Nuclear Matrix Protein MATR3. MBio 9:1–13.
302. Rao S, Amorim R, Niu M, Temzi A, Mouland AJ. 2018. The RNA surveillance proteins UPF1, UPF2 and SMG6 affect HIV-1 reactivation at a post-transcriptional level. Retrovirology 15:1–12.
303. Besnard E, Hakre S, Kampmann M, Lim HW, Hosmane NN, Martin

A, Bassik MC, Verschueren E, Battivelli E, Chan J, Svensson JP, Gramatica A, Conrad RJ, Ott M, Greene WC, Krogan NJ, Siliciano RF, Weissman JS, Verdin E. 2016. The mTOR Complex Controls HIV Latency. Cell Host Microbe 20:785–797.

304. García F, León A, Gatell JM, Plana M, Gallart T. 2012. Therapeutic vaccines against HIV infection. Hum Vaccin Immunother 8:569–81.
305. Excler J-L, Kim JH. 2019. Novel prime-boost vaccine strategies against HIV-1. Expert Rev Vaccines 18:765–779.
306. Jones LD, Moody MA, Thompson AB. 2020. Innovations in HIV-1 Vaccine Design. Clin Ther 42:499–514.
307. Rahman MA, Robert-Guroff M. 2019. Accelerating HIV vaccine development using non-human primate models. Expert Rev Vaccines 18:61–73.
308. Gallinaro A, Borghi M, Pirillo MF, Cecchetti S, Bona R, Canitano A, Michelini Z, Di Virgilio A, Olvera A, Brander C, Negri D, Cara A. 2020. Development and Preclinical Evaluation of an Integrase Defective Lentiviral Vector Vaccine Expressing the HIVACAT T Cell Immunogen in Mice. Mol Ther Methods Clin Dev 17:418–428.
309. Mothe B, Manzardo C, Sanchez-Bernabeu A, Coll P, Morón-López S, Puertas MC, Rosas-Umbert M, Cobarsi P, Escrig R, Perez-Alvarez N, Ruiz I, Rovira C, Meulbroek M, Crook A, Borthwick N, Wee EG, Yang H, Miró JM, Dorrell L, Clotet B, Martinez-Picado J, Brander C, Hanke T. 2019. Therapeutic Vaccination Refocuses T-cell Responses Towards Conserved Regions of HIV-1 in Early Treated Individuals (BCN 01 study). EClinicalMedicine 11:65–80.
310. de Jong W, Aerts J, Allard S, Brander C, Buyze J, Florence E, van Gorp E, Vanham G, Leal L, Mothe B, Thielemans K, Plana M, Garcia F, Gruters R, iHIVARNA consortium. 2019. iHIVARNA phase IIa, a randomized, placebo-controlled, double-blinded trial to evaluate the safety and immunogenicity of iHIVARNA-01 in chronically HIV-infected patients under stable combined antiretroviral therapy. Trials 20:361.
311. Jong W de, Leal L, Buyze J, Pannus P, Guardo A, Salgado M, Mothe B, Molto J, Moron-Lopez S, Gálvez C, Florence E, Vanham G, Gorp

E van, Brander C, Allard S, Thielemans K, Martinez-Picado J, Plana M, García F, Gruters RA. 2019. Therapeutic Vaccine in Chronically HIV-1-Infected Patients: A Randomized, Double-Blind, Placebo-Controlled Phase IIa Trial with HTI-TriMix. Vaccines 7:1–17.

312. Deeks SG. 2012. HIV: Shock and kill. Nature 487:439–440.
313. Kim Y, Anderson JL, Lewin SR. 2018. Getting the “Kill” into “Shock and Kill”: Strategies to Eliminate Latent HIV. Cell Host Microbe 23:14–26.
314. Prins JM, Jurriaans S, van Praag RMEE, Blaak H, van Rij R, Schellekens PTAA, ten Berge IJMM, Yong S-LL, Fox CH, Roos MTLL, de Wolf F, Goudsmit J, Schuitemaker H, Lange JMA. 1999. Immuno-activation with anti-CD3 and recombinant human IL-2 in HIV-1-infected patients on potent antiretroviral therapy. AIDS 13:2405–10.
315. Lehrman G, Hogue IB, Palmer S, Jennings C, Spina CA, Wiegand A, Landay AL, Coombs RW, Richman DD, Mellors JW, Coffin JM, Bosch RJ, Margolis DM. 2005. Depletion of latent HIV-1 infection in vivo: a proof-of-concept study. Lancet (London, England) 366:549–55.
316. Lindkvist A, Edén A, Norström MM, Gonzalez VD, Nilsson S, Svennerholm B, Karlsson AC, Sandberg JK, Sönnerborg A, Gisslén M. 2009. Reduction of the HIV-1 reservoir in resting CD4+ T-lymphocytes by high dosage intravenous immunoglobulin treatment: a proof-of-concept study. AIDS Res Ther 6:15-32 .
317. Scripture-Adams DD, Brooks DG, Korin YD, Zack JA. 2002. Interleukin-7 induces expression of latent human immunodeficiency virus type 1 with minimal effects on T-cell phenotype. J Virol 76:13077–82.
318. van Praag RME, Prins JM, Roos MTL, Schellekens PTA, Ten Berge IJM, Yong S-LL, Schuitemaker H, Eerenberg AJM, Jurriaans S, De Wolf F, Fox CH, Goudsmit J, Miedema F, Lange JM. 2001. OKT3 and IL-2 treatment for purging of the latent HIV-1 reservoir in vivo results in selective long-lasting CD4+ T cell depletion. J Clin Immunol 21:218–26.
319. Kulkosky J, Nunnari G, Otero M, Calarota S, Dornadula G, Zhang H, Malin A, Sullivan J, Xu Y, DeSimone J, Babinchak T, Stern J, Cavert

W, Haase A, Pomerantz RJ. 2002. Intensification and stimulation therapy for human immunodeficiency virus type 1 reservoirs in infected persons receiving virally suppressive highly active antiretroviral therapy. J Infect Dis 186:1403–1411.

320. Spivak AM, Planelles V. 2016. HIV-1 eradication: early trials (and tribulations). Trends Mol Med 22:10–27.
321. Rasmussen TA, Søgaard OS, Brinkmann C, Wightman F, Lewin SR, Melchjorsen J, Dinarello C, Østergaard L, Tolstrup M. 2013. Comparison of HDAC inhibitors in clinical development. Hum Vaccin Immunother 9:993–1001.
322. Wightman F, Ellenberg P, Churchill M, Lewin SR. 2012. HDAC inhibitors in HIV. Immunol Cell Biol 90:47–54.
323. Lim S-Y, Osuna CE, Hraber PT, Hesselgesser J, Gerold JM, Barnes TL, Sanisetty S, Seaman MS, Lewis MG, Geleziunas R, Miller MD, Cihlar T, Lee WA, Hill AL, Whitney JB. 2018. TLR7 agonists induce transient viremia and reduce the viral reservoir in SIV-infected rhesus macaques on antiretroviral therapy. Sci Transl Med 10:4521.
324. Xing S, Bullen CK, Shroff NS, Shan L, Yang H-C, Manucci JL, Bhat S, Zhang H, Margolick JB, Quinn TC, Margolis DM, Siliciano JD, Siliciano RF. 2011. Disulfiram Reactivates Latent HIV-1 in a Bcl-2-Transduced Primary CD4 + T Cell Model without Inducing Global T Cell Activation. J Virol 85:6060–6064.
325. Torchilin VP. 1998. Polymer-coated long-circulating microparticulate pharmaceuticals. J Microencapsul 15:1–19.
326. Elliott JH, McMahon JH, Chang CC, Lee SA, Hartogensis W, Bumpus N, Savic R, Roney J, Hoh R, Solomon A, Piatak M, Gorelick RJ, Lifson J, Bacchetti P, Deeks SG, Lewin SR. 2015. Short-term administration of disulfiram for reversal of latent HIV infection: a phase 2 dose-escalation study. Lancet HIV 2:520–529.
327. Xing S, Siliciano RF. 2013. Targeting HIV latency: pharmacologic strategies toward eradication. Drug Discov Today 18:541–551.
328. Jiang G, Dandekar S. 2015. Targeting NF-κB signaling with protein kinase C agonists as an emerging strategy for combating HIV latency. AIDS Res Hum Retroviruses 31:4–12.

329. Trushin SA, Pennington KN, Carmona EM, Asin S, Savoy DN, Billadeau DD, Paya C V. 2003. Protein kinase Calpha (PKCalpha) acts upstream of PKCtheta to activate IkappaB kinase and NF-kappaB in T lymphocytes. Mol Cell Biol 23:7068–81.
330. Davidson SK, Allen SW, Lim GE, Anderson CM, Haygood MG. 2001. Evidence for the biosynthesis of bryostatins by the bacterial symbiont “Candidatus Endobugula sertula” of the bryozoan Bugula neritina. Appl Environ Microbiol 67:4531–7.
331. Mehla R, Bivalkar-Mehla S, Zhang R, Handy I, Albrecht H, Giri S, Nagarkatti P, Nagarkatti M, Chauhan A. 2010. Bryostatin modulates latent HIV-1 infection via PKC and AMPK signaling but inhibits acute infection in a receptor independent manner. PLoS One 5:11160.
332. Perez M, de Vinuesa A, Sanchez-Duffhues G, Marquez N, Bellido M, Munoz-Fernandez M, Moreno S, Castor T, Calzado M, Munoz E. 2010. Bryostatin-1 Synergizes with Histone Deacetylase Inhibitors to Reactivate HIV-1 from Latency. Curr HIV Res 8:418–429.
333. Díaz L, Martínez-Bonet M, Sánchez J, Fernández-Pineda A, Jiménez JL, Muñoz E, Moreno S, Álvarez S, Muñoz-Fernández MÁMÁ. 2015. Bryostatin activates HIV-1 latent expression in human astrocytes through a PKC and NF-κB-dependent mechanism. Sci Rep 5:12442.
334. Plimack ER, Tan T, Wong Y-NN, von Mehren MM, Malizzia L, Roethke SK, Litwin S, Li T, Hudes GR, Haas NB. 2014. A phase I study of temsirolimus and bryostatin-1 in patients with metastatic renal cell carcinoma and soft tissue sarcoma. Oncologist 19:354–355.
335. Morgan RJ, Leong L, Chow W, Gandara D, Frankel P, Garcia A, Lenz H-J, Doroshow JH. 2012. Phase II trial of bryostatin-1 in combination with cisplatin in patients with recurrent or persistent epithelial ovarian cancer: a California cancer consortium study. Invest New Drugs 30:723–728.
336. Gray LR, On H, Roberts E, Lu HK, Moso MA, Raison JA, Papaioannou C, Cheng W-J, Ellett AM, Jacobson JC, Purcell DFJ, Wesselingh SL, Gorry PR, Lewin SR, Churchill MJ. 2016. Toxicity and in vitro activity of HIV-1 latency-reversing agents in primary CNS cells. J Neurovirol 22:455–463.

337. Clutton G, Xu Y, Baldoni PL, Mollan KR, Kirchherr J, Newhard W, Cox K, Kuruc JD, Kashuba A, Barnard R, Archin N, Gay CL, Hudgens MG, Margolis DM, Goonetilleke N. 2016. The differential short- and long-term effects of HIV-1 latency-reversing agents on T cell function. Sci Rep 6:30749.
338. Laird GM, Bullen CK, Rosenbloom DISS, Martin AR, Hill AL, Durand CM, Siliciano JD, Siliciano RF. 2015. Ex vivo analysis identifies effective HIV-1 latency–reversing drug combinations. J Clin Invest 125:1901–1912.
339. Williams SA, Chen L-F, Kwon H, Fenard D, Bisgrove D, Verdin E, Greene WC. 2004. Prostratin antagonizes HIV latency by activating NF-kappaB. J Biol Chem 279:42008–17.
340. Kulkosky J, Culnan DM, Roman J, Dornadula G, Schnell M, Boyd MR, Pomerantz RJ. 2001. Prostratin: activation of latent HIV-1 expression suggests a potential inductive adjuvant therapy for HAART. Blood 98:3006–15.
341. Biancotto A, Grivel J-C, Gondois-Rey F, Bettendroffer L, Vigne R, Brown S, Margolis LB, Hirsch I. 2004. Dual role of prostratin in inhibition of infection and reactivation of human immunodeficiency virus from latency in primary blood lymphocytes and lymphoid tissue. J Virol 78:10507–15.
342. Wang P, Lu P, Qu X, Shen Y, Zeng H, Zhu X, Zhu Y, Li X, Wu H, Xu J. 2017. Reactivation of HIV-1 from latency by an ingenol derivative from Euphorbia kansui. Sci Rep 7:9451.
343. Clutton G, Xu Y, Baldoni PL, Mollan KR, Kirchherr J, Newhard W, Cox K, Kuruc JD, Kashuba A, Barnard R. 2016. Corrigendum: The differential short-and long-term effects of HIV-1 latency-reversing agents on T cell function. Sci Rep 6:34430.
344. Jiang G, Mendes EA, Kaiser P, Wong DP, Tang Y, Cai I, Fenton A, Melcher GP, Hildreth JEKK, Thompson GR, Wong JK, Dandekar S. 2015. Synergistic Reactivation of Latent HIV Expression by Ingenol-3-Angelate, PEP005, Targeted NF-kB Signaling in Combination with JQ1 Induced p-TEFb Activation. PLoS Pathog 11:55-66.
345. Treatment C for SA. 2009. Incorporating Alcohol Pharmacotherapies

Into Medical Practice. Chapter 3—Disulfiram. Treatment Improvement Protocol (TIP) Series.

346. Spivak AM, Andrade A, Eisele E, Hoh R, Bacchetti P, Bumpus NN, Emad F, Buckheit R, McCance-Katz EF, Lai J, Kennedy M, Chander G, Siliciano RF, Siliciano JD, Deeks SG. 2014. A Pilot Study Assessing the Safety and Latency-Reversing Activity of Disulfiram in HIV-1-Infected Adults on Antiretroviral Therapy. Clin Infect Dis 58:883–890.
347. Sun SC. 2017. The non-canonical NF-κB pathway in immunity and inflammation. Nat Rev Immunol. Nature Publishing Group.
348. Zarnegar BJ, Wang Y, Mahoney DJ, Dempsey PW, Cheung HH, He J, Shiba T, Yang X, Yeh WC, Mak TW, Korneluk RG, Cheng G. 2008. Noncanonical NF-κB activation requires coordinated assembly of a regulatory complex of the adaptors cIAP1, cIAP2, TRAF2 and TRAF3 and the kinase NIK. Nat Immunol 9:1371–1378.
349. Bobardt M, Kuo J, Chatterji U, Chanda S, Little SJ, Wiedemann N, Vuagniaux G, Gallay PA. 2019. The inhibitor apoptosis protein antagonist Debio 1143 Is an attractive HIV-1 latency reversal candidate. PLoS One 14:1–12.
350. Pache L, Dutra MS, Spivak AM, Marlett JM, Murry JP, Hwang Y, Maestre AM, Manganaro L, Vamos M, Teriete P, Martins LJ, König R, Simon V, Bosque A, Fernandez-Sesma A, Cosford NDP, Bushman FD, Young JAT, Planelles V, Chanda SK. 2015. BIRC2/cIAP1 is a Negative Regulator of HIV-1 Transcription and Can Be Targeted by Smac Mimetics to Promote Reversal of Viral Latency. Cell Host Microbe 18:345–353.
351. Campbell GR, Bruckman RS, Chu YL, Trout RN, Spector SA. 2018. SMAC Mimetics Induce Autophagy-Dependent Apoptosis of HIV-1-Infected Resting Memory CD4+ T Cells. Cell Host Microbe 24:689–702.
352. Hattori SI, Matsuda K, Tsuchiya K, Gatanaga H, Oka S, Yoshimura K, Mitsuya H, Maeda K. 2018. Minimizes secondary HIV-1 Infection in vitro. Front Microbiol 9:2022–2034.
353. Roth SY, Allis CD. 1996. Histone acetylation and chromatin assembly:

a single escort, multiple dances? Cell1996/10/04. 87:5–8.

354. Verdin E, Dequiedt F, Kasler HG. 2003. Class II histone deacetylases: versatile regulators. Trends Genet 19:286–293.
355. Chen HP, Zhao YT, Zhao TC. 2015. Histone Deacetylases and Mechanisms of Regulation of Gene Expression. Crit Rev Oncog 20:35–47.
356. Schemies J, Uciechowska U, Sippl W, Jung M. 2010. NAD + -dependent histone deacetylases (sirtuins) as novel therapeutic targets. Med Res Rev2009/10/14. 30:861–889.
357. Keedy KS, Archin NM, Gates AT, Espeseth A, Hazuda DJ, Margolis DM. 2009. A Limited Group of Class I Histone Deacetylases Acts To Repress Human Immunodeficiency Virus Type 1 Expression. J Virol 83:4749–4756.
358. Ceccacci E, Minucci S. 2016. Inhibition of histone deacetylases in cancer therapy: lessons from leukaemia. Br J Cancer. 114:605–611.
359. Bubna A. 2015. Vorinostat-An overview. Indian J Dermatol 60:419.
360. Mann BS, Johnson JR, Cohen MH, Justice R, Pazdur R. 2007. FDA Approval Summary: Vorinostat for Treatment of Advanced Primary Cutaneous T-Cell Lymphoma. Oncologist 12:1247–1252.
361. Elliott JH, Wightman F, Solomon A, Ghneim K, Ahlers J, Cameron MJ, Smith MZ, Spelman T, McMahon J, Velayudham P, Brown G, Roney J, Watson J, Prince MH, Hoy JF, Chomont N, Fromentin R, Procopio FA, Zeidan J, Palmer S, Odevall L, Johnstone RW, Martin BP, Sinclair E, Deeks SG, Hazuda DJ, Cameron PU, Sékaly R-P, Lewin SR. 2014. Activation of HIV Transcription with Short-Course Vorinostat in HIV-Infected Patients on Suppressive Antiretroviral Therapy. PLoS Pathog 10:44-73.
362. Mota TM, Rasmussen TA, Rhodes A, Tennakoon S, Dantanarayana A, Wightman F, Hagenauer M, Roney J, Spelman T, Purcell DFJJ, McMahon J, Hoy JF, Prince HM, Elliott JH, Lewin SR. 2017. No adverse safety or virological changes 2 years following vorinostat in HIV-infected individuals on antiretroviral therapy. AIDS2017/03/17. 31:1137–1141.
363. Archin NM, Bateson R, Tripathy MK, Crooks AM, Yang K-H, Dahl NP,

Kearney MF, Anderson EM, Coffin JM, Strain MC. 2014. HIV-1 expression within resting CD4+ T cells after multiple doses of vorinostat. J Infect Dis 210:728–735.

364. Pearse BMF. 1976. Clathrin: a unique protein associated with intracellular transfer of membrane by coated vesicles. Proc Natl Acad Sci U S A 73:1255–9.
365. Rasmussen TA, Tolstrup M, Brinkmann CR, Olesen R, Erikstrup C, Solomon A, Winckelmann A, Palmer S, Dinarello C, Buzon M, Lichterfeld M, Lewin SR, Ostergaard L, Sogaard OS. 2014. Panobinostat, a histone deacetylase inhibitor, for latent-virus reactivation in HIV-infected patients on suppressive antiretroviral therapy: a phase 1/2, single group, clinical trial. Lancet HIV 1:13–21.
366. Valdez BC, Brammer JE, Li Y, Murray D, Liu Y, Hosing C, Nieto Y, Champlin RE, Andersson BS. 2015. Romidepsin targets multiple survival signaling pathways in malignant T cells. Blood Cancer J 5:357.
367. Subramanian S, Bates SE, Wright JJ, Espinoza-Delgado I, Piekarz RL. 2010. Clinical Toxicities of Histone Deacetylase Inhibitors. Pharm 3:2751–2767.
368. Grant C, Rahman F, Piekarz R, Peer C, Frye R, Robey RW, Gardner ER, Figg WD, Bates SE. 2010. Romidepsin: a new therapy for cutaneous T-cell lymphoma and a potential therapy for solid tumors. Expert Rev Anticancer Ther 10:997–1008.
369. Wei DG, Chiang V, Fyne E, Balakrishnan M, Barnes T, Graupe M, Hesselgesser J, Irrinki A, Murry JP, Stepan G, Stray KM, Tsai A, Yu H, Spindler J, Kearney M, Spina CA, McMahon D, Lalezari J, Sloan D, Mellors J, Geleziunas R, Cihlar T. 2014. Histone Deacetylase Inhibitor Romidepsin Induces HIV Expression in CD4 T Cells from Patients on Suppressive Antiretroviral Therapy at Concentrations Achieved by Clinical Dosing. PLoS Pathog 10:1004071.
370. Søgaard OS, Graversen ME, Leth S, Olesen R, Brinkmann CR, Nissen SK, Kjaer AS, Schleimann MH, Denton PW, Hey-Cunningham WJ, Koelsch KK, Pantaleo G, Krogsgaard K, Sommerfelt M, Fromentin R, Chomont N, Rasmussen TA, Østergaard L, Tolstrup M.

2015. The Depsipeptide Romidepsin Reverses HIV-1 Latency In Vivo. PLoS Pathog 11:e1005142.

371. McMahon DK, Zheng L, Cyktor JC, Aga E, Macatangay BJ, Godfrey C, Para M, Mitsuyasu RT, Hesselgesser J, Dragavon J, Dobrowolski C, Karn J, Acosta EP, Gandhi RT, Mellors JW. 2021. A Phase 1/2 Randomized, Placebo-Controlled Trial of Romidespin in Persons With HIV-1 on Suppressive Antiretroviral Therapy. J Infect Dis 224:648–656.
372. Winckelmann A, Barton K, Hiener B, Schlub TE, Shao W, Rasmussen TA, Østergaard L, Søgaard OS, Tolstrup M, Palmer S. 2017. Romidepsin-induced HIV-1 viremia during effective antiretroviral therapy contains identical viral sequences with few deleterious mutations. AIDS 31:771–779.
373. Winckelmann A, Morcilla V, Shao W, Schleimann MH, Hojen JF, Schlub TE, Benton PW, Østergaard L, Søgaard OS, Tolstrup M, Palmer S. 2018. Genetic characterization of the HIV-1 reservoir after Vacc-4x and romidepsin therapy in HIV-1-infected individuals. AIDS 32:1793–1802.
374. Walker-Sperling VE, Pohlmeyer CW, Tarwater PM, Blankson JN. 2016. The Effect of Latency Reversal Agents on Primary CD8 + T Cells: Implications for Shock and Kill Strategies for Human Immunodeficiency Virus Eradication. EBioMedicine 8:217–229.
375. Rasmussen TA, Lewin SR. 2016. Shocking HIV out of hiding: where are we with clinical trials of latency reversing agents? Curr Opin HIV AIDS2016/03/15. 11:394–401.
376. Jones RB, O'Connor R, Mueller S, Foley M, Szeto GL, Karel D, Lichterfeld M, Kovacs C, Ostrowski MA, Trocha A, Irvine DJ, Walker BD, O'Connor R, Mueller S, Foley M, Szeto GL, Karel D, Lichterfeld M, Kovacs C, Ostrowski MA, Trocha A, Irvine DJ, Walker BD, O'Connor R, Mueller S, Foley M, Szeto GL, Karel D, Lichterfeld M, Kovacs C, Ostrowski MA, Trocha A. 2014. Histone deacetylase inhibitors impair the elimination of hiv-infected cells by cytotoxic t-lymphocytes. PLoS Pathog2008/02/12. 10:e1004287.
377. Reardon B, Beliakova-Bethell N, Spina CA, Singhania A, Margolis

DM, Richman DR, Woelk CH. 2015. Dose-responsive gene expression in suberoylanilide hydroxamic acid-treated resting CD4+ T cells. AIDS2015/08/11. 29:2235–2244.

378. Olesen R, Vigano S, Rasmussen TA, Sogaard OS, Ouyang Z, Buzon M, Bashirova A, Carrington M, Palmer S, Brinkmann CR, Yu XG, Ostergaard L, Tolstrup M, Lichterfeld M, Søgaard OS, Ouyang Z, Buzon M, Bashirova A, Carrington M, Palmer S, Brinkmann CR. 2015. Innate immune activity correlates with CD4 T cell-associated HIV-1 DNA decline during latency-reversing treatment with panobinostat. J Virol2015/08/01. 89:10176–10189.
379. ElKassar N, Gress RE. 2010. An overview of IL-7 biology and its use in immunotherapy. J Immunotoxicol 7:1–7.
380. Levy Y, Lacabaratz C, Weiss L, Viard J-P, Goujard C, Lelièvre J-D, Boué F, Molina J-M, Rouzioux C, Avettand-Fénoêl V. 2009. Enhanced T cell recovery in HIV-1–infected adults through IL-7 treatment. J Clin Invest 119:997–1007.
381. Wang F-X, Xu Y, Sullivan J, Souder E, Argyris EG, Acheampong EA, Fisher J, Sierra M, Thomson MM, Najera R. 2005. IL-7 is a potent and proviral strain–specific inducer of latent HIV-1 cellular reservoirs of infected individuals on virally suppressive HAART. J Clin Invest 115:128–137.
382. Vandergeeten C, Fromentin R, DaFonseca S, Lawani MB, Sereti I, Lederman MM, Ramgopal M, Routy J-P, Sékaly R-P, Chomont N. 2013. Interleukin-7 promotes HIV persistence during antiretroviral therapy. Blood 121:4321–4329.
383. Bosque A, Famiglietti M, Weyrich AS, Goulston C, Planelles V. 2011. Homeostatic proliferation fails to efficiently reactivate HIV-1 latently infected central memory CD4+ T cells. PLoS Pathog 7:112–126.
384. Jones RB, Mueller S, O'Connor R, Rimpel K, Sloan DD, Karel D, Wong HC, Jeng EK, Thomas AS, Whitney JB, Lim SY, Kovacs C, Benko E, Karandish S, Huang SH, Buzon MJ, Lichterfeld M, Irrinki A, Murry JP, Tsai A, Yu H, Geleziunas R, Trocha A, Ostrowski MA, Irvine DJ, Walker BD. 2016. A Subset of Latency-Reversing Agents Expose HIV-Infected Resting CD4+T-Cells to Recognition by Cytotoxic T-

Lymphocytes. PLoS Pathog 12:e1005545.

385. Huang SH, Ren Y, Thomas AS, Chan D, Mueller S, Ward AR, Patel S, Bollard CM, Cruz CR, Karandish S, Truong R, Macedo AB, Bosque A, Kovacs C, Benko E, Piechocka-Trocha A, Wong H, Jeng E, Nixon DF, Ho YC, Siliciano RF, Walker BD, Brad Jones R. 2018. Latent HIV reservoirs exhibit inherent resistance to elimination by CD8+ t cells. J Clin Invest 128:876–889.
386. Kawai T, Akira S. 2008. Toll-like receptor and RIG-I-like receptor signaling. Ann N Y Acad Sci 1143:1–20.
387. Akira S, Uematsu S, Takeuchi O. 2006. Pathogen recognition and innate immunity. Cell 124:783–801.
388. Komai-Koma M, Jones L, Ogg GS, Xu D, Liew FY. 2004. TLR2 is expressed on activated T cells as a costimulatory receptor. Proc Natl Acad Sci U S A 101:3029–3034.
389. Kawai T, Akira S. 2010. The role of pattern-recognition receptors in innate immunity: update on Toll-like receptors. Nat Immunol 11:373–84.
390. Hornef MW, Henriques-Normark B, Normark S. 2008. The function and biological role of toll-like receptors in infectious diseases: an update. Curr Opin Infect Dis 21:304–12.
391. Alvarez-Carbonell D, Garcia-Mesa Y, Milne S, Das B, Dobrowolski C, Rojas R, Karn J. 2017. Toll-like receptor 3 activation selectively reverses HIV latency in microglial cells. Retrovirology 14:9–15.
392. Novis CL, Archin NM, Buzon MJ, Verdin E, Round JL, Lichterfeld M, Margolis DM, Planelles V, Bosque A. 2013. Reactivation of latent HIV-1 in central memory CD4+T cells through TLR-1/2 stimulation. Retrovirology2013/10/26. 10:119.
393. Tsai A, Irrinki A, Kaur J, Cihlar T, Kukolj G, Sloan DD, Murry JP. 2017. Toll-Like Receptor 7 Agonist GS-9620 Induces HIV Expression and HIV-Specific Immunity in Cells from HIV-Infected Individuals on Suppressive Antiretroviral Therapy. J Virol 91:1–14.
394. Del Prete GQ, Alvord WG, Li Y, Deleage C, Nag M, Oswald K, Thomas JA, Pyle C, Bosche WJ, Coalter V, Wiles A, Wiles R, Berkemeier B, Hull M, Chipriano E, Silipino L, Fast R, Kiser J, Kiser

R, Malys T, Kramer J, Breed MW, Trubey CM, Estes JD, Barnes TL, Hesselgesser J, Geleziunas R, Lifson JD. 2019. TLR7 agonist administration to SIV-infected macaques receiving early initiated cART does not induce plasma viremia. JCI insight 4:1–16.

395. Bekerman E, Hesselgesser J, Carr B, Nagel M, Hung M, Wang A, Stapleton L, von Gegerfelt A, Elyard HA, Lifson JD, Geleziunas R. 2019. PD-1 Blockade and TLR7 Activation Lack Therapeutic Benefit in Chronic Simian Immunodeficiency Virus-Infected Macaques on Antiretroviral Therapy. Antimicrob Agents Chemother 63:4–21.
396. Borducchi EN, Cabral C, Stephenson KE, Liu J, Abbink P, Ng'ang'a D, Nkolola JP, Brinkman AL, Peter L, Lee BC, Jimenez J, Jetton D, Mondesir J, Mojta S, Chandrashekar A, Molloy K, Alter G, Gerold JM, Hill AL, Lewis MG, Pau MG, Schuitemaker H, Hesselgesser J, Geleziunas R, Kim JH, Robb ML, Michael NL, Barouch DH, Ng'ang'a D, Nkolola JP, Brinkman AL, Peter L, Lee BC, Jimenez J, Jetton D, Mondesir J, Mojta S, Chandrashekar A, Molloy K, Alter G, Gerold JM, Hill AL, Lewis MG, Pau MG, Schuitemaker H, Hesselgesser J, Geleziunas R, Kim JH, Robb ML, Michael NL, Barouch DH. 2016. Ad26/MVA therapeutic vaccination with TLR7 stimulation in SIV-infected rhesus monkeys. Nature 540:284–287.
397. Borducchi EN, Liu J, Nkolola JP, Cadena AM, Yu W-H, Fischinger S, Broge T, Abbink P, Mercado NB, Chandrashekar A, Jetton D, Peter L, McMahan K, Moseley ET, Bekerman E, Hesselgesser J, Li W, Lewis MG, Alter G, Geleziunas R, Barouch DH. 2018. Publisher Correction: Antibody and TLR7 agonist delay viral rebound in SHIV-infected monkeys. Nature 564:8–22.
398. Bricker KM, Obregon-Perko V, Uddin F, Williams B, Uffman EA, Garrido C, Fouda GG, Geleziunas R, Robb M, Michael N, Barouch DH, Chahroudi A. 2020. Therapeutic vaccination of SIV-infected, ART-treated infant rhesus macaques using Ad48/MVA in combination with TLR-7 stimulation. PLoS Pathog 16:1008954.
399. Riddler SA, Para M, Benson CA, Mills A, Ramgopal M, DeJesus E, Brinson C, Cyktor J, Jacobs J, Koontz D, Mellors JW, Laird GM, Wrin T, Patel H, Guo S, Wallin J, Boice J, Zhang L, Humeniuk R, Begley

R, German P, Graham H, Geleziunas R, Brainard DM, SenGupta D. 2021. Vesatolimod, a Toll-like Receptor 7 Agonist, Induces Immune Activation in Virally Suppressed Adults Living With Human Immunodeficiency Virus-1. Clin Infect Dis 72:815–824.

400. Offersen R, Nissen SK, Rasmussen TA, Østergaard L, Denton PW, Søgaard OS, Tolstrup M. 2016. A Novel Toll-Like Receptor 9 Agonist, MGN1703, Enhances HIV-1 Transcription and NK Cell-Mediated Inhibition of HIV-1-Infected Autologous CD4 + T Cells. J Virol 90:4441–4453.
401. Vibholm LK, Konrad C V., Schleimann MH, Frattari G, Winckelmann A, Klastrup V, Jensen NM, Jensen SS, Schmidt M, Wittig B, Zuwala K, Mack K, Olesen R, Hua S, Lichterfeld M, Østergaard L, Denton PW, Tolstrup M, Søgaard OS. 2019. Effects of 24-week Toll-like receptor 9 agonist treatment in HIV type 1+ individuals. AIDS 33:1315–1325.
402. Barik S. 2016. What Really Rigs Up RIG-I? J Innate Immun 8:429–36.
403. Garcia-Vidal E, Castellví M, Pujantell M, Badia R, Jou A, Gomez L, Puig T, Clotet B, Ballana E, Riveira-Muñoz E, Esté JA. 2017. Evaluation of the Innate Immune Modulator Acitretin as a Strategy To Clear the HIV Reservoir. Antimicrob Agents Chemother 61:e01368-17.
404. Palermo E, Acchioni C, Di Carlo D, Zevini A, Muscolini M, Ferrari M, Castiello L, Virtuoso S, Borsetti A, Antonelli G, Turriziani O, Sgarbanti M, Hiscott J. 2019. Activation of Latent HIV-1 T Cell Reservoirs with a Combination of Innate Immune and Epigenetic Regulators. J Virol 93:1194–1213.
405. Sarabia I, Novis CL, Macedo AB, Takata H, Nell R, Kakazu JC, Furler RL, Shakya B, Schubert HL, Hill CP, DePaula-Silva AB, Spivak AM, Trautmann L, Planelles V, Bosque A. 2021. Activation of the Anti-Oxidative Stress Response Reactivates Latent HIV-1 Through the Mitochondrial Antiviral Signaling Protein Isoform MiniMAVS. Front Immunol 12:1–14.
406. Bullen CK, Laird GM, Durand CM, Siliciano JD, Siliciano RF. 2014.

New ex vivo approaches distinguish effective and ineffective single agents for reversing HIV-1 latency in vivo. Nat Med2014/03/25. 20:425–429.

407. Postow MA, Callahan MK, Wolchok JD. 2015. Immune Checkpoint Blockade in Cancer Therapy. J Clin Oncol 33:1974–1982.
408. Waldman AD, Fritz JM, Lenardo MJ. 2020. A guide to cancer immunotherapy: from T cell basic science to clinical practice. Nat Rev Immunol 20:651–668.
409. Jahangirian H, Kalantari K, Izadiyan Z, Rafiee-Moghaddam R, Shameli K, Webster TJ. 2019. A review of small molecules and drug delivery applications using gold and iron nanoparticles. Int J Nanomedicine Volume 14:1633–1657.
410. Chauhan G, Madou MJ, Kalra S, Chopra V, Ghosh D, Martinez-Chapa SO. 2020. Nanotechnology for COVID-19: Therapeutics and Vaccine Research. ACS Nano 14:7760–7782.
411. Kalaydina R-V, Bajwa K, Qorri B, DeCarlo A, Szewczuk MR. 2018. Recent advances in “smart” delivery systems for extended drug release in cancer therapy. Int J Nanomedicine 13:4727–4745.
412. Park JH, Jiang Y, Zhou J, Gong H, Mohapatra A, Heo J, Gao W, Fang RH, Zhang L. 2021. Genetically engineered cell membrane-coated nanoparticles for targeted delivery of dexamethasone to inflamed lungs. Sci Adv 7:7820–7836.
413. Ma W, Zhu D, Li J, Chen X, Xie W, Jiang X, Wu L, Wang G, Xiao Y, Liu Z, Wang F, Li A, Shao D, Dong W, Liu W, Yuan Y. 2020. Coating biomimetic nanoparticles with chimeric antigen receptor T cell-membrane provides high specificity for hepatocellular carcinoma photothermal therapy treatment. Theranostics 10:1281–1295.
414. Mandal S, Sunagawa SW, Prathipati PK, Belshan M, Shibata A, Destache CJ. 2020. Targeted immuno-antiretroviral HIV therapeutic approach to provide dual protection and boosts cellular immunity: A proof-of-concept study. bioRxiv 121:34–46.
415. Polack FP, Thomas SJ, Kitchin N, Absalon J, Gurtman A, Lockhart S, Perez JL, Pérez Marc G, Moreira ED, Zerbini C, Bailey R, Swanson KA, Roychoudhury S, Koury K, Li P, Kalina W V., Cooper D, Frenck

RW, Hammitt LL, Türeci Ö, Nell H, Schaefer A, Ünal S, Tresnan DB, Mather S, Dormitzer PR, Şahin U, Jansen KU, Gruber WC. 2020. Safety and Efficacy of the BNT162b2 mRNA Covid-19 Vaccine. N Engl J Med 383:2603–2615.

416. Cevaal PM, Ali A, Czuba-Wojnilowicz E, Symons J, Lewin SR, Cortez-Jugo C, Caruso F. 2021. In Vivo T Cell-Targeting Nanoparticle Drug Delivery Systems: Considerations for Rational Design. ACS Nano 15:3736–3753.
417. Bowen A, Sweeney EE, Fernandes R. 2020. Nanoparticle-Based Immunoengineered Approaches for Combating HIV. Front Immunol 11:1–9.
418. Wojnilowicz M, Besford QA, Wu Y-L, Loh XJ, Braunger JA, Glab A, Cortez-Jugo C, Caruso F, Cavalieri F. 2018. Glycogen-nucleic acid constructs for gene silencing in multicellular tumor spheroids. Biomaterials 176:34–49.
419. Mitchell MJ, Billingsley MM, Haley RM, Wechsler ME, Peppas NA, Langer R. 2021. Engineering precision nanoparticles for drug delivery. Nat Rev Drug Discov 20:101–124.
420. van Vlerken LE, Amiji MM. 2006. Multi-functional polymeric nanoparticles for tumour-targeted drug delivery. Expert Opin Drug Deliv2006/03/02. 3:205–216.
421. Rizvi SAA, Saleh AM. 2018. Applications of nanoparticle systems in drug delivery technology. Saudi Pharm J. Elsevier B.V.
422. Zuhorn IS, Kalicharan R, Hoekstra D. 2002. Lipoplex-mediated Transfection of Mammalian Cells Occurs through the Cholesterol-dependent Clathrin-mediated Pathway of Endocytosis. J Biol Chem2002/03/05. 277:18021–18028.
423. Doherty GJ, McMahon HT. 2009. Mechanisms of endocytosis. Annu Rev Biochem2009/03/26. 78:857–902.
424. Sahay G, Alakhova DY, Kabanov A V. 2010. Endocytosis of nanomedicines. J Control release 145:182–195.
425. Nel AE, Mädler L, Velegol D, Xia T, Hoek EM V, Somasundaran P, Klaessig F, Castranova V, Thompson M. 2009. Understanding biophysicochemical interactions at the nano–bio interface. Nat Mater

8:543.

426. Bhavsar MD, Tiwari SB, Amiji MM. 2006. Formulation optimization for the nanoparticles-in-microsphere hybrid oral delivery system using factorial design. J Control Release2005/12/13. 110:422–430.
427. Lammers T, Hennink WE, Storm G. 2008. Tumour-targeted nanomedicines: principles and practice. Br J Cancer 99:392.
428. Detering L, Abdilla A, Luehmann HP, Williams JW, Huang LH, Sultan D, Elvington A, Heo GS, Woodard PK, Gropler RJ, Randolph GJ, Hawker CJ, Liu Y. 2021. CC Chemokine Receptor 5 Targeted Nanoparticles Imaging the Progression and Regression of Atherosclerosis Using Positron Emission Tomography/Computed Tomography. Mol Pharm 18:1386–1396.
429. Umotoy JC, de Taeye SW. 2021. Antibody Conjugates for Targeted Therapy Against HIV-1 as an Emerging Tool for HIV-1 Cure. Front Immunol. Frontiers.
430. Kumar B V., Connors TJ, Farber DL. 2018. Human T Cell Development, Localization, and Function throughout Life. Immunity 48:202–213.
431. Terwilliger T, Abdul-Hay M. 2017. Acute lymphoblastic leukemia: a comprehensive review and 2017 update. Blood Cancer J 7:577–589.
432. Varghese MT, Alsubait S. 2021. T-Cell LymphomaStatPearls. StatPearls Publishing.
433. Hirons A, Khoury G, Purcell DFJ. 2021. Human T-cell lymphotropic virus type-1: a lifelong persistent infection, yet never truly silent. Lancet Infect Dis 21:2–10.
434. Zhao M, De Crignis E, Rokx C, Verbon A, van Gelder T, Mahmoudi T, Katsikis PD, Mueller YM. 2019. T cell toxicity of HIV latency reversing agents. Pharmacol Res2018/10/27. 139:524–534.
435. Alberts B, Johnson A, Lewis J, Raff M, Roberts K, And Walter P. 2007. Molecular Biology of the CellAmino Acids. New York.
436. Khor SY, Vu MN, Pilkington EH, Johnston APR, Whittaker MR, Quinn JF, Truong NP, Davis TP. 2018. Elucidating the Influences of Size, Surface Chemistry, and Dynamic Flow on Cellular Association of Nanoparticles Made by Polymerization-Induced Self-Assembly. Small

14:1801702.

437. Mann SK, Czuba E, Selby LI, Such GK, Johnston APR. 2016. Quantifying Nanoparticle Internalization Using a High Throughput Internalization Assay. Pharm Res 33:2421–2432.
438. McMahon HT, Boucrot E. 2011. Molecular mechanism and physiological functions of clathrin-mediated endocytosis. Nat Rev Mol Cell Biol 12:517–533.
439. Lim JP, Gleeson PA. 2011. Macropinocytosis: An endocytic pathway for internalising large gulps. Immunol Cell Biol. Immunol Cell Biol.
440. Hillaireau H, Couvreur P. 2009. Nanocarriers' entry into the cell: relevance to drug delivery. Cell Mol Life Sci 66:2873–96.
441. Rejman J, Oberle V, Zuhorn IS, Hoekstra D. 2004. Size-dependent internalization of particles via the pathways of clathrin- and caveolae-mediated endocytosis. Biochem J2003/09/25. 377:159–69.
442. Cureton DK, Massol RH, Saffarian S, Kirchhausen TL, Whelan SPJ. 2009. Vesicular stomatitis virus enters cells through vesicles incompletely coated with clathrin that depend upon actin for internalization. PLoS Pathog2009/04/25. 5:394–412.
443. Marsh M, McMahon HT. 1999. The structural era of endocytosis. Science 285:215–20.
444. Crowther RA, Pearse BM. 1981. Assembly and packing of clathrin into coats. J Cell Biol1981/12/01. 91:790–797.
445. Villanueva-Flores F, Castro-Lugo A, Ramírez OT, Palomares LA. 2020. Understanding cellular interactions with nanomaterials: towards a rational design of medical nanodevices. Nanotechnology 31:132–156.
446. He C, Hu Y, Yin L, Tang C, Yin C. 2010. Effects of particle size and surface charge on cellular uptake and biodistribution of polymeric nanoparticles. Biomaterials 31:3657–3666.
447. Progatzky F, Dallman MJ, Lo Celso C. 2013. From seeing to believing: labelling strategies for in vivo cell-tracking experiments. Interface Focus 3:20130001.
448. Fromen CA, Rahhal TB, Robbins GR, Kai MP, Shen TW, Luft JC, DeSimone JM. 2016. Nanoparticle surface charge impacts

distribution, uptake and lymph node trafficking by pulmonary antigen-presenting cells. Nanomedicine2015/12/15. 12:677–687.

449. Glass JJ, Chen L, Alcantara S, Crampin EJ, Thurecht KJ, De Rose R, Kent SJ. 2017. Charge Has a Marked Influence on Hyperbranched Polymer Nanoparticle Association in Whole Human Blood. ACS Macro Lett 6:586–592.
450. Tenzer S, Docter D, Kuharev J, Musyanovych A, Fetz V, Hecht R, Schlenk F, Fischer D, Kiouptsi K, Reinhardt C, Landfester K, Schild H, Maskos M, Knauer SK, Stauber RH. 2013. Rapid formation of plasma protein corona critically affects nanoparticle pathophysiology. Nat Nanotechnol 8:772–781.
451. Chakraborty D, Ethiraj KR, Mukherjee A. 2020. Understanding the relevance of protein corona in nanoparticle-based therapeutics and diagnostics. RSC Adv 10:27161–27172.
452. Prabhakar U, Maeda H, Jain RK, Sevick-Muraca EM, Zamboni W, Farokhzad OC, Barry ST, Gabizon A, Grodzinski P, Blakey DC. 2013. Challenges and key considerations of the enhanced permeability and retention effect for nanomedicine drug delivery in oncology. Cancer Res 73:2412–7.
453. Ju Y, Kelly HG, Dagley LF, Reynaldi A, Schlub TE, Spall SK, Bell CA, Cui J, Mitchell AJ, Lin Z, Wheatley AK, Thurecht KJ, Davenport MP, Webb AI, Caruso F, Kent SJ. 2020. Person-Specific Biomolecular Coronas Modulate Nanoparticle Interactions with Immune Cells in Human Blood. ACS Nano 14:15723–15737.
454. Danhier F, Ansorena E, Silva JM, Coco R, Le Breton A, Préat V. 2012. PLGA-based nanoparticles: An overview of biomedical applications. J Control Release 161:505–522.
455. Kovochich M, Marsden MD, Zack JA. 2011. Activation of latent HIV using drug-loaded nanoparticles. PLoS One 6:212–232.
456. Ramishetti S, Kedmi R, Goldsmith M, Leonard F, Sprague AG, Godin B, Gozin M, Cullis PR, Dykxhoorn DM, Peer D. 2015. Systemic Gene Silencing in Primary T Lymphocytes Using Targeted Lipid Nanoparticles. ACS Nano 9:6706–6716.
457. Jones RB, Mueller S, Kumari S, Vrbanac V, Genel S, Tager AM, Allen

TM, Walker BD, Irvine DJ. 2017. Antigen recognition-triggered drug delivery mediated by nanocapsule-functionalized cytotoxic T-cells. Biomaterials2016/12/10. 117:44–53.

458. Cao S, Slack SD, Levy CN, Hughes SM, Jiang Y, Yogodzinski C, Roychoudhury P, Jerome KR, Schiffer JT, Hladik F, Woodrow KA. 2019. Hybrid nanocarriers incorporating mechanistically distinct drugs for lymphatic CD4 + T cell activation and HIV-1 latency reversal. Sci Adv2019/04/05. 5:1–16.
459. Edagwa B, McMillan J, Sillman B, Gendelman HE. 2017. Long-acting slow effective release antiretroviral therapy. Expert Opin Drug Deliv 14:1281–1291.
460. Guo D, Zhou T, Araínga M, Palandri D, Gautam N, Bronich T, Alnouti Y, McMillan J, Edagwa B, Gendelman HE. 2017. Creation of a Long-Acting Nanoformulated 2′,3′-Dideoxy-3′-Thiacytidine. JAIDS J Acquir Immune Defic Syndr 74:75-e83.
461. Kumar P, Lakshmi YS, Kondapi AK. 2017. Triple Drug Combination of Zidovudine, Efavirenz and Lamivudine Loaded Lactoferrin Nanoparticles: an Effective Nano First-Line Regimen for HIV Therapy. Pharm Res 34:257–268.
462. Wei X, Zhang G, Ran D, Krishnan N, Fang RH, Gao W, Spector SA, Zhang L. 2018. T-Cell-Mimicking Nanoparticles Can Neutralize HIV Infectivity. Adv Mater 30:1802233.
463. Tang X, Liang Y, Liu X, Zhou S, Liu L, Zhang F, Xie C, Cai S, Wei J, Zhu Y, Hou W. 2015. PLGA-PEG Nanoparticles Coated with Anti-CD45RO and Loaded with HDAC Plus Protease Inhibitors Activate Latent HIV and Inhibit Viral Spread. Nanoscale Res Lett 10:413.
464. Freeling JP, Koehn J, Shu C, Sun J, Ho RJY. 2014. Long-acting three-drug combination anti-HIV nanoparticles enhance drug exposure in primate plasma and cells within lymph nodes and blood. AIDS 28:2625–2627.
465. Battivelli E, Dahabieh MS, Abdel-Mohsen M, Svensson JP, Tojal Da Silva I, Cohn LB, Gramatica A, Deeks S, Greene WC, Pillai SK, Verdin E. 2018. Distinct chromatin functional states correlate with HIV latency reactivation in infected primary CD4+ T cells. Elife 7:1–14.

466. Shahbazi R, Sghia-Hughes G, Reid JL, Kubek S, Haworth KG, Humbert O, Kiem H-P, Adair JE. 2019. Targeted homology-directed repair in blood stem and progenitor cells with CRISPR nanoformulations. Nat Mater 18:1124–1132.
467. Jayant RD, Atluri VSR, Agudelo M, Sagar V, Kaushik A, Nair M. 2015. Sustained-release nanoART formulation for the treatment of neuroAIDS. Int J Nanomedicine 10:1077–93.
468. Anselmo AC, Mitragotri | Samir, Mitragotri S, Paulson JA. 2019. Nanoparticles in the clinic: An update. Bioeng Transl Med 4:11–23.
469. Idrees H, Zaidi SZJ, Sabir A, Khan RU, Zhang X, Hassan SU. 2020. A Review of Biodegradable Natural Polymer-Based Nanoparticles for Drug Delivery Applications. Nanomaterials 10:1–22.
470. Zheng M, Pan M, Zhang W, Lin H, Wu S, Lu C, Tang S, Liu D, Cai J. 2021. Poly(α-l-lysine)-based nanomaterials for versatile biomedical applications: Current advances and perspectives. Bioact Mater 6:1878–1909.
471. Tong R, Gabrielson NP, Fan TM, Cheng J. 2012. Polymeric Nanomedicines Based on Poly(lactide) and Poly(lactide-co-glycolide). Curr Opin Solid State Mater Sci 16:323–332.
472. Chen M, Yin M. 2014. Design and development of fluorescent nanostructures for bioimaging. Prog Polym Sci 39:365–395.
473. Baba M, Matsumoto Y, Kashio A, Cabral H, Nishiyama N, Kataoka K, Yamasoba T. 2012. Micellization of cisplatin (NC-6004) reduces its ototoxicity in guinea pigs. J Control Release 157:112–117.
474. Zielińska A, Carreiró F, Oliveira AM, Neves A, Pires B, Venkatesh DN, Durazzo A, Lucarini M, Eder P, Silva AM, Santini A, Souto EB. 2020. Polymeric Nanoparticles: Production, Characterization, Toxicology and Ecotoxicology. Molecules 25:3731–3746.
475. Cheng CJ, Tietjen GT, Saucier-Sawyer JK, Saltzman WM. 2015. A holistic approach to targeting disease with polymeric nanoparticles. Nat Rev Drug Discov 2015 144 14:239–247.
476. Li B, Li Q, Mo J, Dai H. 2017. Drug-loaded polymeric nanoparticles for cancer stem cell targeting. Front Pharmacol 8:23–51.
477. Gagliardi A, Giuliano E, Venkateswararao E, Fresta M, Bulotta S,

Awasthi V, Cosco D. 2021. Biodegradable Polymeric Nanoparticles for Drug Delivery to Solid Tumors. Front Pharmacol. Frontiers Media S.A.

478. Dinu MV, Dragan ES. 2010. Evaluation of Cu2+, Co2+ and Ni2+ ions removal from aqueous solution using a novel chitosan/clinoptilolite composite: Kinetics and isotherms. Chem Eng J 160:157–163.
479. Qi X, Wei W, Li J, Zuo G, Pan X, Su T, Zhang J, Dong W. 2017. Salecan-Based pH-Sensitive Hydrogels for Insulin Delivery. Mol Pharm 14:431–440.
480. Qi X, Wei W, Li J, Liu Y, Hu X, Zhang J, Bi L, Dong W. 2015. Fabrication and Characterization of a Novel Anticancer Drug Delivery System: Salecan/Poly(methacrylic acid) Semi-interpenetrating Polymer Network Hydrogel. ACS Biomater Sci Eng 1:1287–1299.
481. Prajapati SK, Jain A, Jain A, Jain S. 2019. Biodegradable polymers and constructs: A novel approach in drug delivery. Eur Polym J. Pergamon.
482. Filippov SK, Sedlacek O, Bogomolova A, Vetrik M, Jirak D, Kovar J, Kucka J, Bals S, Turner S, Stepanek P, Hruby M. 2012. Glycogen as a Biodegradable Construction Nanomaterial for in vivo Use. Macromol Biosci 12:1731–1738.
483. Gálisová A, Jirátová M, Rabyk M, Sticová E, Hájek M, Hrubý M, Jirák D. 2020. Glycogen as an advantageous polymer carrier in cancer theranostics: Straightforward in vivo evidence. Sci Reports 2020 101 10:1–11.
484. Okishima A, Koide H, Hoshino Y, Egami H, Hamashima Y, Oku N, Asai T. 2019. Design of Synthetic Polymer Nanoparticles Specifically Capturing Indole, a Small Toxic Molecule. Biomacromolecules 20:1644–1654.
485. Decher G, Hong J -D. 1991. Buildup of ultrathin multilayer films by a self-assembly process, 1 consecutive adsorption of anionic and cationic bipolar amphiphiles on charged surfaces. Makromol Chemie Macromol Symp 46:321–327.
486. Caruso F, Caruso RA, Möhwald H. 1998. Nanoengineering of inorganic and hybrid hollow spheres by colloidal templating. Science

(80-) 282:1111–1114.

487. Zelikin AN, Quinn JF, Caruso F. 2006. Disulfide cross-linked polymer capsules: en route to biodeconstructible systems. Biomacromolecules2006/01/10. 7:27–30.
488. Richardson JJ, Cui J, Björnmalm M, Braunger JA, Ejima H, Caruso F. 2016. Innovation in Layer-by-Layer Assembly. Chem Rev 116:14828–14867.
489. Becker AL, Zelikin AN, Johnston APR, Caruso F. 2009. Tuning the formation and degradation of layer-by-layer assembled polymer hydrogel microcapsules. Langmuir 25:14079–14085.
490. Zelikin AN, Li Q, Caruso F. 2008. Disulfide-stabilized poly(methacrylic acid) capsules: Formation, cross-linking, and degradation behavior. Chem Mater 20:2655–2661.
491. Cui J, Yan Y, Wang Y, Caruso F. 2012. Templated Assembly of pH-Labile Polymer-Drug Particles for Intracellular Drug Delivery. Adv Funct Mater 22:4718–4723.
492. Wang Y, Yan Y, Cui J, Hosta-Rigau L, Heath JK, Nice EC, Caruso F. 2010. Encapsulation of water-insoluble drugs in polymer capsules prepared using mesoporous silica templates for intracellular drug delivery. Adv Mater2010/06/22. 22:4293–4297.
493. de Planque MRRR, Aghdaei S, Roose T, Morgan H. 2011. Electrophysiological characterization of membrane disruption by nanoparticles. ACS Nano2018/09/08. 5:3599–606.
494. Yano K, Fukushima Y. 2003. Particle size control of mono-dispersed super-microporous silica spheres. J Mater Chem 13:2577–2581.
495. Yamada Y, Yano K. 2006. Synthesis of monodispersed super-microporous/mesoporous silica spheres with diameters in the low submicron range. Microporous Mesoporous Mater 93:190–198.
496. Cortez C, Tomaskovic-Crook E, Johnston APR, Scott AM, Nice EC, Heath JK, Caruso F. 2007. Influence of Size, Surface, Cell Line, and Kinetic Properties on the Specific Binding of A33 Antigen-Targeted Multilayered Particles and Capsules to Colorectal Cancer Cells. ACS Nano 1:93–102.
497. Besford QA, Cavalieri F, Caruso F. 2020. Glycogen as a Building

Block for Advanced Biological Materials. Adv Mater 32:1904625.

498. Yang L, Liu Z, Gong H, Zeng R, Liang X, Zhang L-M, Lan Y. 2015. Efficient delivery of NF-κB siRNA to human retinal pigment epithelial cells with hyperbranched cationic polysaccharide derivative-based nanoparticles. Int J Nanomedicine 10:2735.
499. Ahmed M, Lai BFL, Kizhakkedathu JN, Narain R. 2012. Hyperbranched Glycopolymers for Blood Biocompatibility. Bioconjug Chem 23:1050–1058.
500. Selby LI, Cortez-Jugo CM, Such GK, Johnston APR. 2017. Nanoescapology: progress toward understanding the endosomal escape of polymeric nanoparticlesWiley Interdisciplinary Reviews: Nanomedicine and Nanobiotechnology. Wiley Interdiscip Rev Nanomed Nanobiotechnol.
501. Kim HJ, Kim A, Miyata K, Kataoka K. 2016. Recent progress in development of siRNA delivery vehicles for cancer therapy. Adv Drug Deliv Rev 104:61–77.
502. Ma Y, Bjornmalm M, Wise AK, Cortez-Jugo C, Revalor E, Ju Y, Feeney OM, Richardson RT, Hanssen E, Shepherd RK, Porter CJHH, Caruso F, Björnmalm M, Wise AK, Cortez-Jugo C, Revalor E, Ju Y, Feeney OM, Richardson RT, Hanssen E, Shepherd RK, Porter CJHH, Caruso F. 2018. Gel-Mediated Electrospray Assembly of Silica Supraparticles for Sustained Drug Delivery. ACS Appl Mater Interfaces2018/09/08. 10:31019–31031.
503. Cui J, Alt K, Ju Y, Gunawan ST, Braunger JA, Wang T-YY, Dai Y, Dai Q, Richardson JJ, Guo J, Björnmalm M, Hagemeyer CE, Caruso F. 2019. Ligand-Functionalized Poly(ethylene glycol) Particles for Tumor Targeting and Intracellular Uptake. Biomacromolecules 20:3592–3600.
504. Wang J-G, Zhou H-J, Sun P-C, Ding D-T, Chen T-H. 2010. Hollow Carved Single-Crystal Mesoporous Silica Templated by Mesomorphous Polyelectrolyte−Surfactant Complexes. Chem Mater 22:3829–3831.
505. Zhang K, Xu L-L, Jiang J-G, Calin N, Lam K-F, Zhang S-J, Wu H-H, Wu G-D, Albela B, Bonneviot L, Wu P. 2013. Facile Large-Scale

Synthesis of Monodisperse Mesoporous Silica Nanospheres with Tunable Pore Structure. J Am Chem Soc 135:2427–2430.

506. Schustak J, Twarog M, Wu X, Wu HY, Huang Q, Bao Y. 2021. Mechanism of Nucleic Acid Sensing in Retinal Pigment Epithelium (RPE): RIG-I Mediates Type I Interferon Response in Human RPE. J Immunol Res 2021:1–14.
507. Tsuchiya S, Yamabe M, Yamaguchi Y, Kobayashi Y, Konno T, Tada K. 1980. Establishment and characterization of a human acute monocytic leukemia cell line (THP-1). Int J Cancer 26:171–176.
508. Weiss A, Stobo JD, A Weiss, R L Wiskocil JDS. 2015. The role of T3 surface molecules in the activation of human T cells: a two-stimulus requirement for IL 2 production reflects events occurring at a pre-translational level - PubMed. Front Immunol 6:72–84.
509. Copy TD. 2007. Item Details 59–73.
510. Derdeyn CA, Decker JM, Sfakianos JN, Wu X, O'Brien WA, Ratner L, Kappes JC, Shaw GM, Hunter E. 2000. Sensitivity of human immunodeficiency virus type 1 to the fusion inhibitor T-20 is modulated by coreceptor specificity defined by the V3 loop of gp120. J Virol 74:8358–67.
511. Schreiber G. 2017. The molecular basis for differential type I interferon signaling. J Biol Chem 292:7285–7294.
512. Abràmoff MD, Magalhães PJ, Ram SJ. 2004. Image Processing with ImageJ Second EditionBiophotonics International. Laurin Publishing.
513. De Rose R, Zelikin AN, Johnston APRR, Sexton A, Chong SF, Cortez C, Mulholland W, Caruso F, Kent SJ. 2008. Binding, internalization, and antigen presentation of vaccine-loaded nanoengineered capsules in blood. Adv Mater 20:4698–4703.
514. Nelson TJ, Sen A, Alkon DL, Sun M-K. 2014. Adduct formation in liquid chromatography-triple quadrupole mass spectrometric measurement of bryostatin 1. J Chromatogr B2013/12/03. 944:55–62.
515. Chassaing C, Marshall JL, Wainer IW. 1998. Determination of the antitumor agent depsipeptide in plasma by liquid chromatography on serial octadecyl stationary phases. J Chromatogr B Biomed Sci Appl 719:169–176.

516. Goldeck M, Schlee M, Hartmann G, Hornung V. 2014. Enzymatic synthesis and purification of a defined RIG-I ligand. Methods Mol Biol 1169:15–25.
517. Anand G, Perry AM, Cummings CL, St. Raymond E, Clemens RA, Steed AL. 2021. Surface Proteins of SARS-CoV-2 Drive Airway Epithelial Cells to Induce IFN-Dependent Inflammation. J Immunol 206:3000–3009.
518. Rebendenne A, Chaves Valadão AL, Tauziet M, Maarifi G, Bonaventure B, McKellar J, Planès R, Nisole S, Arnaud-Arnould M, Moncorgé O, Goujon C. 2021. SARS-CoV-2 Triggers an MDA-5-Dependent Interferon Response Which Is Unable To Control Replication in Lung Epithelial Cells. J Virol 95:1–13.
519. Hirn S, Semmler-Behnke M, Schleh C, Wenk A, Lipka J, Schäffler M, Takenaka S, Möller W, Schmid G, Simon U, Kreyling WG. 2011. Particle size-dependent and surface charge-dependent biodistribution of gold nanoparticles after intravenous administration. Eur J Pharm Biopharm 77:407–416.
520. Furtado D, Björnmalm M, Ayton S, Bush AI, Kempe K, Caruso F. 2018. Overcoming the Blood–Brain Barrier: The Role of Nanomaterials in Treating Neurological Diseases. Adv Mater 30:1801362.
521. Gheibi Hayat SM, Bianconi V, Pirro M, Sahebkar A. 2019. Stealth functionalization of biomaterials and nanoparticles by CD47 mimicry. Int J Pharm 569:118628.
522. Ivask A, Mitchell AJ, Hope CM, Barry SC, Lombi E, Voelcker NH. 2017. Single Cell Level Quantification of Nanoparticle–Cell Interactions Using Mass Cytometry. Anal Chem2017/07/12. 89:8228–8232.
523. Elsaesser A, Taylor A, de Yanés GS, McKerr G, Kim E-M, O'Hare E, Howard CV. 2010. Quantification of nanoparticle uptake by cells using microscopical and analytical techniques. Nanomedicine 5:1447–1457.
524. Ivask A, Mitchell AJ, Malysheva A, Voelcker NH, Lombi E. 2018. Methodologies and approaches for the analysis of cell–nanoparticle

interactions. Wiley Interdiscip Rev Nanomedicine Nanobiotechnology. Wiley-Blackwell.

525. Görgens A, Bremer M, Ferrer-Tur R, Murke F, Tertel T, Horn PA, Thalmann S, Welsh JA, Probst C, Guerin C, Boulanger CM, Jones JC, Hanenberg H, Erdbrügger U, Lannigan J, Ricklefs FL, El-Andaloussi S, Giebel B. 2019. Optimisation of imaging flow cytometry for the analysis of single extracellular vesicles by using fluorescence-tagged vesicles as biological reference material. J Extracell Vesicles 8:1587567.
526. Glass JJ, Yuen D, Rae J, Johnston APRR, Parton RG, Kent SJ, De Rose R. 2016. Human immune cell targeting of protein nanoparticles–caveospheres. Nanoscale2016/04/01. 8:8255–8265.
527. Wei X, Zheng D-H, Cai Y, Jiang R, Chen M-L, Yang T, Xu Z-R, Yu Y-L, Wang J-H. 2018. High-Throughput/High-Precision Sampling of Single Cells into ICP-MS for Elucidating Cellular Nanoparticles. Anal Chem 90:14543–14550.
528. Yang Y-SS, Atukorale PU, Moynihan KD, Bekdemir A, Rakhra K, Tang L, Stellacci F, Irvine DJ. 2017. High-throughput quantitation of inorganic nanoparticle biodistribution at the single-cell level using mass cytometry. Nat Commun2017/01/18. 8:14069.
529. Gottstein C, Wu G, Wong BJ, Zasadzinski JA. 2013. Precise quantification of nanoparticle internalization. ACS Nano 7:4933–4945.
530. Zucker RM, Massaro EJ, Sanders KM, Degn LL, Boyes WK. 2010. Detection of TiO2 nanoparticles in cells by flow cytometry. Cytometry A 77:677–85.
531. Muraca F, Alahmari A, Giannone VA, Adumeau L, Yan Y, McCafferty MM, Dawson KA. 2019. A Three-Dimensional Cell Culture Platform for Long Time-Scale Observations of Bio-Nano Interactions. ACS Nano 13:13524–13536.
532. Akinc A, Battaglia G. 2013. Exploiting Endocytosis for Nanomedicines. Cold Spring Harb Perspect Biol 5:16980–16980.
533. Zhang S, Li J, Lykotrafitis G, Bao G, Suresh S. 2009. Size-Dependent Endocytosis of Nanoparticles. Adv Mater 21:419–424.

534. Shang L, Nienhaus K, Nienhaus GU. 2014. Engineered nanoparticles interacting with cells: size matters. J Nanobiotechnology 12:5.
535. Severino P, da Silva CF, Andrade LN, de Lima Oliveira D, Campos J, Souto EB. 2019. Alginate Nanoparticles for Drug Delivery and Targeting. Curr Pharm Des 25:1312–1334.
536. Albanese A, Tang PS, Chan WCW. 2012. The Effect of Nanoparticle Size, Shape, and Surface Chemistry on Biological Systems. Annu Rev Biomed Eng 14:1–16.
537. Clausen J, Vergeiner B, Enk M, Petzer AL, Gastl G, Gunsilius E. 2003. Functional significance of the activation-associated receptors CD25 and CD69 on human NK-cells and NK-like T-cells. Immunobiology 207:85–93.
538. Radulovic K, Rossini V, Manta C, Holzmann K, Kestler HA, Niess JH. 2013. The Early Activation Marker CD69 Regulates the Expression of Chemokines and CD4 T Cell Accumulation in Intestine. PLoS One 8:65413.
539. Ng WF, Duggan PJ, Ponchel F, Matarese G, Lombardi G, Edwards AD, Isaacs JD, Lechler RI. 2001. Human CD4+CD25+ cells: a naturally occurring population of regulatory T cells. Blood 98:2736–2744.
540. D'Souza WN, Lefrançois L. 2003. IL-2 Is Not Required for the Initiation of CD8 T Cell Cycling but Sustains Expansion. J Immunol 171:5727–5735.
541. Lee E, Bacchetti P, Milush J, Shao W, Boritz E, Douek D, Fromentin R, Liegler T, Hoh R, Deeks SG, Hecht FM, Chomont N, Palmer S. 2019. Memory CD4 + T-Cells Expressing HLA-DR Contribute to HIV Persistence During Prolonged Antiretroviral Therapy. Front Microbiol 10:2214.
542. Peterlin BM. 1991. Transcriptional regulation of HLA-DRA gene. Res Immunol 142:393–399.
543. Fytianos K, Drasler B, Blank F, von Garnier C, Seydoux E, Rodriguez-Lorenzo L, Petri-Fink A, Rothen-Rutishauser B. 2016. Current in vitro approaches to assess nanoparticle interactions with lung cells. Nanomedicine 11:2457–2469.

544. La-Beck NM, Gabizon AA. 2017. Nanoparticle Interactions with the Immune System: Clinical Implications for Liposome-Based Cancer Chemotherapy. Front Immunol 8:416.
545. Zupke O, Distler E, Jürchott A, Paiphansiri U, Dass M, Thomas S, Hartwig UF, Theobald M, Landfester K, Mailänder V, Herr W. 2015. Nanoparticles and antigen-specific T-cell therapeutics: a comprehensive study on uptake and release. Nanomedicine 10:1063–1076.
546. Boraschi D, Duschl A. 2014. Nanoparticles and the Immune SystemNanoparticles and the Immune System: Safety and Effects. Elsevier.
547. Fytianos K, Rodriguez-Lorenzo L, Clift MJD, Blank F, Vanhecke D, von Garnier C, Petri-Fink A, Rothen-Rutishauser B. 2015. Uptake efficiency of surface modified gold nanoparticles does not correlate with functional changes and cytokine secretion in human dendritic cells in vitro. Nanomedicine Nanotechnology, Biol Med 11:633–644.
548. Blank F, Gerber P, Rothen-Rutishauser B, Sakulkhu U, Salaklang J, De Peyer K, Gehr P, Nicod LP, Hofmann H, Geiser T, Petri-Fink A, Von Garnier C. 2011. Biomedical nanoparticles modulate specific CD4 + T cell stimulation by inhibition of antigen processing in dendritic cells. Nanotoxicology 5:606–621.
549. Villiers CL, Freitas H, Couderc R, Villiers M-B, Marche PN. 2010. Analysis of the toxicity of gold nano particles on the immune system: effect on dendritic cell functions. J Nanoparticle Res 12:55–60.
550. Ma B, Zhuang W, Wang Y, Luo R, Wang Y. 2018. pH-sensitive doxorubicin-conjugated prodrug micelles with charge-conversion for cancer therapy. Acta Biomater 70:186–196.
551. Alberg I, Kramer S, Schinnerer M, Hu Q, Seidl C, Leps C, Drude N, Möckel D, Rijcken C, Lammers T, Diken M, Maskos M, Morsbach S, Landfester K, Tenzer S, Barz M, Zentel R. 2020. Polymeric Nanoparticles with Neglectable Protein Corona. Small 16:1–14.
552. Gelderman KA, Hultqvist M, Holmberg J, Olofsson P, Holmdahl R. 2006. T cell surface redox levels determine T cell reactivity and arthritis susceptibility. Proc Natl Acad Sci 103:12831–12836.

553. Sahaf B, Heydari K, Herzenberg LA, Herzenberg LA. 2003. Lymphocyte surface thiol levels. Proc Natl Acad Sci 100:4001–4005.
554. Matthias LJ, Yam PTW, Jiang XM, Vandegraaff N, Li P, Poumbourios P, Donoghue N, Hogg PJ. 2002. Disulfide exchange in domain 2 of CD4 is required for entry of HIV-I. Nat Immunol 3:727–732.
555. Abegg D, Gasparini G, Hoch DG, Shuster A, Bartolami E, Matile S, Adibekian A. 2017. Strained cyclic disulfides enable cellular uptake by reacting with the transferrin receptor. J Am Chem Soc 139:231–238.
556. Chuard N, Gasparini G, Moreau D, Lörcher S, Palivan C, Meier W, Sakai N, Matile S. 2017. Strain-Promoted Thiol-Mediated Cellular Uptake of Giant Substrates: Liposomes and Polymersomes. Angew Chemie Int Ed 56:2947–2950.
557. Mosquera J, García I, Liz-Marzán LM. 2018. Cellular Uptake of Nanoparticles versus Small Molecules: A Matter of Size. Acc Chem Res 51:2305–2313.
558. Bayer AL, Baliga P, Woodward JE. 1998. Transferrin receptor in T cell activation and transplantation. J Leukoc Biol 64:19–24.
559. Batista A, Millán J, Mittelbrunn M, Sánchez-Madrid F, Alonso MA. 2004. Recruitment of Transferrin Receptor to Immunological Synapse in Response to TCR Engagement. J Immunol 172:6709–6714.
560. Cano E, Pizarro A, Redondo JM, Sánchez-Madrid F, Bernabeu C, Fresno M. 1990. Induction of T cell activation by monoclonal antibodies specific for the transferrin receptor. Eur J Immunol 20:765–770.
561. Rausch K, Reuter A, Fischer K, Schmidt M. 2010. Evaluation of nanoparticle aggregation in human blood serum. Biomacromolecules 11:2836–9.
562. Cui J, De Rose R, Alt K, Alcantara S, Paterson BM, Liang K, Hu M, Richardson JJ, Yan Y, Jeffery CM, Price RI, Peter K, Hagemeyer CE, Donnelly PS, Kent SJ, Caruso F. 2015. Engineering Poly(ethylene glycol) Particles for Improved Biodistribution. ACS Nano 9:1571–1580.
563. Weiss ACG, Kelly HG, Faria M, Besford QA, Wheatley AK, Ang C-S,

Crampin EJ, Caruso F, Kent SJ. 2019. Link between Low-Fouling and Stealth: A Whole Blood Biomolecular Corona and Cellular Association Analysis on Nanoengineered Particles. ACS Nano 13:4980–4991.

564. Dai Q, Walkey C, Chan WCW. 2014. Polyethylene glycol backfilling mitigates the negative impact of the protein corona on nanoparticle cell targeting. Angew Chem Int Ed Engl 53:5093–6.
565. Bobo D, Robinson KJ, Islam J, Thurecht KJ, Corrie SR. 2016. Nanoparticle-Based Medicines: A Review of FDA-Approved Materials and Clinical Trials to DatePharmaceutical Research.
566. Suk JS, Xu Q, Kim N, Hanes J, Ensign LM. 2016. PEGylation as a strategy for improving nanoparticle-based drug and gene deliveryAdvanced Drug Delivery Reviews. Elsevier.
567. Baker DP, Lin EY, Lin K, Pellegrini M, Petter RC, Chen LL, Arduini RM, Brickelmaier M, Wen D, Hess DM, Chen L, Grant D, Whitty A, Gill A, Lindner DJ, Pepinsky RB. 2006. N-Terminally PEGylated Human Interferon-β-1a with Improved Pharmacokinetic Properties and in Vivo Efficacy in a Melanoma Angiogenesis Model §. Bioconjug Chem 17:179–188.
568. Truong NP, Zhang C, Nguyen TAH, Anastasaki A, Schulze MW, Quinn JF, Whittaker AK, Hawker CJ, Whittaker MR, Davis TP. 2018. Overcoming Surfactant-Induced Morphology Instability of Noncrosslinked Diblock Copolymer Nano-Objects Obtained by RAFT Emulsion Polymerization. ACS Macro Lett 7:159–165.
569. Verma A, Stellacci F. 2010. Effect of surface properties on nanoparticle-cell interactions. Small. John Wiley & Sons, Ltd.
570. Hoshyar N, Gray S, Han H, Bao G. 2016. The effect of nanoparticle size on in vivo pharmacokinetics and cellular interaction. Nanomedicine 11:673–692.
571. Li SD, Huang L. 2010. Stealth nanoparticles: High density but sheddable PEG is a key for tumor targeting. J Control Release. NIH Public Access.
572. Salmaso S, Caliceti P. 2013. Stealth Properties to Improve Therapeutic Efficacy of Drug Nanocarriers. J Drug Deliv 2013:1–19.
573. Khutoryanskiy V V. 2018. Beyond PEGylation: Alternative surface-

modification of nanoparticles with mucus-inert biomaterials. Adv Drug Deliv Rev 124:140–149.

574. Huckaby JT, Lai SK. 2018. PEGylation for enhancing nanoparticle diffusion in mucus. Adv Drug Deliv Rev 124:125–139.
575. Photos PJ, Bacakova L, Discher B, Bates FS, Discher DE. 2003. Polymer vesicles in vivo: correlations with PEG molecular weight. J Control Release 90:323–34.
576. Hoang Thi TT, Pilkington EH, Nguyen DH, Lee JS, Park KD, Truong NP. 2020. The Importance of Poly(ethylene glycol) Alternatives for Overcoming PEG Immunogenicity in Drug Delivery and Bioconjugation. Polymers (Basel) 12:298.
577. Garbuzenko O, Barenholz Y, Priev A. 2005. Effect of grafted PEG on liposome size and on compressibility and packing of lipid bilayer. Chem Phys Lipids 135:117–129.
578. Nag O, Awasthi V. 2013. Surface Engineering of Liposomes for Stealth Behavior. Pharmaceutics 5:542–569.
579. McSweeney MD, Price LSL, Wessler T, Ciociola EC, Herity LB, Piscitelli JA, DeWalle AC, Harris TN, Chan AKP, Saw RS, Hu P, Jennette JC, Forest MG, Cao Y, Montgomery SA, Zamboni WC, Lai SK. 2019. Overcoming anti-PEG antibody mediated accelerated blood clearance of PEGylated liposomes by pre-infusion with high molecular weight free PEG. J Control Release 311–312:138–146.
580. Veronese FM, Mero A. 2008. The Impact of PEGylation on Biological Therapies. BioDrugs 22:315–329.
581. Sebak AA. 2018. Limitations of pegylated nanocarriers: Unfavourable physicochemical properties, biodistribution patterns and cellular and subcellular fates. Int J Appl Pharm. Innovare Academics Sciences Pvt. Ltd.
582. Estapé Senti M, de Jongh CA, Dijkxhoorn K, Verhoef JJF, Szebeni J, Storm G, Hack CE, Schiffelers RM, Fens MH, Boross P. 2022. Anti-PEG antibodies compromise the integrity of PEGylated lipid-based nanoparticles via complement. J Control Release 341:475–486.
583. Sayes CM, Gobin AM, Ausman KD, Mendez J, West JL, Colvin VL. 2005. Nano-C60 cytotoxicity is due to lipid peroxidation.

Biomaterials2005/07/12. 26:7587–7595.

584. Hirano S, Kanno S, Furuyama A. 2008. Multi-walled carbon nanotubes injure the plasma membrane of macrophages. Toxicol Appl Pharmacol2008/07/29. 232:244–251.

585. Li S-Q, Zhu R-R, Zhu H, Xue M, Sun X-Y, Yao S-D, Wang S-L. 2008. Nanotoxicity of TiO(2) nanoparticles to erythrocyte in vitro. Food Chem Toxicol2008/10/09. 46:3626–31.

586. Wightman F, Solomon A, Khoury G, Green JA, Gray L, Gorry PR, Ho YS, Saksena NK, Hoy J, Crowe SM, Cameron PU, Lewin SR. 2010. Both CD31(+) and CD31$^-$ naive CD4(+) T cells are persistent HIV type 1-infected reservoirs in individuals receiving antiretroviral therapy. J Infect Dis2010/10/29. 202:1738–48.

587. Zerbato JM, Purves H V, Lewin SR, Rasmussen TA. 2019. Between a shock and a hard place: challenges and developments in HIV latency reversal. Curr Opin Virol2019/05/03. 38:1–9.

588. Deng K, Pertea M, Rongvaux A, Wang L, Durand CM, Ghiaur G, Lai J, McHugh HL, Hao H, Zhang H, Margolick JB, Gurer C, Murphy AJ, Valenzuela DM, Yancopoulos GD, Deeks SG, Strowig T, Kumar P, Siliciano JD, Salzberg SL, Flavell RA, Shan L, Siliciano RF. 2015. Broad CTL response is required to clear latent HIV-1 due to dominance of escape mutations. Nature 517:381–385.

589. Pitman MC, Lau JSY, McMahon JH, Lewin SR. 2018. Barriers and strategies to achieve a cure for HIV. Lancet HIV 5:317–328.

590. Cummins NW, Badley AD. 2010. Mechanisms of HIV-associated lymphocyte apoptosis: 2010. Cell Death Dis 1:1–13.

591. Cummins NW, Sainski-Nguyen AM, Natesampillai S, Aboulnasr F, Kaufmann S, Badley AD. 2017. Maintenance of the HIV Reservoir Is Antagonized by Selective BCL2 Inhibition. J Virol 91.

592. Schwartz C, Bouchat S, Marban C, Gautier V, Van Lint C, Rohr O, Le Douce V. 2017. On the way to find a cure: Purging latent HIV-1 reservoirs. Biochem Pharmacol 146:10–22.

593. Jain S, Zain J, Jain S, Zain J. 2011. Romidepsin in the treatment of cutaneous T-cell lymphoma. J Blood Med 2:37–47.

594. Woo S, Gardner ER, Chen X, Ockers SB, Baum CE, Sissung TM,

Price DK, Frye R, Piekarz RL, Bates SE, Figg WD. 2009. Population pharmacokinetics of romidepsin in patients with cutaneous T-cell lymphoma and relapsed peripheral T-cell lymphoma. Clin Cancer Res 15:1496–503.

595. Yurek-George A, Cecil ARL, Mo AHK, Wen S, Rogers H, Habens F, Maeda S, Yoshida M, Packham G, Ganesan A. 2007. The First Biologically Active Synthetic Analogues of FK228, the Depsipeptide Histone Deacetylase Inhibitor. J Med Chem 50:5720–5726.
596. Cao S, Woodrow KA. 2019. Nanotechnology approaches to eradicating HIV reservoirs. Eur J Pharm Biopharm 138:48–63.
597. Cirelli KM, Carnathan DG, Nogal B, Martin JT, Rodriguez OL, Upadhyay AA, Enemuo CA, Gebru EH, Choe Y, Viviano F, Nakao C, Pauthner MG, Reiss S, Cottrell CA, Smith ML, Bastidas R, Gibson W, Wolabaugh AN, Melo MB, Cossette B, Kumar V, Patel NB, Tokatlian T, Menis S, Kulp DW, Burton DR, Murrell B, Schief WR, Bosinger SE, Ward AB, Watson CT, Silvestri G, Irvine DJ, Crotty S. 2019. Slow Delivery Immunization Enhances HIV Neutralizing Antibody and Germinal Center Responses via Modulation of Immunodominance. Cell2019/05/14. 177:1153-1171 e28.
598. Tian X, Angioletti-Uberti S, Battaglia G. 2020. On the design of precision nanomedicines. Sci Adv 6:919.
599. Tu B, Zhang M, Liu T, Huang Y. 2020. Nanotechnology-Based Histone Deacetylase Inhibitors for Cancer Therapy. Front Cell Dev Biol. Frontiers Media S.A.
600. Kuai Q, Wang Y, Gao F, Qi Y, Wang R, Wang Y, Lu X, Zhao Y, Nie G, He M, Zhou H, Jiang X, Ren S, Yu Q. 2019. Peptide Self-Assembly Nanoparticles Loaded with Panobinostat to Activate Latent Human Immunodeficiency Virus. J Biomed Nanotechnol 15:979–992.
601. Denis I, Bahhaj F el, Collette F, Delatouche R, Gueugnon F, Pouliquen D, Pichavant L, Héroguez V, Grégoire M, Bertrand P, Blanquart C. 2014. Vorinostat–Polymer Conjugate Nanoparticles for Acid-Responsive Delivery and Passive Tumor Targeting. Biomacromolecules 15:4534–4543.
602. Chandler WL, Yeung W, Tait JF. 2011. A new microparticle size

calibration standard for use in measuring smaller microparticles using a new flow cytometer. J Thromb Haemost2011/04/13. 9:1216–24.

603. Erdbrügger U, Rudy CK, E. Etter M, Dryden KA, Yeager M, Klibanov AL, Lannigan J, Erdbrugger U, Rudy CK, Etter ME, Dryden KA, Yeager M, Klibanov AL, Lannigan J. 2014. Imaging flow cytometry elucidates limitations of microparticle analysis by conventional flow cytometry. Cytom A2014/06/07. 85:756–770.
604. Botha J, Pugsley HR, Handberg A. 2021. Conventional, High-Resolution and Imaging Flow Cytometry: Benchmarking Performance in Characterisation of Extracellular Vesicles. Biomedicines 9:1–24.
605. Gratton SEA, Ropp PA, Pohlhaus PD, Luft JC, Madden VJ, Napier ME, DeSimone JM. 2008. The effect of particle design on cellular internalization pathways. Proc Natl Acad Sci U S A 105:11613–8.
606. Conde J, Dias JT, GrazÃº V, Moros M, Baptista P V., de la Fuente JM. 2014. Revisiting 30 years of biofunctionalization and surface chemistry of inorganic nanoparticles for nanomedicine. Front Chem 2:48.
607. Sexton A, Whitney PG, Chong S-F, Zelikin AN, Johnston APR, De Rose R, Brooks AG, Caruso F, Kent SJ. 2009. A Protective Vaccine Delivery System for In Vivo T Cell Stimulation Using Nanoengineered Polymer Hydrogel Capsules. ACS Nano 3:3391–3400.
608. Rodríguez R, Rodríguez IR, Sánchez RJ, Pavicic C, Muñoz E, Ángeles M, Fernández M, Relaño-Rodríguez I, Juárez-Sánchez R, Pavicic C, Muñoz E, Muñoz-Fernández MÁ. 2019. Polyanionic carbosilane dendrimers as a new adjuvant in combination with latency reversal agents for HIV treatment. J Nanobiotechnology 17:1–8.
609. Martínez-Bonet M, Clemente MI, Serramía MJ, Muñoz E, Moreno S, Muñoz-Fernández MÁ, Isabel Clemente M, Jesús Serramía M, Muñoz E, Moreno S, Ángeles Muñoz-Fernández M, Martinez-Bonet M, Clemente MI, Serramia MJ, Munoz E, Moreno S, Munoz-Fernandez MA. 2015. Synergistic Activation of Latent HIV-1 Expression by Novel Histone Deacetylase Inhibitors and Bryostatin-1. Sci Rep2015/11/14. 5:16445.
610. Yang H, Wu H, Hancock G, Clutton G, Sande N, Xu X, Yan H, Huang

X, Angus B, Kuldanek K, Fidler S, Denny TN, Birks J, McMichael A, Dorrell L. 2012. Antiviral Inhibitory Capacity of CD8+ T cells Predicts the Rate of CD4+ T-Cell Decline in HIV-1 Infection. J Infect Dis 206:552–561.

611. Rosás-Umbert M, Ruiz-Riol M, Fernández MA, Marszalek M, Coll P, Manzardo C, Cedeño S, Miró JM, Clotet B, Hanke T, Moltó J, Mothe B, Brander C, Ligero C. 2020. In vivo Effects of Romidepsin on T-Cell Activation, Apoptosis and Function in the BCN02 HIV-1 Kick&Kill Clinical Trial. Front Immunol 11:1–11.
612. Moltó J, Rosás-Umbert M, Miranda C, Manzardo C, Puertas MC, Ruiz-Riol M, López M, Miró JM, Martinez-Picado J, Clotet B, Brander C, Mothe B, Valle M. 2021. Pharmacokinetic/pharmacodynamic analysis of romidepsin used as an HIV latency reversing agent. J Antimicrob Chemother 76:1032–1040.
613. Chung C-H, Mele AR, Allen AG, Costello R, Dampier W, Nonnemacher MR, Wigdahl B. 2020. Integrated Human Immunodeficiency Virus Type 1 Sequence in J-Lat 10.6. Microbiol Resour Announc 9.
614. Bieniasz PD, Cullen BR. 2000. Multiple Blocks to Human Immunodeficiency Virus Type 1 Replication in Rodent Cells. J Virol 74:9868–9877.
615. Han S, Tie X, Meng L, Wang Y, Wu A. 2013. PMA and Ionomycin Induce Glioblastoma Cell Death: Activation-Induced Cell-Death-Like Phenomena Occur in Glioma Cells. PLoS One 8:e76717.
616. Lehnert C, Weiswange M, Jeremias I, Bayer C, Grunert M, Debatin K-M, Strauss G. 2014. TRAIL-receptor costimulation inhibits proximal TCR signaling and suppresses human T cell activation and proliferation. J Immunol 193:4021–31.
617. Clutton GT, Jones RB. 2018. Diverse Impacts of HIV Latency-Reversing Agents on CD8+ T-Cell Function: Implications for HIV CureFrontiers in Immunology.
618. Cao S, Jiang Y, Zhang H, Kondza N, Woodrow KA. 2018. Core-shell nanoparticles for targeted and combination antiretroviral activity in gut-homing T cells. Nanomedicine Nanotechnology, Biol

Med2018/07/03. 14:2143–2153.

619. Yan Y, Lai ZW, Goode RJA, Cui J, Bacic T, Kamphuis MMJ, Nice EC, Caruso F. 2013. Particles on the Move: Intracellular Trafficking and Asymmetric Mitotic Partitioning of Nanoporous Polymer Particles. ACS Nano 7:5558–5567.
620. Kleinman AJ, Xu C, Cottrell ML, Sivanandham R, Brocca-Cofano E, Dunsmore T, Kashuba A, Pandrea I, Apetrei C. 2020. Pharmacokinetics and Immunological Effects of Romidepsin in Rhesus Macaques. Front Immunol 11:579158.
621. Zelikin AN, Becker AL, Johnston APR, Wark KL, Turatti F, Caruso F. 2007. A general approach for DNA encapsulation in degradable polymer microcapsules. ACS Nano 1:63–69.
622. Bates SE, Zhan Z, Steadman K, Obrzut T, Luchenko V, Frye R, Robey RW, Turner M, Gardner ER, Figg WD, Steinberg SM, Ling A, Fojo T, To KW, Piekarz RL. 2010. Laboratory correlates for a phase II trial of romidepsin in cutaneous and peripheral T-cell lymphoma. Br J Haematol 148:256–67.
623. Piekarz RL, Robey RW, Zhan Z, Kayastha G, Sayah A, Abdeldaim AH, Torrico S, Bates SE. 2004. T-cell lymphoma as a model for the use of histone deacetylase inhibitors in cancer therapy: impact of depsipeptide on molecular markers, therapeutic targets, and mechanisms of resistance. Blood 103:4636–4643.
624. Pearson RM, Hsu H, Bugno J, Hong S. 2014. Understanding nano-bio interactions to improve nanocarriers for drug delivery. MRS Bull 39:227–237.
625. Dominska M, Dykxhoorn DM. 2010. Breaking down the barriers: siRNA delivery and endosome escape. J Cell Sci 123:1183–1189.
626. Sahay G, Querbes W, Alabi C, Eltoukhy A, Sarkar S, Zurenko C, Karagiannis E, Love K, Chen D, Zoncu R, Buganim Y, Schroeder A, Langer R, Anderson DG. 2013. Efficiency of siRNA delivery by lipid nanoparticles is limited by endocytic recycling. Nat Biotechnol 31:653–658.
627. Yang B, Ming X, Cao C, Laing B, Yuan A, Porter MA, Hull-Ryde EA, Maddry J, Suto M, Janzen WP, Juliano RL. 2015. High-throughput

screening identifies small molecules that enhance the pharmacological effects of oligonucleotides. Nucleic Acids Res 43:1987–1996.

628. Cosenza M, Civallero M, Fiorcari S, Pozzi S, Marcheselli L, Bari A, Ferri P, Sacchi S. 2016. The histone deacetylase inhibitor romidepsin synergizes with lenalidomide and enhances tumor cell death in T-cell lymphoma cell lines. Cancer Biol Ther 17:1094–1106.
629. McDonald AJ, Curt KM, Patel RP, Kozlowski H, Sackett DL, Robey RW, Gottesman MM, Bates SE. 2019. Targeting mitochondrial hexokinases increases efficacy of histone deacetylase inhibitors in solid tumor models. Exp Cell Res 375:106–112.
630. Robers MB, Dart ML, Woodroofe CC, Zimprich CA, Kirkland TA, Machleidt T, Kupcho KR, Levin S, Hartnett JR, Zimmerman K, Niles AL, Ohana RF, Daniels DL, Slater M, Wood MG, Cong M, Cheng Y-Q, Wood K V. 2015. Target engagement and drug residence time can be observed in living cells with BRET. Nat Commun 2015 61 6:1–10.
631. Koblan LW, Buckley DL, Ott CJ, Fitzgerald ME, Ember SWJ, Zhu J-Y, Liu S, Roberts JM, Remillard D, Vittori S, Zhang W, Schonbrunn E, Bradner JE. 2016. Assessment of Bromodomain Target Engagement by a Series of BI2536 Analogues with Miniaturized BET-BRET. ChemMedChem 11:2575–2581.
632. Gallastegui E, Marshall B, Vidal D, Sanchez-Duffhues G, Collado JA, Alvarez-Fernandez C, Luque N, Terme J-M, Gatell JM, Sanchez-Palomino S, Munoz E, Mestres J, Verdin E, Jordan A. 2012. Combination of Biological Screening in a Cellular Model of Viral Latency and Virtual Screening Identifies Novel Compounds That Reactivate HIV-1. J Virol 86:3795–3808.
633. Lusic M, Marcello A, Cereseto A, Giacca M. 2003. Regulation of HIV-1 gene expression by histone acetylation and factor recruitment at the LTR promoter. EMBO J 22:6550–61.
634. Jordan A, Defechereux P, Verdin E. 2001. The site of HIV-1 integration in the human genome determines basal transcriptional activity and response to Tat transactivation. EMBO J 20:1726–38.
635. Verdin E. 1991. DNase I-hypersensitive sites are associated with both

long terminal repeats and with the intragenic enhancer of integrated human immunodeficiency virus type 1. J Virol 65:6790–9.

636. Shukla A, Ramirez N-GP, D'Orso I. 2020. HIV-1 Proviral Transcription and Latency in the New Era. Viruses 12:555.
637. Brady T, Agosto LM, Malani N, Berry CC, O'Doherty U, Bushman F. 2009. HIV integration site distributions in resting and activated CD4 + T cells infected in culture. AIDS 23:1461–1471.
638. Pion M, Jordan A, Biancotto A, Dequiedt F, Gondois-Rey F, Rondeau S, Vigne R, Hejnar J, Verdin E, Hirsch I. 2003. Transcriptional suppression of in vitro-integrated human immunodeficiency virus type 1 does not correlate with proviral DNA methylation. J Virol 77:4025–32.
639. Cummins NW, Sainski AM, Dai H, Natesampillai S, Pang Y-P, Bren GD, de Araujo Correia MCM, Sampath R, Rizza SA, O'Brien D, Yao JD, Kaufmann SH, Badley AD. 2016. Prime, Shock, and Kill: Priming CD4 T Cells from HIV Patients with a BCL-2 Antagonist before HIV Reactivation Reduces HIV Reservoir Size. J Virol 90:4032–4048.
640. Brumme ZL, Chopera DR, Brockman MA. 2012. Modulation of HIV reservoirs by host HLA: Bridging the gap between vaccine and cure. Curr Opin Virol. Curr Opin Virol.
641. Ferrari G, Pollara J, Tomaras GD, Haynes BF. 2017. Humoral and Innate Antiviral Immunity as Tools to Clear Persistent HIV Infection. J Infect Dis 215:152–159.
642. Shan L, Deng K, Shroff NS, Durand CM, Rabi SA, Yang H-C, Zhang H, Margolick JB, Blankson JN, Siliciano RF. 2012. Stimulation of HIV-1-specific cytolytic T lymphocytes facilitates elimination of latent viral reservoir after virus reactivation. Immunity 36:491–501.
643. Badley AD, Sainski A, Wightman F, Lewin SR. 2013. Altering cell death pathways as an approach to cure HIV infection. Cell Death Dis2013/07/13. 4:718–729.
644. Loo Y-M, Gale M. 2011. Immune Signaling by RIG-I-like Receptors. Immunity 34:680–692.
645. Ramos HJ, Gale M. 2011. RIG-I like receptors and their signaling crosstalk in the regulation of antiviral immunity. Curr Opin Virol 1:167–

176.

646. Doehle BP, Hladik F, McNevin JP, McElrath MJ, Gale M. 2009. Human immunodeficiency virus type 1 mediates global disruption of innate antiviral signaling and immune defenses within infected cells. J Virol 83:10395–10405.

647. Goulet M-L, Olagnier D, Xu Z, Paz S, Belgnaoui SM, Lafferty EI, Janelle V, Arguello M, Paquet M, Ghneim K, Richards S, Smith A, Wilkinson P, Cameron M, Kalinke U, Qureshi S, Lamarre A, Haddad EK, Sekaly RP, Peri S, Balachandran S, Lin R, Hiscott J. 2013. Systems Analysis of a RIG-I Agonist Inducing Broad Spectrum Inhibition of Virus Infectivity. PLoS Pathog 9:10032–98.

648. Wang Y, Wang X, Li J, Zhou Y, Ho W. 2013. RIG-I activation inhibits HIV replication in macrophages. J Leukoc Biol 94:337–341.

649. Martin-Gayo E, Buzon MJ, Ouyang Z, Hickman T, Cronin J, Pimenova D, Walker BD, Lichterfeld M, Yu XG. 2015. Potent Cell-Intrinsic Immune Responses in Dendritic Cells Facilitate HIV-1-Specific T Cell Immunity in HIV-1 Elite Controllers. PLoS Pathog 11:1–13.

650. Schlee M. 2013. Master sensors of pathogenic RNA - RIG-I like receptors. Immunobiology2013/07/31. 218:1322–1335.

651. Yoneyama M, Kikuchi M, Natsukawa T, Shinobu N, Imaizumi T, Miyagishi M, Taira K, Akira S, Fujita T. 2004. The RNA helicase RIG-I has an essential function in double-stranded RNA-induced innate antiviral responses. Nat Immunol 5:730–737.

652. Kell AM, Gale Jr. M, Gale M. 2015. RIG-I in RNA virus recognition. Virology2015/03/10. 479–480:110–121.

653. Schlee M, Roth A, Hornung V, Hagmann CA, Wimmenauer V, Barchet W, Coch C, Janke M, Mihailovic A, Wardle G, Juranek S, Kato H, Kawai T, Poeck H, Fitzgerald KA, Takeuchi O, Akira S, Tuschl T, Latz E, Ludwig J, Hartmann G. 2009. Recognition of 5′ Triphosphate by RIG-I Helicase Requires Short Blunt Double-Stranded RNA as Contained in Panhandle of Negative-Strand Virus. Immunity 31:25–34.

654. Tomalka J, Ghneim K, Bhattacharyya S, Aid M, Barouch DH, Sekaly RP, Ribeiro SP. 2016. The sooner the better: innate immunity as a

path toward the HIV cure. Curr Opin Virol 19:85–91.

655. Finkel TH, Tudor-Williams G, Banda NK, Cotton MF, Curiel T, Monks C, Baba TW, Ruprecht RM, Kupfer A. 1995. Apoptosis occurs predominantly in bystander cells and not in productively infected cells of HIV- and SIV-infected lymph nodes. Nat Med 1:129–134.
656. Fraietta JA, Mueller YM, Yang G, Boesteanu AC, Gracias DT, Do DH, Hope JL, Kathuria N, McGettigan SE, Lewis MG, Giavedoni LD, Jacobson JM, Katsikis PD. 2013. Type I Interferon Upregulates Bak and Contributes to T Cell Loss during Human Immunodeficiency Virus (HIV) Infection. PLoS Pathog 9.
657. Berg RK, Melchjorsen J, Rintahaka J, Diget E, Søby S, Horan KA, Gorelick RJ, Matikainen S, Larsen CS, Ostergaard L, Paludan SR, Mogensen TH. 2012. Genomic HIV RNA Induces Innate Immune Responses through RIG-I-Dependent Sensing of Secondary-Structured RNA. PLoS One 7:1–16.
658. Solis M, Nakhaei P, Jalalirad M, Lacoste J, Douville R, Arguello M, Zhao T, Laughrea M, Wainberg MA, Hiscott J. 2011. RIG-I-Mediated Antiviral Signaling Is Inhibited in HIV-1 Infection by a Protease-Mediated Sequestration of RIG-I. J Virol2010/11/19. 85:1224–1236.
659. Britto AMA, Amoedo ND, Pezzuto P, Afonso AO, Martínez AMB, Silveira J, Sion FS, Machado ES, Soares MA, Giannini ALM. 2013. Expression levels of the innate response gene RIG-I and its regulators RNF125 and TRIM25 in HIV-1-infected adult and pediatric individuals. AIDS 27:1879–1885.
660. Naji S, Ambrus G, Cimermančič P, Reyes JR, Johnson JR, Filbrandt R, Huber MD, Vesely P, Krogan NJ, Yates JR, Saphire AC, Gerace L. 2012. Host Cell Interactome of HIV-1 Rev Includes RNA Helicases Involved in Multiple Facets of Virus Production. Mol Cell Proteomics 11:153–166.
661. Soto-Rifo R, Rubilar PS, Limousin T, de Breyne S, Décimo D, Ohlmann T. 2012. DEAD-box protein DDX3 associates with eIF4F to promote translation of selected mRNAs. EMBO J 31:3745–56.
662. Gringhuis SI, Hertoghs N, Kaptein TM, Zijlstra-Willems EM, Sarrami-Forooshani R, Sprokholt JK, van Teijlingen NH, Kootstra NA,

Booiman T, van Dort KA, Ribeiro CMS, Drewniak A, Geijtenbeek TBH. 2016. HIV-1 blocks the signaling adaptor MAVS to evade antiviral host defense after sensing of abortive HIV-1 RNA by the host helicase DDX3. Nat Immunol 2016 182 18:225–235.

663. Takahama S, Yamamoto T. 2020. Pattern Recognition Receptor Ligands as an Emerging Therapeutic Agent for Latent HIV-1 Infection. Front Cell Infect Microbiol 10:216.
664. Rasmussen TA, Anderson JL, Wightman F, Lewin SR. 2017. Cancer therapies in HIV cure research. Curr Opin HIV AIDS 12:96–104.
665. Kanasty R, Dorkin JR, Vegas A, Anderson D. 2013. Delivery materials for siRNA therapeutics. Nat Mater2013/10/24. 12:967–977.
666. Pack DW, Hoffman AS, Pun S, Stayton PS. 2005. Design and development of polymers for gene delivery. Nat Rev Drug Discov 4:581–93.
667. Schlee M, Hartmann E, Coch C, Wimmenauer V, Janke M, Barchet W, Hartmann G. 2009. Approaching the RNA ligand for RIG-I? Immunol Rev 227:66–74.
668. Wang Y, Ludwig J, Schuberth C, Goldeck M, Schlee M, Li H, Juranek S, Sheng G, Micura R, Tuschl T, Hartmann G, Patel DJ. 2010. Structural and functional insights into 5′-ppp RNA pattern recognition by the innate immune receptor RIG-I. Nat Struct Mol Biol 17:781–787.
669. Schlee M, Hartmann G. 2010. The Chase for the RIG-I Ligand—Recent Advances. Mol Ther2010/05/13. 18:1254–1262.
670. Zhang L, Xia Q, Li W, Peng Q, Yang H, Lu X, Wang G. 2019. The RIG-I pathway is involved in peripheral T cell lymphopenia in patients with dermatomyositis. Arthritis Res Ther 21:131.
671. Kuruganti S, Accavitti-Loper MA, Walter MR. 2014. Production and characterization of thirteen human type-I interferon-α subtypes. Protein Expr Purif 103:75–83.
672. Overall ML, Hertzog PJ. 1992. Functional analysis of interferon-α subtypes using monoclonal antibodies to interferon-α 4a—subtype reactivity, neutralisation of biological activities and epitope analysis. Mol Immunol 29:391–399.
673. Schindler C, Plumlee C. 2008. Inteferons pen the JAK–STAT

pathway. Semin Cell Dev Biol 19:311–318.

674. Borden EC, Sen GC, Uze G, Silverman RH, Ransohoff RM, Foster GR, Stark GR. 2007. Interferons at age 50: past, current and future impact on biomedicine. Nat Rev Drug Discov 6:975–990.
675. Malmgaard L. 2004. Induction and regulation of IFNs during viral infections. J Interf Cytokine Res.
676. Stark GR. 2007. How cells respond to interferons revisited: From early history to current complexity. Cytokine Growth Factor Rev 18:419–423.
677. Yang H, Fung SY, Bao A, Li Q, Turvey SE. 2017. Screening Bioactive Nanoparticles in Phagocytic Immune Cells for Inhibitors of Toll-like Receptor Signaling. J Vis Exp 8:56075.
678. Kato H, Takeuchi O, Mikamo-Satoh E, Hirai R, Kawai T, Matsushita K, Hiiragi A, Dermody TS, Fujita T, Akira S. 2008. Length-dependent recognition of double-stranded ribonucleic acids by retinoic acid–inducible gene-I and melanoma differentiation–associated gene 5. J Exp Med 205:1601–1610.
679. Marques JT, Devosse T, Wang D, Zamanian-Daryoush M, Serbinowski P, Hartmann R, Fujita T, Behlke MA, Williams BR. 2006. A structural basis for discriminating between self and nonself double-stranded RNAs in mammalian cells. Nat Biotechnol 24:559–565.
680. Brisse M, Ly H. 2019. Comparative Structure and Function Analysis of the RIG-I-Like Receptors: RIG-I and MDA5Frontiers in Immunology.
681. Schmidt A, Schwerd T, Hamm W, Hellmuth JC, Cui S, Wenzel M, Hoffmann FS, Michallet M-C, Besch R, Hopfner K-P, Endres S, Rothenfusser S. 2009. 5’-triphosphate RNA requires base-paired structures to activate antiviral signaling via RIG-I. Proc Natl Acad Sci 106:12067–12072.
682. Kolakofsky D, Kowalinski E, Cusack S. 2012. A structure-based model of RIG-I activation. RNA 18:2118–2127.
683. Lu C, Xu H, Ranjith-Kumar CT, Brooks MT, Hou TY, Hu F, Herr AB, Strong RK, Kao CC, Li P. 2010. The Structural Basis of 5′ Triphosphate Double-Stranded RNA Recognition by RIG-I C-

Terminal Domain. Structure 18:1032–1043.

684. Strahle L, Garcin D, Kolakofsky D. 2006. Sendai virus defective-interfering genomes and the activation of interferon-beta. Virology 351:101–111.

685. Takahasi K, Yoneyama M, Nishihori T, Hirai R, Kumeta H, Narita R, Gale M, Inagaki F, Fujita T. 2008. Nonself RNA-Sensing Mechanism of RIG-I Helicase and Activation of Antiviral Immune Responses. Mol Cell 29:428–440.

686. McNab F, Mayer-Barber K, Sher A, Wack A, O'Garra A. 2015. Type I interferons in infectious disease. Nat Rev Immunol 15:87–103.

687. Prabakaran T, Troldborg A, Kumpunya S, Alee I, Marinković E, Windross SJ, Nandakumar R, Narita R, Zhang B, Carstensen M, Vejvisithsakul P, Marqvorsen MH, Iversen MB, Holm CK, Østergaard LJ, Pedersen FS, Pisitkun T, Behrendt R, Pisitkun P, Paludan SR. 2021. A STING antagonist modulating the interaction with STIM1 blocks ER-to-Golgi trafficking and inhibits lupus pathology. EBioMedicine 66:103314.

688. Mejía-Calvo I, Muñoz-García L, Jiménez-Uribe A, Camacho-Sandoval R, González-González E, Mellado-Sánchez G, Tenorio-Calvo A V., López-Morales CA, Velasco-Velázquez MA, Pavón L, Pérez-Tapia SM, Medina-Rivero E. 2019. Validation of a cell-based colorimetric reporter gene assay for the evaluation of Type I Interferons. Biotechnol Reports 22:e00331.

689. Jiang M, Österlund P, Sarin LP, Poranen MM, Bamford DH, Guo D, Julkunen I, Osterlund P, Sarin LP, Poranen MM, Bamford DH, Guo D, Julkunen I. 2011. Innate immune responses in human monocyte-derived dendritic cells are highly dependent on the size and the 5' phosphorylation of RNA molecules. J Immunol 187:1713–21.

690. Hornung V, Ellegast J, Kim S, Brzózka K, Jung A, Kato H, Poeck H, Akira S, Conzelmann K-K, Schlee M, Endres S, Hartmann G. 2006. 5'-Triphosphate RNA is the ligand for RIG-I. Science 314:994–7.

691. Rock KL, Lai J-J, Kono H. 2011. Innate and adaptive immune responses to cell death. Immunol Rev 243:191–205.

692. van den Boorn JG, Hartmann G. 2013. Turning Tumors into Vaccines:

Co-opting the Innate Immune System. Immunity 39:27–37.

693. Palchetti S, Starace D, De Cesaris P, Filippini A, Ziparo E, Riccioli A. 2015. Transfected Poly(I:C) Activates Different dsRNA Receptors, Leading to Apoptosis or Immunoadjuvant Response in Androgen-independent Prostate Cancer Cells. J Biol Chem 290:5470–5483.
694. Besch R, Poeck H, Hohenauer T, Senft D, Häcker G, Berking C, Hornung V, Endres S, Ruzicka T, Rothenfusser S, Hartmann G. 2009. Proapoptotic signaling induced by RIG-I and MDA-5 results in type I interferon-independent apoptosis in human melanoma cells. J Clin Invest 119:2399–2411.
695. Jacobson ME, Wang-Bishop L, Becker KW, Wilson JT. 2019. Delivery of 5′-triphosphate RNA with endosomolytic nanoparticles potently activates RIG-I to improve cancer immunotherapy. Biomater Sci 7:547–559.
696. Rasmussen TA, Søgaard OS. 2018. Clinical interventions in HIV cure research, p. 285–318. *In* Advances in Experimental Medicine and Biology. Adv Exp Med Biol.
697. Thorlund K, Horwitz MS, Fife BT, Lester R, Cameron DW. 2017. Landscape review of current HIV “kick and kill” cure research - some kicking, not enough killing. BMC Infect Dis2017/08/31. 17:595.
698. Sengupta S, Siliciano RF. 2018. Targeting the Latent Reservoir for HIV-1Immunity. Immunity.
699. Ke R, Lewin SR, Elliott JH, Perelson AS. 2015. Modeling the Effects of Vorinostat In Vivo Reveals both Transient and Delayed HIV Transcriptional Activation and Minimal Killing of Latently Infected Cells. PLoS Pathog 11:e1005237.
700. Singh V, Dashti A, Mavigner M, Chahroudi A. 2021. Latency Reversal 2.0: Giving the Immune System a Seat at the Table. Curr HIV/AIDS Rep 18:117–127.
701. Kasumba DM, Grandvaux N. 2019. Therapeutic Targeting of RIG-I and MDA5 Might Not Lead to the Same Rome. Trends Pharmacol Sci 40:116–127.
702. Helms MW, Jahn-Hofmann K, Gnerlich F, Metz-Weidmann C, Braun M, Dietert G, Scherer P, Grandien K, Theilhaber J, Cao H, Wagenaar

TR, Schnurr MM, Endres S, Wiederschain D, Scheidler S, Rothenfußer S, Brunner B, König LM. 2019. Utility of the RIG-I Agonist Triphosphate RNA for Melanoma Therapy. Mol Cancer Ther 18:2343–2356.

703. Elion DL, Cook RS. 2018. Harnessing RIG-I and intrinsic immunity in the tumor microenvironment for therapeutic cancer treatment. Oncotarget 9:29007–29017.
704. Iurescia S, Fioretti D, Rinaldi M. 2020. The Innate Immune Signalling Pathways: Turning RIG-I Sensor Activation against Cancer. Cancers (Basel) 12:3158.
705. Such L, Zhao F, Liu D, Thier B, Le-Trilling VTK, Sucker A, Coch C, Pieper N, Howe S, Bhat H, Kalkavan H, Ritter C, Brinkhaus R, Ugurel S, Köster J, Seifert U, Dittmer U, Schuler M, Lang KS, Kufer TA, Hartmann G, Becker JC, Horn S, Ferrone S, Liu D, Van Allen EM, Schadendorf D, Griewank K, Trilling M, Paschen A. 2020. Targeting the innate immunoreceptor RIG-I overcomes melanoma-intrinsic resistance to T cell immunotherapy. J Clin Invest 130:4266–4281.
706. Buccheri L, Katchen BR, Karter AJ, Cohen SR. 1997. Acitretin therapy is effective for associated with human immunodeficiency virus infection. Arch Dermatol 133:711–715.
707. Dowdy SF. 2017. Overcoming cellular barriers for RNA therapeutics. Nat Biotechnol. Nature Publishing Group.
708. Whitehead KA, Langer R, Anderson DG. 2009. Knocking down barriers: advances in siRNA delivery. Nat Rev Drug Discov 8:129–138.
709. Durymanov M, Reineke J. 2018. Non-viral Delivery of Nucleic Acids: Insight Into Mechanisms of Overcoming Intracellular Barriers. Front Pharmacol 9:971.
710. Putnam D. 2006. Polymers for gene delivery across length scales. Nat Mater 5:439–451.
711. Schumann K, Lin S, Boyer E, Simeonov DR, Subramaniam M, Gate RE, Haliburton GE, Ye CJ, Bluestone JA, Doudna JA, Marson A. 2015. Generation of knock-in primary human T cells using Cas9 ribonucleoproteins. Proc Natl Acad Sci U S A 112:10437–42.

712. Das M, Shen L, Liu Q, Goodwin TJ, Huang L. 2019. Nanoparticle Delivery of RIG-I Agonist Enables Effective and Safe Adjuvant Therapy in Pancreatic Cancer. Mol Ther 27:507–517.
713. Poeck H, Besch R, Maihoefer C, Renn M, Tormo D, Morskaya SS, Kirschnek S, Gaffal E, Landsberg J, Hellmuth J, Schmidt A, Anz D, Bscheider M, Schwerd T, Berking C, Bourquin C, Kalinke U, Kremmer E, Kato H, Akira S, Meyers R, Häcker G, Neuenhahn M, Busch D, Ruland J, Rothenfusser S, Prinz M, Hornung V, Endres S, Tüting T, Hartmann G. 2008. 5′-triphosphate-siRNA: turning gene silencing and Rig-I activation against melanoma. Nat Med 14:1256–1263.
714. Jiang X, Muthusamy V, Fedorova O, Kong Y, Kim DJ, Bosenberg M, Pyle AM, Iwasaki A. 2019. Intratumoral delivery of RIG-I agonist SLR14 induces robust antitumor responses. J Exp Med 216:2854–2868.
715. Linehan MM, Dickey TH, Molinari ES, Fitzgerald ME, Potapova O, Iwasaki A, Pyle AM. 2018. A minimal RNA ligand for potent RIG-I activation in living mice. Sci Adv 4:1–10.
716. Ellermeier J, Wei J, Duewell P, Hoves S, Stieg MR, Adunka T, Noerenberg D, Anders H-J, Mayr D, Poeck H, Hartmann G, Endres S, Schnurr M. 2013. Therapeutic Efficacy of Bifunctional siRNA Combining TGF-β1 Silencing with RIG-I Activation in Pancreatic Cancer. Cancer Res 73:1709–1720.
717. Czerkies M, Korwek Z, Prus W, Kochańczyk M, Jaruszewicz-Błońska J, Tudelska K, Błoński S, Kimmel M, Brasier AR, Lipniacki T. 2018. Cell fate in antiviral response arises in the crosstalk of IRF, NF-κB and JAK/STAT pathways. Nat Commun 9:493.
718. Yoboua F, Martel A, Duval A, Mukawera E, Grandvaux N. 2010. Respiratory Syncytial Virus-Mediated NF-κB p65 Phosphorylation at Serine 536 Is Dependent on RIG-I, TRAF6, and IKKβ. J Virol 84:7267–7277.
719. Rückle A, Haasbach E, Julkunen I, Planz O, Ehrhardt C, Ludwig S. 2012. The NS1 Protein of Influenza A Virus Blocks RIG-I-Mediated Activation of the Noncanonical NF-κB Pathway and p52/RelB-Dependent Gene Expression in Lung Epithelial Cells. J Virol

86:10211–10217.

720. Krapp C, Jønsson K, Jakobsen MR. 2018. STING dependent sensing – Does HIV actually care? Cytokine Growth Factor Rev 40:68–76.

721. Lau JSY, McMahon JH, Gubser C, Solomon A, Chiu CYH, Dantanarayana A, Chea S, Tennakoon S, Zerbato JM, Garlick J, Morcilla V, Palmer S, Lewin SR, Rasmussen TA. 2021. The impact of immune checkpoint therapy on the latent reservoir in HIV-infected individuals with cancer on antiretroviral therapy. AIDS 35:1631–1636.

722. Rasmussen TA, Rajdev L, Rhodes A, Dantanarayana A, Tennakoon S, Chea S, Spelman T, Lensing S, Rutishauser R, Bakkour S, Busch M, Siliciano JD, Siliciano RF, Einstein MH, Dittmer DP, Chiao E, Deeks SG, Durand C, Lewin SR. 2021. Impact of Anti–PD-1 and Anti–CTLA-4 on the Human Immunodeficiency Virus (HIV) Reservoir in People Living With HIV With Cancer on Antiretroviral Therapy: The AIDS Malignancy Consortium 095 Study. Clin Infect Dis 1530:1–9.

723. Macedo AB, Novis CL, De Assis CM, Sorensen ES, Moszczynski P, Huang S-H, Ren Y, Spivak AM, Jones RB, Planelles V, Bosque A. 2018. Dual TLR2 and TLR7 agonists as HIV latency-reversing agents. JCI insight 3:1–16.

724. van der Sluis RM, Zerbato JM, Rhodes JW, Pascoe RD, Solomon A, Kumar NA, Dantanarayana AI, Tennakoon S, Dufloo J, McMahon J, Chang JJ, Evans VA, Hertzog PJ, Jakobsen MR, Harman AN, Lewin SR, Cameron PU. 2020. Diverse effects of interferon alpha on the establishment and reversal of HIV latency. PLOS Pathog 16:1008151.

725. van der Pol E, Coumans FAW, Grootemaat AE, Gardiner C, Sargent IL, Harrison P, Sturk A, van Leeuwen TG, Nieuwland R. 2014. Particle size distribution of exosomes and microvesicles determined by transmission electron microscopy, flow cytometry, nanoparticle tracking analysis, and resistive pulse sensing. J Thromb Haemost 12:1182–92.

726. Vibholm L, Schleimann MH, Højen JF, Benfield T, Offersen R, Rasmussen K, Olesen R, Dige A, Agnholt J, Grau J, Buzon M, Wittig B, Lichterfeld M, Petersen AM, Deng X, Abdel-Mohsen M, Pillai SK, Rutsaert S, Trypsteen W, De Spiegelaere W, Vandekerchove L,

Østergaard L, Rasmussen TA, Denton PW, Tolstrup M, Søgaard OS. 2017. Short-Course Toll-Like Receptor 9 Agonist Treatment Impacts Innate Immunity and Plasma Viremia in Individuals With Human Immunodeficiency Virus Infection. Clin Infect Dis2017/03/23. 64:1686–1695.

727. Jarrell JA, Twite AA, Lau KHWJ, Kashani MN, Lievano AA, Acevedo J, Priest C, Nieva J, Gottlieb D, Pawell RS. 2019. Intracellular delivery of mRNA to human primary T cells with microfluidic vortex shedding. Sci Rep 9:3214.
728. Lou J, Heater A, Zheng G. 2021. Improving the Delivery of Drugs and Nucleic Acids to T Cells Using Nanotechnology. Small Struct 2:2100026.
729. Glass JJ, Kent SJ, De Rose R. 2016. Enhancing dendritic cell activation and HIV vaccine effectiveness through nanoparticle vaccination. Expert Rev Vaccines 15:719–729.
730. Wang C, He C, Tong Z, Liu X, Ren B, Zeng F. 2006. Combination of adsorption by porous CaCO3 microparticles and encapsulation by polyelectrolyte multilayer films for sustained drug delivery. Int J Pharm 308:160–167.
731. Jafari S, Derakhshankhah H, Alaei L, Fattahi A, Varnamkhasti BS, Saboury AA. 2019. Mesoporous silica nanoparticles for therapeutic/diagnostic applications. Biomed Pharmacother 109:1100–1111.
732. Ahuja G, Pathak K. 2009. Porous carriers for controlled/modulated drug delivery. Indian J Pharm Sci 71:599–607.
733. Fujiwara M, Yamamoto F, Okamoto K, Shiokawa K, Nomura R. 2005. Adsorption of Duplex DNA on Mesoporous Silicas: Possibility of Inclusion of DNA into Their Mesopores. Anal Chem 77:8138–8145.
734. Jia L, Shen J, Li Z, Zhang D, Zhang Q, Duan C, Liu G, Zheng D, Liu Y, Tian X. 2012. Successfully tailoring the pore size of mesoporous silica nanoparticles: Exploitation of delivery systems for poorly water-soluble drugs. Int J Pharm 439:81–91.
735. Gao Y, Chen Y, Ji X, He X, Yin Q, Zhang Z, Shi J, Li Y. 2011. Controlled Intracellular Release of Doxorubicin in Multidrug-Resistant

Cancer Cells by Tuning the Shell-Pore Sizes of Mesoporous Silica Nanoparticles. ACS Nano 5:9788–9798.

736. Li J, Shen S, Kong F, Jiang T, Tang C, Yin C. 2018. Effects of pore size on in vitro and in vivo anticancer efficacies of mesoporous silica nanoparticles. RSC Adv 8:24633–24640.
737. Takimoto A, Shiomi T, Ino K, Tsunoda T, Kawai A, Mizukami F, Sakaguchi K. 2008. Encapsulation of cellulase with mesoporous silica (SBA-15). Microporous Mesoporous Mater 116:601–606.
738. Xu C, Lei C, Yu C. 2019. Mesoporous Silica Nanoparticles for Protein Protection and Delivery. Front Chem 7:290.
739. Imamichi H, Smith M, Adelsberger JW, Izumi T, Scrimieri F, Sherman BT, Rehm CA, Imamichi T, Pau A, Catalfamo M, Fauci AS, Lane HC. 2020. Defective HIV-1 proviruses produce viral proteins. Proc Natl Acad Sci 117:3704–3710.
740. Finzi D, Plaeger SF, Dieffenbach CW. 2006. Defective Virus Drives Human Immunodeficiency Virus Infection, Persistence, and Pathogenesis. Clin Vaccine Immunol 13:715–721.
741. Eisele E, Siliciano RF. 2012. Redefining the viral reservoirs that prevent HIV-1 eradication. Immunity 37:377–88.
742. Schudel A, Francis DM, Thomas SN. 2019. Material design for lymph node drug delivery. Nat Rev Mater 4:415–428.
743. Rosenblum D, Joshi N, Tao W, Karp JM, Peer D. 2018. Progress and challenges towards targeted delivery of cancer therapeutics. Nat Commun 9:1410.
744. Egusquiaguirre SP, Igartua M, Hernández RM, Pedraz JL. 2012. Nanoparticle delivery systems for cancer therapy: advances in clinical and preclinical research. Clin Transl Oncol 14:83–93.
745. Dykman L, Khlebtsov N. 2012. Gold nanoparticles in biomedical applications: recent advances and perspectives. Chem Soc Rev 41:2256–2282.
746. Cao S, Jiang Y, Levy CN, Hughes SM, Zhang H, Hladik F, Woodrow KA. 2018. Optimization and comparison of CD4-targeting lipid-polymer hybrid nanoparticles using different binding ligands. J Biomed Mater Res Part A 106:1177–1188.

747. Tan KX, Danquah MK, Sidhu A, Yon LS, Ongkudon CM. 2018. Aptamer-Mediated Polymeric Vehicles for Enhanced Cell-Targeted Drug Delivery. Curr Drug Targets 19.
748. Shi J, Kantoff PW, Wooster R, Farokhzad OC. 2017. Cancer nanomedicine: Progress, challenges and opportunities. Nat Rev Cancer. Nat Rev Cancer.
749. Field LD, Delehanty JB, Chen Y, Medintz IL. 2015. Peptides for Specifically Targeting Nanoparticles to Cellular Organelles: Quo Vadis ? Acc Chem Res 48:1380–1390.
750. Kandil R, Xie Y, Heermann R, Isert L, Jung K, Mehta A, Merkel OM. 2019. Coming in and Finding Out: Blending Receptor-Targeted Delivery and Efficient Endosomal Escape in a Novel Bio-Responsive siRNA Delivery System for Gene Knockdown in Pulmonary T Cells. Adv Ther 2:1900047.
751. Lee J, Yun K-SS, Choi CS, Shin S-HH, Ban H-SS, Rhim T, Lee SK, Lee KY. 2012. T cell-specific siRNA delivery using antibody-conjugated chitosan nanoparticles. Bioconjug Chem2012/05/23. 23:1174–1180.
752. Yang Y-SS, Moynihan KD, Bekdemir A, Dichwalkar TM, Noh MM, Watson N, Melo M, Ingram J, Suh H, Ploegh H, Stellacci FR, Irvine DJ. 2019. Targeting small molecule drugs to T cells with antibody-directed cell-penetrating gold nanoparticles. Biomater Sci2018/11/18. 7:113–124.
753. Schmid D, Park CG, Hartl CA, Subedi N, Cartwright AN, Puerto RB, Zheng Y, Maiarana J, Freeman GJ, Wucherpfennig KW, Irvine DJ, Goldberg MS. 2017. T cell-targeting nanoparticles focus delivery of immunotherapy to improve antitumor immunity. Nat Commun2017/11/25. 8:1–11.
754. Kumar P, Ban H-S, Kim S-S, Wu H, Pearson T, Greiner DL, Laouar A, Yao J, Haridas V, Habiro K, Yang Y-G, Jeong J-H, Lee K-Y, Kim Y-H, Kim SW, Peipp M, Fey GH, Manjunath N, Shultz LD, Lee S-K, Shankar P. 2008. T Cell-Specific siRNA Delivery Suppresses HIV-1 Infection in Humanized Mice. Cell 134:577–586.
755. Iglesias-Ussel M, Vandergeeten C, Marchionni L, Chomont N,

Romerio F. 2013. High Levels of CD2 Expression Identify HIV-1 Latently Infected Resting Memory CD4 + T Cells in Virally Suppressed Subjects. J Virol 87:9148–9158.

756. Paiardini M, Lichterfeld M. 2016. Follicular T helper cells: hotspots for HIV-1 persistence. Nat Med 22:711–712.
757. Fromentin R, Bakeman W, Lawani MB, Khoury G, Hartogensis W, DaFonseca S, Killian M, Epling L, Hoh R, Sinclair E, Hecht FM, Bacchetti P, Deeks SG, Lewin SR, Sékaly R-PP, Chomont N. 2016. CD4+ T Cells Expressing PD-1, TIGIT and LAG-3 Contribute to HIV Persistence during ART. PLOS Pathog 12:1–13.
758. Hogan LE, Vasquez J, Hobbs KS, Hanhauser E, Aguilar-Rodriguez B, Hussien R, Thanh C, Gibson EA, Carvidi AB, Smith LCB, Khan S, Trapecar M, Sanjabi S, Somsouk M, Stoddart CA, Kuritzkes DR, Deeks SG, Henrich TJ. 2018. Increased HIV-1 transcriptional activity and infectious burden in peripheral blood and gut-associated CD4+T cells expressing CD30. PLoS Pathog 14.
759. Darcis G, Kootstra NA, Hooibrink B, van Montfort T, Maurer I, Groen K, Jurriaans S, Bakker M, van Lint C, Berkhout B, Pasternak AO. 2020. CD32+CD4+ T Cells Are Highly Enriched for HIV DNA and Can Support Transcriptional Latency. Cell Rep 30:2284-2296.e3.
760. Shi Y, Fu Y, Zhang X, Zhao G, Yao Y, Guo Y, Ma G, Bai S, Li H. 2021. Romidepsin (FK228) regulates the expression of the immune checkpoint ligand PD-L1 and suppresses cellular immune functions in colon cancer. Cancer Immunol Immunother 70:61–73.
761. Gay CL, Bosch RJ, Ritz J, Hataye JM, Aga E, Tressler RL, Mason SW, Hwang CK, Grasela DM, Ray N, Cyktor JC, Coffin JM, Acosta EP, Koup RA, Mellors JW, Eron JJ. 2017. Clinical trial of the anti-PD-L1 antibody BMS-936559 in HIV-1 infected participants on suppressive antiretroviral therapy. J Infect Dis 215:1725–1733.
762. Wykes MN, Lewin SR. 2018. Immune checkpoint blockade in infectious diseases. Nat Rev Immunol 18:91–104.
763. Smith TT, Stephan SB, Moffett HF, McKnight LE, Ji W, Reiman D, Bonagofski E, Wohlfahrt ME, Pillai SPSSS, Stephan MT. 2017. In situ programming of leukaemia-specific t cells using synthetic DNA

nanocarriers. Nat Nanotechnol2017/04/19. 12:813–822.

764. Zheng Y, Stephan MT, Gai SA, Abraham W, Shearer A, Irvine DJ. 2013. In vivo targeting of adoptively transferred T-cells with antibody- and cytokine-conjugated liposomes. J Control Release 172:426–435.
765. Glass JJ, Yuen D, Rae J, Johnston APR, Parton RG, Kent SJ, De Rose R. 2016. Human immune cell targeting of protein nanoparticles – caveospheres. Nanoscale 8:8255–8265.
766. Licht A, Alter G. 2016. A Drug-Free Zone—Lymph Nodes as a Safe Haven for HIV. Cell Host Microbe 19:275–276.
767. Barton K, Hiener B, Winckelmann A, Rasmussen TA, Shao W, Byth K, Lanfear R, Solomon A, McMahon J, Harrington S, Buzon M, Lichterfeld M, Denton PW, Olesen R, Østergaard L, Tolstrup M, Lewin SR, Søgaard OS, Palmer S. 2016. Broad activation of latent HIV-1 in vivo. Nat Commun 7:12731.
768. Yukl S, Wong JK. 2008. Blood and Guts and HIV: Preferential HIV Persistence in GI Mucosa. J Infect Dis 197:640–642.
769. Kinman L, Brodie SJ, Tsai CC, Bui T, Larsen K, Schmidt A, Anderson D, Morton WR, Hu S-L, Ho RJY. 2003. Lipid–Drug Association Enhanced HIV-1 Protease Inhibitor Indinavir Localization in Lymphoid Tissues and Viral Load Reduction: A Proof of Concept Study in HIV-2287-Infected Macaques. JAIDS J Acquir Immune Defic Syndr 34:387–397.
770. Brogdon J, Ziani W, Wang X, Veazey RS, Xu H. 2016. In vitro effects of the small-molecule protein kinase C agonists on HIV latency reactivation. Sci Rep 6:39032.
771. Subeha MR, Telleria CM. 2020. The Anti-Cancer Properties of the HIV Protease Inhibitor Nelfinavir. Cancers (Basel) 12:3437.
772. Sainte-Marie G. 2010. The Lymph Node Revisited: Development, Morphology, Functioning, and Role in Triggering Primary Immune Responses. Anat Rec Adv Integr Anat Evol Biol 293:320–337.
773. Huang B, Abraham WD, Zheng Y, Bustamante López SC, Luo SS, Irvine DJ. 2015. Active targeting of chemotherapy to disseminated tumors using nanoparticle-carrying T cells. Sci Transl Med2015/06/13. 7:291–294.

774. Swartz M. 2001. The physiology of the lymphatic system. Adv Drug Deliv Rev 50:3–20.
775. De Koker S, Cui J, Vanparijs N, Albertazzi L, Grooten J, Caruso F, De Geest BG. 2016. Engineering Polymer Hydrogel Nanoparticles for Lymph Node-Targeted Delivery. Angew Chemie Int Ed 55:1334–1339.
776. Thomas SN, Schudel A. 2015. Overcoming transport barriers for interstitial-, lymphatic-, and lymph node-targeted drug delivery. Curr Opin Chem Eng 7:65–74.
777. Kaminskas LM, Kota J, McLeod VM, Kelly BD, Karellas P, Porter CJ. 2009. PEGylation of polylysine dendrimers improves absorption and lymphatic targeting following SC administration in rats. J Control Release 140:108–116.
778. Rohner NA, Thomas SN. 2017. Flexible Macromolecule versus Rigid Particle Retention in the Injected Skin and Accumulation in Draining Lymph Nodes Are Differentially Influenced by Hydrodynamic Size. ACS Biomater Sci Eng 3:153–159.
779. Ou W, Thapa RK, Jiang L, Soe ZC, Gautam M, Chang J-HH, Jeong J-HH, Ku SK, Choi H-GG, Yong CS, Kim JO, Soe C, Gautam M, Chang J-HH, Jeong J-HH, Kwang Ku S, Choi H-GG, Yong CS, Kim JO. 2018. Regulatory T cell-targeted hybrid nanoparticles combined with immuno-checkpoint blockage for cancer immunotherapy. J Control Release2018/05/20. 281:84–96.
780. Zheng Y, Tang L, Mabardi L, Kumari S, Irvine DJ. 2017. Enhancing Adoptive Cell Therapy of Cancer through Targeted Delivery of Small-Molecule Immunomodulators to Internalizing or Noninternalizing Receptors. ACS Nano 11:3089–3100.
781. Davenport MP, Khoury DS, Cromer D, Lewin SR, Kelleher AD, Kent SJ. 2019. Functional cure of HIV: the scale of the challenge. Nat Rev Immunol 19:45–54.
782. Ait-Ammar A, Kula A, Darcis G, Verdikt R, De Wit S, Gautier V, Mallon PWG, Marcello A, Rohr O, Van Lint C. 2019. Current Status of Latency Reversing Agents Facing the Heterogeneity of HIV-1 Cellular and Tissue Reservoirs. Front Microbiol 10:3060.

783. Archin NM, Kirchherr JL, Sung JAM, Clutton G, Sholtis K, Xu Y, Allard B, Stuelke E, Kashuba AD, Kuruc JD, Eron J, Gay CL, Goonetilleke N, Margolis DM. 2017. Interval dosing with the HDAC inhibitor vorinostat effectively reverses HIV latency. J Clin Invest 127:3126–3135.
784. Brinkmann CR, Højen JF, Rasmussen TA, Kjær AS, Olesen R, Denton PW, Østergaard L, Ouyang Z, Lichterfeld M, Yu X, Søgaard OS, Dinarello C, Tolstrup M. 2018. Treatment of HIV-Infected Individuals with the Histone Deacetylase Inhibitor Panobinostat Results in Increased Numbers of Regulatory T Cells and Limits Ex Vivo Lipopolysaccharide-Induced Inflammatory Responses. mSphere 3:16–17.
785. Cary DC, Fujinaga K, Peterlin BM. 2016. Molecular mechanisms of HIV latency. J Clin Invest2016/01/06. 126:448–54.
786. Bouchat S, Delacourt N, Kula A, Darcis G, Van Driessche B, Corazza F, Gatot J-S, Melard A, Vanhulle C, Kabeya K, Pardons M, Avettand-Fenoel V, Clumeck N, De Wit S, Rohr O, Rouzioux C, Van Lint C. 2016. Sequential treatment with 5-aza-2′-deoxycytidine and deacetylase inhibitors reactivates HIV -1. EMBO Mol Med 8:117–138.
787. Spivak AM, Nell RA, Petersen M, Martins L, Sebahar P, Looper RE, Planelles V. 2018. Synthetic Ingenols Maximize Protein Kinase C-Induced HIV-1 Latency Reversal. Antimicrob Agents Chemother 62.
788. Hashemi P, Sadowski I. 2020. Diversity of small molecule HIV-1 latency reversing agents identified in low- and high-throughput small molecule screens. Med Res Rev 40:881–908.
789. Zerbato JM, Khoury G, Zhao W, Gartner MJ, Pascoe RD, Rhodes A, Dantanarayana A, Gooey M, Anderson J, Bacchetti P, Deeks SG, McMahon J, Roche M, Rasmussen TA, Purcell DF, Lewin SR. 2021. Multiply spliced HIV RNA is a predictive measure of virus production ex vivo and in vivo following reversal of HIV latency. EBioMedicine 65:103–241.
790. Mcmahon JH, Evans VA, Lau JSY, Symons J, Zerbato JM, Chang J, Solomon A, Tennakoon S, Dantanarayana A, Hagenauer M, Lee S, Palmer S, Fisher K, Bumpus N, Heck CJS, Burger D, Wu G, Zuck P,

Howell BJ, Zetterberg HH, Blennow K, Gisslen M, Rasmussen TA, Lewin SR. 2021. Neurotoxicity with high dose disulfiram and vorinostat used for HIV latency reversal. AIDS https://doi.org/10.1097/QAD.0000000000003091.

791. Raverdeau M, Mills KHG. 2014. Modulation of T Cell and Innate Immune Responses by Retinoic Acid. J Immunol 192:2953–2958.
792. Abbas W, Herbein G. 2013. T-Cell Signaling in HIV-1 Infection. Open Virol J 7:57–71.
793. Cummins NW, Badley AD. 2013. Anti-apoptotic mechanisms of HIV: lessons and novel approaches to curing HIV. Cell Mol Life Sci 70:3355–3363.
794. López-Huertas MR, Mateos E, Sánchez Del Cojo M, Gómez-Esquer F, Díaz-Gil G, Rodríguez-Mora S, López JA, Calvo E, López-Campos G, Alcamí J, Coiras M. 2013. The presence of HIV-1 Tat protein second exon delays fas protein-mediated apoptosis in CD4+ T lymphocytes: a potential mechanism for persistent viral production. J Biol Chem 288:7626–7644.
795. Wolf D, Witte V, Laffert B, Blume K, Stromer E, Trapp S, D'Aloja P, Schürmann A, Baur AS. 2001. HIV-1 Nef associated PAK and PI3-Kinases stimulate Akt-independent Bad-phosphorylation to induce anti-apoptotic signals. Nat Med 7:1217–1224.
796. Kaplan AH, Manchester M, Swanstrom R. 1994. The activity of the protease of human immunodeficiency virus type 1 is initiated at the membrane of infected cells before the release of viral proteins and is required for release to occur with maximum efficiency. J Virol 68:6782–6786.
797. Conti L, Rainaldi G, Matarrese P, Varano B, Rivabene R, Columba S, Sato A, Belardelli F, Malorni W, Gessani S. 1998. The HIV-1 vpr Protein Acts as a Negative Regulator of Apoptosis in a Human Lymphoblastoid T Cell Line: Possible Implications for the Pathogenesis of AIDS. J Exp Med 187:403–413.
798. Kato Y, Salumbides BC, Wang XF, Qian DZ, Williams S, Wei Y, Sanni TB, Atadja P, Pili R. 2007. Antitumor effect of the histone deacetylase inhibitor LAQ824 in combination with 13-cis-retinoic acid in human

malignant melanoma. Mol Cancer Ther 6:70–81.

799. Gustafson HH, Holt-Casper D, Grainger DW, Ghandehari H. 2015. Nanoparticle uptake: The phagocyte problem. Nano Today 10:487–510.
800. Herd HL, Bartlett KT, Gustafson JA, McGill LD, Ghandehari H. 2015. Macrophage silica nanoparticle response is phenotypically dependent. Biomaterials 53:574–582.
801. Blanco E, Shen H, Ferrari M. 2015. Principles of nanoparticle design for overcoming biological barriers to drug delivery. Nat Biotechnol 33:941–951.
802. Pinheiro WO, Fascineli ML, Farias GR, Horst FH, de Andrade LR, Corrêa LH, Magalhães KG, Sousa MH, de Almeida MC, Azevedo RB, Lacava ZG. 2019. The influence of female mice age on biodistribution and biocompatibility of citrate-coated magnetic nanoparticles. Int J Nanomedicine 14:3375–3388.
803. Zhang X-D, Chen, Song, Wang, Shen, Wu, Fan, Fan, Sun Y-M, Liu P-X, Long W. 2013. Sex differences in the toxicity of polyethylene glycol-coated gold nanoparticles in miceInternational Journal of Nanomedicine. Dove Press.
804. Lavender KJ, Pace C, Sutter K, Messer RJ, Pouncey DL, Cummins NW, Natesampillai S, Zheng J, Goldsmith J, Widera M, Van Dis ES, Phillips K, Race B, Dittmer U, Kukolj G, Hasenkrug KJ. 2018. An advanced BLT-humanized mouse model for extended HIV-1 cure studies. AIDS 32:1–10.
805. Llewellyn GN, Seclén E, Wietgrefe S, Liu S, Chateau M, Pei H, Perkey K, Marsden MD, Hinkley SJ, Paschon DE, Holmes MC, Zack JA, Louie SG, Haase AT, Cannon PM. 2019. Humanized Mouse Model of HIV-1 Latency with Enrichment of Latent Virus in PD-1+ and TIGIT+ CD4 T Cells. J Virol 93.
806. Choudhary SK, Archin NM, Cheema M, Dahl NP, Garcia J V., Margolis DM. 2012. Latent HIV-1 Infection of Resting CD4+ T Cells in the Humanized Rag2-/- c-/- Mouse. J Virol 86:114–120.
807. Joshi P, Maidji E, Stoddart CA. 2016. Inhibition of Heat Shock Protein 90 Prevents HIV Rebound. J Biol Chem 291:10332–10346.

808. Marsden MD, Zack JA. 2015. Studies of retroviral infection in humanized mice. Virology 479–480:297–309.
809. Marsden MD, Zack JA. 2017. Humanized Mouse Models for Human Immunodeficiency Virus Infection. Annu Rev Virol 4:393–412.
810. Lin Z, Monteiro-Riviere NA, Riviere JE. 2015. Pharmacokinetics of metallic nanoparticles. Wiley Interdiscip Rev Nanomedicine Nanobiotechnology. Wiley Interdiscip Rev Nanomed Nanobiotechnol.
811. Kozics K, Sramkova M, Kopecka K, Begerova P, Manova A, Krivosikova Z, Sevcikova Z, Liskova A, Rollerova E, Dubaj T, Puntes V, Wsolova L, Simon P, Tulinska J, Gabelova A. 2021. Pharmacokinetics, Biodistribution, and Biosafety of PEGylated Gold Nanoparticles In Vivo. Nanomaterials 11:7–22.
812. Chenthamara D, Subramaniam S, Ramakrishnan SG, Krishnaswamy S, Essa MM, Lin F-H, Qoronfleh MW. 2019. Therapeutic efficacy of nanoparticles and routes of administration. Biomater Res 23:1–20.
813. Parker SE, Davey PG. 1992. Pharmacoeconomics of Intravenous Drug Administration. Pharmacoeconomics. Pharmacoeconomics.
814. Coelho T, Adams D, Silva A, Lozeron P, Hawkins PN, Mant T, Perez J, Chiesa J, Warrington S, Tranter E, Munisamy M, Falzone R, Harrop J, Cehelsky J, Bettencourt BR, Geissler M, Butler JS, Sehgal A, Meyers RE, Chen Q, Borland T, Hutabarat RM, Clausen VA, Alvarez R, Fitzgerald K, Gamba-Vitalo C, Nochur S V., Vaishnaw AK, Sah DWY, Gollob JA, Suhr OB. 2013. Safety and Efficacy of RNAi Therapy for Transthyretin Amyloidosis. N Engl J Med 369:819–829.
815. Fraser N, Snyman JR, Wessels F, Nel G. 2007. Intravenous fluid therapy: A randomized controlled trial to investigate the effectiveness of the IV2TM flow medical device. J Clin Nurs 16:1593–1601.
816. Xu H, Shen L, Xu L, Yang Y. 2015. Controlled delivery of hollow corn protein nanoparticles via non-toxic crosslinking: in vivo and drug loading study. Biomed Microdevices 17:1–14.
817. Cunha-Reis C, Machado A, Barreiros L, Araújo F, Nunes R, Seabra V, Ferreira D, Segundo MA, Sarmento B, das Neves J. 2016. Nanoparticles-in-film for the combined vaginal delivery of anti-HIV microbicide drugs. J Control Release 243:43–53.

818. Desai P, Patlolla RR, Singh M. 2010. Interaction of nanoparticles and cell-penetrating peptides with skin for transdermal drug delivery. Mol Membr Biol. Mol Membr Biol.
819. Sailaja I, Kumar Baghel M, Anand Shaker I. 2021. Nanotechnology Based Drug Delivery for HIV-AIDS TreatmentAIDS Updates - Recent Advances and New Perspectives. IntechOpen.
820. Dölen Y, Valente M, Tagit O, Jäger E, Van Dinther EAW, van Riessen NK, Hruby M, Gileadi U, Cerundolo V, Figdor CG. 2020. Nanovaccine administration route is critical to obtain pertinent iNKt cell help for robust anti-tumor T and B cell responses. Oncoimmunology 9.